Listening to the Ear

Thesis by
Christopher A. Shera

In Partial Fulfillment of the Requirements
for the Degree of
Doctor of Philosophy

California Institute of Technology
Pasadena, California
1992
(Defended 2 January 1992)

Listening to the Ear

"Your tale, Sir, would cure deafness."

—Shakespeare, *The Tempest* (act I, scene ii)

For the closest of friends,

κοινὰ γὰρ τὰ τῶν φίλων.

—Plato's *Phaedrus*

Acknowledgements

"It takes two to speak the truth—one to speak, and another to hear."

—Thoreau

The best listening is never done alone, and mine has been no exception. Thanks go foremost to my advisor, George Zweig, who imparted his own unshakeable 'commitment to reality' and attention to detail. While working with him, and while listening as he worked with others, I have been privileged to learn much about answering his reiterated and provocative question, What constitutes 'success'?; a question he posed—and answered incisively with his own example—not only when wrestling meaning from the data at hand, but also in recognizing just what other questions needed to be asked.

I thank my committee members—Steven Frautschi, Jim Bower, Ricardo Gomez, Charlie Peck, and David Van Essen—for their guidance and support, and for their continuing interest in a thesis part physics, part neurobiology; part theory, part experiment; and in a graduate student part here, part there.

I am indebted to many, for this thesis is not mine alone. My interest in hearing and language, in the unfathomable (and anything but quiet) inner life and culture of the deaf, first arose from conversations with Mark Medoff and an open rehearsal of his then work-in-progress, *Children of a Lesser God.* For the inspiration of their passionate example in blending the life of the mind with the practical and romantic life of the soul, I owe much to Haverford professors Richard Bernstein (philosophy) and Tamara Brooks (music).

On a more tangible level, Jennifer McDowell—too modest ever to believe it—made invaluable contributions, as both technical assistant and patient subject, to the experiments described here. Mickey Chorn cheerfully provided many of the signal-processing routines used in the data analysis, and a bottle of Stolichnaya (still, fortunately, far from finished) as consolation until they worked. Scott Konishi's causal-function programs—undocumented, inscrutable, and perhaps nondeterministic—proved indispensable in 'debugging' the experiments. Klaus Lackner contributed exquisitely crafted numerical-analysis and graphics software; and, more important, taught me how to write my own. And thanks go to my

many subjects, especially Jennifer McDowell, Cindy Little, and Erica Jen, for lending me their ears.

Over the years the Hearing Research group has cast a true gallimaufry of players. Their contributions ring on (some, fortunately, more highly damped than others), and I thank them all for allowing me to teach and for what they've taught. For the sheer joy of the unexpected, Ngeci Bowman, David Goldhaber, and Tom Tromey deserve special mention.

Outside the lab, I thank my family—still, after all these years, never more crazy—for their care and support. Although our center could never have held, Rachel Carnell, perhaps unwittingly, helped catalyze my journey toward self-acceptance. And I remember with affection the many friends—you know who you are—who have enriched my days here. Worthy of special note are Candace Magner and the members of *Coro de Cámara*, who shared with me their love of chamber music; and my *chaverim* in the Jewish community, especially Jack Shlachter and Kate Bowman, who befriended a stranger, Shemaya, sojourning among them.

Finally, to those special, happy few—Jim Knierim, Jeffrey Carr, George Zweig, Erica Jen, Cindy Little, Rebecca Meketa, Jennifer McDowell, Melissa Klein, Mordena Babich—who have been with me, over these seven wonderful and sometimes difficult years, my closest friends; it is to each of you, individually and together, that this thesis is dedicated, and for whom, as now, I will always be listening.

Pasadena–Los Alamos, 1984–1991

Abstract

Otoacoustic emissions demonstrate that the ear creates sound while listening to sound, offering a promising acoustic window on the mechanics of hearing in awake, listening human beings. That window is clouded, however, by an incomplete knowledge of wave reflection and transmission, both forth and back within the cochlea and through the middle ear. This thesis "does windows," addressing wave propagation and scattering on both sides of the middle ear. A summary of highlights follows. Measurements of the cochlear input impedance in cat are used to identify a new symmetry in cochlear mechanics—termed "tapering symmetry" after its geometric interpretation in simple models—that guarantees that the wavelength of the traveling wave changes slowly with position near the stapes. Waves therefore propagate without reflection through the basal turns of the cochlea. Analytic methods for solving the cochlear wave equations using a perturbative scattering series are given and used to demonstrate that, contrary to common belief, conventional cochlear models exhibit negligible internal reflection whether or not they accurately represent the tapering symmetries of the inner ear. Frameworks for the systematic "deconstruction" of eardrum and middle-ear transduction characteristics are developed and applied to the analysis of noninvasive measurements of middle-ear and cochlear mechanics. A simple phenomenological model of inner-ear compressibility that correctly predicts hearing thresholds in patients with missing or disarticulated middle-ear ossicles is developed and used to establish an upper bound on cochlear compressibility several orders of magnitude smaller than that provided by direct measurements. Accurate measurements of stimulus-frequency evoked otoacoustic emissions are performed and used to determine the form and frequency variation of the cochlear traveling-wave ratio noninvasively. Those measurements are inverted to obtain the spatial distribution of mechanical inhomogeneities responsible for evoked emission. Although current models require that the periodicities found in emission spectra and threshold hearing curves originate in a corresponding corrugation in the mechanics of the cochlea, it is shown that the observed spectral periodicities can arise spontaneously through the dynamics of wave propagation and reflection and that the organ of Corti, as suggested by the anatomy, need manifest no particular translational symmetries.

Contents

---

1 Published (March 1991) in *J. Acoust. Soc. Am.* **89**:1276–1289.
2 Published (March 1991) in *J. Acoust. Soc. Am.* **89**:1290–1305.
3 Published (July 1991) in *J. Acoust. Soc. Am.* **90**:253–262.
4 Submitted to *J. Acoust. Soc. Am.*
5 Submitted to *J. Acoust. Soc. Am.*
6 Submitted to *J. Acoust. Soc. Am.*
7 Submitted to *J. Acoust. Soc. Am.*
8 Submitted to *J. Acoust. Soc. Am.*

Introduction

The mammalian ear has evolved a remarkable mechanism for the detection and analysis of sound. Far from being an objective, passive recorder of sense impressions, the ear is an energy-producing mechanical system that creates sound in response to sound. Those sounds can be recorded noninvasively in the ear canal with sensitive microphones. Thus, by listening seriously to what the ear is saying, one can explore the mechanics of hearing in awake, listening human beings.

Blow on an Aeolian harp. As the strings vibrate they move air molecules surrounding the harp and sound waves are created that travel outwards to the listening ear. Upon entering the ear canal those waves vibrate the eardrum, whose oscillations are transmitted by the bones of the middle ear (the three smallest of the human body: the malleus, incus, and stapes) to the oval window of the cochlea.

Helmholtz pictured the cochlea itself as a miniature harp, connected string by string to neural fibers (Helmholtz 1863). Sensations of tone were created as sound waves induced the strings to resonate in sympathetic vibration, exciting corresponding fibers, which sent electrical signals to the brain. This view of cochlear mechanics was overturned, however, by the experiments of Georg von Békésy who showed that, unlike the strings of a harp, the structures within the cochlea are not under tension (von Békésy 1960).

Rather, the cochlea consists of three fluid-filled chambers coiled into a spiral like a snail's shell about the size of a large pea. (Applied to the ear by the Sicilian philosopher Empedocles,[1] the word "cochlea" comes from the Greek $\kappa o \chi \lambda \acute{\iota} \alpha \varsigma$, referring to the spiny, spiral-shelled Mediterranean gastropod *Murex trunculus*, source of the coveted royal dye, Tyrian purple.) Separated by membranes from the other two, the central chamber contains a longitudinal array of specialized sensory cells, the hair cells of the organ of Corti. By directly observing the motion of the basilar membrane in human cadavers, von Békésy demonstrated that vibration of the stapes sets the cochlear fluids into motion, generating a wave that travels along the organ of Corti until it reaches a point where its energy excites the nearby hair cells and is transduced into electrical potentials. The location of the point

[1] Empedocles' (d. circa 430 B.C.E.) contributions to physics include the famous theory of the four elements (earth, air, fire, and water) and their manipulation by the two powers, affinity and antipathy.

of transduction varies monotonically with the frequency of the stimulus. Tones of low frequency stimulate hair cells near the apex of the cochlea; higher-frequency tones excite regions closer to the stapes. The cochlea thus acts like an acoustic prism, separating sounds into their component frequencies and mapping those frequencies onto different points along the organ of Corti. This "textbook" understanding of traveling-wave excitation in the cochlea was, until recently, believed correct at all stimulus levels.[2] Although the classical view applies for loud sounds (and in the dead), a remarkably different picture now pertains at lower sound intensities.

It is now known that the ear creates sound while listening to sound (Kemp 1978). A recent model of cochlear mechanics deduced from measurements of basilar-membrane motion (Zweig 1991) predicts that cellular force generators in the cochlea—presumably the outer hair cells, which are motile, exhibiting a voltage-dependent contraction in isolated preparations (Brownell et al. 1985; Zenner et al. 1987), and receive extensive innervation from the brain (Spoendlin 1979)—boost the energy of incoming sound, amplifying traveling waves somewhat as a laser amplifies light. Consequently, small backward-traveling waves, originating from the scattering of forward-traveling waves by mechanical inhomogeneities in the organ of Corti (Manley 1983; Lonsbury-Martin et al. 1988), are amplified as they travel backwards to the stapes, from which they are partially reflected. Unreflected waves vibrate the middle-ear bones and ultimately appear in the ear canal as sound ("otoacoustic emissions"). The generation of large backward-traveling waves radically changes our view of wave motion in the cochlea at low sound-pressure levels. The superposition of forward- and backward-traveling waves leads to a standing-wave component in the cochlear response, thereby increasing the overall sensitivity of hearing.

The threshold hearing curve shows periodic minima (Elliot 1958; Thomas 1975) at frequencies that correlate strongly with maxima in the spectra of otoacoustic emissions (Horst et al. 1983; Zwicker and Schloth 1984). The ear emits most loudly at those frequencies for which it is most sensitive. Since the cellular force generators are limited in the energy they

[2] See, however, the work of LePage (LePage 1987; LePage 1990), who describes experiments identifying another possible component—a "summating baseline shift"—in the response of the organ of Corti and suggests that they provide evidence for the dynamic control of cochlear tuning, achieved by varying the tension in the radial fibers of the pars pectinata. The outer hair cells then serve—returning to Helmholtz—much like the pedals on an orchestral harp.

can emit, cochlear excitation patterns produced when the ear listens to quiet sounds are qualitatively different from those produced in response to louder sounds. The extensive innervation of hair cells by neurons from the brain suggests that the brain may, according to its expectations, purposefully alter the mechanical state of the ear to facilitate the extraction of signal from noise; the ear may actively modify and control its own experience.

Background

More than forty years ago, Gold (1948) proposed that the viscous damping of the organ of Corti might be overcome by a "regenerative mechanism" through which electrochemical energy was converted into mechanical forces that counteracted the damping. Gold suggested that such feedback might occasionally drive a region of the cochlea into self-oscillation, and that such sustained oscillations could underly the familiar phenomenon of "ringing in the ear." Although Gold predicted that those mechanical oscillations would generate acoustic counterparts detectable in the ear canal, his hypothesis remained unexplored for thirty years, until Kemp (1978), working with sensitive microphones, demonstrated the existence of otoacoustic emissions originating within the cochlea.

To supply background and context for the work described here—which investigates the unexpected experimental finding that when listening to quiet sounds the ear emits, at certain regularly-spaced frequencies corresponding to those at which it is most sensitive, nearly as much energy as it receives Kemp (1978)—this section provides a brief synopsis of some of the more interesting features of otoacoustic emissions. Probst et al. (1991) provide a recent, comprehensive review of the field, which they find represented, to date, by more than 300 published papers.

- Otoacoustic emissions (OAEs) can occur in the absence of acoustic stimuli (spontaneous OAEs) or they can be generated by the cochlea in response to sound (evoked OAEs).
- Click- or toneburst-evoked otoacoustic emissions, known as cochlear echoes, can be evoked from essentially all normal human ears. Their ubiquity and the close correlation between the spectra of the evoking stimulus and that of the resulting echo (Norton and Neely 1987) indicate that evoked emissions reflect normal cochlear mechanics,

not cochlear pathology. Indeed, the presence and level of evoked emission offers an objective, clinical measure of cochlear function (Kemp et al. 1986).

- Human spontaneous and evoked OAEs are found most often in the frequency range 1–2 kHz. This frequency window may be a reflection of the transfer characteristics of the middle ear (Shera and Zweig 1992d; Shera and Zweig 1992g).
- The amplitude of stimulus-frequency and transiently-evoked OAEs grows linearly with the level of the evoking stimulus below approximately 10 dB; at higher stimulus levels they saturate (Zwicker and Schloth 1984).
- Spontaneous otoacoustic emissions produce a non-Gaussian probability distribution for the pressure amplitude in the ear canal, suggesting that they arise as the result of instabilities in an active feedback system, rather than through the passive filtering of thermal noise (Bialek and Wit 1983).
- Evidence suggests that spontaneous OAEs may arise through damage to the cochlea (Zurek and Clark 1981; Ruggero et al. 1983) and are not important for the normal process of hearing. Characterization of their properties, however, could give insight into the structure of the active processes that contribute to normal hearing.
- Surveys of emission prevalence (see Probst et al. 1991) find that spontaneous OAEs occur more frequently in females (52%) than in males (30%). Similar gender differences occur in both infants and adults (Strickland et al. 1985). These surprising statistics may reflect differences in the stapes reflection coefficient originating through gender-related variations in middle-ear size.
- Spontaneous OAEs display typical nonlinear behavior. They show both suppression and entrainment in response to external tones at nearby frequencies (e.g., Rabinowitz and Widin 1984), suggesting that they may be characterized phenomenologically as originating from the motion of a nonlinear harmonic oscillator.
- Measurements of the minimum stimulus energy needed to entrain a spontaneous emission yield results on the order of 1 eV (Wit and Ritsma 1983), suggesting that emission phenomena could be triggered by or originate in processes at the level of a single molecule.

- Pairs of adjacent spontaneous emissions (and sometimes even groups of noncontiguous emissions) can be "linked" (Burns et al. 1984; Jones et al. 1986), meaning that they appear to switch on and off alternately in time, as though the emission energy were somehow shared between two quasi-stable states.
- When the ear is driven by two primary tones of frequency f_1 and f_2, combination tones at frequencies $nf_1 \pm mf_2$, where n and m are integers, are generated in the cochlea. These combination tones can be detected both psychophysically (Goldstein 1967) and by microphones in the human ear canal (Kemp 1979). Spontaneous OAEs have been found to generate their own intermodulation distortion products (Burns et al. 1984; Jones et al. 1986).
- If, in addition to the two primaries, a third cancellation tone at a combination-tone frequency is presented, its amplitude and phase can be adjusted so that the combination tone is no longer heard. In conjunction with a model of the middle ear, a nonlinear model of the cochlea can predict the amplitude and phase of the required cancellation tone and the results of other psychophysical null experiments (Shera and Zweig 1992b).
- The behavior of otoacoustic emissions is controlled via feedback from the central nervous system. Experiments have shown that contralateral tones can alter the amplitude and frequency of both spontaneous and evoked OAEs (Mott et al. 1989). Whitehead (1991) has described similar, centrally-mediated variations in emission characteristics.

Evoked emission and the thesis

Measurement of the pressure in the human ear canal as a stimulus tone is swept slowly in frequency yields two surprises. First, as demonstrated by Kemp (1978) more than a decade ago, the measured pressure contains a surprising amount of spectral structure, revealing the presence of an additional tone evoked by the stimulus and generated within the cochlea. Second, and perhaps even more surprising, that spectral structure typically assumes a remarkably simple form, consisting of regular, almost periodic oscillations in the amplitude and phase.

This thesis attempts to understand the origin of that simple pattern and explores a number of interesting qualitative features of evoked otoacoustic emissions:

- Close examination of the human threshold hearing curve reveals a substantial microstructure (Elliot 1958; Thomas 1975). Threshold sensitivity can vary by more than 10 dB over intervals of 50 Hz. The microstructure of the human threshold hearing curve suggests that the cochlea, at least at low stimulus levels, is characterized by a discrete (rather than the often presumed continuous) spatial symmetry. The threshold hearing curve defines a "cochlear reticule." The cochlear reticule may result from the generation of standing-wave patterns in the inner ear (Kemp 1980) or may reflect an intrinsic corrugation or washboarding in the mechanics of the organ of Corti.
- Maxima in the spectra of evoked emissions are correlated strongly with minima in the threshold microstructure (Kemp 1979; Horst et al. 1983; Zwicker and Schloth 1984). The ear emits preferentially at those frequencies at which it is most sensitive.
- The frequency spacing of adjacent maxima in both the spectra of evoked OAEs and the threshold hearing curve varies systematically with the frequency of the stimulus. Psychophysically, the observed frequency interval represents roughly half a critical bandwidth (Zwicker and Schloth 1984). When converted to a length using the cochlear frequency-position map, the frequency spacing corresponds to a constant distance (roughly half a millimeter) along the organ of Corti. Perhaps significantly, this distance is nearly the same as that traversed by outer hair cell afferent auditory nerve fibers, which travel basally some distance after entering the cochlea before synapsing with the outer hair cells (Spoendlin 1978).
- Evidence suggests that the microstructure of the human threshold hearing curve may be correlated between the two ears (Probst et al. 1986). If this is so, otoacoustic emissions may play an important role in signal processing at low and intermediate sound-pressure levels (e.g. in the localization of low intensity sounds or the extraction of unvoiced speech from ambient noise). If otoacoustic emissions do function in signal processing, and are not merely an epiphenomenon of cochlear activity, then it is possible that the boundary condition at the basal end of the cochlea (which helps determine the distribution of sound created in the inner ear) evolved to facilitate this

function. A model of the middle ear (Shera and Zweig 1992a) can be used to explore this possibility.

- The data of Zwicker and Schloth (1984) indicate that at low stimulus levels where emissions are strong the analytic structure of the ear-canal pressure is not what one would expect from a causal system (Shera and Zweig, unpublished observation). The real and imaginary parts of a causal function are Hilbert transforms of one another; the real and imaginary parts of Zwicker's measured ear-canal pressure do not satisfy these relations, raising the intriguing possibility that feedback from the brain plays a major role in the generation or control of evoked emission.

Overview

Otoacoustic emissions thus offer a promising acoustic window on the mechanics of hearing. That window is clouded, however, by an incomplete knowledge of wave reflection and transmission, both forth and back within the cochlea and through the middle ear. This thesis "does windows," addressing wave propagation and scattering on both sides of the middle ear to provide an understanding of the striking spectral periodicities found in emission spectra and the microstructure of the threshold hearing curve. Organized as a series of self-contained chapters (corresponding to papers, either published or submitted for publication, written in collaboration with George Zweig), the thesis is unified thematically by its concern with understanding how measurements made in the ear canal can be used as a noninvasive probe of cochlear mechanics.

The thesis—organized as a round-trip journey outwards from the cochlea to the eardrum and middle ear and then back again to the cochlea—explores two principle themes. Since quantitative interpretation of otoacoustic emissions requires knowledge of middle-ear transfer functions not currently available, the thesis first develops (in chapters III, IV, and VI) frameworks for the systematic "deconstruction" of eardrum (§III) and middle-ear mechanics (§IV), providing a common ground for the comparison between theory and experiment. For example, the framework is used to establish an upper bound on inner-ear compressibility several orders of magnitude smaller than those provided by direct measurements (§VI).

Second, the thesis explores (in chapters I, II, V, VII, and VIII) the propagation and reflection of cochlear waves. Measurements of cochlear input impedance in cat are used to identify a new symmetry in cochlear mechanics—termed "tapering symmetry" after its geometric interpretation in simple models—that guarantees that the wavelength of the traveling wave changes slowly with position near the stapes (§I). Waves therefore propagate without reflection through the basal turns of the cochlea. Analytic methods of solving the cochlear wave equations that incorporate both scattering by mechanical inhomogeneities in the organ of Corti (§II) and reflection and transmission at the cochlear boundary with the middle ear are developed. Those methods are used to demonstrate that measurements of otoacoustic emissions can be employed to determine middle-ear transfer functions noninvasively (§V). Accurate measurements of stimulus-frequency evoked otoacoustic emissions are made and, after "dividing out" the unknown transfer characteristics of the middle ear, used to determine the form and principle frequency variation of the cochlear traveling-wave ratio (§VII). Finally, those measurements are "inverted" and solutions to the inverse scattering problem obtained for the distribution of mechanical inhomogeneities responsible for evoked emission (§VIII). Although current models require that the periodicities found in emission spectra and threshold hearing curves originate in a corresponding corrugation in the structure of the cochlea (e.g., Strube 1985; Peisl 1988; Strube 1989), the thesis demonstrates that the striking spectral periodicities can arise spontaneously through the dynamics of wave propagation and reflection and that the remarkable spectral order, as suggested by the anatomy of the organ of Corti, need have no objective spatial correlate.

A Symmetry Suppresses the Cochlear Catastrophe

Christopher A. Shera and George Zweig

Hearing Research Laboratory
Signition, Inc.
P.O. Box 1020
Los Alamos, New Mexico 87544

ABSTRACT

When the independent spatial variable is defined appropriately, the empirical finding that the phase of the cochlear input impedance is small (Lynch et al. 1982) is shown to imply that the wavelength of the pressure wave in the cochlea changes slowly with position near the stapes. As a result, waves traveling in either direction through the basal turn undergo little reflection, and the transfer of energy between the middle and inner ears remains efficient at low frequencies. The slow variation of the wavelength implies that the series impedance $\bar{Z}$ and shunt admittance Y of the cochlear transmission line are approximately proportional at low frequencies and thus requires that the width of the basilar membrane and the cross-sectional areas of the cochlear scalae taper in opposite directions. Maintenance of the symmetry between $\bar{Z}$ and Y is both necessary and sufficient to ensure that the spatial derivative of the wavelength, and hence the phase of the cochlear input impedance, remains small.

Although introduced in another context, the model of Zweig (1987; 1991) manifests the symmetry between $\bar{Z}$ and Y. In other transmission-line models of cochlear mechanics, however, that symmetry is absent, and the spatial derivative of the wavelength diverges at low frequencies—the "cochlear catastrophe." Those models therefore contradict the impedance measurements and predict little transfer of energy between the middle and inner ears.

Contents

Introduction

Measurements of the velocity of the basilar membrane in response to tones of different frequency (e.g., Rhode 1971; Robles et al. 1986) and the absence of spectral ripples in non-invasive measurements of middle-ear input impedance (Kemp and Chum 1980; Zwicker and Schloth 1984) both indicate that little reflection of forward-traveling waves occurs within the cochlea at high sound-pressure levels. Indeed, it is widely believed that the cochlea evolved to suppress such reflection at stimulus levels sufficiently above threshold (Zweig et al. 1976; Zweig 1976). A number of authors have argued, however, that the cochlea is strikingly asymmetric with respect to wave travel in the two directions along the organ of Corti and that the internal reflection of backward-traveling waves is significant at all sound levels (de Boer and Viergever 1984; de Boer et al. 1986ab; Viergever 1986; Kaernbach et al. 1987). Such reflection, if present, would have important consequences for understanding the nature of otoacoustic emissions and their contribution to auditory signal processing (Kemp 1978; Kemp 1979).

This paper demonstrates, however, that measurements of the cochlear input impedance,

(Lynch et al. 1982; Nedzelnitsky 1974a; Nedzelnitsky 1980) which indicate that its phase is nearly zero, imply—when the independent spatial variable is appropriately defined—that the wavelength of the traveling pressure wave changes slowly with position near the stapes. Consequently, reflection of waves traveling in either direction through the basal turn must be small. The slow variation of the wavelength implies that the longitudinal impedance $\bar{Z}$ of the cochlea and the shunt admittance Y of the organ of Corti are approximately proportional. Maintenance of that symmetry between $\bar{Z}$ and Y is both necessary and sufficient for transmission-line models to agree with the impedance measurements. If the symmetry is broken, however, the spatial derivative of the wavelength diverges at low frequencies. That divergence, manifest in nearly all models of cochlear mechanics, we call the "cochlear catastrophe."[1] Those models are thus in contradiction with measurements

[1] The cochlear catastrophe takes its name by analogy with the apparent divergence at low photon energy in the scattering cross-section of an electron, the so-called "infrared catastrophe" of quantum electrodynamics (Bloch and Nordsieck 1937; Feynman 1961). The word "catastrophe" comes from the Greek *καταστρέφειν* meaning "to turn down" and describes the ironic reversal in fortune characteristic of the dénouement of a classical tragedy. Appropriately, models of cochlear mechanics exhibiting the catastrophe display a pronounced decrease in the magnitude of the cochlear input impedance and a sharp fall-off in energy transfer to the cochlea at low frequencies.

of the cochlear input impedance. Whereas the measured input impedance is essentially real and constant over a wide frequency range, the models predict a nonzero phase and a considerable variation in amplitude arising from the broken symmetry. Another model of cochlear mechanics (Zweig 1987; Zweig 1991) enforces the symmetry and so avoids the cochlear catastrophe, remaining approximately consistent with the impedance data.

The rate of change of the wavelength near the stapes is also shown to affect the sensitivity of the ear. Models of cochlear mechanics that exhibit the catastrophe predict a decrease in the transfer of acoustic energy to the cochlea at low frequencies. Suppression of the cochlear catastrophe prevents that dramatic decline in middle-ear efficiency.

A. Overview

The paper consists of two parts. In the first, the cochlear input impedance is defined, its measurement in the cat reviewed, and an approximate analytic expression for it obtained. Consistency with the measurements of Lynch et al. (1982) is shown to require that the wavelength of the traveling wave change slowly at the basal end of the cochlea. The implications of a slowly changing wavelength for the reflection of traveling waves, for the geometric structure of the cochlea, and for the sensitivity of hearing are then discussed. The second part parallels the first, illustrating the results in a simple class of cochlear models. Those models fall into two categories differing in the spatial variation of their parameters: those in which the wavelength changes slowly near the stapes (e.g., Zweig 1987; Zweig 1991), and those, such as the models used to discuss the reflection of retrograde waves (Viergever 1986; de Boer et al. 1986ab and Kaernbach et al. 1987), that exhibit the cochlear catastrophe. The companion paper (Shera and Zweig 1991b) explores the consequences of breaking the symmetry between $\bar{Z}$ and Y for the reflection of traveling waves.

I. The Symmetry

A. The cochlear input impedance

As seen from the basal end of the cochlea, the response at the driving frequency to a pure tone of angular frequency ω and amplitude A can, if the organ of Corti is essentially incompressible (cf. Shera and Zweig 1992a), be characterized by the cochlear

input impedance, which is defined as the ratio of the pressure difference $P(x,\omega;A)$ across the organ of Corti to the volume velocity $U(x,\omega;A)$ of the cochlear fluids in the scala vestibuli:

$$\overrightarrow{Z_0}(\omega;A) \equiv \left.\frac{P}{U}\right|_{x=0;\ \text{cochlea driven forward}} . \tag{1}$$

The position $x = 0$ corresponds to the basal opening of the cochlear spiral, and the diacritical arrow indicates that the cochlea is being driven in the "natural," or forward, direction.

B. Amplitude and frequency range of interest

At moderate intensities nonlinearities in cochlear mechanics make significant contributions to $\overrightarrow{Z_0}(\omega;A)$, which varies strongly with A (Kemp 1979a). At high intensities, however, the relative amplitude of those nonlinear contributions is always small (Kemp and Chum 1980; Zwicker and Schloth 1984), and the function $\overrightarrow{Z_0}(\omega;A)$ becomes independent of the amplitude of the stimulating tone:[2]

$$\overrightarrow{Z_0}(\omega;A) \equiv Z_0(\omega), \quad \text{for } A > A_\infty. \tag{2}$$

In humans, the stimulus amplitude A_∞ corresponds to roughly 60 dB above threshold at frequencies $\omega/2\pi \sim 1$ kHz.

At the lowest frequencies ($\omega/2\pi \lesssim 100$ Hz) interpretation of $Z_0(\omega)$ is complicated by viscosity and the effects of the geometry of the apical scalae and helicotrema (Koshigoe et al. 1983; Puria and Allen 1991). For example, the termination of the organ of Corti at the helicotrema may result, at very low frequencies, in the partial reflection of waves back toward the stapes. Such waves can have significant effects on the cochlear input impedance (Puria and Allen 1991). By restricting attention to higher frequencies ($\omega/2\pi \gtrsim 100$ Hz), at which stimulus energy is absorbed before reaching the apical end of the cochlea, such complications are avoided and measurements of $Z_0(\omega)$ can be compared with the predictions of models that do not specify cochlear responses to the lowest frequencies.

---

[2] The situation in non-mammals may be more complex (e.g., Rosowski et al. 1984).

C. Measurements of $Z_0(\omega)$

Lynch et al. (1982) and Nedzelnitsky (1974a; 1980) have measured the input impedance of the cat inner ear at high stimulus amplitudes. At the lowest frequencies ($\omega/2\pi \lesssim 80$ Hz) their measurements include effects due to the impedance of the round window, but at higher frequencies the impedance they measure reduces to $Z_0(\omega)$ and is determined solely by the internal mechanics of the cochlea.[3] Their measurements of $Z_0(\omega)$, together with smoothed, minimum-phase fits (Zweig and Konishi 1987; Konishi and Zweig 1989) to the data, are shown in Fig. 1.

The measurements indicate that the phase $\angle Z_0(\omega)$ of the cochlear input impedance is small over a broad range of frequencies greater than approximately 100 Hz (see also Nedzelnitsky 1974b):

$$\left|\angle Z_0(\omega)\right| \equiv \tan^{-1}\left|\frac{\mathrm{Im}Z_0(\omega)}{\mathrm{Re}Z_0(\omega)}\right| \ll 1 \qquad (\omega/2\pi \gtrsim 100 \text{ Hz}), \tag{3}$$

where Re and Im indicate the real and imaginary parts of their arguments. Note, in addition, that $\mathrm{Re}Z_0(\omega)$ is roughly constant.

The measurement errors are not precisely known, but since driving-point impedances are minimum-phase functions (Bode 1945), a lower bound on the error is given by the deviations from the minimum-phase fit, which do not exceed ± 2 dB in the amplitude and $\pm 10°$ in the phase. Lynch et al. (1982) provide an upper bound on the error of ± 10 dB in the amplitude and roughly $\pm 40°$ in the phase (Nedzelnitsky 1974a) but believe those limits substantially overestimate the actual error at frequencies greater than 100 Hz (Lynch et al. 1982; Peake 1989).

---

[3] Lynch et al. (1982) measure the ratio P_v/U, where P_v is the pressure in the scala vestibuli. As defined by Eq. (1), however, the cochlear input impedance $Z_0(\omega)$ is the ratio of the pressure *difference*,

$$P \equiv P_v - P_t \,, \tag{3.1}$$

between the scala vestibuli and scala tympani to the fluid volume velocity U in the scala vestibuli. The measurements of Nedzelnitsky (1980) indicate, however, that

$$P_v \gg P_t \qquad (\omega/2\pi \gtrsim 100 \text{ Hz}), \tag{3.2}$$

so that $P \approx P_v$ at frequencies greater than 100 Hz in the basal turn of the cat cochlea. Lynch et al. (1982) refer to Z_0 as the "input impedance *across* the cochlear partition" and denote it by Z'_C.

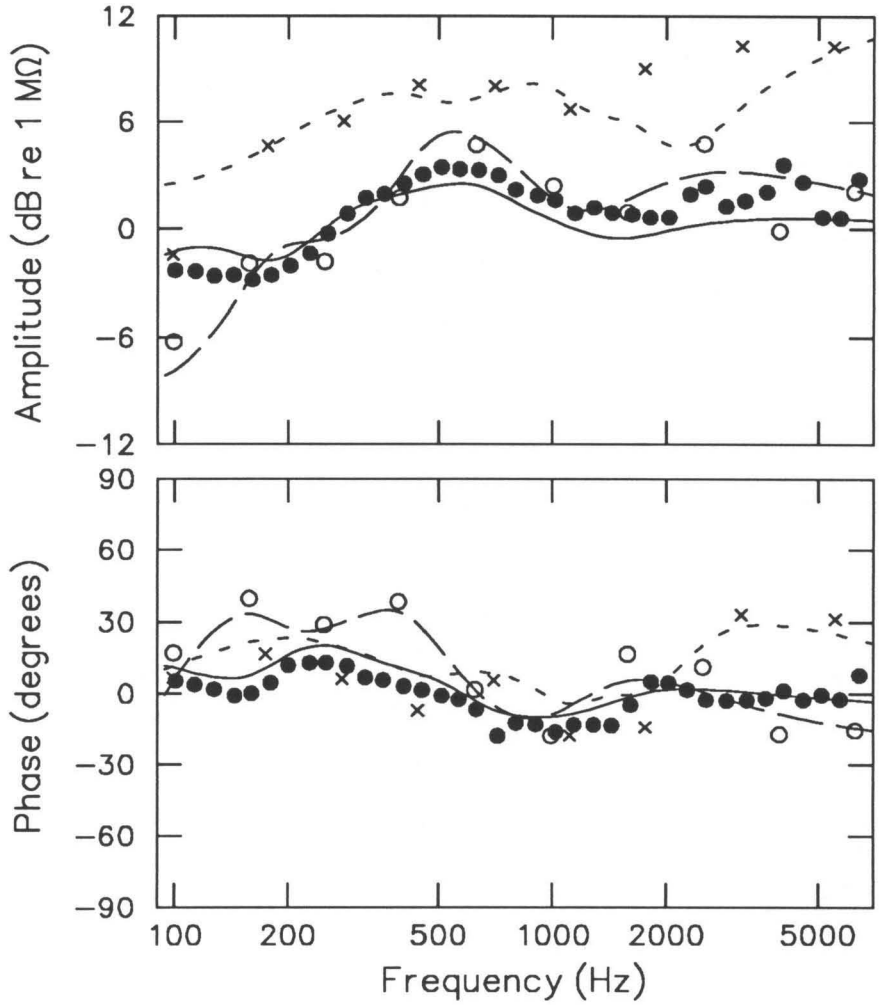

Figure 1. Amplitude and phase of the cochlear input impedance $Z_0(\omega)$ of the cat measured by Lynch et al. (1982) together with smoothed, minimum-phase fits to the measurements (Zweig and Konishi 1987; Konishi and Zweig 1989). Key to symbols: measurements for cat 25 (o) from Fig. 15 of Lynch et al. and corresponding fit (—— ——); measurements for cat 18 (×) from Fig. 15 of Lynch et al. and corresponding fit (- - - -); averaged measurements for 29 cats (•) from Fig. 24 of Lynch et al. and corresponding fit (———). Lynch et al. report measurements for an additional cat (cat 27); those measurements are not shown here because they include only a few points above 100 Hz. Note that the deviations from the minimum-phase fit are less than approximately ±2 dB in the amplitude and ±10° in the phase. Those errors were used as inputs to the fitting procedure and determined the relative weighting of amplitude and phase data (Zweig and Konishi 1987). The data indicate that the phase of $Z_0(\omega)$ is small in the frequency range 100–7000 Hz.

D. Transmission-line models of cochlear mechanics

An approximate analytic form for $Z_0(\omega)$ can be derived from transmission-line models of cochlear mechanics, enabling one to understand the constraints that measurements of $Z_0(\omega)$ impose on such models. Those constraints can be expected to take the form of a symmetry principle enforcing the empirical relation $\angle Z_0(\omega) \approx 0$.

At intensities $A > A_\infty$ and frequencies $\omega \ll \omega_{c_0}$, where ω_{c_0} is the characteristic angular frequency at the beginning of the organ of Corti ($x = 0$), the basal turn of the cochlea is analogous to a linear, one-dimensional mechanical transmission line (Zwislocki-Mościcki 1948; Peterson and Bogert 1950; Zweig 1991) with series impedance $\bar{Z}(x,\omega)$ and shunt admittance $Y(x,\omega)$ per unit length. A section of the cochlear transmission line is illustrated schematically in Fig. 2. Application of Kirchoff's circuit laws yields a pair of coupled, first-order transmission-line equations,

$$\frac{dP}{dx} = -\bar{Z}U \tag{4}$$

and

$$\frac{dU}{dx} = -YP\,, \tag{5}$$

describing the variation of P and U.

Validity of the simple transmission-line analogue used here requires that the cochlear response be linear and that the long-wavelength approximation hold in the basal turn of the cochlea at low frequencies. The motion of the organ of Corti is nonlinear primarily in the region of maximal velocity (Rhode 1971; Robles et al. 1986), which for angular frequencies $\omega \ll \omega_{c_0}$ occurs in the more apical turns of the cochlea. In addition, for frequencies $\omega \ll \omega_{c_0}$ the wavelengths of the waves on the organ of Corti are long relative to the heights of the scalae (Nedzelnitsky 1980). The pressure then depends only on position along the organ of Corti and not on the two orthogonal directions; the geometry of the basal turn is thus effectively one-dimensional.[4]

[4] Sondhi (1978) has shown, for example, that the input impedance of a two-dimensional cochlear model is essentially identical with the one-dimensional result. However, the effects of the vestibule have yet to be carefully investigated.

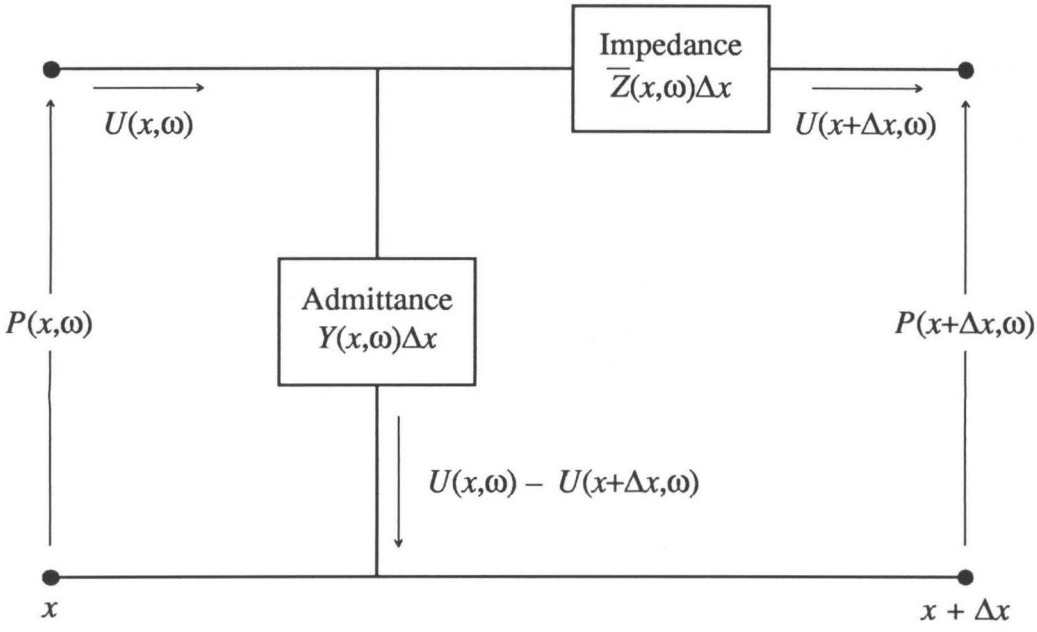

Figure 2. A transmission-line analog for a section of the basal turn of the cochlea. The series impedance $\overline{Z}(x,\omega)\Delta x$ includes the inertia of the cochlear fluids oscillating in the longitudinal direction, whereas the shunt admittance $Y(x,\omega)\Delta x$ characterizes the transverse response of the organ of Corti to a pressure difference across the scala media.

E. A change of coordinates

Solution of the transmission-line equations is simplified by regarding P and U as functions of the "spatial" variable[5]

$$\chi(x,\omega) = -i \int_0^x \bar{Z}(\acute{x},\omega)\, d\acute{x} \; . \tag{6}$$

Two points are then separated by a "distance" equal to $-i$ times the total series impedance between them. Conventional cochlear models predict that the impedance of the cochlear fluids to motion in the longitudinal direction is predominantly inertial. The series impedance $\bar{Z}(x,\omega)$ is thus essentially imaginary, and the factor $-i$, where $i \equiv \sqrt{-1}$, thus makes $\chi(x > 0,\omega)$ a positive, real-valued, monotonically-increasing function of x. Written in terms of χ the transmission-line equations become

$$\frac{dP}{d\chi} = -iU \tag{7}$$

and

$$\frac{dU}{d\chi} = -\frac{i}{\lambda^2} P \; , \tag{8}$$

where $\lambda(\chi,\omega)$ is the characteristic impedance $Z_c(\chi,\omega)$ of the transmission line:

$$\lambda(\chi,\omega) \equiv Z_c(\chi,\omega) \equiv \left(\frac{\bar{Z}}{Y}\right)^{1/2} \; . \tag{9}$$

Equations (7) and (8) describe a transmission line with series impedance i and shunt admittance i/λ^2 per unit length $d\chi$.

---

[5] Three related spatial variables (x, χ, and ζ) are used in this paper. The first, with dimensions

$$[x] = \text{length}, \tag{5.1}$$

represents distance along the organ of Corti. The second, with dimensions of acoustic impedance,

$$[\chi] = \text{mass/length}^4 \cdot \text{time}, \tag{5.2}$$

is used to transform the transmission-line equations (4) and (5) into a form [namely Eq. 10 for P] without explicit first derivatives of the dependent variable. The coordinate χ will later be shown to be the most natural for a description of wave propagation in the cochlea. The third spatial variable, ζ, represents length measured in units of the distance over which the characteristic frequency changes by about an octave in the basal turn and is introduced to simplify expressions involving the dependence of model parameters on position.

Throughout this paper when a function, say $\bar{Z}(x,\omega)$, is written as a function of another spatial variable, say χ, we adopt the notational convention that

$$\bar{Z}(\chi,\omega) \equiv \bar{Z}\big(x(\chi,\omega),\ \omega\big) \; . \tag{5.3}$$

Decoupling Eqs. (7) and (8) yields a wave equation for the pressure difference $P(\chi,\omega)$ across the scala media:

$$\frac{d^2P}{d\chi^2} + \frac{1}{\lambda^2}P = 0\,. \tag{10}$$

When distance is measured in terms of χ, $\lambda(\chi,\omega)$ is just $1/2\pi$ times the local wavelength $\lambda(\chi,\omega)$ of the wave on the basilar membrane (Zweig et al. 1976). Throughout this paper $\lambda(\chi,\omega)$ is thus referred to as the wavelength (and $\lambda' \equiv d\lambda/d\chi$ as its spatial derivative). Note, in addition, that the symbols $\lambda(\chi,\omega)$ and $Z_c(\chi,\omega)$ are used interchangeably.

F. Theoretical input impedance

If the wavelength $\lambda(\chi,\omega)$ varies slowly with position χ, waves traveling down the organ of Corti undergo little reflection. Equation (10) for the pressure can then be solved by expanding P in an asymptotic WKB series (e.g., Bender and Orszag 1978), which yields (e.g., Green 1837; Jeffreys 1924; Zweig et al. 1976)

$$P(\chi,\omega) \sim e^{-i\int^{\chi} d\check{\chi}/\lambda \,+\, \frac{1}{2}\ln\lambda \,+\, \cdots} \tag{11}$$

for the forward-traveling pressure wave. Equation (7) for U then implies that

$$Z_0^{-1}(\omega) = i\frac{d\ln P}{d\chi} \sim i\frac{d}{d\chi}\left\{-i\int^{\chi} d\check{\chi}/\lambda \,+\, \tfrac{1}{2}\ln\lambda \,+\, \cdots\right\}\Bigg|_{\chi=0}\,. \tag{12}$$

When the wavelength has the form predicted by transmission-line models at frequencies $\omega \ll \omega_{c_0}$, truncating the series after the first two terms is optimal and yields[6]

$$Z_0(\omega) \approx \frac{\lambda_0}{1 + i\lambda_0'/2}\,. \tag{13}$$

The subscripts "0" indicate that the quantities are evaluated at the basal end of the organ of Corti; for example,

$$\lambda_0(\omega) \equiv \lambda(0,\omega)\,. \tag{14}$$

The prime[7] denotes differentiation with respect to χ:

$$\lambda_0'(\omega) \equiv \frac{d\lambda(\chi,\omega)}{d\chi}\Bigg|_{\chi=0}\,. \tag{15}$$

---

[6] Viergever and de Boer (1987) obtained a similar approximate form [to which Eq. (13) reduces when the series impedance $\bar{Z}$ is independent of position] for the "matching impedance" of a nonuniform transmission line and found it to be in excellent agreement with numerical calculations.

[7] The traditional accent of the ecstasy of catastrophe.

Note that $\lambda'(\chi,\omega)$ is dimensionless.

Recall that by restricting attention to frequencies $\omega/2\pi \gtrsim 100$ Hz and stimulus amplitudes $A > A_\infty$, contributions to the input impedance due to reflection from the helicotrema and the amplification by the "cochlear laser" (Zweig 1991; Zweig 1989) of wavelets scattered from mechanical inhomogeneities in the organ of Corti can be assumed small. Reflections from apical regions of the cochlea may, however, be responsible for the fine structure in the measured impedance curves (Puria and Allen 1991). If reflections are not too large, $Z_0(\omega)$ can be approximated by an expression depending only on the mechanics at the basal end of the cochlea.

G. A limit on the rate of change of the wavelength

The measurements of Lynch et al. (1982) place important constraints on transmission-line models of cochlear mechanics. As shown later in the examples (Sec. II), those models predict that at frequencies much less than the characteristic frequencies near the stapes (i.e., at $\omega \ll \omega_{c_0}$), the wavelength $\lambda(\chi,\omega)$ is approximately real and the imaginary part of its spatial derivative $\lambda'(\chi,\omega)$ is small:

$$\left|\frac{\mathrm{Im}\lambda_0}{\mathrm{Re}\lambda_0}\right| \ll 1 , \tag{16}$$

and

$$\left|\mathrm{Im}\lambda_0'\right| \ll 1 . \tag{17}$$

Since forward-traveling waves have the approximate form (Zweig et al. 1976)

$$P_+(\chi,\omega) \approx A_+(\omega)\sqrt{\lambda}e^{-i\int^\chi d\check{\chi}/\lambda} , \tag{18}$$

the real nature of the wavelength guarantees that waves of low frequency propagate through the basal turn of the cochlea without substantial change in amplitude.

Applied to Eq. (13) for Z_0, inequalities (16) and (17) imply that

$$\angle Z_0 \approx -\tan^{-1}\left(\mathrm{Re}\lambda_0'/2\right) . \tag{19}$$

Combining Eq. (17) with the empirical finding that

$$\left|\angle Z_0(\omega)\right| \ll 1 \tag{20}$$

above 100 Hz (cf. Fig. 1) therefore yields

$$|\lambda_0'(\omega)| \ll 1 \qquad (\omega \ll \omega_{c_0}). \tag{21}$$

As an immediate consequence, note that the rough constancy of the measured $Z_0(\omega)$ implies

$$\lambda_0(\omega) \approx \text{constant} \qquad (\omega \ll \omega_{c_0}). \tag{22}$$

Inequality (21), which constitutes the central result upon which this paper elaborates, depends for its validity on the empirical finding that $\angle Z_0(\omega)$ is small (Lynch et al. 1982) and on inequalities (16) and (17), which follow from basic assumptions underlying models of cochlear mechanics. Should those assumptions prove inapplicable to the real cochlea, the mechanics of hearing must be considerably different from that currently conceived.

H. Relation to cochlear reflection of traveling waves

The inequality

$$|\lambda_0'(\omega)| \ll 1 \qquad (\omega \ll \omega_{c_0}), \tag{23}$$

which transmission-line models of cochlear mechanics must satisfy if they are to be consistent with the measurements of Lynch et al. (1982), can be interpreted physically in terms of the reflection of waves traveling along the organ of Corti. Inequality (23) is equivalent to the condition that the change in wavelength over distances on the order of a wavelength be less than the wavelength. That statement implies, by analogy with the propagation of light through a medium of variable refractive index (e.g., Born and Wolf 1959), that waves traveling in *either* direction along the organ of Corti undergo little reflection. Mathematically, the statement means that the WKB approximation may be used when solving the transmission-line equations, at least within the basal turn of the cochlea (Schroeder 1973; Zweig et al. 1976). Note that Eq. (23) thus provides *ex post facto* justification for the WKB expansion of the pressure used to obtain Eq. (13) for $Z_0(\omega)$.

I. A symmetry between $\bar{Z}$ and Y

The limit on the spatial derivative of the wavelength imposed by the measurements,

$$|\lambda_0'| = \left| \frac{d}{d\chi} \left(\frac{\bar{Z}}{Y} \right)^{1/2} \right|_{\chi=0} \ll 1 \qquad (\omega \ll \omega_{c_0}), \tag{24}$$

implies that near the basal end of the cochlea the longitudinal impedance $\bar{Z}(\chi,\omega)$ of the cochlea and the shunt admittance $Y(\chi,\omega)$ of the organ of Corti are constrained to be be roughly proportional at low frequencies:

$$Y(\chi,\omega) \approx \phi^2(\omega)\bar{Z}(\chi,\omega) \qquad (|\chi| \ll |\lambda_0/\lambda_0'| \text{ and } \omega \ll \omega_{c_0}), \tag{25}$$

where $\phi(\omega)$ is independent of χ. Conversely, if $\bar{Z}$ and Y are roughly proportional, the derivative of their ratio will be small. Based on its geometric interpretation in conventional cochlear models (see below), we call the proportionality between $\bar{Z}$ and Y the "tapering symmetry."

In deriving Eq. (25) we assume that the derivative $\lambda' = \lambda(d\ln\lambda/d\chi)$ is small because $\lambda(\chi,\omega)$ is essentially independent of χ (at small χ) and not because the wavelength itself is small. Support for that assumption comes from measurements of the magnitude the cochlear input impedance (Lynch et al. 1982). When combined with Eq. (13) for Z_0, those measurements indicate that at low frequencies the wavelength of the pressure wave within the basal turn of the cochlea is long; i.e., that λ_0 is not small.

Technically, the impedance measurements require only that the symmetry hold at the point of measurement (i.e., at $\chi = 0$). We assume that the approximate symmetry continues to hold at least within the basal turn of the cochlea. An estimate of the length scale over which the symmetry might be expected to hold can be obtained from the Taylor expansion of $\lambda(\chi,\omega)$ about $\chi = 0$:

$$\lambda(\chi,\omega) \approx \lambda_0 + \lambda_0'\chi + \cdots . \tag{26}$$

Thus,

$$\lambda(\chi,\omega) \approx \lambda_0 \qquad (|\chi| \ll |\lambda_0/\lambda_0'|). \tag{27}$$

Note that if the symmetry between $\bar{Z}$ and Y is broken, the derivative $\lambda'(\chi,\omega)$ can become large. As shown below, for example, transmission-line models in which such symmetry breaking occurs predict that $\lambda(\chi,\omega \ll \omega_{c_0})$ is independent of frequency in the basal turn. Since in those models the series impedance $\bar{Z}$, and hence the differential element $d\chi$, is proportional to ω, the derivative $d\lambda/d\chi$ can be expected to diverge like $1/\omega$ at low frequencies.

The symmetry between $\bar{Z}$ and Y implies a symmetry between P and U. When $|\lambda'|$ is small—and in the absence of reflections from elsewhere in the cochlea—Eq. (7) for U implies that the ratio of P to U is simply the wavelength, or characteristic impedance, $\lambda(\chi,\omega)$:

$$U \approx \frac{P}{\lambda} . \tag{28}$$

The approximate proportionality between $\bar{Z}$ and Y implies that λ is nearly constant near the stapes. Consequently,

$$U \approx \frac{P}{\lambda_0} \qquad (|\chi| \ll |\lambda_0/\lambda_0'| \text{ and } \omega \ll \omega_{c_0}), \tag{29}$$

so that P and U are roughly proportional in the basal turn. The symmetry between P and U follows immediately from the symmetry between $\bar{Z}$ and Y and the observation that the transmission-line equations (4) and (5) are invariant under the simultaneous substitutions $\bar{Z} \leftrightarrow Y$ and $P \leftrightarrow U$.

The symmetry between $\bar{Z}$ and Y relates two distinct aspects of cochlear mechanics. Whereas the impedance $\bar{Z}$ characterizes the geometry of the scalae and the longitudinal motion of the cochlear fluids, the shunt admittance Y describes the transverse response of an individual section of the organ of Corti to a pressure difference across the scala media. Remarkably, the symmetry imposed by the measurements implies that at low frequencies those functions are roughly proportional in the basal turn of the cochlea.

J. Spatial coordinates revisited

The symmetry between $\bar{Z}$ and Y selects the χ coordinate system—originally introduced as a mathematical convenience for solving the transmission-line equations—as the most natural for describing the variation of pressure and volume velocity in the basal

turn of the cochlea. Since $\bar{Z}$ and Y are approximately proportional, the wavelength λ measured in units defined by χ is nearly constant at frequencies $\omega \ll \omega_{c_0}$ near the stapes. Consequently, P can be written as a simple superposition of plane waves of the form

$$e^{\pm i\chi/\lambda_0} \qquad (|\chi| \ll |\lambda_0/\lambda_0'| \text{ and } \omega \ll \omega_{c_0}). \tag{30}$$

The same is not true, however, for the familiar wavelength λ_x measured in units of length x. The familiar wavelength and its derivative are related to λ and λ' through the equations

$$\lambda_x = \frac{dx}{d\chi}\lambda = i\lambda/\bar{Z}\ , \tag{31}$$

and

$$\frac{d\lambda_x}{dx} = \frac{d\chi}{dx}\frac{d\lambda_x}{d\chi} = \lambda' - \lambda\frac{d\ln\bar{Z}}{d\chi}\ . \tag{32}$$

Recall that $\lambda(\chi,\omega \ll \omega_{c_0})$ is approximately constant in the basal turn [see Eq. (22)]. Since both $\bar{Z}$ and $d\chi$ are, in standard models, proportional to ω, the familiar wavelength λ_x and its spatial derivative $d\lambda_x/dx$ thus diverge like $1/\omega$ at low frequencies.

K. Application to conventional cochlear models

Earlier it was shown that consistency with the measurements of Lynch et al. requires that the wavelength change slowly near the stapes and therefore that $\bar{Z}$ and Y be roughly proportional. At low frequencies in the basal turn, conventional cochlear models predict that the series impedance $\bar{Z}$ is determined by the acoustic inertia $\bar{M}(x)$ of the cochlear fluids and the shunt admittance Y is dominated by the compliance $C(x)$ of the organ of Corti and its basilar membrane. $\bar{Z}$ and Y thus have the limiting asymptotic forms[8]

$$\bar{Z} \underset{\beta\to 0}{\longrightarrow} i\omega\bar{M}(x) \qquad \text{and} \qquad Y \underset{\beta\to 0}{\longrightarrow} i\omega C(x)\ , \tag{33}$$

[8] At the lowest frequencies $\bar{Z}$ may acquire a real part arising from viscous effects. That contribution should be small in the basal turn if the ratio ϵ_v of the viscous boundary layer thickness to the radius of the scala vestibuli (or tympani) satisfies

$$\epsilon_v = \sqrt{\frac{\pi\eta}{\omega\rho S}} \ll 1\ . \tag{8.1}$$

Here, ρ and η are, respectively, the density and coefficient of viscosity of the cochlear fluids, and S is the cross-sectional area of the scala. The values $\rho \approx 1$ g/cm^3, $\eta \approx 0.02$ g/cm · s (von Békésy 1960), and $S \approx 0.01$ cm^2 (e.g., Wever 1949; Dallos 1970) indicate that the inequality is satisfied at frequencies

$$\omega/2\pi \gg 3 \text{ Hz}. \tag{8.2}$$

and therefore

$$\lambda \underset{\beta \to 0}{\longrightarrow} \left(\frac{\bar{M}}{C}\right)^{1/2} . \tag{34}$$

Here, the variable

$$\beta(x,\omega) \equiv \omega/\omega_c(x) , \tag{35}$$

where $\omega_c(x)$ is the mapping between characteristic frequency and position. Near the stapes the symmetry thus constrains the spatial variation of the effective compliance of the organ of Corti $C(x)$ to be that of the effective inertia of the cochlear fluids $\bar{M}(x)$:

$$C(x) \approx \phi^2 \bar{M}(x) , \tag{36}$$

where ϕ is a constant independent of position and frequency. (Note that $\bar{Z}$ and Y, shown to be proportional when considered as functions of χ, maintain their proportionality when considered as functions of x.)

Calculation of the derivative of the wavelength yields

$$\lambda_0'(\omega) = -\frac{\omega_\kappa}{\omega} \qquad (\omega \ll \omega_{c_0}), \tag{37}$$

where the frequency scale ω_κ is defined by

$$\omega_\kappa \equiv -\frac{1}{\bar{M}_0} \frac{d}{dx} \left(\frac{\bar{M}}{C}\right)^{1/2} \Bigg|_{x=0} . \tag{38}$$

Thus, when the symmetry between $\bar{M}$ and C is broken, $\lambda_0'(\omega)$ diverges like $1/\omega$ at low frequencies—the cochlear catastrophe.

L. Relation to scaling symmetry

The symmetry between $\bar{Z}$ and Y at low frequencies can be obtained as a limiting case of the scaling symmetry (Zweig 1976) suggested by Rhode's (1971) measurements of basilar-membrane transfer functions in the squirrel monkey and also found in the pigeon (Gummer et al. 1987). Applied to cochlear transfer functions, scaling symmetry implies (Zweig 1976) that the envelopes of the response of the basilar membrane to tones of nearby frequency are "shift-similar;" that is, one can be made to overlay the other simply by translating its envelope and adjusting its overall height. In the model of Zweig

(1987; 1991) the circuit elements $\bar{Z}(x,\omega)$ and $Y(x,\omega)$, and consequently the transfer functions, "scale;" that is, they are functions not of x and ω independently, but only of the single variable $\beta(x,\omega)$ defined by Eq. (35). At small β in that model,

$$\bar{Z}(x,\omega) = i\beta(x,\omega)\omega_{c_0}\bar{M}_0 \quad \text{and} \quad Y(x,\omega) \approx i\beta(x,\omega)\omega_{c_0}C_0 \,, \tag{39}$$

where $\bar{M}_0$ and C_0 are constants. Hence,

$$\bar{M}(x) = \frac{\omega_{c_0}}{\omega_c(x)}\bar{M}_0 \quad \text{and} \quad C(x) = \frac{\omega_{c_0}}{\omega_c(x)}C_0 \tag{40}$$

near the stapes, so that the model automatically reproduces the required proportionality between $\bar{M}$ and C.[9]

M. Implications for cochlear geometry

The symmetry between $\bar{M}$ and C does not hold in other cochlear models. For example, C is typically assumed to increase exponentially with position, corresponding to the approximately exponential variation in characteristic frequency at the basal end of the cochlea (e.g., von Békésy 1960; Greenwood 1961; Eldredge et al. 1981; Liberman 1982). The series inductance $\bar{M}$, however, is often assumed to be independent of position. An acoustic inertance, $\bar{M}$ is usually taken to have the form

$$\bar{M}(x) \propto \frac{\rho_0}{S(x)} \,, \tag{41}$$

where ρ_0 is the density of the cochlear fluids and $S(x)$ represents the effective cross-sectional area of the two scalae. Simple treatments (e.g., Zwislocki 1965; Dallos 1973) give

$$S = S_v \parallel S_t \equiv \frac{S_v S_t}{S_v + S_t} \,, \tag{42}$$

---

[9] The predictions of scaling symmetry are consistent with Greenwood's (1961) demonstration that von Békésy's post-mortem measurements of the static volume elasticity $E(x)$ of the organ of Corti obey the approximate scaling relation

$$E(x) \approx \frac{\omega_{c_0}}{\omega_c(x)}E_0 \tag{9.1}$$

in a variety of animals, from mice to elephants.

where S_v and S_t are, respectively, the cross-sectional areas of the scala vestibuli and the scala tympani.[10] Thus, $\bar{M}$ is constant when the scalae are approximated as boxes of constant cross-section (de Boer 1980; Viergever 1980). In such models the spatial variation of $\bar{M}$ and C are therefore quite different, breaking the tapering symmetry required by measurements of the cochlear input impedance.

The symmetry deduced from measurements of the input impedance finds support in a consilience with measurements of cochlear anatomy, which indicate that whereas the width, and hence the compliance (von Békésy 1960), of the basilar membrane increases toward the helicotrema, the cross-sectional areas of the scalae decrease, especially at the basal end of the cochlea where the variation is roughly exponential (Wever 1949; Fernández 1952; Zwislocki 1965). Those opposing tapers tend to make $\bar{M}$ and C proportional, thereby preserving the symmetry between $\bar{Z}$ and Y.

N. Corroboration from cadavers[11]

Unfortunately, existing anatomical measurements do not permit a definitive quantitative examination of the proportionality between $\bar{M}$ and C. For example, the relationship between measured properties of the cochlea—the point stiffness of the basilar membrane (Gummer et al. 1981; Olson 1990), for example—and the effective impedances appearing in the model equations is not well understood. Even if one were to adopt the correspondences suggested by simple models—such as Eq. (42) for S appearing in Eq. (41) for $\bar{M}$—appropriate measurements have yet to be made in a single animal. Comparing measurements across preparations is complicated both by uncertainties in the location of the measurement coordinate system and by differences in the overall size of the cochlea (Bohne and Carr 1979).

Despite such uncertainties, a qualitative comparison of measurements on human cadavers is suggestive. Figure 3 compares the spatial variation of the effective cross-sectional area S, computed from Eq. (42) using the measurements of Wever (1949), with that of

[10] Although a typical mammalian cochlea consists of a coiled tube containing three chambers (the scala vestibuli, the scala media, and the scala tympani), simple models of cochlear mechanics approximate the structure by two chambers (the scala vestibuli and scala tympani) separated by the organ of Corti with its basilar membrane. In that simplified view, the quantity S_v appearing in Eq. (42) does not represent the true area of the scala vestibuli but should include some fraction of the area S_m of the scala media. Since $S_m \ll S_v$ at the basal end of the cochlea, however, that correction is small.

[11] Symmetry under a cemetery wall.

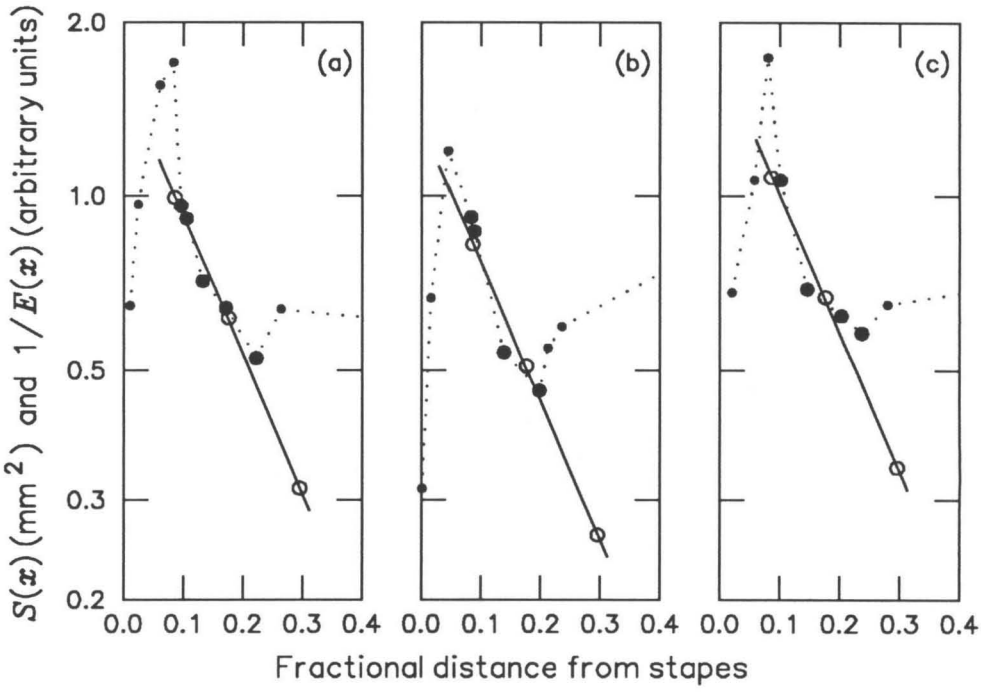

Figure 3. Comparison of the spatial variation of the effective cross-sectional area S (•) computed from measurements of the scala vestibuli and scala tympani in three cadavers by Wever (1949) with that of the reciprocal of the static volume elasticity E (○) of the basal region of the organ of Corti (from Fig. 11-73 of von Békésy 1960). Panels (a), (b), and (c) correspond to measurements from Figs. 73, 74, and 75 of Wever (1949), respectively. The effective cross-sectional area S was computed from Wever's measurements using Eq. (42). The points are connected by straight dotted lines (·····) to aid the eye. The solid line (———) represents the best exponential fit to the measurements of $1/E$. The absolute scale for the stiffness measurements is varied between panels so that the region (containing large symbols) in which the two functions have similar slopes, can be more easily discerned. Although the precise location of the beginning of the organ of Corti is not known—and end effects may complicate the interpretation of the area measurements near the oval window—for the first 15% of the length of the organ of Corti, S and $1/E$ both vary exponentially and are roughly proportional.

the reciprocal of the static volume elasticity E of the organ of Corti measured by von Békésy (1960). Since von Békésy's elasticity measurements were made in cadavers, they do not include contributions from physiologically active mechanical elements. Since the symmetry between $\bar{Z}$ and Y evolved in living ears, there is little reason to expect it to hold after death. The figure indicates, however, that S and $1/E$, and hence—by adopting the naive correspondences $\bar{M} \propto 1/S$ and $C \propto E$—$\bar{M}$ and C, are indeed proportional near the base of the cochlea. Although the location of the beginning of the organ of Corti is not precisely known and end effects complicate the interpretation near the stapes, the proportionality appears to hold for roughly the first 15% of the distance along the organ of Corti.[12]

O. Consequences for the sensitivity of hearing

The slow variation of the wavelength has important consequences for the detection of sound. The efficiency of the middle-ear is defined as the fraction of the time-averaged power entering the middle ear that is absorbed by the cochlea (Rosowski et al. 1986):

$$\eta_{\mathrm{me}}(\omega) \equiv \frac{\text{Power into cochlea}}{\text{Power into middle ear}} = \frac{\mathrm{Re}\{P_0\, U_0^*\}}{\mathrm{Re}\{P_{\mathrm{e}}\, U_{\mathrm{e}}^*\}} = \left|Z_{\mathrm{e}} T_{\mathrm{me}}\right|^2 \frac{\mathrm{Re}Z_0}{\mathrm{Re}Z_{\mathrm{e}}} \,. \tag{43}$$

Here, $P_{\mathrm{e}}(\omega)$ and $U_{\mathrm{e}}(\omega)$ are the pressure and volume velocity measured in the ear canal at the eardrum. The middle-ear input impedance $Z_{\mathrm{e}}(\omega)$ and transfer function $T_{\mathrm{me}}(\omega)$ are defined more precisely in the Appendix.

Although cochlear contributions to middle-ear efficiency are complicated, a qualitative understanding of the effect of tapering symmetry on energy transfer to the cochlea at low frequencies can be obtained by examining the factor $\mathrm{Re}Z_0$. Since λ_0 and λ_0' are both approximately real at low frequencies,

$$\mathrm{Re}Z_0 \approx \mathrm{Re}\left\{\frac{\lambda_0}{1 + i\lambda_0'/2}\right\} \approx \frac{\lambda_0}{1 + (\lambda_0'/2)^2} \qquad (\omega \ll \omega_{\mathrm{c_0}}) \,. \tag{44}$$

[12] Similar results are obtained in guinea pigs by combining the anatomical measurements of Fernández (1952) with the basilar membrane stiffness measurements of Gummer et al. (1981). The analysis, however, is not definitive, both because Gummer et al.'s estimate of the slope of the stiffness variation is uncertain (their measurements are confined to only a small patch of the basilar membrane) and because the relationship between the point stiffness they measure and the effective volume compliance C appearing in the equations is not well understood.

Because $\lambda_0'(\omega)$ is small at auditory frequencies, $\mathrm{Re}Z_0$, and consequently middle-ear efficiency, stays roughly constant. Conversely, for $\eta_{\mathrm{me}}(\omega)$ to remain roughly constant at low frequencies—given the measured transfer characteristics of the cat middle ear, the approximate value of $\mathrm{Re}Z_0$, and the theoretical result that λ_0 varies only slowly with frequency—requires that λ_0' be small.

Note, however, that were $\lambda_0'(\omega)$ to diverge as $\omega \to 0$, as it does in models exhibiting the cochlear catastrophe, $\mathrm{Re}Z_0$ would approach zero. In that limit (i.e., the limit $\mathrm{Re}Z_0 \to 0$), η_{me} becomes proportional to $\mathrm{Re}Z_0$ (see the Appendix), and the transfer of energy into the cochlea becomes vanishingly small. Thus, in a world differing from ours only in that the wavelength changes rapidly in the basal turn of the cochlea, the sensitivity of hearing would be considerably reduced at low frequencies.

II. The Catastrophe

The remainder of this paper illustrates the comments made above by explicit computations for two categories of models, distinguished by the extent to which they exhibit the cochlear catastrophe. Note that the issues addressed—the cochlear input impedance and middle-ear efficiency—depend only on the form of the model at low frequencies near the stapes. The reflection of retrograde waves discussed in the companion paper (Shera and Zweig 1991b) depends on more global characteristics of the model cochleas. The following sections also serve to justify by example the statements [i.e., Eqs. (16) and (17)] that λ_0 and λ_0' are approximately real, which were used to derive the limit on the rate of change of the wavelength [i.e., Eq. (21)].

A. Conventional transmission-line models

In many transmission-line models, including those used to investigate reflection of waves in the cochlea (de Boer and Viergever 1984; Viergever 1986; de Boer et al. 1986ab and Kaernbach et al. 1987), the series impedance $\bar{Z}(x,\omega)$ and shunt admittance $Y(x,\omega)$ per unit length have the form

$$\bar{Z}(x,\omega) = i\omega\bar{M}(x) \quad \text{and} \quad Y(x,\omega) = \left\{ i\omega M(x) + R(x) + \frac{1}{i\omega C(x)} \right\}^{-1}, \qquad (45)$$

where $\bar{M}$, M, R, and C are real-valued functions of x. The wavelength thus becomes

$$\lambda(x,\omega) = \left(\frac{\bar{M}}{C}\right)^{1/2} \sqrt{1 - \beta^2 + i\delta\beta}\,, \tag{46}$$

where $\beta(x,\omega) \equiv \omega/\omega_c(x)$ in accord with Eq. (35), $\omega_c(x) \equiv 1/\sqrt{MC}$ is the characteristic angular frequency, and $\delta(x) \equiv \omega_c RC$ is the dimensionless damping parameter. For future reference, note that

$$\lambda_0(\omega \ll \omega_{c_0}) \approx \lambda(0,0) = \left(\frac{\bar{M}_0}{C_0}\right)^{1/2} \equiv \lambda_{00}\,; \tag{47}$$

that is, $\lambda_0(\omega \ll \omega_{c_0})$ is essentially real, in agreement with Eq. (16).

At the basal end of the cochlea, the derivative $\lambda'(\chi,\omega)$ has the value

$$\lambda_0'(\omega \ll \omega_{c_0}) \approx \frac{1}{4N_0}\left(\frac{\omega_{c_0}}{\omega}\frac{d\gamma}{d\zeta} + i\frac{\delta_0}{2}\frac{d\ln(\delta/\omega_c)}{d\zeta}\right)\Bigg|_{\zeta=0}\,. \tag{48}$$

The dimensionless spatial variable

$$\zeta \equiv x/l \tag{49}$$

used here (see note 5) is defined in terms of the length scale l over which the characteristic frequency changes by a factor of e in the basal turn (Liberman 1982):

$$\omega_c(\zeta) = \omega_{c_0} e^{-\zeta}\,. \tag{50}$$

The dimensionless parameter N_0 is defined by

$$N_0 \equiv \frac{l}{4}\left(\frac{\bar{M}_0}{M_0}\right)^{1/2}\,, \tag{51}$$

and the real dimensionless function $\gamma(\zeta)$ by

$$\gamma(\zeta) \equiv \lambda_{00}^{-1}\left(\frac{\bar{M}}{C}\right)^{1/2}\,. \tag{52}$$

Note that $\gamma(0) = 1$.

B. The reality and divergence of $\lambda_0'(\omega)$

Equation (48) for the derivative can now be used to find the conditions under which $\lambda_0'(\omega)$ becomes large, giving $Z_0(\omega)$ a nonzero phase. Comparison of transmission-line models with measured basilar membrane transfer functions (e.g., Zweig et al. 1976; de Boer 1980) suggests that the damping parameter δ_0 is small whereas N_0 is relatively large. The values

$$\delta_0 \sim \frac{1}{20} \quad \text{and} \quad N_0 \sim 5 \tag{53}$$

are typical. If $\delta(\zeta)$ is roughly constant (as it is in the models discussed here), then

$$\frac{d\ln(\delta/\omega_c)}{d\zeta} \sim 1 \,. \tag{54}$$

Hence,

$$\left|\mathrm{Im}\,\lambda_0'\right| \ll 1 \,, \tag{55}$$

in agreement with Eq. (17).

The derivative of the wavelength then becomes, in agreement with Eq. (37),

$$\lambda_0'(\omega) \approx -\frac{\omega_\kappa}{\omega} \qquad (\omega \ll \omega_{c_0}), \tag{56}$$

where the frequency scale,

$$\omega_\kappa = -\omega_{c_0}\left(\frac{1}{4N_0}\frac{d\gamma}{d\zeta}\right)\bigg|_{\zeta=0} = -\frac{1}{\bar{M}_0}\,\frac{d}{dx}\left(\frac{\bar{M}}{C}\right)^{1/2}\bigg|_{x=0} \,, \tag{57}$$

indicates the frequency at which $\left|\lambda_0'\right| = 1$ and therefore provides a measure of the severity of the cochlear catastrophe. Typically the dimensionless quantity $-d\gamma/d\zeta$ is of order one, so that

$$\omega_\kappa \sim \frac{1}{20}\omega_{c_0} \,. \tag{58}$$

However, if the circuit elements $\bar{Z}$ and Y scale, as they do in the model of Zweig (1987; 1991), then $d\gamma/d\zeta$ vanishes and

$$\omega_\kappa = 0 \,. \tag{59}$$

C. Predictions for $Z_0(\omega)$

Reference to Eq. (13) for the input impedance thus yields[13]

$$Z_0(\omega) \approx \frac{\lambda_{00}}{1 - i\omega_\kappa/2\omega} \qquad (\omega \ll \omega_{c_0}). \tag{60}$$

Unless ω_κ is small enough to suppress the divergence and guarantee that $|\lambda_0'(\omega)| \ll 1$ in the frequency range of hearing, the model input impedance will contain a substantial imaginary part at low frequencies ($\omega \ll \omega_\kappa$) and, in particular, the phase of $Z_0(\omega)$ will approach 90°.[14]

Theoretical predictions for the cochlear input impedance computed from Eq. (1) are shown in Figs. 4, 5, and 6 for the models of Viergever (1986) and de Boer et al. (1986ab and Kaernbach et al. 1987). The parameter values used by de Boer et al. were selected, on the basis of measurements in other animals, to approximate a human cochlea (de Boer 1980). To compare the model with measurements on cats, the parameter values must be rescaled. Shown are predictions using both the original parameter values and those rescaled by changing the frequency-position map (Liberman 1982).[15] The parameter

---

[13] Equation (60) for the model input impedance implies that $Z_0(\omega)$ can, at low frequencies, be represented by an equivalent circuit consisting of an inductor and a resistor in parallel (cf. Allen 1979). More explicitly,

$$Z_0 \approx (i\omega L_0) \parallel R_0 \equiv \frac{i\omega L_0 R_0}{R_0 + i\omega L_0} \qquad (\omega \ll \omega_{c_0}), \tag{13.1}$$

where

$$R_0 \equiv \lambda_{00} \quad \text{and} \quad L_0 \equiv 2\frac{\lambda_{00}}{\omega_\kappa}\,. \tag{13.2}$$

Note that Lynch et al. (1982) represented their averaged measurements with a phenomenological network model, which reduces, at frequencies greater than approximately 100 Hz, to a resistance R_C in parallel with an inductance M_0 (their notation). Like Dallos (1970), Lynch et al. (1982) speculate that the inductive term arises from effects at the apical end of the cochlea. As shown here and in Allen (1979) and Puria and Allen (1991), inductive effects can arise from the spatial variation of the wavelength near the stapes.

[14] The Appendix of the companion paper (Shera and Zweig 1991b) shows that Eq. (60) for $Z_0(\omega)$ captures the leading-order behavior of the cochlear input impedance, even in models that exhibit the cochlear catastrophe.

[15] Measurements on the cat (Liberman 1982) imply that

$$\omega_c(x)/\omega_{c_0} \approx (1+\epsilon)\, e^{-x/l} - \epsilon\,, \tag{15.1}$$

where $\omega_{c_0}/2\pi \approx 57$ kHz, $\epsilon \approx 1/156$, and $l \approx 5$ mm. For the purposes of rescaling the model of de Boer et al. (1986ab and Kaernbach et al. 1987), the small parameter ϵ was set to zero so that the frequency-position map remained purely exponential. When necessary, values $x > x_h$, where x_h is the ostensible position of the helicotrema, were permitted to keep the minimum frequency below 100 Hz and so prevent spurious reflections from the apex of the cochlea (cf. Puria and Allen 1991). Taking $\epsilon = 0$ then has a negligible effect on the model predictions discussed in this paper.

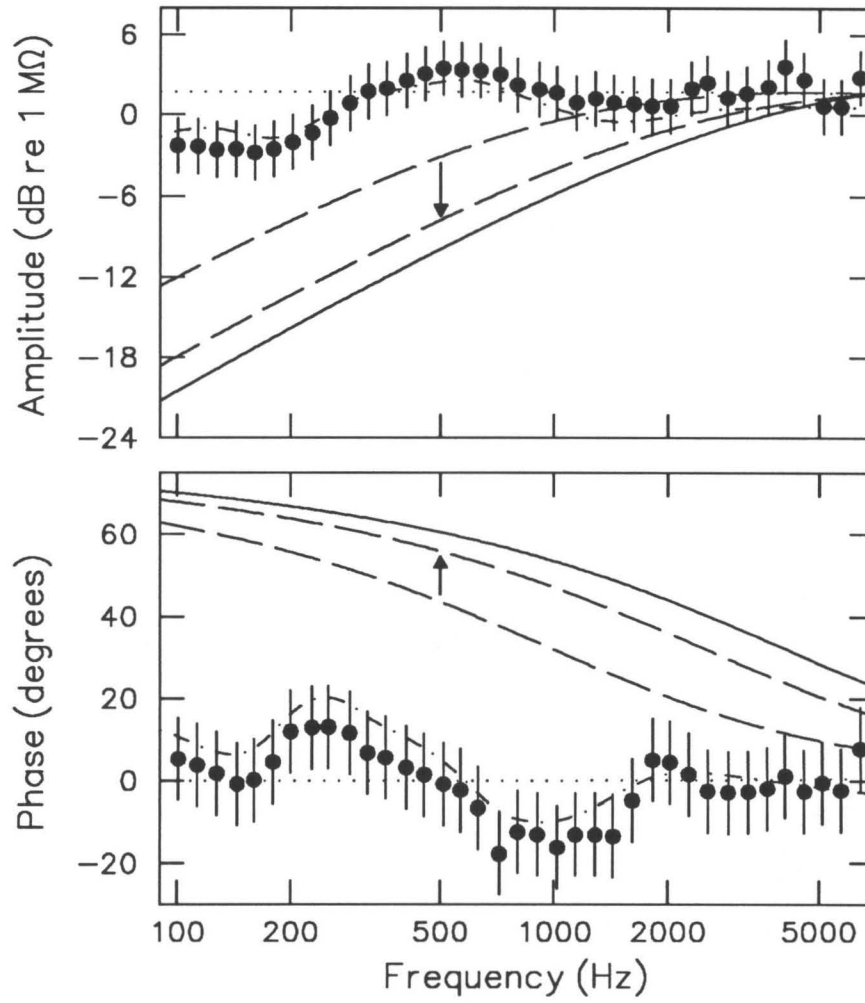

Figure 4. Amplitude and phase of $Z_0(\omega)$ computed numerically for several models of cochlear mechanics compared with the averaged measurements (•) of Lynch et al. (1982) shown in Fig. 1: (———) the model of Viergever (1986); (— —) the model of de Boer et al. (1986ab and Kaernbach et al. 1987) with original parameter values and with those obtained by rescaling (⟶) the frequency-position map to correspond with that of the cat[14] [$\omega_{c_0}/2\pi \rightarrow 57$ kHz and $l \rightarrow 5$ mm from Liberman (1982); N and δ were kept constant at their original values]; (· · · ·) the model of Zweig (1987; 1991), derived for low SPL at frequencies greater than approximately 3 kHz but here extrapolated to low frequencies and high stimulus levels (parameter values are those of Zweig except that the feedback strength $\rho = 0$ and the damping constant $\delta > 0$; i.e., only the passive component of the admittance Y of the scala media has been included). The minimum-phase fit from Fig. 1 (· — · —) is shown for comparison. The amplitudes of the model impedances are normalized at 7 kHz to the value given by the phenomenological network model of Lynch et al. (1982). The errors on the measurements are estimates based on a comparison with the minimum-phase fits. Note that the averaging performed by Lynch et al. has decreased the random errors but revealed systematic errors of the same order as the random errors in cats 18 and 25. Unless measurement errors are substantially greater than the lower bounds shown here, most models of cochlear mechanics—of which those of Viergever and de Boer et al. are but examples—are in disagreement with the measurements.

values used by Viergever apparently represent a "generic" cochlea; the frequency-position map, however, is sufficiently similar to the cat's that no rescaling is necessary.

Unless the measurement errors are substantially greater than the lower bounds estimated from the minimum-phase fits, the model predictions disagree significantly with the empirical values. Although they were not developed to address low-frequency reflection phenomena, many other models of cochlear mechanics, as noted by Wickesberg and Geisler (1986), also exhibit such behavior (e.g., Zweig et al. 1976; Allen 1979; Sondhi 1978; Neely 1981; Wickesberg and Geisler 1986). Shown for comparison is $Z_0(\omega)$ for the model of Zweig (1987; 1991). Introduced in another context, that model was shown to be valid at high frequencies ($\omega/2\pi \gtrsim 3$ kHz) and low sound-pressure levels but has here been extrapolated to lower frequencies and higher intensities. Nevertheless, because it manifests scaling symmetry that model agrees better with the measured impedance functions.

Any disagreement with the empirical values occurs at frequencies $\omega \lesssim \omega_\kappa$ for which the imaginary part of $Z_0(\omega)$ becomes substantial. The approximate value of ω_κ for each model can be determined from the phase of $Z_0(\omega)$ by using the relation

$$\omega_\kappa \approx 2\omega \tan \angle Z_0 \; . \tag{61}$$

Table I gives values of ω_κ for the models of cochlear mechanics shown in the figures. Also given in the table are the derivatives,

$$\left|\lambda_0'(1/40\,\omega_{c_0})\right| \approx 40 \left|\frac{\omega_\kappa}{\omega_{c_0}}\right| , \tag{62}$$

evaluated at a fixed value of $\omega/\omega_{c_0} = 1/40$ chosen to represent a typical low frequency in the model. For the cat the frequency $1/40(\omega_{c_0}/2\pi) \approx 1.5$ kHz (Liberman 1982). Except for the model of Zweig (1987; 1991), which has $\omega_\kappa = 0$ and therefore completely avoids the cochlear catastrophe, all have $\omega_\kappa/2\pi \gg 100$ Hz and $\left|\lambda_0'(1/40\,\omega_{c_0})\right| > 1$.

The measurements of Lynch et al. can be used to estimate the values of ω_κ and λ_0' that would bring such models into agreement with their data. Those estimates, computed from parameters of their phenomenological network model (which represent a best fit to their averaged measurements), are given for comparison; as expected, $\omega_\kappa/2\pi \sim 100$ Hz. The estimate is, of course, only approximate; other factors not related to symmetry breaking in the basal turn (and not accounted for in standard models), such as the presence of reflections from more apical regions of the cochlea (cf. Puria and Allen 1991), may affect the apparent value of ω_κ.

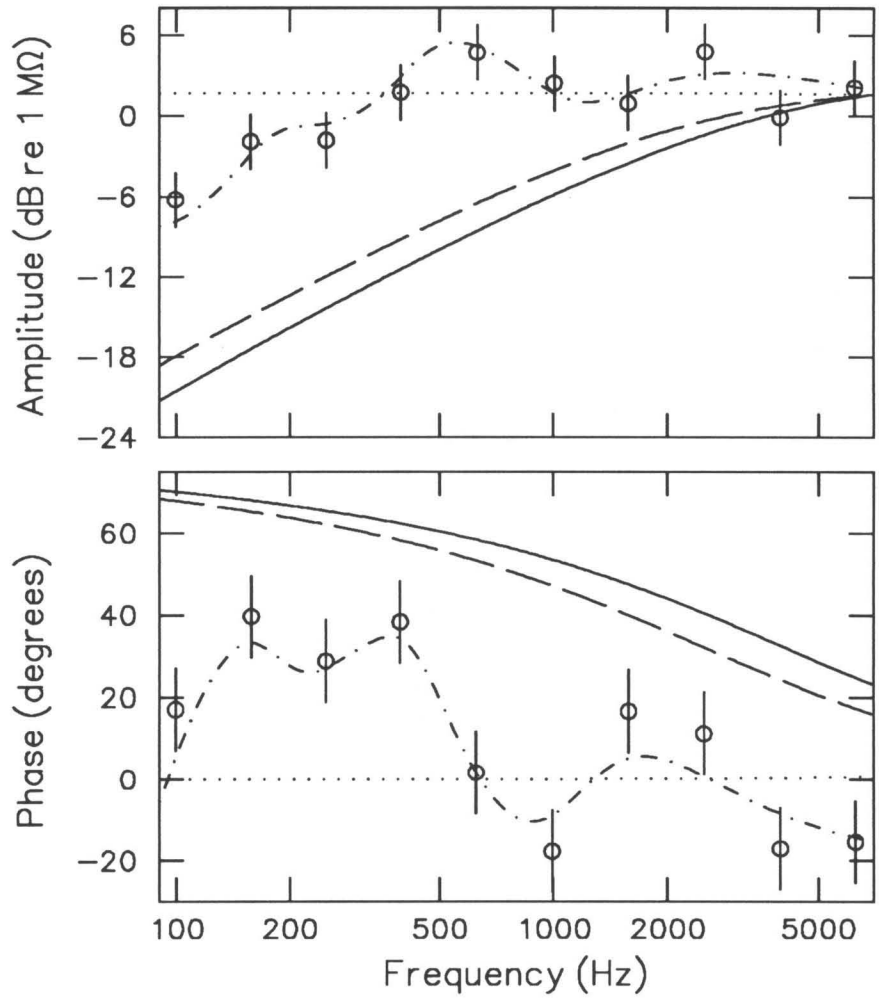

Figure 5. Amplitude and phase of $Z_0(\omega)$ for the models of cochlear mechanics shown in Fig. 4 compared with the measured values (o) and the minimum-phase fit (· — · —) for cat 25 shown in Fig. 1. The errors on the measurements, which appear to be randomly distributed, are estimates based on a comparison with the minimum-phase fits. Again, the amplitudes of the model impedances are normalized at 7 kHz to the value given by the phenomenological network model.

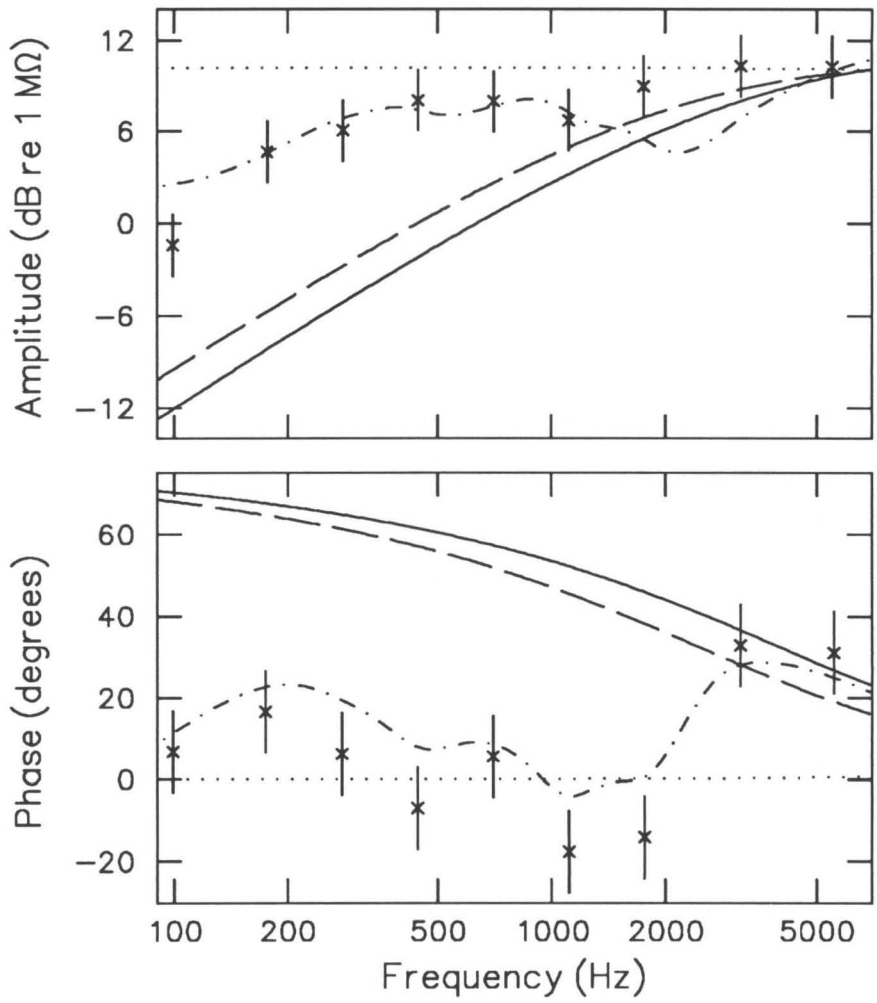

Figure 6. Amplitude and phase of $Z_0(\omega)$ for the models of cochlear mechanics shown in Fig. 4 compared with the measured values ($\times$) and the minimum-phase fit ($\cdot\!-\!\cdot\!-$) for cat 18 shown in Fig. 1. The errors are as described in Fig. 5, and the amplitudes of the model impedances are normalized to agree with the data at approximately 7 kHz.

Cochlear Models	$\omega_\kappa/2\pi$	$\lvert\lambda_0'(1/40\,\omega_{c_0})\rvert$
de Boer (1980) ..... de Boer et al. (1986a) de Boer et al. (1986b) Kaernbach et al. (1987)	1688	3.0
de Boer (1980, rescaled to the cat)	4275	3.0
Viergever (1986)	6917	5.5
Zweig (1987; 1991)	0	0.0
Empirical Values		
Estimated from Lynch et al. (1982)	170	0.12

Table I. Values of ω_κ and λ_0' characterizing the cochlear catastrophe. The first column contains values of $\omega_\kappa/2\pi$ (in Hz) such that $|\lambda_0'(\omega_\kappa)| = 1$. For each model, $\omega_\kappa/2\pi$ corresponds to the frequency at which the phase of the model input impedance passes through approximately $\tan^{-1}(1/2) \approx 25°$ and indicates the approximate frequency below which the model input impedance differs significantly from the empirical value. Since $Z_0(\omega)$ is essentially real above 100 Hz (cf. Fig. 1), any model with $\omega_\kappa/2\pi \gtrsim 100$ Hz is in disagreement with the measurements. Note that to explore cochlear reflection phenomena at low frequencies, de Boer et al. (1986ab and Kaernbach et al. 1987) use the model developed in another context by de Boer (1980). The empirical value based on the measurements of Lynch et al. (1982) was estimated from the parameters of their phenomenological network model by using the formula [in their notation; cf. Eq. (13.2)]:

$$\omega_\kappa \approx 2\frac{R_C}{M_0} .$$

Since other mechanisms not related to symmetry breaking may give rise to an apparent inductive behavior at low frequencies, the empirical estimate is only approximate. The second column contains values of the magnitude of the spatial derivative of the wavelength at a typical low frequency in each model:

$$\left|\lambda_0'(1/40\,\omega_{c_0})\right| \approx 40\left|\frac{\omega_\kappa}{\omega_{c_0}}\right| .$$

Note that for the cat $\omega_{c_0}/2\pi \approx 57$ kHz (Liberman 1982), and so $1/40(\omega_{c_0}/2\pi) \approx 1.5$ kHz. Nonzero model values of $|\lambda_0'|$ result from a symmetry-breaking that occurs between the series impedance $\bar{Z}$ and the shunt admittance Y [cf. Eq. (24)].

D. Middle-ear efficiency

This section illustrates the effects of the cochlear catastrophe on the efficiency $\eta_{\rm me}(\omega)$ of the middle ear. By using measurements on the cat, it can be shown (see the Appendix) that $\eta_{\rm me}(\omega)$ has the approximate form

$$\eta_{\rm me} \approx \frac{\alpha {\rm Re} Z_0}{{\rm Re} Z_0 + R_{\rm C}/3} \qquad (\omega/2\pi \lesssim 700 \text{ Hz}) \,. \tag{63}$$

Here, $R_{\rm C}$ is the cochlear resistance measured by Lynch et al. (1982) and α is a dimensionless constant of order one determined by middle-ear mechanics. Equation (60) for the model input impedance implies that

$${\rm Re} Z_0 \approx \frac{\lambda_{00}}{1 + (\omega_\kappa/2\omega)^2} \,. \tag{64}$$

Therefore, ${\rm Re} Z_0$, and consequently $\eta_{\rm me}(\omega)$, becomes small at frequencies below $\frac{1}{2}\omega_\kappa$.

Figure 7 plots $\eta_{\rm me}(\omega)$, computed from Eq. (63), based on the models of Viergever (1986) and de Boer et al. (1986ab and Kaernbach et al. 1987, rescaled to the cat). Shown for comparison are results based on the model of Zweig (1987; 1991), the averaged measurements of Lynch et al. (1982), and the minimum-phase fit to those measurements from Fig. 1. Although the absolute efficiencies are not reliable because the constant α was determined by combining measurements from a gallimaufry of cats, the indicated frequency dependence is approximately correct. In addition, it is reassuring to note that the constraint $0 \le \eta_{\rm me} \le 1$ applicable to a passive system is everywhere satisfied. Inclusion of the empirical finding that $|\lambda_0'| \ll 1$ causes $\eta_{\rm me}(\omega)$ to remain roughly constant throughout the frequency range of the figure. As expected, however, the symmetry-breaking exhibited by the models of Viergever (1986) and de Boer et al. (1986ab and Kaernbach et al. 1987) significantly decreases middle-ear efficiency at low frequencies.

III. Summary

Recent theoretical arguments for significant asymmetry in the reflection of cochlear waves (de Boer and Viergever 1984; de Boer et al. 1986ab; Viergever 1986; Kaernbach et al. 1987) are based on models that, unless measurement errors are substantially greater than the lower bounds estimated from minimum-phase fits to the data, disagree with measurements of the cochlear input impedance (Lynch et al. 1982). This paper demonstrates

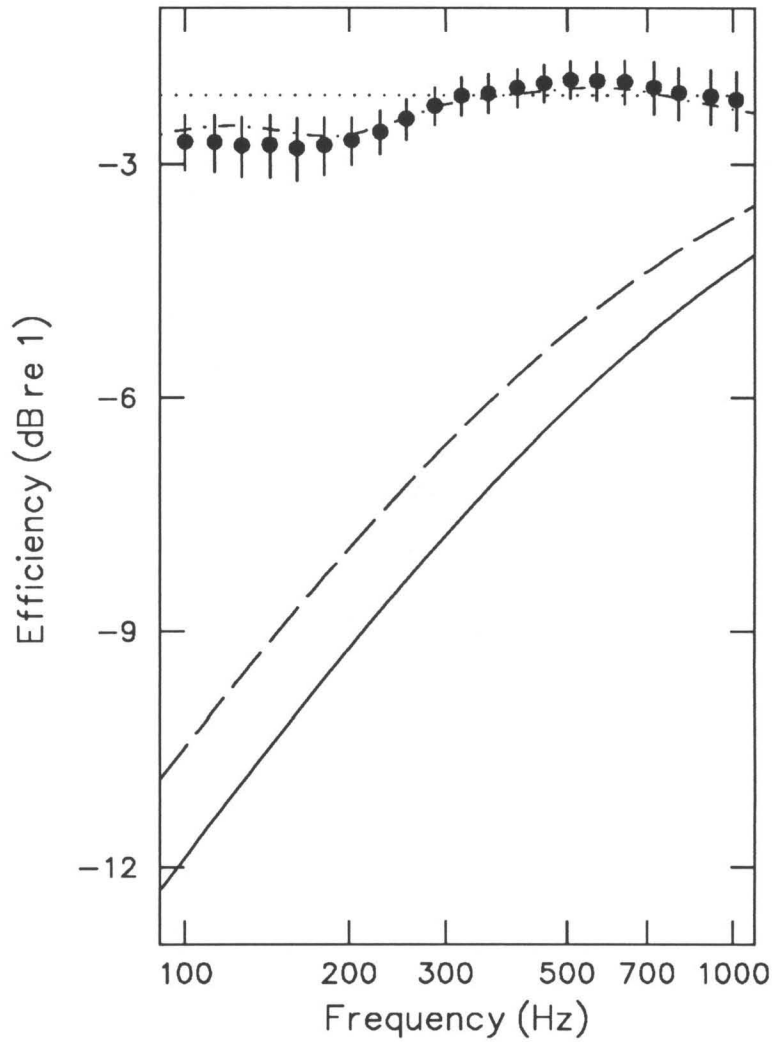

Figure 7. Middle-ear efficiency $\eta_{\rm me}(\omega)$ in dB (i.e., $10\log_{10}\eta_{\rm me}$) computed from Eq. (63) for three models of cochlear mechanics: (———) the model of Viergever (1986); (— —) the model of de Boer et al. (1986ab and Kaernbach et al. 1987), rescaled to the cat as in Fig. 4; (·····) the model of Zweig (1987; 1991) extrapolated to low frequencies and high SPL as in Fig. 4. Values computed by using the averaged measurements (•) of Lynch et al. (1982), with error estimates from Fig. 4, and the corresponding minimum-phase fit from Fig. 1 (· — · —) are shown for comparison. The constant α appearing in Eq. (63) was taken to have the value $\alpha = 0.8$ (see the Appendix), and the model impedances were normalized as in Fig. 4. The catastrophe exhibited by the models of Viergever and de Boer et al. decreases middle-ear efficiency considerably.

that those measurements require that the wavelength change slowly in the basal turn of the cochlea and hence that waves traveling in either direction undergo little reflection.[16]

More generally, linear, one-dimensional transmission-line models are expected to describe the mechanics of the basal turn of the cochlea at low frequencies and high sound-pressure levels. The cochlear input impedance therefore has the approximate form

$$Z_0(\omega) \approx \frac{\lambda_0}{1 + i\lambda_0'/2} \qquad (\omega \ll \omega_{c_0}). \tag{65}$$

In that regime transmission-line models predict that both the wavelength $\lambda(\chi,\omega)$ and its spatial derivative $\lambda'(\chi,\omega)$ are approximately real. Since Lynch et al.'s (1982) measurements of the cochlear input impedance indicate that the phase of $Z_0(\omega)$ is small above 100 Hz, those transmission-line models must also satisfy

$$|\lambda'(\chi,\omega)| \ll 1 \qquad (|\chi| \ll |\lambda_0/\lambda_0'| \text{ and } \omega \ll \omega_{c_0}); \tag{66}$$

i.e., the wavelength changes slowly at the basal end of the cochlea. That result has the following consequences, the logical interrelations of which are diagramed in Fig. 8.

- The series impedance $\bar{Z}(\chi,\omega)$ and shunt admittance $Y(\chi,\omega)$ are roughly proportional at low frequencies near the stapes:

$$Y(\chi,\omega) \approx \phi^2(\omega)\bar{Z}(\chi,\omega)\,. \tag{67}$$

  For the broad class of cochlear models defined by Eqs. (33), that symmetry between $\bar{Z}$ and Y reduces to a proportionality between the longitudinal inductance $\bar{M}$ representing the inertia of the cochlear fluids and the shunt capacitance C representing the effective compliance of the organ of Corti and its basilar membrane. The width of the basilar membrane and the cross-sectional areas of the scalae taper in opposite directions, providing independent support for that proportionality.

- The WKB approximation can be used when solving the cochlear transmission-line equations, at least in the basal turn of the cochlea. Little internal reflection of waves

[16] The companion paper (Shera and Zweig 1991b)—which explores whether violation of tapering symmetry leads to wave reflection in the cochlea—demonstrates that the empirical conclusion that cochlear reflection must be small in the basal turn applies to a broad class of cochlear models whether or not they accurately represent the symmetries of the inner ear.

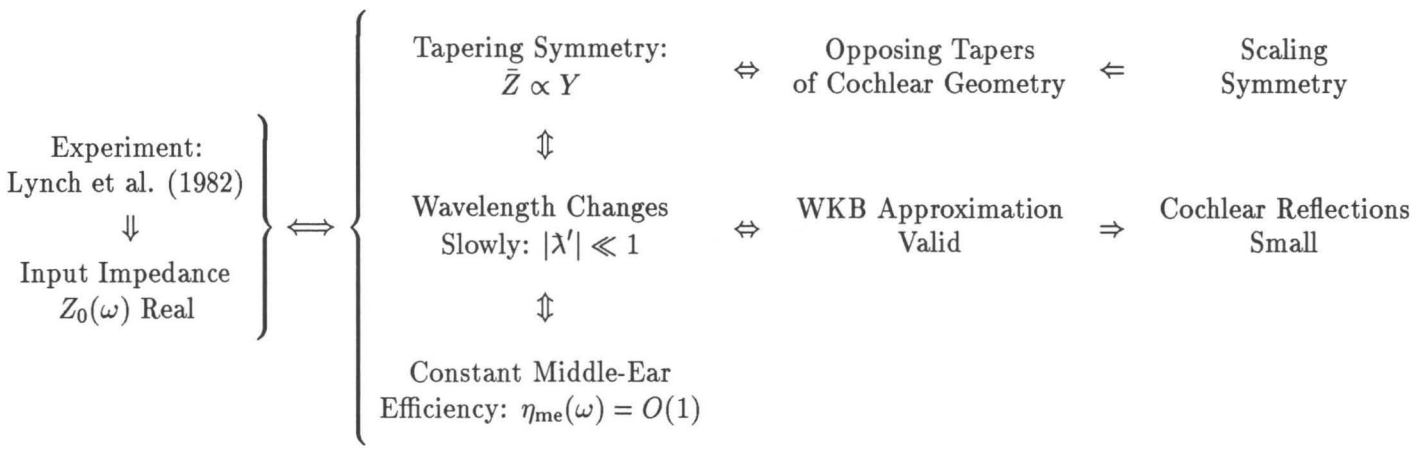

Figure 8. Summary diagram of the logical interrelations between the major findings of the paper. The notation $p \Rightarrow q$ means "p implies q." Assumptions underlying and regions of validity associated with the inferences are discussed in the text.

traveling in either direction along the organ of Corti can therefore be expected. The absence of waves traveling in two directions presumably simplifies the analysis of sound.

- The efficiency of the middle ear at transferring acoustic power into the cochlea remains roughly constant below 700 Hz. The rate of change of the wavelength near the stapes is thus an important determinant of the sensitivity of the ear at low frequencies.

Acknowledgments

This work was supported by DARPA and AFOSR contract N00014-86-C0399.

Appendix A: Estimating Middle-Ear Efficiency

The efficiency $\eta_{\rm me}(\omega)$ of the middle ear at transferring acoustic power to the cochlea depends both on the characteristics of the middle ear and on the cochlear input impedance $Z_0(\omega)$. By combining measurements on the cat to estimate and separate out the contribution made by the middle ear, this appendix derives an expression for middle-ear efficiency as an explicit function of $\mathrm{Re}Z_0$. The appendix thus finds an expression $\eta_{\rm me}(\omega;\mathrm{Re}Z_0)$ that enables one to estimate—by imagining different cochlear models connected to a fixed, empirically-characterized middle ear—the middle-ear efficiency associated with each model.

As in Rosowski et al. (1986), the middle-ear efficiency $\eta_{\rm me}(\omega)$ is defined to be the fraction of the time-averaged power entering the middle ear that is absorbed by the cochlea:

$$\eta_{\rm me} \equiv \frac{\mathrm{Re}\{P_0\,U_0^*\}}{\mathrm{Re}\{P_{\rm e}\,U_{\rm e}^*\}} = \left|Z_{\rm e}T_{\rm me}\right|^2 \frac{\mathrm{Re}Z_0}{\mathrm{Re}Z_{\rm e}}\,. \tag{A1}$$

Here, $P_{\rm e}$ and $U_{\rm e}$ are the pressure and volume velocity measured in the ear canal at the eardrum, and

$$Z_{\rm e}(\omega) \equiv \left.\frac{P_{\rm e}}{U_{\rm e}}\right|_{\text{middle ear driven forward}} \tag{A2}$$

is the middle-ear input impedance. The transfer function $T_{\rm me}$ is defined by

$$T_{\rm me}(\omega) \equiv \left.\frac{U_0}{P_{\rm e}}\right|_{\text{middle ear driven forward}}\,. \tag{A3}$$

Of the two quantities $\left|Z_{\rm e}T_{\rm me}\right|^2$ and $\mathrm{Re}Z_{\rm e}$ that depend on the middle ear in Eq. (A1), the following discussion first considers $\left|Z_{\rm e}T_{\rm me}\right|^2$ and shows that at low frequencies it is nearly independent of the cochlear input impedance $Z_0(\omega)$. An expression for $\mathrm{Re}Z_{\rm e}$, valid in the same frequency range, is then found as a function of $\mathrm{Re}Z_0$.

Measurements on the cat (Guinan and Peake 1967; Lynch 1981; Allen 1986) indicate that for frequencies less than approximately 700 Hz, $Z_{\rm e}$ and $T_{\rm me}$ have the form

$$Z_{\rm e} \approx \frac{1}{i\omega C_{\rm e}}\,. \quad \text{and} \quad T_{\rm me} \approx i\omega C_{\rm me} \tag{A4}$$

Models of the cat middle ear (e.g., Lynch 1981; Carr and Zweig 1984) suggest that the constants $C_{\rm e}$ and $C_{\rm me}$ are proportional to the combined compliances of such middle-ear

structures as the eardrum, cavities, and ossicular joints and are thus essentially independent of Z_0.

Allen (1986) explicitly demonstrated that independence for Z_e by measuring $|Z_e(\omega)|$ both before and after setting $Z_0 \approx 0$ by removing the basilar membrane and draining the cochlear fluids.[17] The implications of that experiment can be understood most readily by noting that

$$Z_e = \frac{aZ_0 + b}{cZ_0 + d} , \tag{A5}$$

where $\left(\begin{smallmatrix} a & b \\ c & d \end{smallmatrix}\right)$ are the elements of the transfer matrix $\mathbf{T}$ of the middle ear (Shera and Zweig 1992a), defined by

$$\begin{pmatrix} P_e \\ U_e \end{pmatrix} = \mathbf{T} \begin{pmatrix} P_0 \\ U_0 \end{pmatrix} . \tag{A6}$$

When the basilar membrane is removed and the cochlear fluids drained,

$$|Z_e|_{Z_0=0} = \left|\frac{b}{d}\right| . \tag{A7}$$

Removing the cochlear load had a negligible effect on $|Z_e|$ below approximately 700 Hz. Hence,

$$\left|\frac{aZ_0 + b}{cZ_0 + d}\right| \approx \left|\frac{b}{d}\right| \qquad (\omega/2\pi \lesssim 700 \text{ Hz}) , \tag{A8}$$

so that[18]

$$|aZ_0| \ll |b| , \qquad |cZ_0| \ll |d| , \tag{A9}$$

and[19]

$$Z_e \approx \frac{b}{d} . \tag{A10}$$

Thus, since

$$T_{me} = \frac{1}{aZ_0 + b} \approx \frac{1}{b} , \tag{A11}$$

---

[17] Allen (1986) measured the ratio of pressure to particle velocity in the ear canal at the eardrum, which is everywhere proportional to Z_e. The proportionality constant is approximately the cross-sectional area of the ear canal which has a typical value of 0.15 cm^2 in cats (Shaw 1974).

[18] The other possibility consistent with Eq. (A8), namely that

$$aZ_0 = (p-1)b \quad \text{and} \quad cZ_0 = (\pm p - 1)d , \tag{18.1}$$

where $p(\omega)$ is some function of frequency, can be excluded because no function p can be found that is simultaneously consistent both with the principle of reciprocity, which requires $\det \mathbf{T} = +1$, and the expected forms (see text) of the matrix elements at low frequencies.

[19] Additional support for the inequality $|cZ_0| \ll |d|$ comes from the observations that at low frequencies the cat eardrum moves much like a rigid plate (Khanna and Tonndorf 1972; Decraemer et al. 1989) and that the ossicular joints are expected to be quite stiff (e.g., Lynch 1981; Carr and Zweig 1984).

the structure of the middle and inner ears are such that

$$|Z_e T_{me}| \approx \left|\frac{1}{d}\right| \approx \left|\frac{C_{me}}{C_e}\right| \tag{A12}$$

and so depends only on the middle ear below 700 Hz.

To estimate middle-ear contributions to $\mathrm{Re}Z_e$, note that at low frequencies models of the cat middle ear (e.g., Lynch 1981; Carr and Zweig 1984) predict that the matrix elements a and d are both approximately positive real, whereas b and c are, respectively, negative imaginary and positive imaginary. In addition, they suggest that $|bc| \ll |ad|$. Thus, by Eq. (A5),

$$\mathrm{Re}Z_e \approx k\mathrm{Re}Z_0 + R_{me} \ , \tag{A13}$$

where

$$k \approx \frac{a}{d} \quad \text{and} \quad R_{me} \approx \mathrm{Re}\left\{\frac{b}{d}\right\} \tag{A14}$$

are constants.

Allen (1986) has measured $\mathrm{Re}Z_e$ while varying the cochlea load,[20] and those measurements can be used to estimate the value of the resistance R_{me}. According to Allen's measurements, removing the cochlear load decreases $\mathrm{Re}Z_e$ by approximately 10–15 dB (or roughly a factor of 4) below 700 Hz. Hence,

$$R_{me} \equiv \mathrm{Re}Z_e\big|_{Z_0=0} \approx \frac{1}{3}kR_C \ , \tag{A15}$$

where R_C represents the resistance of the cochlea. Equation (A15) gives the approximate value of R_{me}, determined by middle-ear mechanics, in terms of the known cochlear resistance. Thus,

$$\mathrm{Re}Z_e \approx k\big(\mathrm{Re}Z_0 + R_C/3\big) \ . \tag{A16}$$

Using Eqs. (A12) and (A16) in Eq. (A1) for $\eta_{me}(\omega)$ yields the expression, namely Eq. (63), used in the text:

$$\eta_{me}(\omega; \mathrm{Re}Z_0) \approx \frac{\alpha \mathrm{Re}Z_0}{\mathrm{Re}Z_0 + R_C/3} \qquad (\omega/2\pi \lesssim 700 \text{ Hz}) \ , \tag{A17}$$

[20] Allen's measurements were made with the middle-ear cavities widely open. At frequencies much lower than the middle-ear cavity resonance near 4 kHz that modification should have little effect on $\mathrm{Re}Z_e$. Calculations using models of the middle ear (e.g., Carr and Zweig 1984) support that contention.

where

$$\alpha \equiv \frac{1}{k}\left(\frac{C_{\mathrm{me}}}{C_{\mathrm{e}}}\right)^2 . \tag{A18}$$

The measurements of Guinan and Peake (1967) indicate that $C_{\mathrm{me}} \approx 2.5 \times 10^{-9}$ cm^5/dyne and Lynch (1981) provides the average value $C_{\mathrm{e}} \approx 2.36 \times 10^{-7}$ cm^5/dyne. Combining the measurements of Allen (1986) with Lynch et al.'s (1982) determination of R_{C} and Shaw's (1974) measurements of the cross-sectional area of the ear canal yields the estimate $k \approx 1/85^2$. Consequently, $\alpha \approx 0.8$. Note that the value relies on measurements from many cats and thus provides only a rough estimate of its value in any individual. Nonetheless, Eq. (A17) can be used, when combined with model predictions of $\mathrm{Re}Z_0(\omega)$, to explore the predicted frequency variation of middle-ear efficiency.

References

Allen, J. B. (1979). "Cochlear models — 1978," *Scand. Audiol. Suppl.* **9**, 1–16.

Allen, J. B. (1986). "Measurement of eardrum acoustic impedance," in *Peripheral Auditory Mechanisms*, edited by J. B. Allen, J. L. Hall, A. Hubbard, S. T. Neely, and A. Tubis, 44–51. Berlin: Springer–Verlag.

von Békésy, G. (1960). *Experiments in Hearing.*New York: McGraw-Hill.

Bender, C. M. and S. A. Orszag (1978). *Advanced Mathematical Methods for Scientists and Engineers.*New York: McGraw-Hill.

Bloch, F. and A. Nordsieck (1937). "Note on the radiation field of the electron," *Phys. Rev.* **52**, 54–59.

Bode, H. (1945). *Network Analysis and Feedback Amplifier Design.*Princeton: Van Nostrand Reinhold.

de Boer, E. (1980). "Auditory physics. Physical principles in hearing theory. I," *Phys. Rep.* **62**, 88–174.

de Boer, E. and M. A. Viergever (1984). "Wave propagation and dispersion in the cochlea," *Hearing Res.* **13**, 101–112.

de Boer, E., C. Kaernbach, P. König, and T. Schillen (1986a). "An isolated sound emitter in the cochlea: Notes on modelling," in *Peripheral Auditory Mechanisms*, edited by J. B. Allen, J. L. Hall, A. Hubbard, S. T. Neely, and A. Tubis, 197–204. Berlin: Springer–Verlag.

de Boer, E., C. Kaernbach, P. König, and T. Schillen (1986b). "Forward and reverse waves in the one-dimensional model of the cochlea," *Hearing Res.* **23**, 1–7.

Bohne, B. B. and C. D. Carr (1979). "Location of structurally similar areas in chinchilla cochleas of different lengths," *J. Acoust. Soc. Am.* **66**, 411–414.

Born, M. and E. Wolf (1959). *Principles of Optics: Electromagnetic Theory of Propagation, Interference and Diffraction of Light.*Oxford: Pergamon Press.

Carr, J. N. and G. Zweig (1984). "A mechanical model of the middle ear of anesthetized cats," unpublished report.

Dallos, P. (1970). "Low-frequency auditory characteristics: Species dependence," *J. Acoust. Soc. Am.* **48**, 489–499.

Dallos, P. (1973). *The Auditory Periphery: Biophysics and Physiology.*New York: Academic Press.

Decraemer, W. F., S. M. Khanna, and W. R. J. Funnell (1989). "Interferometric measurement of the amplitude and phase of tympanic membrane vibrations in cat," *Hearing Res.* **38**, 1–18.

Eldredge, D. H., J. D. Miller, and B. A. Bohne (1981). "A frequency-position map for the chinchilla cochlea," *J. Acoust. Soc. Am.* **69**, 1091–1095.

Fernández, C. (1952). "Dimensions of the cochlea (guinea pig)," *J. Acoust. Soc. Am.* **24**, 519–523.

Feynman, R. P. (1961). *Quantum Electrodynamics.*New York: W. A. Benjamin.

Green, G. (1837). "On the motion of waves in a variable canal of small depth and width," *Trans. Camb. Phil. Soc.* **6**, 457–462.

Greenwood, D. D. (1961). "Critical bandwidth and the frequency coordinates of the basilar membrane," *J. Acoust. Soc. Am.* **33**, 1344–1356.

Guinan, J. J. and W. T. Peake (1967). "Middle-ear characteristics of anesthetized cats," *J. Acoust. Soc. Am.* **41**, 1237–1261.

Gummer, A. W., B. M. Johnstone, and N. J. Armstrong (1981). "Direct measurement of basilar membrane stiffness in the guinea pig," *J. Acoust. Soc. Am.* **70**, 1298–1309.

Gummer, A. W., J. W. T. Smolders, and R. Klinke (1987). "Basilar membrane motion in the pigeon measured with the Mössbauer technique," *Hearing Res.* **29**, 63–92.

Jeffreys, H. (1924). "On certain approximate solutions of linear differential equations of the second order," *Proc. Lond. Math. Soc.* **23**, 428–436.

Kaernbach, C., P. König, and T. Schillen (1987). "On Riccati equations describing impedance relations for forward and backward excitation in the one-dimensional cochlea model," *J. Acoust. Soc. Am.* **81**, 408–411.

Kemp, D. T. (1978). "Stimulated acoustic emissions from within the human auditory system," *J. Acoust. Soc. Am.* **64**, 1386–1391.

Kemp, D. T. (1979). "Evidence of mechanical nonlinearity and frequency selective wave amplification in the cochlea," *Arch. Otorhinolaryngol.* **224**, 37–45.

Kemp, D. T. (1979a). "The evoked cochlear mechanical response and the auditory microstructure — Evidence for a new element in cochlear mechanics," *Scand. Audiol. Suppl.* **9**, 35–47.

Kemp, D. T. and R. A. Chum (1980). "Observations on the generator mechanism of stimulus frequency acoustic emissions — Two tone suppression," in *Psychophysical Physiological and Behavioural Studies in Hearing*, edited by G. Van Den Brink and F. A. Bilsen, 34–42. Delft: Delft University Press.

Khanna, S. M. and J. Tonndorf (1972). "Tympanic membrane vibrations in cats studied by time-averaged holography," *J. Acoust. Soc. Am.* **51**, 1904–1920.

Konishi, S. and G. Zweig (1989). "Smoothing causal functions," in preparation.

Koshigoe, S., W. K. Kwok, and A. Tubis (1983). "Effects of perilymph viscosity on low-frequency intracochlear pressures and the cochlear input impedance of the cat," *J. Acoust. Soc. Am.* **74**, 486–492.

Liberman, M. C. (1982). "The cochlear frequency map for the cat: Labeling auditory-nerve fibers of known characteristic frequency," *J. Acoust. Soc. Am.* **72**, 1441–1449.

Lynch, T. J. (1981). "Signal processing by the cat middle ear: Admittance and transmission, measurements and models," Ph.D. thesis, Massachusetts Institute of Technology.

Lynch, T. J., V. Nedzelnitsky, and W. T. Peake (1982). "Input impedance of the cochlea in cat," *J. Acoust. Soc. Am.* **72**, 108–130.

Nedzelnitsky, V. (1974a). "Measurements of sound pressure in the cochleae of anesthetized cats," Ph.D. thesis, Massachusetts Institute of Technology.

Nedzelnitsky, V. (1974b). "Measurements of sound pressure in the cochleae of anesthetized cats," in *Facts and Models of Hearing*, edited by E. Zwicker and E. Terhardt, 45–55. Berlin: Springer–Verlag.

Nedzelnitsky, V. (1980). "Sound pressures in the basal turn of the cat cochlea," *J. Acoust. Soc. Am.* **68**, 1676–1689.

Neely, S. T. (1981). "Finite difference solution of a two-dimensional mathematical model of the cochlea," *J. Acoust. Soc. Am.* **69**, 1386–1393.

Olson, E. S. (1990). "*In vivo* measure of basilar membrane stiffness," Abstracts of the 13th ARO Midwinter Research Meeting.

Peake, W. T. (1989), private communication.

Peterson, L. C. and B. P. Bogert (1950). "A dynamical theory of the cochlea," *J. Acoust. Soc. Am.* **22**, 369–381.

Puria, S. and J. Allen (1991). "A parametric study of the cochlear input impedance," *J. Acoust. Soc. Am.* **89**, 287–309.

Rhode, W. S. (1971). "Observations of the vibration of the basilar membrane in squirrel monkeys using the Mössbauer technique," *J. Acoust. Soc. Am.* **49**, 1218–1231.

Robles, L., M. A. Ruggero, and N. C. Rich (1986). "Basilar membrane mechanics at the base of the chinchilla cochlea I. Input-output functions, tuning curves, and response phases," *J. Acoust. Soc. Am* **80**, 1364–1374.

Rosowski, J. J., W. T. Peake, and T. J. Lynch (1984). "Acoustic input-admittance of the alligator-lizard ear: Nonlinear features," *Hearing Res.* **16**, 205–223.

Rosowski, J. J., L. H. Carney, T. J. Lynch, and W. T. Peake (1986). "The effectiveness of external and middle ears in coupling acoustic power into the cochlea," in *Peripheral Auditory Mechanisms*, edited by J. B. Allen, J. L. Hall, A. Hubbard, S. T. Neely, and A. Tubis, 56–59. Berlin: Springer–Verlag.

Schroeder, M. R. (1973). "An integrable model of the basilar membrane," *J. Acoust. Soc. Am.* **53**, 429–434.

Shaw, E. A. G. (1974). "The external ear," in *Handbook of Sensory Physiology, Vol. V/1: Auditory System*, edited by W. D. Keidel and W. D. Neff, 455–490. Berlin: Springer–Verlag.

Shera, C. A. and G. Zweig (1991b). "Reflection of retrograde waves within the cochlea and at the stapes," *J. Acoust. Soc. Am.* **89**, 1290–1305.

Shera, C. A. and G. Zweig (1992a). "Middle-ear phenomenology: The view from the three windows," submitted to *J. Acoust. Soc. Am.*

Sondhi, M. M. (1978). "Method for computing motion in a two-dimensional cochlear model," *J. Acoust. Soc. Am.* **63**, 1468–1477.

Viergever, M. A. (1980). *Mechanics of the Inner Ear: A Mathematical Approach.*Delft: Delft University Press.

Viergever, M. A. (1986). "Asymmetry in reflection of cochlear waves," in *Auditory Frequency Selectivity*, edited by B. C. J. Moore and R. D. Patterson, 31–38. New York: Plenum.

Viergever, M. A. and E. de Boer (1987). "Matching impedance of a nonuniform transmission line: Application to cochlear modeling," *J. Acoust. Soc. Am.* **81**, 184–186.

Wever, E. G. (1949). *Theory of Hearing.*New York: John Wiley & Sons.

Wickesberg, R. E. and C. D. Geisler (1986). "Longitudinal stiffness coupling in a 1-dimensional model of the peripheral ear," in *Peripheral Auditory Mechanisms*, edited by J. B. Allen, J. L. Hall, A. Hubbard, S. T. Neely, and A. Tubis, 113–120. Berlin: Springer–Verlag.

Zweig, G., R. Lipes, and J. R. Pierce (1976). "The cochlear compromise," *J. Acoust. Soc. Am.* **59**, 975–982.

Zweig, G. (1976). "Basilar membrane motion," in *Cold Spring Harbor Symposia on Quantitative Biology, volume XL, 1975*, 619–633. Cold Spring Harbor: Cold Spring Harbor Laboratory.

Zweig, G. (1987). "The mechanics of hearing," invited paper presented at the conference "Nonlinearity in Biology and Medicine," Center for Nonlinear Studies, Los Alamos National Laboratory.

Zweig, G. and S. Konishi (1987). "Constraints on measurements of causal or minimum-phase systems," accepted for publication in *J. Acoust. Soc. Am.*

Zweig, G. (1989). "Auditory speech preprocessors," in *Proceedings of the DARPA Speech and Natural Language Workshop*, 229–235. San Mateo: Morgan Kauffman.

Zweig, G. (1991). "Finding the impedance of the organ of Corti," *J. Acoust. Soc. Am.* **89**, 1229–1254.

Zwicker, E. and E. Schloth (1984). "Interrelation of different oto-acoustic emissions," *J. Acoust. Soc. Am.* **75**, 1148–1154.

Zwislocki, J. (1965). "Analysis of some auditory characteristics," in *Handbook of Mathematical Psychology*, edited by R. D. Luce, R. R. Bush, and E. Galanter, 1–97. New York: John Wiley & Sons.

Zwislocki-Mościcki, J. (1948). "Theorie der Schneckenmechanik: Qualitative und quantitative Analyse," *Acta Otolaryngol. Suppl.* **72**, 1–112.

Reflection of Retrograde Waves within the Cochlea and at the Stapes

Christopher A. Shera and George Zweig

Theoretical Division
Los Alamos National Laboratory
Los Alamos, New Mexico 87545

and

Physics Department
California Institute of Technology
Pasadena, California 91125

ABSTRACT

A number of authors (de Boer and Viergever 1984; de Boer et al. 1986ab; Viergever 1986; Kaernbach et al. 1987) have argued that backward-traveling waves, in striking contrast to waves traveling forward towards the helicotrema, suffer appreciable reflection as they move through the basal turns of the cochlea. Such reflection, if present, would have important consequences for understanding the nature and strength of otoacoustic emissions. The apparent asymmetry in reflection of cochlear waves is shown, however, to be an artifact of the boundary condition those authors impose at the stapes: conventional cochlear models are found not to generate reflections of waves traveling in *either* direction even when the wavelength changes rapidly and the WKB approximation breaks down.

Although backward-traveling waves are not reflected by the secular variation of the geometrical and mechanical characteristics of the cochlea, they are reflected when they reach the stapes. The magnitude of that boundary reflection is computed for the cat and shown to be a large, rapidly varying function of frequency.

Contents

Introduction

A number of recent papers have found a surprising asymmetry in the reflection of cochlear waves (de Boer and Viergever 1984; de Boer et al. 1986ab; Viergever 1986; Kaernbach et al. 1987). Those papers argue that whereas waves traveling forward towards the helicotrema suffer little reflection, backward-traveling waves are strongly reflected by the secular variation of the mechanical characteristics of the organ of Corti. Such reflection, if present, would have important consequences for understanding the strength of otoacoustic emissions measured in the ear canal.

This paper demonstrates, however, that the reflection of retrograde waves found by other authors is an artifact of the boundary condition they impose at the stapes. The reflection they find occurs not within the cochlea but rather at an impedance mismatch at the cochlear boundary with the middle ear. The ostensible asymmetry in reflection of cochlear waves thus appears as the expected consequence of an asymmetric termination of the cochlear transmission line.

The finding that the models they use generate little internal reflection is unexpected; since their models, like most cochlear models, break the tapering symmetry required by measurements of the cochlear input impedance (Shera and Zweig 1991a) and therefore manifest the cochlear catastrophe (i.e., a divergence in the "spatial" derivative of the wavelength at low frequencies), one might naively expect them to produce considerable reflection of waves traveling through the basal turn. To see this, recall that tapering symmetry implies that the longitudinal impedance $\bar{Z}$ of the cochlea and the shunt admittance Y of the organ of Corti are approximately proportional. That symmetry guarantees that the wavelength, or characteristic impedance, changes slowly at the basal end of the cochlea and therefore that waves traveling in either direction undergo little reflection. The logic of the argument can be summarized with the diagram:

$$\{\text{Real } Z_0\} \iff \{\bar{Z} \propto Y\} \iff \{|\lambda_0'| \ll 1\} \Rightarrow \{\text{cochlear reflections are small}\}, \quad (1)$$

where the notation "$p \Rightarrow q$" means "p implies q."

One might therefore expect, although such is *not* a necessary consequence of diagram (1), that models in which the symmetry between $\bar{Z}$ and Y is broken and the

wavelength changes rapidly produce large reflection of retrograde waves. By computing reflections in models that exhibit the cochlear catastrophe, this paper shows, however, that conventional cochlear models do not create reflections of retrograde waves even when $\bar{Z}$ and Y are not proportional:

$$\{\bar{Z} \not\propto Y\} \iff \{|\lambda_0'| \gg 1\} \not\Rightarrow \{\text{cochlear reflections are large}\} . \tag{2}$$

Although the input impedance of such models has a nonzero phase at low frequencies—in contradiction with experiment—the cochlear reflection of retrograde waves is always small.

A. Overview

Since the solution to any scattering problem first requires defining what is meant by a wave traveling in a particular direction, Sec. I outlines a method for obtaining projection operators that enable one to decompose the solution to the transmission-line equations into waves traveling in opposite directions. The method is illustrated by application to an asymptotic WKB expansion for the pressure. The connection between the resulting WKB series and the geometric-optical series (Bremmer 1951) used by Viergever (1986) for the analysis of cochlear reflections is established. Section II introduces a family of conventional transmission-line models in which a parameter Δ determines the extent of symmetry-breaking between $\bar{Z}$ and Y. Included in the family are those models (e.g., de Boer 1980) used for the investigation of cochlear reflection phenomena. Approximate solutions for the traveling-wave components, valid at low frequencies near the stapes, are found. Those wave components, asymptotically exact as $\beta \to 0$, are matched to the corresponding WKB waves at higher β to obtain approximate solutions valid throughout the cochlea. The results of Secs. I and II are then combined for a discussion of cochlear reflection. By solving for an infinite cochlea the analog of a plane-wave scattering problem, Sec. III demonstrates that the cochlear reflection of retrograde waves predicted by other authors results from an impedance mismatch at the basal boundary. Section IV argues that negligible internal reflection of waves, properly defined, is a general property of conventional cochlear models. The paper concludes with an estimate of the reflection coefficient at the stapes for retrograde waves traveling within the cochlea of the cat.

I. Finding the Wave Components

This section outlines a simple method, based on an arbitrary pair of "basis waves" $\mathcal{B}_\pm$ and their osculating parameters, for defining projection operators that enable one to decompose the total pressure into wave components traveling in opposite directions along the organ of Corti. The procedure does not depend on the form of the basis functions, although the method is most useful if the $\mathcal{B}_\pm$ constitute good approximate solutions to the transmission-line equations. The resulting wave components can be interpreted as originating from multiple scattering of lower-order waves within the cochlea. The projection operators are used to derive expressions for the wave impedances of a nonuniform transmission line. The section concludes with an examination of the relationship of the WKB series to the geometric-optical series (Bremmer 1951) used by Viergever (1986) for the analysis of cochlear reflections.

At high sound pressure levels and low frequencies (i.e., $\omega \ll \omega_{c_0}$ where ω_{c_0} is the maximal characteristic angular frequency represented on the organ of Corti), the basal turn of the cochlea is analogous to a linear, one-dimensional mechanical transmission line (Zwislocki-Mościcki 1948; Peterson and Bogert 1950; Zweig 1991). The transmission-line equations imply that the differential pressure P and volume velocity U satisfy the equations

$$\frac{d^2P}{d\chi^2} + \frac{1}{\lambda^2}P = 0\,, \tag{3}$$

and

$$U = i\frac{dP}{d\chi}\,, \tag{4}$$

where the "spatial" coordinate χ is defined by

$$\chi(x,\omega) = -i\int_0^x \bar{Z}(x',\omega)\,dx'\,, \tag{5}$$

and the characteristic impedance

$$\lambda(\chi,\omega) \equiv Z_c(\chi,\omega) \equiv \left(\frac{\bar{Z}}{Y}\right)^{1/2}\,. \tag{6}$$

represents the corresponding "wavelength." Recall that $\bar{Z}$ and Y represent, respectively, the longitudinal impedance and shunt admittance per unit length of the cochlear transmission line.

For most forms of $\bar{Z}$ and Y, solutions to Eq. (3) do not exist in terms of elementary functions and approximate solutions must therefore be employed. Imagine P to be approximated, in some region of the cochlea, by a superposition of waves $\mathcal{B}_\pm$ traveling in opposite directions along the organ of Corti:

$$P(\chi,\omega) \approx A_+(\omega)\mathcal{B}_+(\chi,\omega) + A_-(\omega)\mathcal{B}_-(\chi,\omega) \,. \tag{7}$$

The direction of wave propagation is indicated by the subscripts on the complex amplitudes: the '+' indicates a wave traveling toward the helicotrema, the '−' a wave traveling back toward the stapes. The choice of "basis functions" $\mathcal{B}_\pm$ is entirely arbitrary, although the formalism is most useful if the $\mathcal{B}_\pm$ constitute good approximate solutions to the transmission-line equations and, in the limit of zero damping, the power flow computed with those basis waves is nearly constant. The complex amplitudes $A_\pm$ may be determined by boundary conditions (applied, for example, at the base and apex of the cochlea) or by matching with solutions valid in adjacent regions. For simplicity, the frequency dependence of most dependent variables will be suppressed.

The basis waves $\mathcal{B}_\pm$, approximate solutions of Eq. (3), are exact solutions of some other equations, assumed to be of the form

$$\frac{d^2\mathcal{B}_\pm}{d\chi^2} + \frac{1+\epsilon_\pm^{\mathcal{B}}}{\lambda^2}\mathcal{B}_\pm = 0 \,. \tag{8}$$

If $|\epsilon_\pm^{\mathcal{B}}| \ll 1$, the functions $\mathcal{B}_\pm$ form good approximate solutions to the transmission-line equations. (In practice, the $\mathcal{B}_\pm$ may be obtained by choosing convenient forms for the $\epsilon_\pm^{\mathcal{B}}$ so that the solutions to Eqs. (8) correspond to well-known special functions.)

A. The osculating parameters $\psi_\pm^{\mathcal{B}}$

Adopting the approximate solutions $\mathcal{B}_\pm$ as "basis waves" permits the *exact* decomposition of the pressure P into corresponding components $P_\pm^{\mathcal{B}}$ whose sum yields the total pressure P:

$$P \equiv P_+^{\mathcal{B}} + P_-^{\mathcal{B}} \,. \tag{9}$$

The superscripts identify the underlying basis waves. The decomposition, affected by generalizing Eq. (7) and allowing the constants $A_\pm$—renamed the $\psi_\pm^{\mathcal{B}}(\chi)$—to vary with position, is defined by

$$P_\pm^{\mathcal{B}}(\chi) \equiv \psi_\pm^{\mathcal{B}}(\chi)\mathcal{B}_\pm(\chi) \,, \tag{10}$$

where the functions $\psi_{\pm}^{B}(\chi)$ are defined by the pair of simultaneous equations

$$P \equiv \psi_{+}^{B}\mathcal{B}_{+} + \psi_{-}^{B}\mathcal{B}_{-} \tag{11}$$

and

$$\frac{dP}{d\chi} \equiv \psi_{+}^{B}\frac{d\mathcal{B}_{+}}{d\chi} + \psi_{-}^{B}\frac{d\mathcal{B}_{-}}{d\chi} \ . \tag{12}$$

At every point χ the functions $\psi_{\pm}^{B}(\chi)$, known as osculating parameters (Mathews and Walker 1964), are defined so that their values give the pressure P and its derivative $dP/d\chi$ exactly.

If the $\mathcal{B}_{\pm}$ constitute exact solutions to Eq. (3) (so that $\epsilon_{\pm}^{B} = 0$), the osculating parameters become independent of position and one can make the identification

$$\psi_{+}^{B}(\chi) = A_{+} \quad \text{and} \quad \psi_{-}^{B}(\chi) = A_{-} \ . \tag{13}$$

The deviation of the $\psi_{\pm}^{B}$ from those constant values provides a measure of the error in Eq. (7) (Kemble 1935; Mathews and Walker 1964; Fröman and Fröman 1965).

The osculating parameters can be found—and their interpretation as scattering amplitudes illuminated—as follows. Solving Eqs. (11) and (12) for the functions $\psi_{\pm}^{B}(\chi)$ yields

$$\psi_{\pm}^{B} = \pm\gamma^{B}\left(\frac{d\mathcal{B}_{\mp}}{d\chi} - \mathcal{B}_{\mp}\frac{d}{d\chi}\right)P \ , \tag{14}$$

where

$$\gamma^{B} \equiv \det{}^{-1}\begin{vmatrix} \mathcal{B}_{+} & \mathcal{B}_{+}' \\ \mathcal{B}_{-} & \mathcal{B}_{-}' \end{vmatrix} \tag{15}$$

is the reciprocal of the Wronksian determinant. The osculating parameters $\psi_{\pm}^{B}$ may then be determined by solving the pair of coupled first-order differential equations

$$\frac{d\psi_{\pm}^{B}}{d\chi} = \mp\left(\sigma_{\pm}^{B}\psi_{\pm}^{B}\mathcal{B}_{+}\mathcal{B}_{-} + \sigma_{\mp}^{B}\psi_{\mp}^{B}\mathcal{B}_{\mp}^{2}\right) \ , \tag{16}$$

obtained by differentiating Eq. (14). Here,

$$\sigma_{\pm}^{B} \equiv \gamma^{B}\frac{\epsilon_{\pm}^{B}}{\lambda^{2}} \ . \tag{17}$$

If the $|\sigma_{\pm}^{B}|$ are sufficiently small, Eqs. (16) can be solved by iteration. For example, if the boundary conditions are such that $\psi_{+}^{B}(0) = 1$ and $\psi_{-}^{B}(\infty) = 0$, a first approximation to P_{-}^{B} is given by

$$P_{-}^{B}(\chi) \approx -\mathcal{B}_{-} \int_{\chi}^{\infty} \mathcal{B}_{+}(\chi')\sigma_{+}^{B}(\chi')\mathcal{B}_{+}(\chi')\,d\chi' \; + \; O(\sigma^{B}\sigma^{B}) \,, \tag{18}$$

representing summed contributions from wavelets $\mathcal{B}_{+}(\chi')$ reflected (a single time) at all points $\chi' > \chi$. Decomposing the solution P in the manner of Eq. (9) is equivalent to finding the exact solution to the transmission-line equations by solving an integral scattering equation in which incident waves $\mathcal{B}_{\pm}$ are scattered by their interaction with potentials $\sigma_{\pm}^{B}$. The wave components $P_{\pm}^{B}$ can thus be interpreted physically as the summed amplitudes at χ of all wavelets traveling in a particular direction.

As is readily apparent from Eq. (18), the value of P_{-}^{B} depends on the choice of wave components $\mathcal{B}_{\pm}$. Thus, nonzero values of the "reflection coefficient"

$$\overrightarrow{R}^{B}(\chi,\omega) \equiv \left.\frac{P_{-}^{B}}{P_{+}^{B}}\right|_{\text{cochlea driven forward}} \tag{19}$$

do not necessarily represent actual reflection of energy back toward the stapes, but may result simply from the use of wave components $\mathcal{B}_{\pm}$ for which the corresponding scattering potentials $\sigma_{\pm}^{B}(\chi,\omega)$ are not small—that is, wave components that do not constitute accurate solutions to the transmission-line equations (see the Appendix for an example).

B. The projection operators $\widehat{P}_{\pm}^{B}$

The wave components $P_{\pm}^{B}$ can also be obtained from the total pressure P by means of the cochlear projection operators $\widehat{P}_{\pm}^{B}$, defined by

$$P_{\pm}^{B} \equiv \widehat{P}_{\pm}^{B}\{P\} \,. \tag{20}$$

Equation (14) then implies that

$$\widehat{P}_{\pm}^{B} = \pm\gamma^{B}\mathcal{B}_{\pm}\left(\frac{d\mathcal{B}_{\mp}}{d\chi} - \mathcal{B}_{\mp}\frac{d}{d\chi}\right) \,. \tag{21}$$

Note that the waves $\mathcal{B}_{\pm}(\chi)$ are, by construction, eigenfunctions of the projection operators with eigenvalues of either zero or one:

$$\widehat{P}_{i}^{B}\{\mathcal{B}_{j}\} = \delta_{ij}\mathcal{B}_{j} \,. \tag{22}$$

C. The wave impedances $Z_{\pm}^{B}$

A simple application of the projection operators $\hat{P}_{\pm}^{B}(\chi)$ yields the wave impedances $Z_{\pm}^{B}(\chi)$, defined by

$$Z_{\pm}^{B} \equiv \pm \frac{P}{U}\bigg|_{P_{\mp}^{B}=0} = \pm \frac{P_{\pm}^{B}}{U_{\pm}^{B}} , \tag{23}$$

where, by Eq. (4) for U,

$$U_{\pm}^{B} \equiv i \frac{dP_{\pm}^{B}}{d\chi} . \tag{24}$$

Application of the projection operators yields

$$P_{\pm}^{B} = \pm \gamma^{B} \mathcal{B}_{\pm} \left(\frac{d\mathcal{B}_{\mp}}{d\chi} P + i \mathcal{B}_{\mp} U \right) . \tag{25}$$

The wave impedances can now be found by setting $P_{\pm}^{B}$ alternately equal to zero and solving for the ratio of P to U:

$$Z_{\pm}^{B}(\chi) = \frac{\mp i}{d \ln \mathcal{B}_{\pm}/d\chi} . \tag{26}$$

Equations (26) can be obtained immediately from Eqs. (10) and (24) by imposing the condition $\psi_{\pm}^{B\prime}(\chi) = 0$. The $Z_{\pm}^{B}$ are thus identical to the wave impedances for the transmission lines described by Eqs. (8); those equations, whose exact solutions are the $\mathcal{B}_{\pm}$, provide an approximate description of the original line [Eq. (3)]. Note that the wave impedances depend on the direction of wave propagation. They provide generalizations to nonuniform media of the concept of characteristic impedance.

D. Examples

This section applies the scattering formalism to approximate solutions of the cochlear transmission-line equations obtained by expanding the pressure P in an asymptotic WKB series. The connection between the first-order WKB series and the geometric-optical series introduced by Bremmer is then illustrated.

1. The WKB scattering series

An asymptotic WKB expansion for P yields (Bender and Orszag 1978)

$$P(\chi) \sim e^{\pm i \int^{\chi} d\chi'/\lambda \, + \, \frac{1}{2} \ln \lambda \, + \, \cdots} . \tag{27}$$

Basis waves obtained by including the first and second terms in the expansion will be denoted $V_{\pm}$ and $W_{\pm}$, respectively.

Truncating the asymptotic WKB series after the second term yields the WKB approximation (e.g., Green 1837; Jeffreys 1924; Zweig et al. 1976); the approximate solution (7) then represents a superposition of WKB basis waves $W_\pm(\chi)$ defined by

$$\mathcal{B}_\pm \longmapsto W_\pm \equiv \sqrt{\lambda}\, e^{\mp i \int_0^x d\chi'/\lambda} \,. \tag{28}$$

Simple substitution into Eqs. (21) and (26) yields expressions for the corresponding projection operators $\widehat{P}_\pm^W$ and wave impedances $Z_\pm^W$ (see the first line of Table I). For future reference, note that the corresponding scattering potential has the form

$$\sigma_\pm^{\mathcal{B}} \longmapsto \sigma_\pm^W \equiv \sigma^W = \gamma^W \frac{\epsilon^W}{\lambda^2} \,, \tag{29}$$

where

$$\gamma^{\mathcal{B}} \longmapsto \gamma^W = \frac{1}{2i} \quad \text{and} \quad \epsilon^{\mathcal{B}} \longmapsto \epsilon^W = -\lambda^2 \frac{1}{\sqrt{\lambda}} \frac{d^2}{d\chi^2} \sqrt{\lambda} \,. \tag{30}$$

The WKB scattering series can be developed by iterative solution of Eqs. (16) for $\psi_\pm^{W\prime}$ in the manner of Eq. (18).

2. Relation to the geometric-optical series

Another scattering series recently used to explore cochlear wave reflection (Viergever 1986) is the geometric-optical series of Bremmer (1951). Whereas the scattering series outlined above is based on the WKB waves $W_\pm$, the geometric-optical series uses as its "basis set" the functions

$$\mathcal{B}_\pm \longmapsto V_\pm(\chi) \equiv e^{\mp i \int_0^x d\chi'/\lambda} \tag{31}$$

obtained by including only the first term in the asymptotic WKB series (27). The functions $V_\pm$ thus lack the factor of $\sqrt{\lambda}$ multiplying the WKB waves $W_\pm$; they therefore violate energy conservation and do not constitute acceptable solutions to the transmission-line equations (Zweig et al. 1976).

Adopting the $V_\pm$ as one's basis waves leads to the following pair of coupled differential equations for the $\psi_\pm^V$, corresponding to Eqs. (16):

$$\frac{d\psi_\pm^V}{d\chi} = \mp\sigma_\pm^V \left(\psi_\pm^V V_\pm V_\mp - \psi_\mp^V V_\mp^2 \right) \,, \tag{32}$$

Series	$\mathcal{B}_\pm$	$\widehat{P}_\pm^{\mathcal{B}}$	$Z_\pm^{\mathcal{B}}$
WKB	$\sqrt{\lambda}e^{\mp i\int_0^\chi d\chi'/\lambda}$	$\frac{1}{2}\left\{\left(1\mp\frac{i}{2}\lambda'\right)\hat{1}\pm i\lambda\frac{d}{d\chi}\right\}$	$\frac{\lambda}{1\pm i\lambda'/2}$
Bremmer	$e^{\mp i\int_0^\chi d\chi'/\lambda}$	$\frac{1}{2}\left\{\hat{1}\pm i\lambda\frac{d}{d\chi}\right\}$	λ

Table I. Projection operators $\widehat{P}_\pm^{\mathcal{B}}$ and wave impedances $Z_\pm^{\mathcal{B}}$ corresponding to basis waves $\mathcal{B}_\pm$ obtained using the WKB approximation and Bremmer's (1951) geometric-optical series.

where

$$\sigma_{\pm}^{B} \longmapsto \sigma_{\pm}^{V} \equiv \gamma^{V} \frac{\epsilon_{\pm}^{V}}{\lambda^{2}} \tag{33}$$

with

$$\gamma^{B} \longmapsto \gamma^{V} = \frac{\lambda}{2i} \quad \text{and} \quad \epsilon_{\pm}^{B} \longmapsto \epsilon_{\pm}^{V} = \mp i\lambda' \,. \tag{34}$$

There are two scattering potentials $\sigma_{\pm}^{V}$, and the corresponding Wronksian determinant $1/\gamma^{V}$ is not constant, because, unlike the WKB waves $W_{\pm}$, the geometric-optical basis waves $V_{\pm}$ do not satisfy a single differential equation. Iterative solution of Eqs. (32) yields Bremmer's geometric-optical series.[1]

As noted by Bremmer (1951), $\sigma_{\pm}^{V}$ can be interpreted as effective reflection coefficient densities (i.e., reflection coefficients per unit length $d\chi$) for plane waves. Note that ϵ^{W} can be written

$$\epsilon^{W} = \gamma^{V} \frac{d\epsilon_{+}^{V}}{d\chi} - \frac{1}{4}\epsilon_{+}^{V}\epsilon_{+}^{V} \,. \tag{35}$$

Equation (35) suggests that

$$|\epsilon^{W}| \ll |\epsilon_{\pm}^{V}| \tag{36}$$

in conventional cochlear models for which $|\epsilon_{\pm}^{V}| = |\lambda'| < 1$; as verified in Sec. III, the $\psi_{\pm}^{V}$ can thus be expected to vary considerably more rapidly with position than the $\psi_{\pm}^{W}$.

As before, one can define projection operators that enable one to decompose the total solution into traveling-wave components. The corresponding operators, with eigenfunctions $V_{\pm}$, are given in Table I. The projection operators $\widehat{P}_{\pm}^{V}$ derived here by use of the

---

[1] Equations (32) may be used to obtain a pair of coupled integral equations for the waves P_{+}^{V} and P_{-}^{V}:

$$P_{+}^{V}(\chi) = \left\{ A_{+} \; - \; \int_{0}^{\chi} W_{-} \frac{\sigma_{-}^{V}}{\lambda} P_{-}^{V} \, d\chi' \right\} W_{+} \,, \tag{1.1}$$

and

$$P_{-}^{V}(\chi) = \left\{ A_{-} \; - \; \int_{\chi}^{\infty} W_{+} \frac{\sigma_{+}^{V}}{\lambda} P_{+}^{V} \, d\chi' \right\} W_{-} \,, \tag{1.2}$$

where

$$W_{\pm} \equiv e^{\mp \int_{0}^{\chi} V_{-} \sigma_{\pm}^{V} V_{+} \, d\chi'} V_{\pm} = \sqrt{\lambda} V_{\pm} \tag{1.3}$$

are simply the WKB functions $W_{\pm}$. Integral equations (1.1) and (1.2) are equivalent to those obtained by Bremmer (1951) by summation of alternate terms of the geometric-optical series.

Thus, if the retrograde wave P_{-}^{V} is small, the anterograde wave P_{+}^{V} is, to first-order, proportional to the WKB wave W_{+} obtained by including the next term in the WKB expansion. Although the geometric-optical series may yield the WKB approximation as its leading term (accounting for the title of Bremmer's paper), the series is nonetheless grounded on the lower-order basis waves $V_{\pm}$, whose presence is betrayed, for example, by the form of the projection operators $\widehat{P}_{\pm}^{V}$ (see Table I).

osculating parameters $\psi_{\pm}^{V}$ agree with those obtained by Bremmer (1951) by summation of the geometric-optical series. As expected, the projection operators for the WKB and geometric-optical series, and their corresponding eigenfunctions, become equivalent in the limit $|\lambda'| \to 0$.

Calculating the wave impedances for the $V_{\pm}$ yields

$$Z_{\pm}^{V} \equiv \pm \frac{P}{U}\bigg|_{P_{\mp}^{V}=0} = Z_{c} \; . \tag{37}$$

Unlike the higher-order wave impedances $Z_{\pm}^{W}$,[2] the $Z_{\pm}^{V}$ simply equal the characteristic impedance Z_{c} of the transmission line and are independent of the direction of wave propagation.

Although the geometric-optical series remains useful for the purposes for which it was developed (namely, for solving for the reflected wave present in a homogeneous medium because of wave reflection by an adjacent inhomogeneous medium), because the $V_{\pm}(\chi,\omega)$ do not provide good approximate solutions to the transmission-line equations, using them as the basis for an exploration of reflection phenomena *within* an inhomogeneous medium such as the cochlea leads to results that are difficult to interpret (cf. Sec. III).

II. Basis Waves Valid Throughout the Cochlea

Section I outlined a formalism, based on an arbitrary pair of basis functions $\mathcal{B}_{\pm}$, for decomposing the total pressure P into waves traveling in opposite directions. Since the underlying basis waves should be chosen to represent accurate solutions to the transmission-line equations, this section introduces a family of passive, conventional transmission-line models and solves the equations for approximate basis waves valid throughout the cochlea. Because different approximate solutions are valid in different regions of the cochlea, the basis waves are given in terms of matched asymptotic expansions. The family of models is characterized by a parameter Δ that determines the extent of model symmetry-breaking. Section III uses basis waves corresponding to different members of the family to explore the reflection of retrograde waves in models appearing in the literature.

---

[2] Note that the WKB wave impedances $Z_{\pm}^{W}$ and the characteristic impedance Z_{c} are related by

$$Z_{c} = 2\left(Z_{+}^{W} \parallel Z_{-}^{W}\right) \equiv 2\frac{Z_{+}^{W} Z_{-}^{W}}{Z_{+}^{W} + Z_{-}^{W}} \; . \tag{2.1}$$

A. A family of conventional cochlear models

In conventional cochlear models the series impedance $\bar{Z}(x,\omega)$ and shunt admittance $Y(x,\omega)$ per unit length have the form

$$\bar{Z}(x,\omega) = i\omega\bar{M}(x) \quad \text{and} \quad Y(x,\omega) = \left\{ i\omega M(x) + R(x) + \frac{1}{i\omega C(x)} \right\}^{-1} . \tag{38}$$

In accord with experiment (e.g., von Békésy 1960; Greenwood 1961; Eldredge et al. 1981; Liberman 1982), the local characteristic frequency decreases exponentially with position in the basal turns:

$$\omega_c(x) \equiv \frac{1}{\sqrt{MC}} = \omega_{c_0} e^{-x/l} . \tag{39}$$

The phenomena discussed in this paper depend principally on the spatial variation of the wavelength λ at low frequencies in the basal turns, that is, at values

$$\beta(x,\omega) \equiv \omega/\omega_c(x) \ll 1 . \tag{40}$$

From the circuit elements one can form several dimensionless parameters: the quality factor, or Q, of the resonance is given by the reciprocal of the dimensionless damping parameter,

$$\frac{1}{Q} \equiv \delta \equiv \omega_c RC ; \tag{41}$$

and the dimensionless parameter

$$N \equiv \frac{l}{4} \left(\frac{\bar{M}}{M} \right)^{1/2} \tag{42}$$

represents the approximate number of wavelengths of the pressure wave in the cochlea in response to sinusoidal stimulation.

Consider the family of conventional cochlear models in which the parameters N and δ are constant and

$$\bar{M}(x) = \bar{M}_0 \left(\frac{\omega_{c_0}}{\omega_c(x)} \right)^{1-\Delta} , \tag{43}$$

and

$$C(x) = C_0 \left(\frac{\omega_{c_0}}{\omega_c(x)} \right)^{1+\Delta} . \tag{44}$$

Note that if $\Delta = 0$, $\bar{M}$ is proportional to C and the circuit elements $\bar{Z}$ and Y scale at low frequencies (Shera and Zweig 1991a; Zweig 1991). Since $\bar{M}$ is usually assumed inversely proportional to the effective cross-sectional area of the cochlear scalae, the traditional case (e.g., de Boer 1980) in which the scalae are approximated as boxes with constant cross-section is obtained by setting $\Delta = 1$. The parameter Δ thus determines the extent of symmetry breaking that occurs in the model; for example, the frequency ω_κ (Shera and Zweig 1991a) at which symmetry-breaking becomes apparent is given by

$$\omega_\kappa = \frac{\Delta}{4N}\omega_{c_0} \,. \tag{45}$$

Consistency with the measurements of Lynch et al. (1982) requires $|\Delta| \ll 1$ (Shera and Zweig 1991a).

B. Solving for the basis waves

The remainder of this section solves the equations for the family of models introduced above to obtain a pair of basis waves $\mathcal{B}_\pm$ valid throughout the cochlea. Those basis waves are given in terms of matched asymptotic expansions. On a first reading the reader may simply wish to note that the basis waves found below are summarized in Eq. (60); the corresponding projection operators and wave impedances appear in Table II.

It is easy to show that the function

$$\pi(\beta) \equiv \beta^{\Delta/2} P(\beta) \tag{46}$$

satisfies the equation

$$\frac{d^2\pi}{d\beta^2} + \frac{1}{\lambda_\beta^2}\pi = 0 \,, \tag{47}$$

where the "wavelength"

$$\lambda_\beta \equiv \frac{\sqrt{1-\beta^2+i\delta\beta}}{4N} \Bigg/ \left\{1 - \frac{\Delta(\Delta-2)}{4(4N)^2}\left(\frac{1-\beta^2+i\delta\beta}{\beta^2}\right)\right\}^{1/2} \,. \tag{48}$$

Note that values $|\Delta| \ll 1$ suppress the singularity in the wavelength (i.e., the cochlear catastrophe) at $\beta = 0$. (The singularity in λ_β is also eliminated when $\Delta = 2$. That value of Δ, however, corresponds to a cochlea in which the input impedance is imaginary and the scalae taper outward from the stapes like a horn.)

1. Approximate solutions for small β

At values of $\beta \ll 1$, Eq. (47) approaches

$$\frac{d^2\pi}{d\hat{\beta}^2} + \left\{1 - \frac{\Delta(\Delta-2)}{4\hat{\beta}^2}\right\}\pi = 0\,, \tag{49}$$

where

$$\hat{\beta} \equiv 4N\beta\,. \tag{50}$$

The general solution has the form

$$\pi(\hat{\beta}) = \sum_{-}^{+}\left\{\sqrt{\hat{\beta}}H_\nu^{\pm}(\hat{\beta})\right\}\,, \tag{51}$$

where $\sum_{-}^{+}\{\cdot\}$ represents any linear combination of its arguments, and the constant

$$\nu \equiv (1-\Delta)/2\,. \tag{52}$$

The Hankel functions,

$$H_\nu^{\pm}(z) \equiv H_\nu^{(2,1)}(z) = J_\nu(z) \mp iY_\nu(z)\,, \tag{53}$$

represent those linear combinations of Bessel functions having the asymptotic form (at large z) of incoming and outgoing plane waves.[3] Equation (46) implies that the pressure has the form

$$P(\hat{\beta}) \approx \sum_{-}^{+}\left\{\hat{\beta}^\nu H_\nu^{\pm}(\hat{\beta})\right\} \qquad (\beta \ll 1). \tag{54}$$

Table II provides expressions for the projection operators $\widehat{P}_{\pm}^{H}$ and wave impedances $Z_{\pm}^{H}$ implied by traveling-wave components of the form given by Eq. (54).[4]

2. Approximate solutions elsewhere

As one moves out of the basal turn the wavelength becomes

$$\lambda_\beta \approx \frac{\sqrt{1-\beta^2+i\delta\beta}}{4N}\,, \qquad \text{for } \beta \gg \sqrt{|\Delta(\Delta-2)|}/8N \tag{55}$$

and is independent of Δ. Since the wavelength then changes more slowly with position, Eq. (46) can be solved using the WKB approximation, which yields (Zweig et al. 1976)

$$P(\beta) \approx \sum_{-}^{+}\left\{\frac{\sqrt{\lambda_\beta}e^{\mp i\int_{\beta_0}^{\beta} d\beta'/\lambda_\beta}}{\beta^{\Delta/2}}\right\}\,. \tag{56}$$

Note that if $|\Delta| \ll 1$, the WKB solution is in fact valid throughout the cochlea.

---

[3] Bessel-function solutions to the cochlear transmission-line equations were first obtained by Zwislocki (1948).

[4] Note that the spatial variable in Eqs. (46) and (49) is β and not χ; the formulas of Sec. I must thus be modified appropriately to obtain, for example, the projection operators given in Table II.

Series	Region	$\mathcal{B}_\pm$	$\widehat{P}_\pm$	$Z_\pm$
Hankel	$\beta \ll 1$	$\tilde{\beta}^\nu H_\nu^\pm(\tilde{\beta})$	$\mp\frac{i\pi}{8}\tilde{\beta}H_\nu^\pm\left\{H_{\nu-1}^\mp + (2\nu/\tilde{\beta})H_\nu^\mp - H_{\nu+1}^\mp - 2H_\nu^\mp\frac{d}{d\tilde{\beta}}\right\}$	$\frac{\mp 2i\alpha H_\nu^\pm}{H_{\nu-1}^\pm + (2\nu/\tilde{\beta})H_\nu^\pm - H_{\nu+1}^\pm}$
WKB	$\beta \gg \frac{\sqrt{\lvert\Delta(\Delta-2)\rvert}}{8N}$	$A_\pm\frac{\sqrt{\lambda_\beta}e^{\mp i\int_{\beta_0}^{\beta} d\beta'/\lambda_\beta}}{\beta^{\Delta/2}}$	$\frac{1}{2}\left\{\left[1 \mp \frac{i}{2}\left(\lambda'_\beta - \Delta\lambda_\beta/\beta\right)\right]\hat{1} \pm i\lambda_\beta\frac{d}{d\beta}\right\}$	$\frac{4N\alpha\lambda_\beta}{1 \pm i(\lambda'_\beta - \Delta\lambda_\beta/\beta)/2}$

Table II. Projection operators $\widehat{P}_\pm^{\mathcal{B}}$ and wave impedances $Z_\pm^{\mathcal{B}}$ for the model parameterization of symmetry breaking outlined in Sec. II. The primes denote differentiation with respect to β and the function

$$\alpha(x) \equiv \left(\bar{M}/C\right)^{1/2} .$$

The constants $A_\pm$, determined by asymptotic matching, are given by Eqs. (61).

3. Asymptotic matching

When N is sufficiently large (or Δ small), the approximate solutions (54) and (56) have an overlapping region of validity, namely those values of β such that

$$\frac{\sqrt{|\Delta(\Delta-2)|}}{8N} \ll \beta \ll 1\,. \tag{57}$$

In that region the solutions can be matched to provide an approximate solution throughout the cochlea.

Consider a anterograde wave traveling along the organ of Corti. As $\hat{\beta} \equiv 4N\beta$ increases, the Hankel wave assumes the form (Abramowitz and Stegun 1964)

$$P \sim \sqrt{\frac{2}{\pi}}\frac{e^{i\pi(1+2\nu)/4}}{(4N)^{\Delta/2}} \times \frac{e^{-i4N\beta}}{\beta^{\Delta/2}} \qquad (4N\beta \gg 1)\,. \tag{58}$$

Similarly, at values $\beta \ll 1$ an anterograde WKB wave becomes

$$P \sim \frac{e^{i4N\beta_0}}{\sqrt{4N}} \times \frac{e^{-i4N\beta}}{\beta^{\Delta/2}} \qquad (\beta \ll 1)\,. \tag{59}$$

Note that the dependence on β is identical with that of the asymptotic form of the Hankel waves. Equating those asymptotic forms yields the relations

$$P \approx \sum_{-}^{+} \begin{cases} \tilde{\beta}^{\nu} H_{\nu}^{\pm}(\tilde{\beta}), & \text{for } \beta \ll 1; \\ A_{\pm}\dfrac{\sqrt{\lambda_\beta}\, e^{\mp i\int_{\beta_0}^{\beta} d\beta/\lambda_\beta}}{\beta^{\Delta/2}}, & \text{for } \beta \gg \sqrt{|\Delta(\Delta-2)|}/8N; \end{cases} \tag{60}$$

where

$$A_{\pm} \equiv \sqrt{\frac{2}{\pi}}(4N)^{\nu} e^{\mp i\left[4N\beta_0 + \pi(1+2\nu)/4\right]}\,, \tag{61}$$

and, once again, $\sum_{-}^{+}\{\cdot\}$ represents any linear combination of its arguments. Equations (60) provide, for any value of Δ, approximate solutions to the transmission-line equations valid throughout the cochlea. Note that a single Hankel wave matches smoothly onto a single WKB wave. The implications of that smooth, one-to-one matching for the reflection of cochlear waves are explored, first in a concrete example and then more generally, in subsequent sections.

III. Reflection of Retrograde Waves

The wave components defined above can now be applied to a discussion of cochlear reflection. Many of the general techniques used here for quantifying cochlear reflection may prove useful in other contexts (e.g., exploring the role of mechanical inhomogeneities in generating otoacoustic emissions). In order to eliminate complications caused by end effects, this section first solves, for an infinite cochlea, the cochlear scattering problem discussed by other authors in a finite cochlea (de Boer et al. 1986b; Viergever 1986; Kaernbach et al. 1987). To explore the effect of basal boundary conditions on the reflection coefficient, the scattering problem is then solved for a finite cochlea using several different boundary conditions at the stapes. Finally, the scattering from a step discontinuity in the stiffness of the organ of Corti is computed and the result interpreted in terms of power flow.

A. Reflection in an infinite cochlea

As emphasized by Viergever (1986) and Kaernbach et al. (1987), exploration of reflection intrinsic to the cochlea requires eliminating reflections from the basal boundary. Such is most simply accomplished by eliminating the boundary altogether and imagining the cochlea as extending infinitely in the negative-x direction. In such an infinite cochlea the local characteristic angular frequency continues to increase without bound beyond ω_{c_0} as one travels basalward past $x = 0$ toward $x = -\infty$.

Consider then the analog of a plane-wave scattering problem in a cochlear model of the family discussed in Sec. II. Imagine driving the model backwards from a point x_{drive} at a frequency such that $1 > \beta_{\text{drive}} \gg \sqrt{|\Delta(\Delta-2)|}/8N$ so that, locally, the WKB approximation is valid and a retrograde WKB wave is launched upon the basilar membrane. As that wave travels basally the local value of β becomes ever smaller, the wavelength changes ever more rapidly, and (if $\Delta \neq 0$) the WKB approximation breaks down. As the wave continues toward $-\infty$, however, the local value of β eventually becomes small enough that the wave assumes the form of a retrograde Hankel wave $\tilde{\beta}^{\nu} H_{\nu}^{-}(\tilde{\beta})$. That form is maintained, becoming more accurate as $\beta \to 0$.

Since the WKB and Hankel waves match smoothly onto one another in their common region of validity (see Sec. II), one might suspect that reflection is small everywhere basal

to the driving point. That suspicion can be quantified by computing the dimensionless traveling-wave ratio $\overleftarrow{R}^{B}$, defined as the ratio of the waves traveling in the two directions along the organ of Corti:

$$\overleftarrow{R}^{B}(x,\omega) \equiv \left.\frac{P_{+}^{B}}{P_{-}^{B}}\right|_{\text{cochlea driven backward}} . \tag{62}$$

Here one imagines the cochlear transmission line to be driven "in reverse" by a pressure source apical to x (i.e., at $x_{\text{drive}} > x$). The diacritical arrow indicates that the primary wave is traveling toward the stapes. $|\overleftarrow{R}^{B}|$ then provides a measure of the relative magnitude of the reflected wave. That wave is a superposition of wavelets scattered (any number of times) from all points in the cochlea basal to x. The primary wave $P_{-}^{B}(x,\omega)$ thus acts as a probe, returning as $P_{+}^{B}(x,\omega)$ with information both about the basal portion of the cochlea and (in a finite cochlea) about the cochlear boundary with the middle ear.

To compute $\overleftarrow{R}^{B}$ for an infinite cochlea one solves (e.g., numerically) the transmission-line equations for P subject to the "boundary condition" that[5]

$$\lim_{x\to-\infty} P(x,\omega) = P_{-}^{H}(x,\omega) \propto \tilde{\beta}^{\nu} H_{\nu}^{-}(\tilde{\beta}) ; \tag{63}$$

that is, at infinite distance from the driving point the solution consists of that linear combination of Bessel functions that at larger values of x represents a single wave traveling away from the driving point. One can then determine the traveling-wave ratio $\overleftarrow{R}^{B}$ at various points in the cochlea by applying the appropriate projection operators $\hat{P}_{\pm}^{B}$ to the solution P:

$$P_{\pm}^{B}(x,\omega) = \hat{P}_{\pm}^{B}(x,\omega)\{P(x,\omega)\} . \tag{64}$$

As the wave travels basally away from x_{drive} the wave components change form (evolving from WKB waves at large positive x to Hankel waves as $x \to -\infty$), and consequently the choice of projection operators will vary with position. Here, the wave components are

[5] As $\tilde{\beta} \to 0$ the Hankel function $H_{\nu}^{-}(\tilde{\beta})$ has the limiting form (Abramowitz and Stegun 1964)

$$H_{\nu}^{-}(\tilde{\beta}) \sim \begin{cases} -(2/i\pi)\ln\tilde{\beta}, & \text{for } \nu = 0 \\ (1/i\pi)\Gamma(\nu)\left(\tilde{\beta}/2\right)^{-\nu}, & \text{for } \mathrm{Re}\nu > 0. \end{cases} \tag{5.1}$$

Thus for positive ν the amplitude of the pressure P approaches a constant value as $x \to -\infty$.

computed using projection operators determined from the matched asymptotic expansion outlined in Sec. II:

$$\widehat{P}_{\pm}^{B} \longmapsto \widehat{P}_{\pm} \equiv \widehat{P}_{\pm}^{H|W} \equiv \begin{cases} \widehat{P}_{\pm}^{H}, & \text{for } \beta \ll 1; \\ \widehat{P}_{\pm}^{W}, & \text{for } \beta \gg \sqrt{|\Delta(\Delta-2)|}/8N. \end{cases} \tag{65}$$

$\widehat{P}_{\pm}^{H}$ and $\widehat{P}_{\pm}^{W}$ are given in Table II.

Figure 1 shows the results of such a calculation for the model ($\Delta = 1$) of de Boer et al. (1986ab and Kaernbach et al. 1987, rescaled to an "infinite cat"). The figure plots

$$\left|\overleftarrow{R}(\beta,\omega_s)\right| \equiv \left|\overleftarrow{R}^{H|W}\left(\beta(x,\omega_s),\omega_s\right)\right| \tag{66}$$

at the fixed stimulus frequency

$$\omega_s/2\pi \equiv 1 \text{ kHz} . \tag{67}$$

When quantities such as $\overleftarrow{R}$ appear without superscripts identifying the underlying basis waves, those waves are understood to be taken in accord with the matched asymptotic expansion. Since ω_s is fixed, the independent variable $\beta(x,\omega_s)$ is simply a remapping of position, small values of β corresponding to regions of large characteristic frequency near the base. At fixed frequency, Eq. (39) for $\omega_c(x)$ implies that $\ln\beta$ is a linear function of x. Since the long-wavelength approximation underlying one-dimensional transmission-line models of cochlear mechanics presumably breaks down when the wavelength becomes small in the region about maximal membrane velocity ($\beta \approx 1$), the present discussion of cochlear reflections is limited to the basal, small-β region of the cochlea ($\beta < 1/2$).

The calculated reflection coefficient is everywhere only a small fraction of a percent ($|\overleftarrow{R}| \sim 1/1000$). Note that nonzero values for $\overleftarrow{R}$ result from the use of projection operators whose eigenfunctions are not exact solutions to the transmission-line equations. Similar values for the reflection coefficient are found in models with other values of Δ, including $\Delta = 0$. Thus wave reflection due to the secular variation of mechanical characteristics along the cochlea appears negligible in conventional transmission-line models, regardless of the degree of symmetry-breaking exhibited by the model (see Sec. IV). The empirical conclusion that wave reflection must be small in the real cochlea at high sound pressure

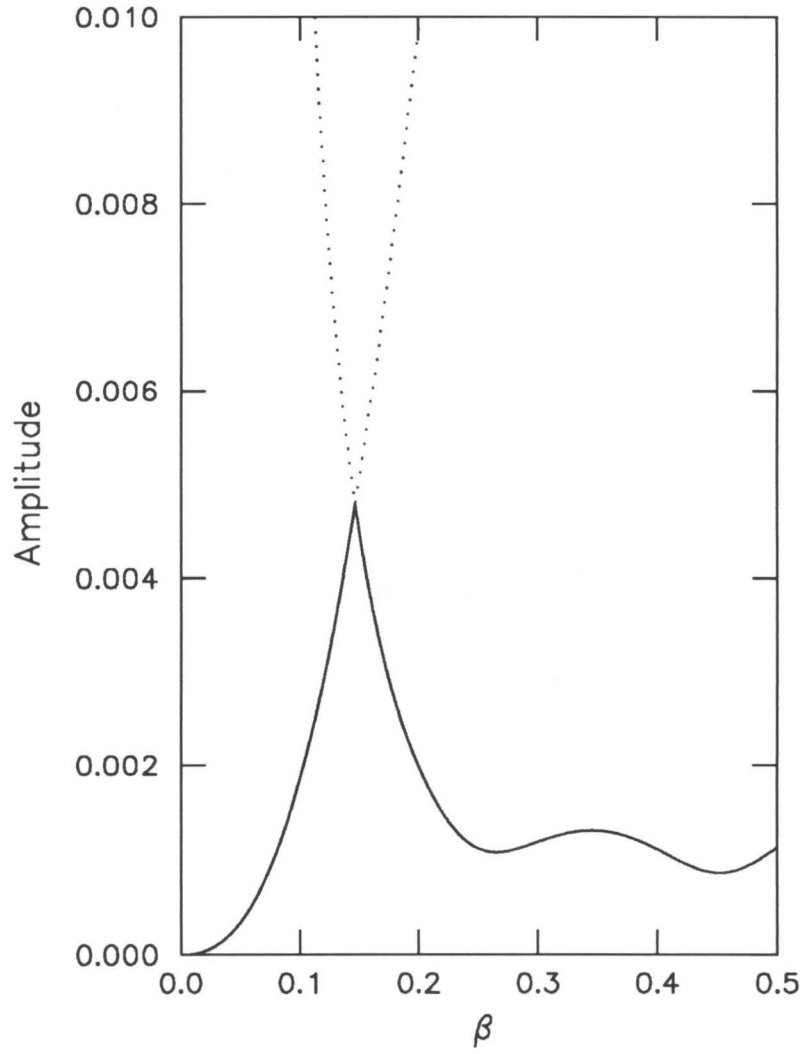

Figure 1. Amplitude of the reflection coefficient $\overleftarrow{R}(\beta, \omega_s)$ (———) for the model ($\Delta = 1$) of de Boer et al. (1986ab and Kaernbach et al. 1987) rescaled to the cat [that is, $\omega_{c_0}/2\pi \rightarrow 57$ kHz and $l \rightarrow 5$ mm from Liberman (1982); N and δ were kept constant at their original values] and then made infinite by continuing all functions to $x = -\infty$ (or, equivalently, to $\beta = 0$). The stimulus frequency is fixed at $\omega_s/2\pi = 1$ kHz. Far from the driving point (i.e., as $x \rightarrow -\infty$), the pressure was required to approach a function proportional to $H_0^-(\tilde{\beta})$. The projection operators $\widehat{P}_\pm$ used to compute the reflection coefficient were selected according to the matched asymptotic expansion [Eqs. (60)] and switch from $\widehat{P}_\pm^H$ to $\widehat{P}_\pm^W$ at the point of intersection of the curves (i.e., near $\beta \approx 0.15$). Note that $|\overleftarrow{R}|$ is everywhere only a fraction of a percent. The dotted lines continue the corresponding solid lines through the overlapping regions of validity and indicate, for example, that whereas at small β a single retrograde Hankel wave H_0^- suffices to represent the solution, WKB waves $W_\pm$ traveling in *both* directions are needed to produce the same pressure distribution.

levels thus extends to a broad class of conventional cochlear models whether or not they accurately represent the geometry of the inner ear.

Note that considerably larger reflections ($|\overleftarrow{R}| \approx 1/2$) have been obtained by other authors in finite cochlear models (de Boer et al. 1986b; Viergever 1986; Kaernbach et al. 1987). Since the model cochlea itself is not the source of those reflections, they must originate at the basal boundary at the stapes.

B. Boundary reflection in a finite cochlea

To understand the origin of the sizable reflections obtained by others, it is convenient to reexpress the scattering problem outlined above in the language of impedances. The impedance $\overleftarrow{Z}$ looking basalward toward the stapes is defined by[6]

$$\overleftarrow{Z}(x,\omega) \equiv -\frac{P}{U} \equiv -\left.\frac{P_+^{\mathcal{B}} + P_-^{\mathcal{B}}}{U_+^{\mathcal{B}} + U_-^{\mathcal{B}}}\right|_{\text{cochlea driven backward}} , \tag{68}$$

where P and U have been decomposed into waves traveling in opposite directions. Reexpressing Eq. (68) in terms of the wave impedances $Z_\pm^{\mathcal{B}}(x,\omega)$ and the traveling-wave ratio $\overleftarrow{R}^{\mathcal{B}}(x,\omega)$ yields (Shera 1986a)

$$\overleftarrow{Z} = Z_-^{\mathcal{B}} \left\{ 1 + \overleftarrow{R}^{\mathcal{B}} \frac{Z_+^{\mathcal{B}} + Z_-^{\mathcal{B}}}{Z_+^{\mathcal{B}} - \overleftarrow{R}^{\mathcal{B}} Z_-^{\mathcal{B}}} \right\} . \tag{69}$$

Note that Eq. (69) is simply Eq. (68) rewritten in the language of wave impedances and reflection coefficients. Solving for the traveling-wave ratio one obtains

$$\overleftarrow{R}^{\mathcal{B}} = \frac{\overleftarrow{Z}/Z_-^{\mathcal{B}} - 1}{\overleftarrow{Z}/Z_+^{\mathcal{B}} + 1} . \tag{70}$$

The value of $\overleftarrow{R}^{\mathcal{B}}$ depends on the choice of wave components through the wave impedances $Z_\pm^{\mathcal{B}}$. Whereas the wave impedances $Z_\pm^{\mathcal{B}}$ contain only local information, the impedance $\overleftarrow{Z}$, like the traveling-wave ratio $\overleftarrow{R}^{\mathcal{B}}$, contains information about the entire cochlea basal to the driving point, including the boundary with the middle ear.

---

[6] Figure 2 of Kaernbach et al. (1987) gives $\overleftarrow{Z}(x,\omega_s)$ at $\omega_s/2\pi = 1$ kHz for their model when the termination impedance at the stapes is the local value of the characteristic impedance $Z_c(0,\omega_s)$. Kaernbach et al. refer to $\overleftarrow{Z}(x,\omega)$ as the "impedance measured to the left."

Note that Eq. (70) for the traveling-wave ratio implies that $\overleftarrow{R}^{\mathcal{B}}$ is zero if $\overleftarrow{Z} = Z_{-}^{\mathcal{B}}$, the local value of the retrograde wave impedance. In the absence of reflections, the ratio

$$\mathcal{A}^{\mathcal{B}}(x,\omega) \equiv \frac{\overleftarrow{Z}}{Z_{-}^{\mathcal{B}}} \tag{71}$$

thus has the value $+1$, and deviations from that value evince the presence of a reflected wave. In addition, terminating the cochlear transmission line with the impedance $Z_{-}^{\mathcal{B}}$ at its basal end [i.e., imposing the condition that $\overleftarrow{Z}_0(\omega) \equiv Z_{-}^{\mathcal{B}}(0,\omega)$] eliminates the reflection of the corresponding retrograde wave component $\mathcal{B}_{-}$ incident upon the boundary.

Figure 2 plots the amplitude and phase of $\mathcal{A}(\beta,\omega_s) \equiv \mathcal{A}^{H|W}(\beta,\omega_s)$ for the model ($\Delta = 1$) of de Boer et al. (1986ab and Kaernbach et al. 1987, rescaled to the cat) for two different termination conditions at the stapes. The first condition requires that $\overleftarrow{Z}_0(\omega_s) \equiv Z_{-}^{H}(0,\omega_s)$. Since the Hankel wave components represent good approximate solutions to the transmission-line equations at small β the termination impedance $Z_{-}^{H}(0,\omega_s)$ creates little reflection. The second condition follows de Boer et al. (de Boer et al. 1986ab; Kaernbach et al. 1987) and terminates the cochlear transmission line in its characteristic impedance [so that $\overleftarrow{Z}_0(\omega_s) \equiv Z_{-}^{V} = Z_c(0,\omega_s)$]. That termination produces significant boundary reflection, as is apparent from the oscillatory variations in the amplitude and phase of $\mathcal{A}$ created by the alternating constructive and destructive interference between the waves $P_{-}(x,\omega_s)$ and $P_{+}(x,\omega_s)$ traveling in opposite directions along the organ of Corti.

Equation (70) can be used to estimate the boundary reflection produced by terminating the cochlear transmission line with its characteristic impedance Z_c (de Boer et al. 1986ab; Viergever 1986; Kaernbach et al. 1987):

$$\overleftarrow{R}\Big|_{\overleftarrow{Z}_0 = Z_c} = \frac{Z_c/Z_{-}^{H} - 1}{Z_c/Z_{+}^{H} + 1} \,. \tag{72}$$

Substituting the Hankel wave impedances $Z_{\pm}^{H}$ from Table II and evaluating the result for the model of de Boer et al. (1986ab and Kaernbach et al. 1987, rescaled to the cat) gives

$$\left|\overleftarrow{R}_0(\omega_s)\right|_{\overleftarrow{Z}_0 = Z_c(0,\omega_s)} \approx 0.55 \,. \tag{73}$$

The impedance mismatch at the basal boundary occurs because whereas the Hankel wave impedance Z_{-}^{H} has a large imaginary part, the termination impedance Z_c is nearly real. Thus by using the characteristic impedance de Boer et al. (1986ab and Kaernbach et al. 1987) overestimate (by at least a factor of 500) the internal reflection actually predicted by their model.

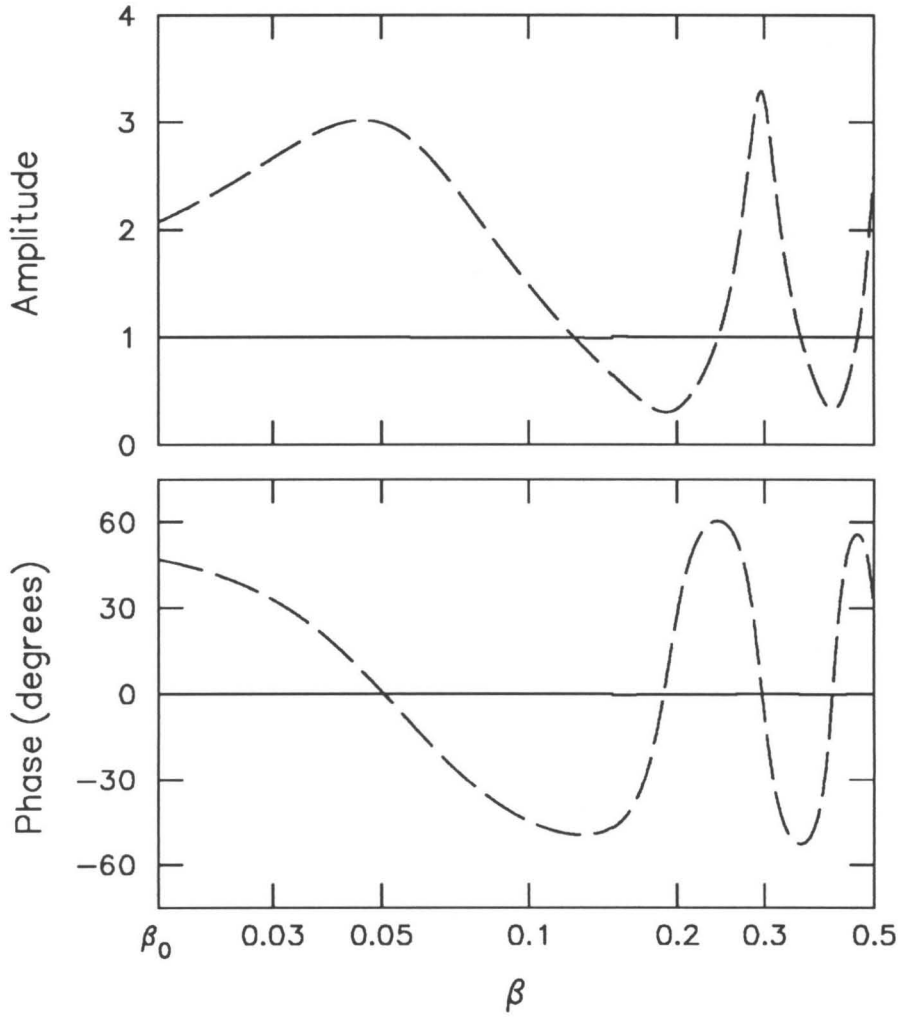

Figure 2. Amplitude and phase of

$$\mathcal{A}(\beta, \omega_s) \equiv \frac{\overleftarrow{Z}}{Z_-}$$

computed for the model ($\Delta = 1$) of de Boer et al. (1986ab and Kaernbach et al. 1987, rescaled to the cat as in Fig. 1) with two different boundary conditions at the stapes: (———) $\mathcal{A}$ computed when the cochlear transmission line is terminated at the stapes with the Hankel wave impedance $Z_-^H(\tilde{\beta}_0)$; (— — —) $\mathcal{A}$ computed when the cochlear transmission line is terminated with its characteristic impedance $Z_c(0, \omega_s)$. The wave impedance Z_- in the definition of $\mathcal{A}$ was selected according to the matched asymptotic expansions and switches from Z_-^H to Z_-^W at $\beta \approx 0.15$. Note that the β-axis is logarithmic; at fixed frequency $\ln \beta$ is a linear function of x [cf. Eq. (39) for $\omega_c(x)$]. Oscillatory variations in the amplitude and phase are created by interference between waves traveling in opposite directions along the organ of Corti. Those oscillations are essentially nonexistent when the cochlear transmission line is terminated with the wave impedance $Z_-^H(\tilde{\beta}_0)$.

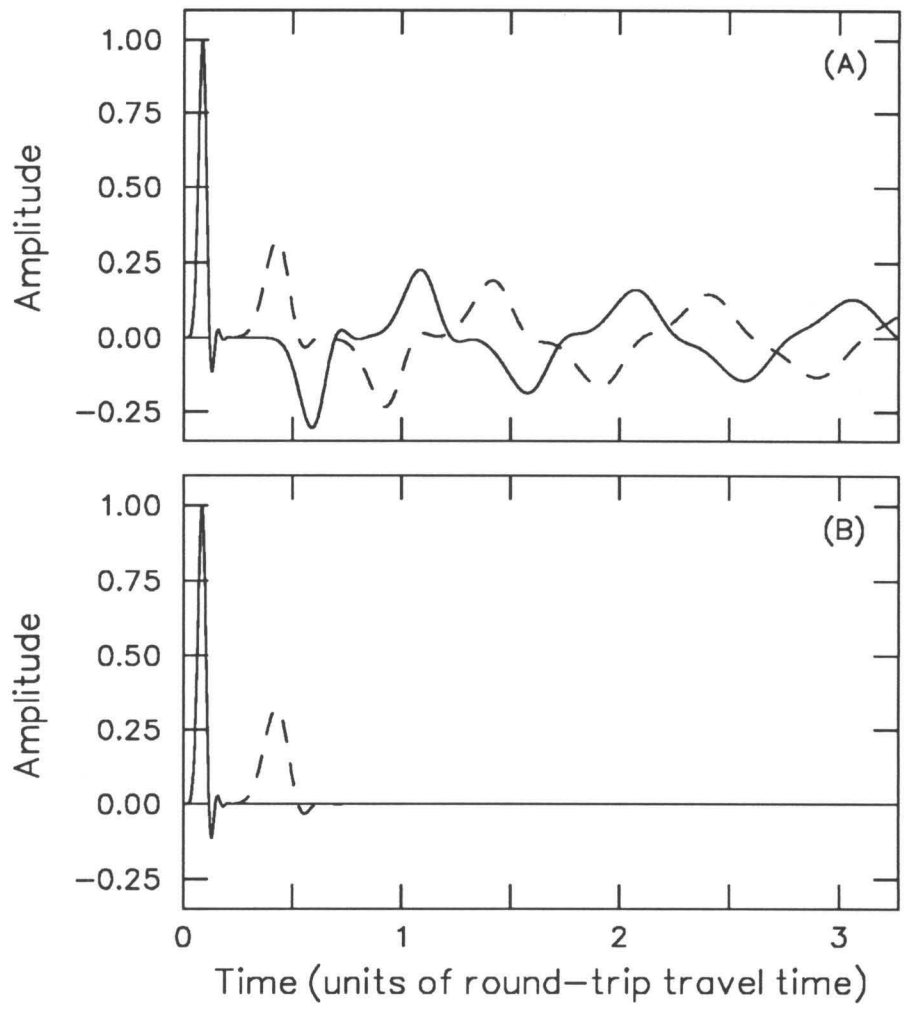

Figure 3. Time-varying amplitudes of the traveling-wave components $p_{\pm}(x_{\text{obs}}, t)$ recorded at an observation point x_{obs} after an impulse $p_0\delta(t)$ is applied at the stapes in a model with $\Delta = 0$: (———) amplitude of the anterograde pressure wave $p_{+}(x_{\text{obs}}, t)$; (— — —) amplitude of the retrograde pressure wave $p_{-}(x_{\text{obs}}, t)$. The total pressure $p(x_{\text{obs}}, t)$ is, at every instant, equal to the sum of the wave components $p_{\pm}(x_{\text{obs}}, t)$. The two panels correspond to different boundary conditions at the stapes: (A) the case $\overleftarrow{Z}_0 = 0$ (short circuit boundary condition) so that $\overleftarrow{R}_0 = -1$; (B) the case $\overleftarrow{Z}_0 = Z^W_-$ so that $\overleftarrow{R}_0 \approx 0$. The observation point x_{obs} was taken so that $\omega_c(x_{\text{obs}})/2\pi = 7$ kHz, and the cochlear transmission line was terminated in an open circuit at a position x_{apical} corresponding to a 3 kHz characteristic frequency (thus, $\overrightarrow{R}_{x_{\text{apical}}} = +1$). In both panels the pressure $p(x_{\text{obs}}, t)$ is normalized to a maximum value of one and times t are expressed in units of the approximate round-trip travel time. The parameters defining the model are those of Fig. 1 except that (for clarity of presentation) $\omega_{c_0}/2\pi = 20$ kHz and $\delta = 0.5$. Whereas in panel (A) waves continue to echo back and forth between the stapes and helicotrema, in panel (B) all energy reflected from the impedance mismatch at the apex subsequently "disappears" at the stapes, where the termination impedance makes the cochlea appear *infinite* to WKB waves incident upon the boundary.

1. Reflections in the time domain

The absence of reflection of retrograde waves from the basal boundary when the model is terminated in the retrograde wave impedance Z_-^B is confirmed by the time-domain calculation illustrated in Fig. 3. That figure plots the time-varying amplitudes of the pressure waves $p_\pm(x_{\rm obs},t)$ resulting from an impulse $p_0\delta(t)$ applied at the stapes in a model with $\Delta = 0$. (The calculations are considerably simplified when $\Delta = 0$—the scaling case corresponding to the cat cochlea—but qualitatively similar results are expected for other values as well.) The waves components $p_\pm(x_{\rm obs},t)$ were computed numerically by implementing the transmission-line equations, their boundary conditions, and Eq. (25) for $P_\pm^W$ in the time-domain (e.g., by replacing impedances with impedance operators acting through convolution).

Two calculations are shown, corresponding to different boundary conditions at the stapes. In both cases, however, the cochlear transmission line is "cut" abruptly at a point $x_{\rm apical}$ well before the helicotrema (but satisfying $x_{\rm apical} > x_{\rm obs}$) so that substantial energy is reflected back toward the stapes (open circuit boundary condition so that $\overrightarrow{R}_{x_{\rm apical}} = +1$). In the first case, the basal termination impedance $\overleftarrow{Z}_0 = 0$ (short circuit boundary condition) so that $\overleftarrow{R}_0 = -1$. Note that energy continues to echo back and forth—passing the observation point $x_{\rm obs}$ in alternating directions—between the stapes and helicotrema, which are both, here, perfect reflectors. Since $\overleftarrow{R}_0\,\overrightarrow{R}_{x_{\rm apical}} = -1$, the pulses $p_\pm(x_{\rm obs},t)$ switch polarity on each round trip. In the second case, the termination impedance $\overleftarrow{Z}_0 = Z_-^W$, and $\overleftarrow{R}_0 \approx 0$. (Since $\Delta = 0$, the WKB waves $W_\pm$ everywhere provide good approximate solutions to the transmission line equations.) All energy initially reflected from the impedance mismatch at the apex subsequently "disappears" at the stapes, where the termination impedance makes the cochlea appear infinite to WKB waves incident upon the boundary.

2. An apparent reflection asymmetry

The previous results can be used to show how terminating a model cochlear transmission line in its characteristic impedance can give rise to an apparent asymmetry in the reflection of cochlear waves. To test for an asymmetry in the reflection characteristics of the line one might imagine, for example, extracting a section of the transmission line

and terminating it with a fixed impedance at one end. While driving the line from the other end, one could measure (at the driving point) the resulting reflection coefficient. If one were then to repeat the measurement after interchanging the termination and driving points, any asymmetry would manifest itself in a different value for the measured reflection coefficient.

Figure 4 plots the expected results of a series of such gedanken experiments performed (numerically) on sections of systematically varying length extracted from the model of de Boer et al. (1986ab and Kaernbach et al. 1987, rescaled to the cat). As always, the stimulus frequency is fixed at $\omega_s/2\pi \equiv 1$ kHz, and the apical end of the extracted section is, in each case, taken to be the point corresponding to a characteristic frequency of $\omega_c/2\pi = 2$ kHz. Thus $\beta = \omega_s/\omega_c = 1/2$ at the apical end of the section. The location x_{basal} of the basal end of the section is varied systematically, beginning at $x_{\text{basal}} = 0$ (i.e., at the point with $\omega_c = \omega_{c_0}$) and proceeding to larger values of x_{basal} so that the sections get progressively shorter at the basal end. A particular section of the transmission line therefore has values of β that vary over the range $\beta_{\text{basal}} \leq \beta \leq 1/2$, where $\beta_{\text{basal}} = \omega_s/\omega_c(x_{\text{basal}})$. The value of β_{basal}, recorded along the abscissa, thus fixes the length (and range of characteristic frequencies) of the section. For small values of β_{basal} the extracted section includes basal regions of the model cochlea in which the wavelength changes rapidly. As β_{basal} increases those regions are "sliced off," and the section appears more homogeneous to waves at the stimulus frequency.

The figure plots both $|\overleftarrow{R}|$, measured at the apical end (i.e., at $\beta = 1/2$) of the section, and $|\overrightarrow{R}|$, measured at the basal end (i.e., at $\beta = \beta_{\text{basal}}$).[7] The reflection coefficients are plotted for two different termination conditions. In the first (panel A), the section is made to appear infinite to Hankel/WKB waves incident upon the boundaries. Thus at the apical end the termination impedance is the local value of Z_+ and at the basal end the value of Z_-. In the second (panel B), the line is made to appear infinite to geometric-optical waves by terminating both ends with the local characteristic impedance Z_c. Unlike the Hankel/WKB waves, the geometric-optical waves are not accurate approximate solutions to the transmission-line equations except in the limit $|\lambda'| \to 0$.

[7] The equation for $\overrightarrow{R}$ can be obtained from Eq. (70) for $\overleftarrow{R}$ by switching the + and − signs and reversing the directions of the diacritical arrows (see the Appendix).

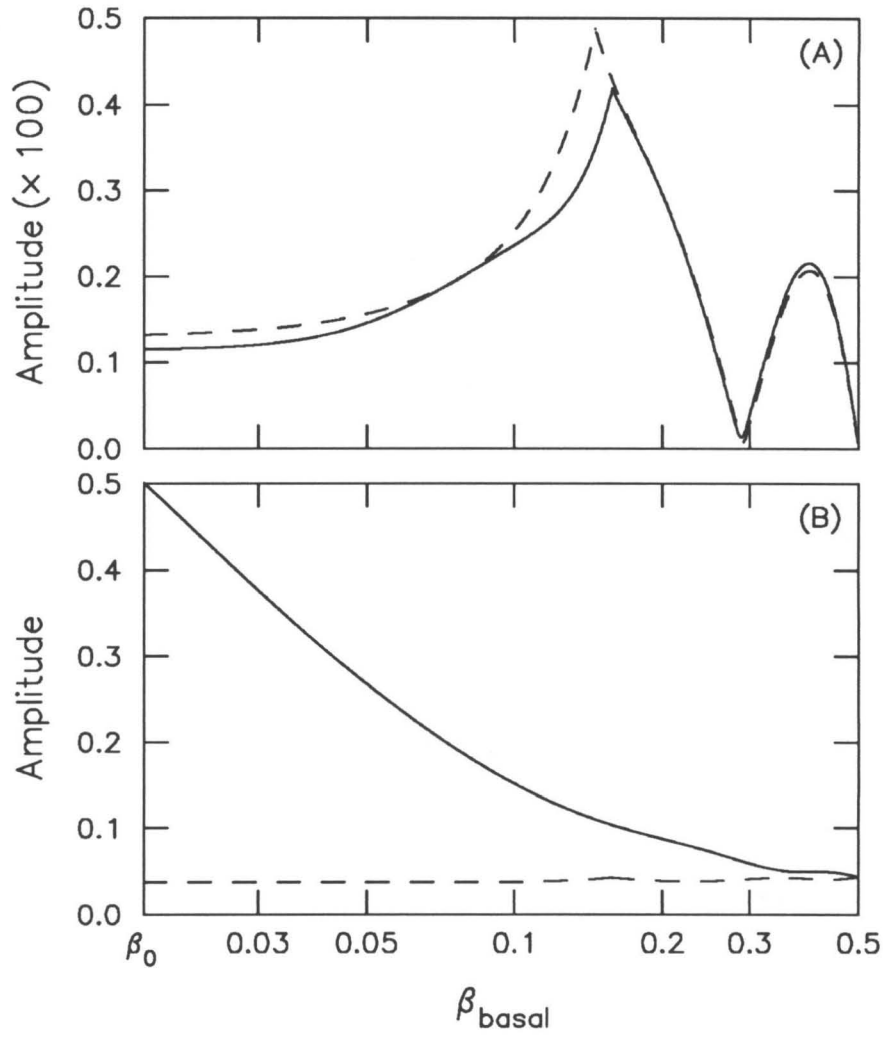

Figure 4. Amplitude of the reflection coefficients $\overleftarrow{R}(\beta_{\text{basal}}, \omega_s)$ (———) and $\overrightarrow{R}(1/2, \omega_s)$ (– – –) at a stimulus frequency of $\omega_s/2\pi = 1$ kHz computed at the basal (i.e., $\beta = \beta_{\text{basal}}$) and apical (i.e., $\beta = 1/2$) ends, respectively, of sections of cochlear transmission line extracted from the cochlear model of de Boer et al. (1986ab and Kaernbach et al. 1987), rescaled to the cat as in Fig. 1. The location of the basal boundary, indicated by β_{basal}, is varied along the abscissa. The projection operators $\widehat{P}_\pm$ used to compute the reflection coefficient were selected according to the matched asymptotic expansions [Eqs. (60)] and switch from $\widehat{P}_\pm^H$ to $\widehat{P}_\pm^W$ at the points where the derivatives change discontinuously (near $\beta \approx 0.15$). Key to panels: (A) reflection coefficients measured when the termination impedances at the ends of the section are the local values of the Hankel/WKB wave impedances $Z_\pm$. (B) reflection coefficients measured when the termination impedances are the local values of the characteristic impedance Z_c. Note that, for clarity, the amplitudes in panel (A) have been multiplied by a factor of 100. Terminating the cochlear transmission line in its characteristic impedance gives rise to a pronounced asymmetry between $|\overrightarrow{R}|$ and $|\overleftarrow{R}|$, which might, mistakenly, be ascribed to an internal reflection asymmetry between forward- and backward-traveling waves.

The figure illustrates clearly how the choice of boundary conditions can give rise to an apparent asymmetry in cochlear reflection characteristics. When a section is made to appear infinite to Hankel/WKB waves at both ends, $|\overrightarrow{R}|$ and $|\overleftarrow{R}|$ are small and nearly identical. When the section is terminated in its characteristic impedance, however, the predicted reflection coefficients $|\overrightarrow{R}|$ and $|\overleftarrow{R}|$ are quite different, especially for small β_{basal} for which the measured section contains regions in which the wavelength changes rapidly and the geometric-optical waves constitute especially poor approximate solutions to the transmission-line equations. The asymmetry arises because boundary reflection from the termination is quite different in magnitude at the two ends, being rather small at $\beta = 1/2$ and rather large at $\beta = \beta_{\text{basal}}$. The asymmetry in wave reflection found by other authors (de Boer et al. 1986b; Viergever 1986; Kaernbach et al. 1987) can thus be traced to their termination of the cochlear transmission line.

3. Comparison with the geometric-optical series

In a nonuniform medium such as the cochlea the definition of forward- and backward-traveling waves is to some extent arbitrary. For the family of conventional models outlined in Sec. II, this paper defines the traveling-wave components $P_{\pm}$ in terms of the Hankel and WKB waves given in Table II. Using Hankel and WKB waves (in their respective regions of validity) as the "basis set" has the advantage that, in addition to having nearly constant power flow, they provide good approximate solutions to the transmission-line equations and so propagate independently without substantial reflection or violation of energy conservation (Zweig et al. 1976). Underlying Bremmer's geometric-optical series used by Viergever (1986) for the analysis of cochlear reflections is a different definition for the traveling-wave components (see Sec. I). By computing the "reflection coefficient" based on the geometric-optical series, this section demonstrates how adopting as one's basis set waves $\mathcal{B}_{\pm}$ that are not good approximate solutions to the transmission-line equations can lead to results that are difficult to interpret.

Using the traveling-wave components resulting from the geometric-optical series leads, of course, to a different definition for the reflection coefficient. In terms of the impedance $\overleftarrow{Z}$, the reflection coefficient for the geometric-optical series is given by

$$\overleftarrow{R}^{V} \equiv \left.\frac{P_{+}^{V}}{P_{-}^{V}}\right|_{\text{cochlea driven backward}} = \frac{\overleftarrow{Z}/Z_{-}^{V} - 1}{\overleftarrow{Z}/Z_{+}^{V} + 1}, \tag{74}$$

where the $Z_{\pm}^{V}$ both equal the characteristic impedance Z_c of the transmission line. Consequently, $\overleftarrow{R}^{V} = 0$ if $\overleftarrow{Z} = Z_c$; terminating a transmission line in its characteristic impedance thus eliminates the reflection of "geometric-optical waves" $V_{\pm}$ incident upon the boundary. Since the functions $V_{\pm}(\chi,\omega)$ are not good approximate solutions to the transmission-line equations, however, the physical interpretation of $\overleftarrow{R}^{V}$ as a reflection coefficient is somewhat problematic.

Shown in Fig. 5 is the "reflection coefficient" $|\overleftarrow{R}^{V}(\beta,\omega_s)|$ for the geometric-optical series computed by using the termination $Z_c(0,\omega_s)$.[8] Shown for comparison is the reflection coefficient $|\overleftarrow{R}(\beta,\omega_s)|$ computed from the curve in Fig. 2 corresponding to the same termination. $|\overleftarrow{R}|$ and $|\overleftarrow{R}^{V}|$ are of similar average amplitude except close to the boundary where they diverge and approach values consistent with the underlying difference in the traveling-wave components. Recall that it is near the boundary ($\beta \lesssim 1/10$) that the model wavelength changes most rapidly and that the difference between the views of the traveling-wave components is most pronounced. For example, whereas $|\overleftarrow{R}|$ approaches the finite value (≈ 0.55) computed above in Eq. (73), $|\overleftarrow{R}^{V}|$ rapidly falls to zero as $\overleftarrow{Z} \to Z_c$.

Farther from the boundary ($\beta \gtrsim 1/10$) the wavelength changes more slowly, and the difference in the definition of traveling-wave components manifests itself in another manner. In that region $|\overleftarrow{R}^{V}|$ oscillates about an average value given by $|\overleftarrow{R}|$. $|\overleftarrow{R}|$ is roughly constant because the WKB waves $W_{\pm}$ provide good approximate solutions to the differential equation, and a fixed linear combination of those waves suffices to satisfy the equation. By contrast, the $V_{\pm}$ constitute poor solutions to the equation, and the linear combination needed to produce a solution varies periodically in space.

To see this more clearly, recall from Sec. I that the osculating parameters provide (as a function of position) the coefficients of the wave components necessary to satisfy

---

[8] The reflection coefficients in this paper have been computed using the appropriate projection operators and are thus correct to "infinite" order. A calculation of $\overleftarrow{R}^{V}$ to first order in the geometric-optical series has been performed by Viergever (1986), yielding [cf. Eq. (1.1)]

$$\overleftarrow{R}^{V}(\chi,\omega)\big|_{\overleftarrow{Z}_0 = Z_c(0,\omega)} = \frac{P_{+}^{V}}{P_{-}^{V}} \tag{8.1}$$

$$\approx -\frac{W_{+}}{W_{-}} \int_0^{\chi} W_{-} \frac{\sigma_{-}^{V}}{\lambda} W_{-}\, d\chi' = \frac{1}{2} \int_{\chi}^{0} \frac{\lambda'}{\lambda} e^{+2i \int_{\chi}^{\chi'} d\chi''/\lambda} d\chi' . \tag{8.2}$$

Figure 2 of Viergever (1986) plots, for his model, the amplitude of Eq. (8.2) at a stimulus frequency of 1 kHz.

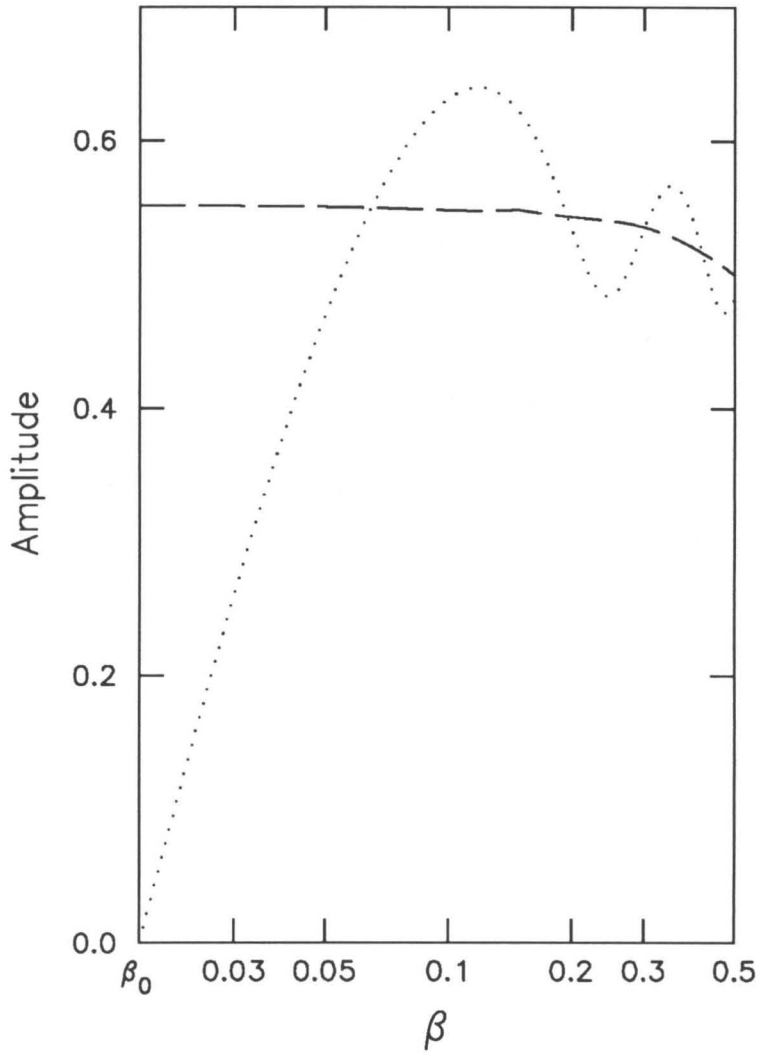

Figure 5. Amplitude of the reflection coefficients $\overleftarrow{R}^V(\beta, \omega_s)$ for the geometric-optical series used by Viergever (1986) and $\overleftarrow{R}(\beta, \omega_s)$ for Hankel/WKB waves compared for the model ($\Delta = 1$) of de Boer et al. (1986ab and Kaernbach et al. 1987, rescaled to the cat as in Fig. 1): (— — —) $|\overleftarrow{R}|$ computed from Eq. (70) with the wave impedances $Z_\pm$ selected according to the matched asymptotic expansion as in Fig. 2; (·····) $|\overleftarrow{R}^V|$ computed from Eq. (74). The boundary condition at the stapes [i.e., $\overleftarrow{Z}_0(\omega) = Z_c(0, \omega)$] guarantees that retrograde "geometric-optical" waves incident upon the boundary are not reflected. Thus $|\overleftarrow{R}^V| \to 0$ at the boundary, and $|\overleftarrow{R}_0| \approx 0.55$, in agreement with the calculation in the text. Away from the boundary, both $|\overleftarrow{R}^V|$ and $|\overleftarrow{R}|$ are large and have similar average amplitudes. The oscillations in $\overleftarrow{R}^V$ indicate, however, that the "geometric-optical" waves $V_\pm$ do not constitute good approximate solutions to the transmission-line equations.

the differential equation. When the wave components $\mathcal{B}_\pm$ satisfy the original differential equation the corresponding osculating parameters $\psi_\pm^{\mathcal{B}}$ are independent of position. The ratio of the osculating parameters is easily obtained from the reflection coefficient. For example, in terms of the "reflection coefficient" $\overleftarrow{R}^V$ the ratio of the osculating parameters for the geometric-optical series is given by

$$\frac{\psi_+^V}{\psi_-^V} = \frac{V_-}{V_+}\overleftarrow{R}^V \; ; \tag{75}$$

analogous expressions hold for other wave components. To obtain the ratio of osculating parameters one multiplies the reflection coefficients given in Fig. 5 by the ratio of the corresponding wave components. At values of $\beta \lesssim 1/2$ the ratio of the wave components is, in each case, almost constant, and the ratio of the osculating parameters can, it turns out, be obtained simply by straightening out the the gentle downward drift in the average value of the reflection coefficients.[9] The ratio of the osculating parameters for the Hankel/WKB approximations is thus essentially constant. The large oscillations apparent in the Bremmer ratio are not, however, eliminated, demonstrating that the $V_\pm$ do not provide good approximate solutions to the transmission-line equations.

C. Reflection from a mechanical inhomogeneity

Although waves are not reflected simply by the secular variation of mechanical characteristics, they can be reflected when discontinuities or other strong inhomogeneities are superimposed upon that more gradual variation. This section solves the scattering problem in a cochlea containing a localized mechanical anomaly in the organ of Corti. The result is interpreted in terms of the power flowing past a point in the cochlea.

In a model of the type introduced in Sec. II.A, assume that the exponential frequency-position map is perturbed to have the form

$$\omega_c(x)/\omega_{c_0} = \begin{cases} (1-\phi)e^{-x/l}, & \text{for } x_0 < x < x_1; \\ e^{-x/l}, & \text{elsewhere.} \end{cases} \tag{76}$$

[9] Because the factors of $\sqrt{\lambda}$ cancel in the ratio,

$$\frac{V_-}{V_+} = \frac{W_-}{W_+} \; ; \tag{9.1}$$

the required "straightening" is the same for each curve.

The anomaly, illustrated in Fig. 6–A for several values of ϕ, corresponds (for $\phi > 0$ in a model with $\Delta = 1$) to a local increase in the compliance C of the organ of Corti.

Imagine driving the model backwards from some point apical to an observation point $x_{\rm obs} > x_1$. The net time-averaged power flowing past the observation point toward the stapes is given by

$$\mathcal{W}_{\rm net} = -\tfrac{1}{2}{\rm Re}PU^* = \tfrac{1}{2}|P|^2{\rm Re}\{1/\overleftarrow{Z}\}\,, \tag{77}$$

where $*$ represents the operation of complex conjugation. Reexpressing the result as a fraction of the incident power flow one obtains

$$\eta \equiv \frac{\mathcal{W}_{\rm net}}{\mathcal{W}_{\rm incident}} = \frac{|P|^2{\rm Re}\{1/\overleftarrow{Z}\}}{|P_-^{\mathcal{B}}|^2{\rm Re}\{1/Z_-^{\mathcal{B}}\}} = |1+\overleftarrow{R}^{\mathcal{B}}|^2\frac{{\rm Re}\{1/\overleftarrow{Z}\}}{{\rm Re}\{1/Z_-^{\mathcal{B}}\}}\,. \tag{78}$$

Figure 6–B plots $\eta(\phi)$ for the model of de Boer et al. (1986ab and Kaernbach et al. 1987, rescaled to the cat) at the stimulus frequency $\omega_{\rm s}/2\pi = 1$ kHz. Since WKB waves represent good approximate solutions to the equations near $x_{\rm obs}$ (the observation point was chosen so that $\beta_{\rm obs} = \frac{1}{2}$), the WKB wave impedances and projection operators were used to determine the incident power flow. The figure plots $\eta(\phi)$ both for an infinite cochlea (of the type introduced in Sec. III.A) and for a model terminated at the stapes in its characteristic impedance. When the discontinuity is small, η is close to unity in the infinite cochlea, indicating that, despite the secular variation of parameters, little reflection of the incident energy occurs in the infinite half-plane basal to the observation point. As the size of the discontinuity increases, however, more and more of that energy is reflected by the anomaly and the net power flowing basally towards the stapes decreases.

Terminating the model in its characteristic impedance gives rise to considerable boundary reflection; the net power flow is correspondingly reduced. An estimate of the value $\eta(\phi = 0)$ can be obtained from Eq. (73):

$$\eta(0) \approx 1 - \left|\overleftarrow{R}_0(\omega_{\rm s})\right|^2\,. \tag{79}$$

Using the value 0.55 obtained above for the reflection coefficient yields $\eta(0) \approx 0.7$; that value slightly underestimates the actual power flow at $x_{\rm obs}$ because of the finite damping in the model.

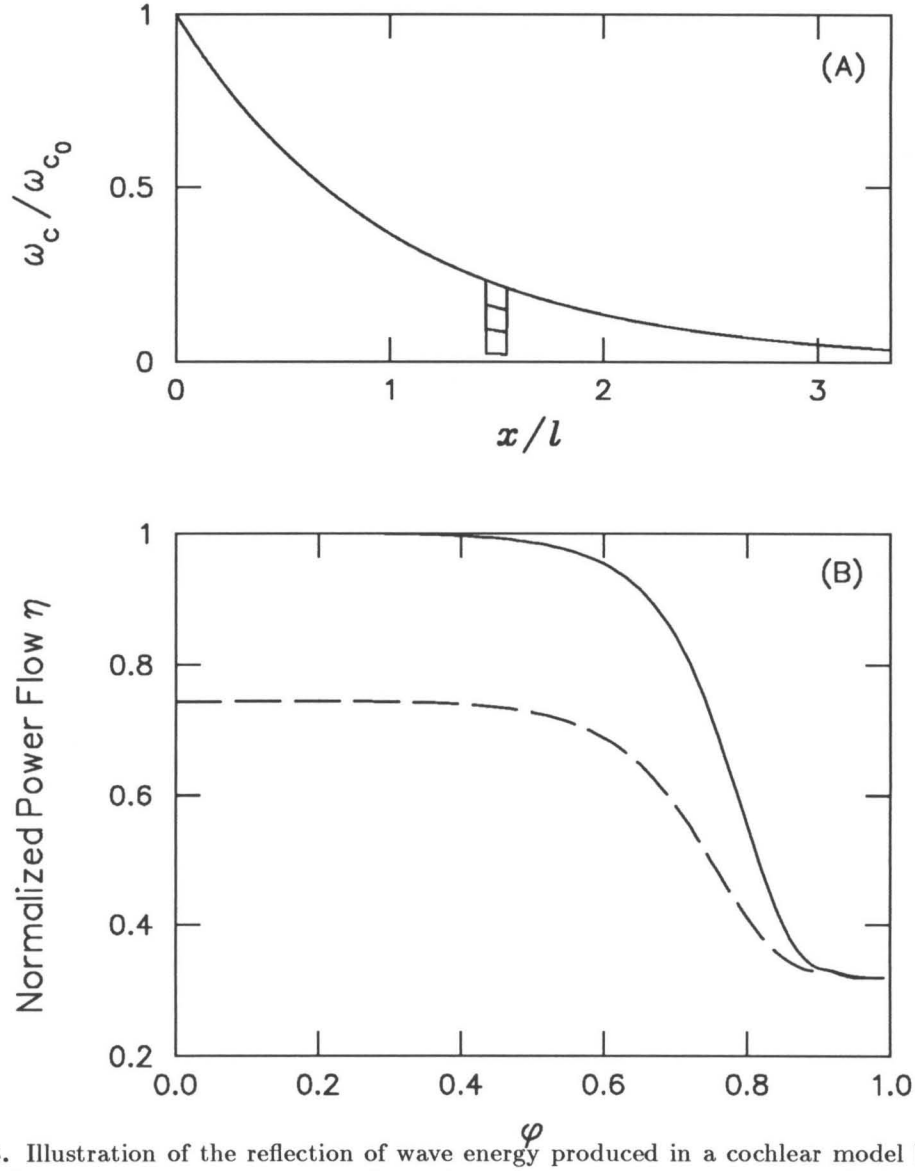

Figure 6. Illustration of the reflection of wave energy produced in a cochlear model by a mechanical inhomogeneity. Panel (A) plots (over the range $0 < x < x_{\rm obs}$) the perturbed frequency-position map ω_c/ω_{c_0} given by Eq. (76) for several values of the perturbation parameter ϕ. When $\phi = 0$ the anomaly in the frequency-position map is eliminated. Panel (B) plots the normalized power $\eta(\phi)$ flowing basally towards the stapes past the observation point $x_{\rm obs}$ for the model of de Boer et al. (1986ab and Kaernbach et al. 1987, rescaled to the cat as in Fig. 1) using two different boundary conditions at the stapes. The stimulus frequency is again fixed at $\omega_s/2\pi = 1$ kHz and the observation point chosen so that $\beta_{\rm obs} = \frac{1}{2}$. The solid line (———) shows $\eta(\phi)$ computed when the cochlea is assumed infinite as in Fig. 1. Although panel (A) shows the frequency-position map only for $x > 0$, the cochlea is here assumed to extend infinitely in the negative–x direction. Despite the strong secular variation in the mechanical characteristics in an infinite cochlea, η is close to unity when $|\phi| \ll 1$. At larger values of ϕ, reflection from the discontinuity reduces the net basal power flow considerably. The dashed line (— —) shows $\eta(\phi)$ computed when the cochlea is terminated at the stapes in its characteristic impedance $Z_c(0,\omega_s)$. The boundary reflection produced by terminating the model in its characteristic impedance reduces the net power flow even in the absence of any inhomogeneity.

IV. When Do Cochlear Reflections Occur?

The negligible cochlear reflection found in the models of Sec. II (see Fig. 1) provides but a specific example of a result conjectured to hold more generally. In a generic cochlear scattering problem the cochlea is divided into two parts in which corresponding approximate solutions to the equations are found: an apical region (A) containing the source of retrograde waves launched upon the basilar membrane and a more basal region (B) in which those waves may be reflected back toward the source. Assume, for simplicity, that the basal region B extends infinitely in the negative-x direction so that there are no boundary reflections to complicate the discussion. For $\beta < 1$ the wavelength λ in conventional cochlear models is essentially real and the wave equation for the pressure has the standard Sturm-Liouville form (Courant and Hilbert 1953; Birkhoff and Rota 1969). In the source region, the solutions can then be presumed oscillatory so that an appropriate linear combination can be taken representing waves traveling independently in opposite directions. For example, in the models of Sec. II.A those approximate traveling-wave solutions are the WKB waves $W_{\pm}$.

When the approximate solutions in regions A and B have overlapping regions of validity, solutions in one region can be matched asymptotically onto solutions in the other. In particular, the two traveling-wave solutions in region A can be matched one-to-one onto corresponding solutions in region B. By asymptotic matching one can thus construct, in principle, two global approximate solutions to the transmission-line equations that, at least in region A and the region of overlap, have the form of traveling waves. Adopting as one's "basis waves" $\mathcal{B}_{\pm}$ those independent global solutions thus guarantees that waves, so defined, propagate essentially without reflection.

When the mechanics of the cochlea do not vary sufficiently smoothly (e.g., when they change discontinuously at a point as illustrated in Sec. III.C), no overlapping region of validity exists between the solutions in regions A and B, and no one-to-one matching of solutions can be made. Consequently no global solutions exist that correspond, in region A, to waves traveling in only a single direction: the discontinuity generates a reflection.

Even in the absence of discontinuities or other strong mechanical inhomogeneities, employing basis waves that constitute poor approximate solutions to the transmission-line

equations (e.g., the geometric-optical waves $V_\pm$) can give rise to an apparent reflection (of those basis waves) because a spatially-varying linear combination of (those) waves traveling in opposite directions is then necessary to accurately approximate the solution (cf. Sec. III.B).

V. Boundary Reflection in the Cat

Although traveling waves are not reflected by the secular variation of the geometrical and mechanical characteristics of the cochlea, they can be reflected at the basal boundary with the middle ear. Discussions of retrograde wave propagation (e.g., de Boer et al. 1986ab; Viergever 1986; Kaernbach et al. 1987) and models for the generation of otoacoustic emissions (e.g., Furst and Lapid 1988) have typically chosen a basal boundary condition for calculational convenience; the qualitative form of the basal reflection coefficient in an actual ear has never been addressed.[10] This section estimates $\overleftarrow{R}_0(\omega)$ for the cat.

The effective "output impedance" $\overleftarrow{Z}_0(\omega)$ at the stapes is determined by the mechanical and acoustical characteristics of the middle and external ears. That impedance can be estimated in the cat by combining a model of the middle ear (Carr and Zweig 1984) with measurements of the radiation impedance of the external ear seen from the eardrum (Rosowski et al. 1986; Rosowski et al. 1988). The approximate reflection coefficient $\overleftarrow{R}_0(\omega)$ can then be found from Eq. (70):

$$\overleftarrow{R}_0^{\,B} = \left. \frac{\overleftarrow{Z}/Z_-^B - 1}{\overleftarrow{Z}/Z_+^B + 1} \right|_{x=0} . \tag{80}$$

To the extent that apical reflections make negligible contributions to the measured input impedance, the wave impedances $Z_\pm^B$ can be estimated from measurements (Lynch et al. 1982) of the cochlear input impedance $Z_0(\omega)$ according to the rule (Shera and Zweig 1991a):

$$Z_+^B(0,\omega) \approx Z_0(\omega) \quad \text{and} \quad Z_-^B(0,\omega) \approx Z_0^*(\omega) . \tag{81}$$

[10] Matthews (1983) has estimated the impedance $\overleftarrow{Z}_0(\omega)$ in the cat under simulated recording conditions in which the middle-ear cavities are widely open and the ear canal terminated with a model stimulus delivery system.

In accord with measurements of the cochlear input impedance (Lynch et al. 1982), the wave impedances $Z_{\pm}^{B}$ can also be approximated by the WKB wave impedances of a cochlear model with $|\Delta| \ll 1$ (Shera and Zweig 1991a).

The resulting reflection coefficient is shown in Fig. 7. Although the precise position of the peaks and dips will vary from animal to animal (and from those in the "composite" cat shown here), the figure demonstrates that the reflection coefficient, typically of order one, can be expected to vary strongly with frequency. Shown for comparison is the reflection coefficient computed under simulated recording conditions in which the ear canal is blocked at the entrance to the concha. The differences between the two conditions are considerable.

VI. Summary

Passive, one-dimensional transmission-line models are expected to describe the mechanics of the basal turns of the cochlea at high sound pressures and angular frequencies ω much less than the maximum frequency of hearing ω_{c_0}. The companion paper (Shera and Zweig 1991a) demonstrates that the inner ear of the cat manifests a symmetry between the longitudinal impedance $\bar{Z}$ of the cochlea and the admittance Y of the organ of Corti that guarantees that the wavelength changes slowly near the stapes. Remarkably, conventional transmission-line models, whether they manifest that symmetry or not, do not appear to generate reflections of waves traveling through the basal turn even when the wavelength changes rapidly.

Unless the model manifests the tapering symmetry required by measurements of the input impedance, terminating a cochlear transmission line in its characteristic impedance, whether explicitly (de Boer et al. 1986ab; Kaernbach et al. 1987) or implicitly (Viergever 1986), generates significant boundary reflection. The ostensible asymmetry in reflection of cochlear waves computed by other authors emerges as the expected consequence of an asymmetric termination of the cochlear transmission line. Viergever's (1986) conclusion that the decline in stiffness (increase in C) of the basilar membrane is primarily responsible for the wave reflection observed in his model is incorrect. In fact, the reflections originate not from the secular variation of the stiffness but from an impedance mismatch at the basal boundary.

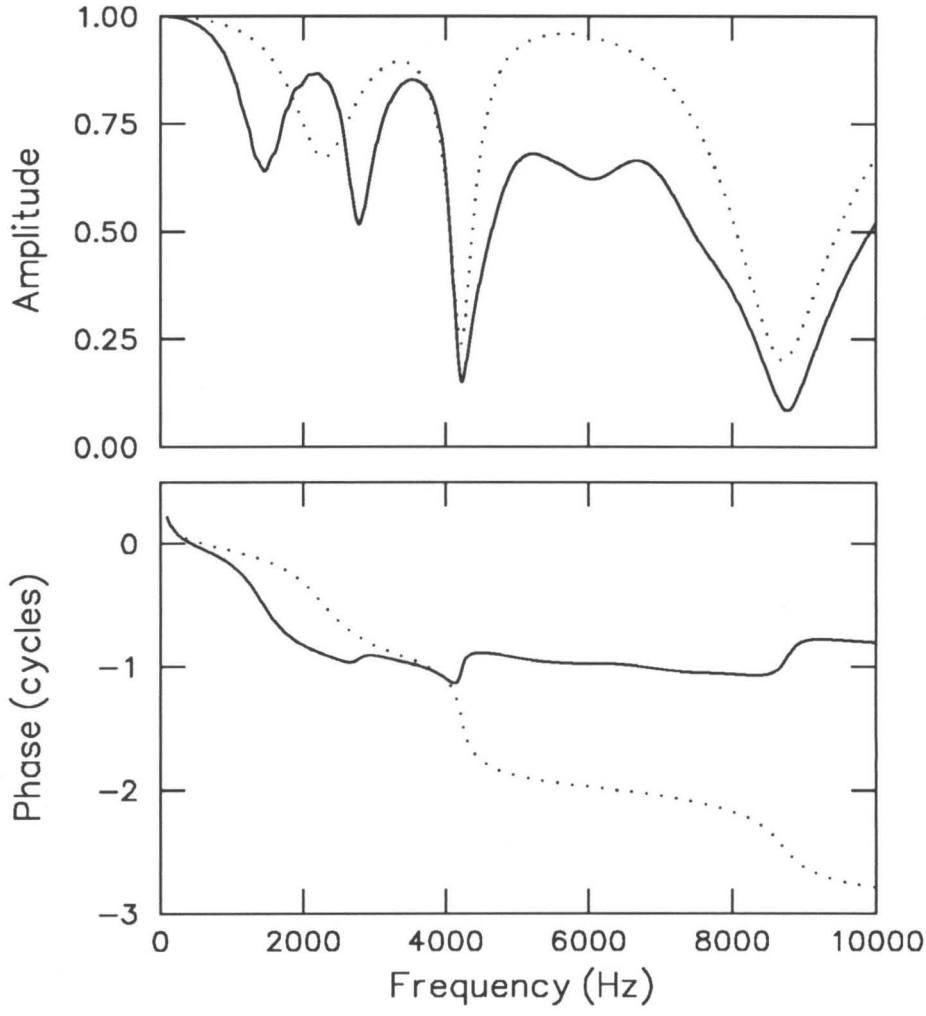

Figure 7. Approximate amplitude and phase of $\overleftarrow{R}_0(\omega)$ for the cat cochlea computed from a model of the middle ear (Carr and Zweig 1984) for two boundary conditions in the ear canal: (———) $\overleftarrow{R}_0(\omega)$ computed using an external-ear radiation impedance $Z_{ee}(\omega)$ at the tympanic membrane obtained from measurements on excised external ears (Rosowski et al. 1986; Rosowski et al. 1988); (· · · · ·) $\overleftarrow{R}_0(\omega)$ computed using Z_{ee} for simulated experimental recording conditions computed from a model consisting of a rigid-walled, closed tube with dimensions typical of the feline ear canal (Shaw 1974; Rosowski et al. 1988). The figure shows that $\overleftarrow{R}_0(\omega)$, which is typically of $O(1)$, can be expected to display strong frequency dependence and depend sensitively on the boundary conditions imposed by the external ear.

Although the extent of symmetry-breaking has little effect on the reflection characteristics of the cochlea itself, it does affect the reflection of retrograde waves at the stapes. The basal reflection coefficient, demonstrated to vary strongly with frequency in the cat, depends on the impedance mismatch between the cochlear "output impedance" $\overleftarrow{Z}_0$ and the wave impedance $Z^B_-(0,\omega)$ and is thus determined both by the characteristics of the middle and external ears and by the form of the retrograde wave components. Quantitative interpretation of spontaneous and other otoacoustic emissions believed to depend on that reflection coefficient thus requires that the model accurately represent the symmetries of the inner ear.

Acknowledgments

We thank Laurel Carney for providing her data for analysis. This work was supported by the Theoretical Division of Los Alamos National Laboratory and a National Science Foundation Graduate Fellowship to C. A. S.

Appendix A: Analytic Approximations to $Z_0(\omega)$

This Appendix justifies the assertion of the companion paper (Shera and Zweig 1991a) that the simple WKB wave impedance $Z_+^W(0,\omega)$ suffices to determine the leading-order behavior of the cochlear input impedance $Z_0(\omega)$, even in models that exhibit the cochlear catastrophe. The cochlear scattering formalism outlined Sec. I is used to derive an analytic expression for $Z_0(\omega)$ in terms of the wave impedances $Z_\pm^{\mathcal{B}}(0,\omega)$ and the corresponding reflection coefficient $\overrightarrow{R}^{\mathcal{B}}(0,\omega)$. In the absence of apical reflections, and if the basis waves $\mathcal{B}_\pm$ constitute good solutions to the transmission-line equations near the stapes, $\overrightarrow{R}^{\mathcal{B}}$ is small and $Z_0(\omega)$ reduces to the anterograde wave impedance $Z_+^{\mathcal{B}}(0,\omega)$. The scattering formalism is then combined with the WKB approximation to derive a perturbative expansion for $Z_0(\omega)$ in powers of the scattering potential $\sigma^W(\chi)$. Successive terms in the expansion are computed for the model of de Boer et al. (1986ab and Kaernbach et al. 1987, rescaled to the cat) and compared to the exact result computed numerically.

At stimulus amplitudes $A > A_\infty$ (Shera and Zweig 1991a), the cochlear input impedance is defined by

$$Z_0(\omega) \equiv \left.\frac{P}{U}\right|_{x=0} \equiv \left.\frac{P_+^{\mathcal{B}} + P_-^{\mathcal{B}}}{U_+^{\mathcal{B}} + U_-^{\mathcal{B}}}\right|_{x=0} , \tag{A1}$$

where P and U have been decomposed into waves traveling in opposite directions. Reexpressing Eq. (A1) in terms of the wave impedances $Z_\pm^{\mathcal{B}}(\chi,\omega)$ and the "reflection coefficient"

$$\overrightarrow{R}^{\mathcal{B}}(\chi,\omega) \equiv \left.\frac{P_-^{\mathcal{B}}}{P_+^{\mathcal{B}}}\right|_{\text{cochlea driven forward}} . \tag{A2}$$

yields

$$Z_0(\omega) = Z_+^{\mathcal{B}} \left\{ 1 + \overrightarrow{R}^{\mathcal{B}} \frac{Z_+^{\mathcal{B}} + Z_-^{\mathcal{B}}}{Z_-^{\mathcal{B}} - \overrightarrow{R}^{\mathcal{B}} Z_+^{\mathcal{B}}} \right\} \Bigg|_{\chi=0} . \tag{A3}$$

Note that if $Z_\pm^{\mathcal{B}} = Z_c$, the right-hand side of Eq. (A3) reduces to the expression

$$\left. Z_c \frac{1 + \overrightarrow{R}}{1 - \overrightarrow{R}} \right|_{\chi=0} \tag{A4}$$

familiar from transmission-line theory (e.g., Slater 1942). Equation (18) in Sec. I implies that, to first order,

$$\overrightarrow{R}_0^{\mathcal{B}} \equiv \overrightarrow{R}^{\mathcal{B}}(0,\omega) \approx -\int_0^\infty \mathcal{B}_+(\chi')\sigma_+^{\mathcal{B}}(\chi')\mathcal{B}_+(\chi')\, d\chi' . \tag{A5}$$

When $\vec{R}_0^{\,B}$ is small, Eq. (A3) for $Z_0(\omega)$ reduces to the wave impedance $Z_+^B(0,\omega)$.

Calculation of the input impedance using WKB waves $W_\pm$ provides an interesting example. Two approximations to $Z_0(\omega)$, namely $Z_{0;0}^W(\omega)$ and $Z_{0;1}^W(\omega)$, are shown in Fig. A1 for the model of de Boer et al. (1986ab and Kaernbach et al. 1987, rescaled to the cat). The approximations are based on an iterative expansion of Eq. (A5) for $\vec{R}_0^{\,W}$ in the manner of Eq. (18). The second subscript denotes the number of interactions with the WKB scattering potential included in the calculation of the reflection coefficient $\vec{R}_0^{\,W}$ appearing in Eq. (A3) for $Z_0(\omega)$:

$$\vec{R}_0^{\,W}(\omega) = \vec{R}_{0;0}^{\,W} + \vec{R}_{0;1}^{\,W} + \vec{R}_{0;2}^{\,W} + \cdots \tag{A6}$$

$$= 0 - \int_0^\infty W_+ \sigma^W W_+ \, d\chi' + O(\sigma^W \sigma^W) \, . \tag{A7}$$

Thus, the zeroth-order approximation $Z_{0;0}^W$, computed by including terms to $O(\vec{R}_{0;0}^{\,W})$, is simply the anterograde WKB wave impedance

$$Z_{0;0}^W = Z_+^W(0,\omega) \, ; \tag{A8}$$

the first-order approximation $Z_{0;1}^W$ includes terms to order $O(\vec{R}_{0;1}^{\,W})$:

$$Z_{0;1}^W(\omega) = Z_+^W \left\{ 1 + \vec{R}_{0;1}^{\,W} \frac{Z_+^W + Z_-^W}{Z_-^W - \vec{R}_{0;1}^{\,W} Z_+^W} \right\} \Bigg|_{\chi=0} \, . \tag{A9}$$

The figure demonstrates that, despite the breakdown in the WKB approximation at low frequencies, the leading-order behavior of $Z_0(\omega)$ is well captured in the zeroth-order approximation $Z_{0;0}^W = Z_+^W(0,\omega)$. By contrast, the corresponding zeroth-order approximation to $Z_0(\omega)$ (namely Z_+^V) obtained by using the geometric-optical series fails completely to indicate the presence of the cochlear catastrophe. That approximation, shown for comparison, is simply the characteristic impedance $Z_c(0,\omega)$ to which $Z_+^W(0,\omega)$ reduces in the limit $|\lambda_0'| \to 0$ (see Sec. I).

The behavior of the first-order approximation $Z_{0;1}^W(\omega)$ at frequencies $\omega/2\pi \lesssim 1$ kHz results from the divergence of the scattering series at low frequencies and can be understood by examining the form of the scattering potential σ^W at low β. At frequencies $\omega \ll \omega_{c_0}$ the function

$$2i\sigma^W(\chi,\omega) = -\frac{1}{2}\frac{\lambda''}{\lambda} + \frac{1}{4}\left(\frac{\lambda'}{\lambda}\right)^2 \, , \tag{A10}$$

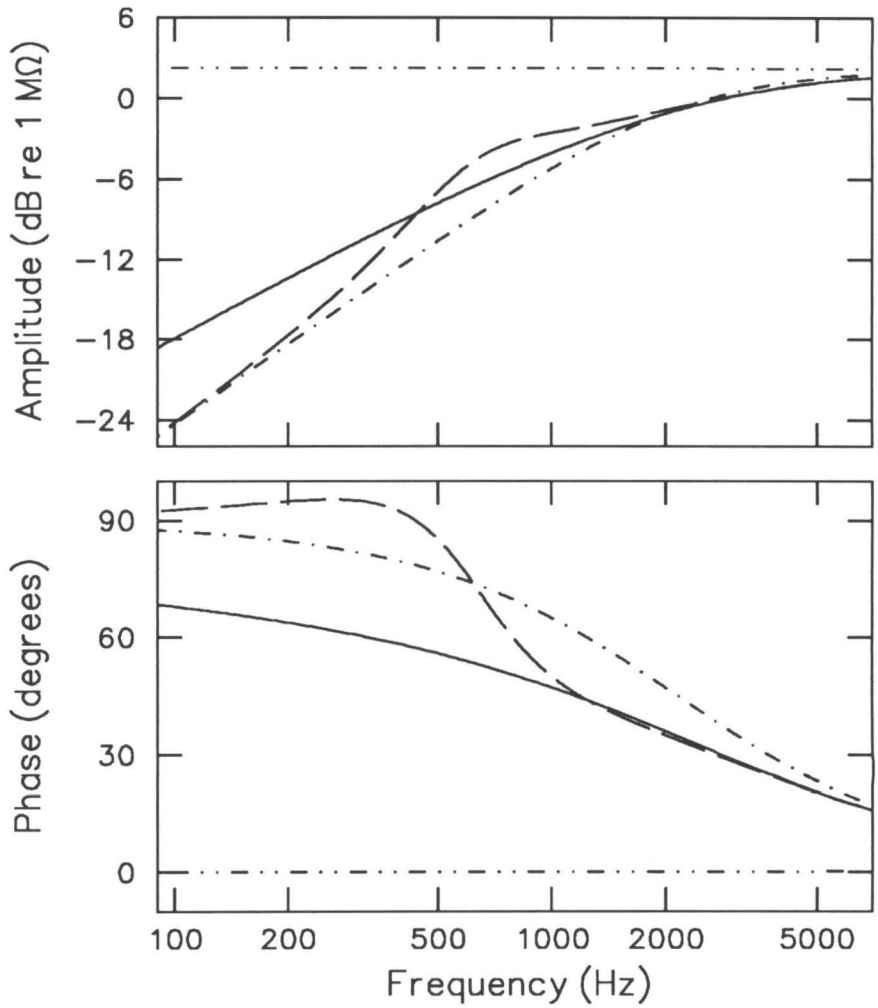

Figure A1. Approximations to the amplitude and phase of $Z_0(\omega)$ for the cochlear model of de Boer et al. (1986ab and Kaernbach et al. 1987), rescaled to the cat as in Fig. 1: (·· — ·· —) the characteristic impedance $Z_c(0,\omega)$; (· — · —) the zeroth-order approximation $Z^W_{0;0} = Z^W_+(0,\omega)$; (— — —) the first-order approximation $Z^W_{0;1}$; (———) the impedance $Z_0(\omega)$ calculated numerically. The anterograde Hankel wave impedance $Z^H_+(\tilde{\beta}_0)$, shown for comparison, is indistinguishable from the numerical result. The impedance amplitudes are normalized at 7 kHz to the value given by the phenomenological network model of Lynch et al. (1982). Unlike the characteristic impedance $Z_c(0,\omega)$, the WKB anterograde wave impedance $Z^W_+(0,\omega)$ correctly captures the leading-order behavior of $Z_0(\omega)$.

is essentially real and diverges like $1/\beta^2$. Thus,

$$\overrightarrow{R}^{W}_{0;1}(\beta) \approx -\frac{ie^{+8iN\beta}}{32N}\int_{\beta}^{1}\frac{e^{-8iN\beta'}}{\beta'^2}\,d\beta' \qquad (\beta \ll 1) \tag{A11}$$

$$\sim -\frac{i}{32N}\left\{\frac{1}{\beta}+8iN\ln\beta+\cdots\right\} \qquad (8N\beta \to 0^{+}) \tag{A12}$$

diverges like $1/\beta$.

Although $\overrightarrow{R}^{W}_{0;1}(\beta)$ diverges at low frequencies, the corresponding approximation to the input impedance, $Z^{W}_{0;1}(\omega)$, remains finite. Indeed, note that when $\overrightarrow{R}^{W}_{0;1}$ diverges, Eq. (A3) for $Z_0(\omega)$ implies that

$$Z^{W}_{0;1}(\omega) \to -Z^{W}_{-}(0,\omega) \qquad (|\overrightarrow{R}^{W}_{0;1}| \to \infty). \tag{A13}$$

Since (see Table I)

$$-Z^{W}_{-} \to Z^{W}_{+} \qquad (|\lambda'| \to \infty), \tag{A14}$$

$Z^{W}_{0;1}(\omega)$ approaches $Z^{W}_{0;0}(\omega)$ at the lowest frequencies, in agreement with Fig. A1. Note that the divergence in $\overrightarrow{R}^{W}_{0;1}$ would occur at higher frequencies were it not for the relatively large value of N, which helps to suppress the magnitude of the reflection coefficient.

Because of its generality and the ease of its physical interpretation, the companion paper (Shera and Zweig 1991a) uses the anterograde WKB wave impedance Z^{W}_{+} to approximate Z_0. For models of the family introduced in Sec. II, however, a better approximation to Z_0 at small β would be the anterograde Hankel wave impedance Z^{H}_{+} given in Table B1. For the model of de Boer et al. (for which $\Delta = 1$), that approximation becomes

$$Z_0(\omega) \approx Z^{H}_{+}(\tilde{\beta}_0) = iZ_{c}(0,0)\frac{H^{+}_{0}(\tilde{\beta}_0)}{H^{+}_{1}(\tilde{\beta}_0)} \qquad (\tilde{\beta}_0 = 4N\omega/\omega_{c_0})\,. \tag{A15}$$

Plotted in the figure for comparison, $Z^{H}_{+}(\tilde{\beta}_0)$ is indistinguishable from the numerical result. The analogue of $\overrightarrow{R}^{W}_{0;1}$ computed using Hankel waves would thus be quite small. The sizable "reflection coefficient" $\overrightarrow{R}^{W}_{0}$ computed above by using WKB waves results entirely from the choice of basis waves, and is not indicative of genuine reflection.

References

Abramowitz, M. and I. A. Stegun (1964). *Handbook of Mathematical Functions,* Applied Mathematics Series, vol. 55.Washington: National Bureau of Standards.

von Békésy, G. (1960). *Experiments in Hearing.*New York: McGraw-Hill.

Bender, C. M. and S. A. Orszag (1978). *Advanced Mathematical Methods for Scientists and Engineers.*New York: McGraw-Hill.

Birkhoff, G. and G.–C. Rota (1969). *Ordinary Differential Equations.*Waltham: Blaisdell.

de Boer, E. (1980). "Auditory physics. Physical principles in hearing theory. I," *Phys. Rep.* **62**, 88–174.

de Boer, E. and M. A. Viergever (1984). "Wave propagation and dispersion in the cochlea," *Hearing Res.* **13**, 101–112.

de Boer, E., C. Kaernbach, P. König, and T. Schillen (1986a). "An isolated sound emitter in the cochlea: Notes on modelling," in *Peripheral Auditory Mechanisms*, edited by J. B. Allen, J. L. Hall, A. Hubbard, S. T. Neely, and A. Tubis, 197–204. Berlin: Springer–Verlag.

de Boer, E., C. Kaernbach, P. König, and T. Schillen (1986b). "Forward and reverse waves in the one-dimensional model of the cochlea," *Hearing Res.* **23**, 1–7.

Bremmer, H. (1951). "The W.K.B. approximation as the first term of a geometric-optical series," *Commun. Pure Appl. Math.* **4**, 105–115.

Carr, J. N. and G. Zweig (1984). "A mechanical model of the middle ear of anesthetized cats," unpublished report.

Courant, R. and D. Hilbert (1953). *Methods of Mathematical Physics.*New York: Wiley Interscience.

Eldredge, D. H., J. D. Miller, and B. A. Bohne (1981). "A frequency-position map for the chinchilla cochlea," *J. Acoust. Soc. Am.* **69**, 1091–1095.

Fröman, N. and P. O. Fröman (1965). *JWKB Approximation: Contributions to the Theory.*Amsterdam: North-Holland.

Furst, M. and M. Lapid (1988). "A cochlear model for acoustic emissions," *J. Acoust. Soc. Am.* **84**, 222–229.

Green, G. (1837). "On the motion of waves in a variable canal of small depth and width," *Trans. Camb. Phil. Soc.* **6**, 457–462.

Greenwood, D. D. (1961). "Critical bandwidth and the frequency coordinates of the basilar membrane," *J. Acoust. Soc. Am.* **33**, 1344–1356.

Jeffreys, H. (1924). "On certain approximate solutions of linear differential equations of the second order," *Proc. Lond. Math. Soc.* **23**, 428–436.

Kaernbach, C., P. König, and T. Schillen (1987). "On Riccati equations describing impedance relations for forward and backward excitation in the one-dimensional cochlea model," *J. Acoust. Soc. Am.* **81**, 408–411.

Kemble, E. C. (1935). "A contribution to the theory of the B.W.K. method," *Phys. Rev.* **48**, 549–561.

Liberman, M. C. (1982). "The cochlear frequency map for the cat: Labeling auditory-nerve fibers of known characteristic frequency," *J. Acoust. Soc. Am.* **72**, 1441–1449.

Lynch, T. J., V. Nedzelnitsky, and W. T. Peake (1982). "Input impedance of the cochlea in cat," *J. Acoust. Soc. Am.* **72**, 108–130.

Mathews, J. and R. Walker (1964). *Mathematical Methods of Physics.*New York: Benjamin.

Matthews, J. W. (1983). "Modeling reverse middle-ear transmission of acoustic distortion products," in *Mechanics of Hearing*, edited by E. de Boer and M. A. Viergever, 11–18. Delft: Delft University Press.

Peterson, L. C. and B. P. Bogert (1950). "A dynamical theory of the cochlea," *J. Acoust. Soc. Am.* **22**, 369–381.

Rosowski, J. J., L. H. Carney, T. J. Lynch, and W. T. Peake (1986). "The effectiveness of external and middle ears in coupling acoustic power into the cochlea," in *Peripheral Auditory Mechanisms*, edited by J. B. Allen, J. L. Hall, A. Hubbard, S. T. Neely, and A. Tubis, 56–59. Berlin: Springer–Verlag.

Rosowski, J. J., L. H. Carney, and W. T. Peake (1988). "The radiation impedance of the external ear of cat: Measurements and applications," *J. Acoust. Soc. Am.* **84**, 1695–1708.

Shaw, E. A. G. (1974). "The external ear," in *Handbook of Sensory Physiology, Vol. V/1: Auditory System*, edited by W. D. Keidel and W. D. Neff, 455–490. Berlin: Springer–Verlag.

Shera, C. A. (1986a). "Boundary conditions on the waves in the cochlea," unpublished progress report.

Shera, C. A. and G. Zweig (1991a). "A symmetry suppresses the cochlear catastrophe," *J. Acoust. Soc. Am.* **89**, 1276–1289.

Slater, J. C. (1942). *Microwave Transmission.*New York: McGraw-Hill.

Viergever, M. A. (1986). "Asymmetry in reflection of cochlear waves," in *Auditory Frequency Selectivity*, edited by B. C. J. Moore and R. D. Patterson, 31–38. New York: Plenum.

Zweig, G., R. Lipes, and J. R. Pierce (1976). "The cochlear compromise," *J. Acoust. Soc. Am.* **59**, 975–982.

Zweig, G. (1991). "Finding the impedance of the organ of Corti," *J. Acoust. Soc. Am.* **89**, 1229–1254.

Zwislocki-Mościcki, J. (1948). "Theorie der Schneckenmechanik: Qualitative und quantitative Analyse," *Acta Otolaryngol. Suppl.* **72**, 1–112.

Phenomenological Characterization of Eardrum Transduction

Christopher A. Shera and George Zweig

Theoretical Division
Los Alamos National Laboratory
Los Alamos, New Mexico 87545

and

Physics Department
California Institute of Technology
Pasadena, California 91125

ABSTRACT

A phenomenological description of the transduction effected by the eardrum is presented. That description is provided by a transfer matrix, whose elements define those measurements sufficient to characterize eardrum transduction. Causality provides constraints on the matrix elements. In addition, measurements of the matrix elements can determine whether they satisfy constraints imposed by minimum-phase behavior and the principle of reciprocity. Those constraints may be used either to reduce the number of measurements necessary to characterize the eardrum or to check the consistency of measurements that overdetermine the system. Within its region of validity, the transfer matrix of the eardrum provides a common ground for the comparison between theory and experiment. As an example, a simple model for the transduction characteristics of the eardrum, defined completely in terms of measurable quantities, is presented.

Contents

Introduction

The eardrum begins the process of auditory transduction, converting incident sound into a mechanical oscillation of the bones of the middle ear. Although detailed measurements of eardrum surface-displacement patterns (Tonndorf and Khanna 1972; Khanna and Tonndorf 1972; von Bally 1976; Løkberg et al. 1980; Decraemer et al. 1989) provide a qualitative picture of the complexity of eardrum vibration, the characteristics of that transduction have not been measured. Such experiments do not, for example, measure the force transmitted to the ossicles and so fail to characterize those properties of the eardrum directly relevant to the process of hearing. Although eardrum dynamics have been explored theoretically at varying levels of complexity (Helmholtz 1868; Shaw 1977; Shaw and Stinson 1986; Funnell et al. 1987; Rabbitt and Holmes 1986) and qualitative agreement between measured and computed surface-displacement patterns obtained, the transformation properties of the eardrum have not been thoroughly examined.

Since measurements are incomplete and eardrum mechanics not well understood, the need exists for a comprehensive framework that identifies those measurements necessary and sufficient to characterize the transduction properties of the eardrum. Such a framework would show one how to prove what is believed known about the system (e.g., its analyticity and symmetry properties), and once proven, how to remove the effects of those constraints from measurements to expose directly the underlying dynamics. This paper proposes such a framework for the phenomenological description of the transformation properties of the eardrum. That description is provided by the transfer matrix $\widehat{\mathbf{T}}_{\mathbf{u}}^{\mathbf{e}}(\omega)$ of the eardrum, which summarizes those dynamical characteristics of the eardrum important for understanding its role in transmitting sound to the middle ear. The transfer-matrix elements are necessarily constrained by causality; in addition, measurements of the matrix elements can be used to determine whether they are minimum-phase functions and whether the eardrum satisfies the principle of reciprocity. If the eardrum is a completely passive mechanical transducer, reciprocity must hold. Those constraints may be used either to reduce the number of measurements necessary to characterize the eardrum or to check the consistency of measurements that overdetermine the system. The transfer-matrix elements provide a concise summary of the functional response of the eardrum—thereby facilitating

incorporation of eardrum transduction characteristics into models of the middle ear—and provide a common ground for comparing theory and experiment.

Just as the overall response of the ear to sound can be factored into parts describing the separate actions of the inner, middle, and external ears, so the response of the middle ear itself can, under certain conditions (Shera and Zweig 1992a), be factored into components describing the individual actions of its constituent parts. Those component factorizations are conveniently summarized by transfer matrices; the overall transfer matrix is simply the product of component matrices. This paper represents the first in a series of papers (Shera and Zweig 1991c; Shera and Zweig 1992a; Shera and Zweig 1992d) devoted to the phenomenological description of eardrum and middle-ear mechanics. Subsequent papers extend the program begun here with the eardrum to provide a phenomenological description of the other major components of the middle ear.

I. Phenomenological Characterization of the Eardrum

The eardrum (illustrated schematically in Fig. 1) forms the lateral wall of the tympanic cavity and vibrates in response to incident sound. Volume displacements of the eardrum create pressure variations $P_{\rm tc}$ in the tympanic cavity. At the same time, the eardrum exerts a force $F_{\rm u}$ on the malleus. That force results from the mechanical response of the eardrum to the driving pressure difference

$$\widehat{P}_{\rm e} \equiv P_{\rm e} - P_{\rm tc} \tag{1}$$

between the ear canal and the tympanic cavity.

The measurements of Guinan and Peake (1967) and Buunen and Vlaming (1981) on the cat indicate that the eardrum and middle ear respond linearly throughout the intensity range of normal hearing below the activation threshold for the acoustic reflex. Linearity implies that the eardrum can be completely characterized in terms of its response to pure tones. For simplicity, all variables in this paper have been written as complex quantities characterizing those responses. For example, the variable $V_{\rm u}$, representing the velocity of the umbo, is defined in terms of the measured amplitude $A(\omega)$ and phase $\phi(\omega)$ relative to the pressure at the eardrum by

$$V_{\rm u}(\omega) \equiv A(\omega)e^{i\phi(\omega)} \ . \tag{2}$$

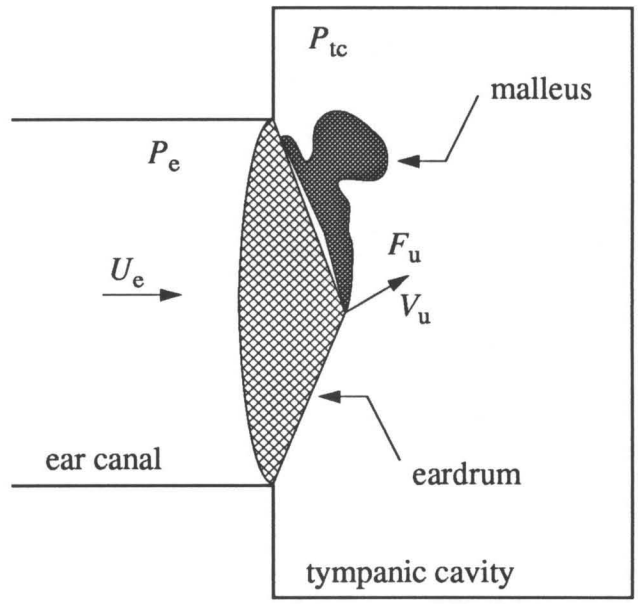

Figure 1. Schematic drawing of the eardrum in cross-section adapted from Fig. 5–6 of von Békésy (1960).

Under conditions discussed below, a phenomenological description of eardrum mechanics is provided by the transfer matrix $\widehat{\mathbf{T}}_{\mathrm{u}}^{\mathrm{e}}(\omega)$ of the eardrum. Illustrated schematically in Fig. 2a, $\widehat{\mathbf{T}}_{\mathrm{u}}^{\mathrm{e}}(\omega)$ is defined by the equation

$$\begin{pmatrix} \widehat{P}_{\mathrm{e}} \\ U_{\mathrm{e}} \end{pmatrix} = \widehat{\mathbf{T}}_{\mathrm{u}}^{\mathrm{e}} \begin{pmatrix} F_{\mathrm{u}} \\ V_{\mathrm{u}} \end{pmatrix} , \tag{3}$$

where U_{e} represents the volume velocity of the eardrum. The input and output variables are identified by super- and subscripts on the matrix. Since $\widehat{\mathbf{T}}_{\mathrm{u}}^{\mathrm{e}}$ is defined in terms of the pressure difference $\widehat{P}_{\mathrm{e}}$—which reduces to P_{e} when the middle-ear cavities are surgically exposed and opened widely to the atmosphere—the matrix depends only on the properties of the eardrum; the effects of the complicated acoustic geometry of the middle-ear cavities, discussed in the next paper in this series (Shera and Zweig 1992a), have been "factored out."

In the language of electrical circuit theory, Eq. (3) views the eardrum as a two-port network characterized in terms of transfer coefficients. (e.g., Brillouin 1946; Friedland et al. 1961; Lampton 1978). Although the phenomenology could have been based on any of the other standard characterizations of two-port networks (e.g., impedance or admittance coefficients), the transfer coefficients of the eardrum have especially simple interpretations—as, for example, effective areas (see below)—and their measurement—based on manipulation of the ossicular load—is convenient. In addition, the transfer-matrix representation, which maintains a separation between input and output ports, is natural for describing a cascade of systems. For example, the transfer matrix describing the combined action of the eardrum and ossicular chain is simply the product of the matrices representing the eardrum and ossicular transformations individually (Shera and Zweig 1992a).

Equation (3) is the most general linear equation relating the four variables defining the eardrum transformation.[1] The relation is independent of the nature or position of any sources or loads presented to the eardrum. (It is ratios such as $\widehat{P}_{\mathrm{e}}/U_{\mathrm{e}}$ or $F_{\mathrm{u}}/V_{\mathrm{u}}$ that depend on the loading of the eardrum by the middle and inner ears.) Furthermore,

[1] Equations similar to Eqs. (3), with a specific form for $\widehat{\mathbf{T}}_{\mathrm{u}}^{\mathrm{e}}$, were obtained by Esser (1947) by considering a simple model of the eardrum. However, Esser seems to have realized neither that equations of that form follow immediately from the linearity of the mechanics, nor that the coefficients in his model were related by the principle of reciprocity.

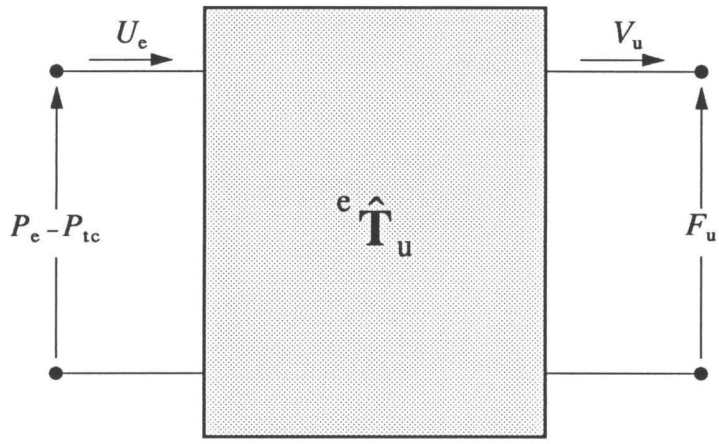

Figure 2a. The eardrum represented as a two-port network that transforms a pressure and volume velocity in the ear canal into a force and velocity at the umbo.

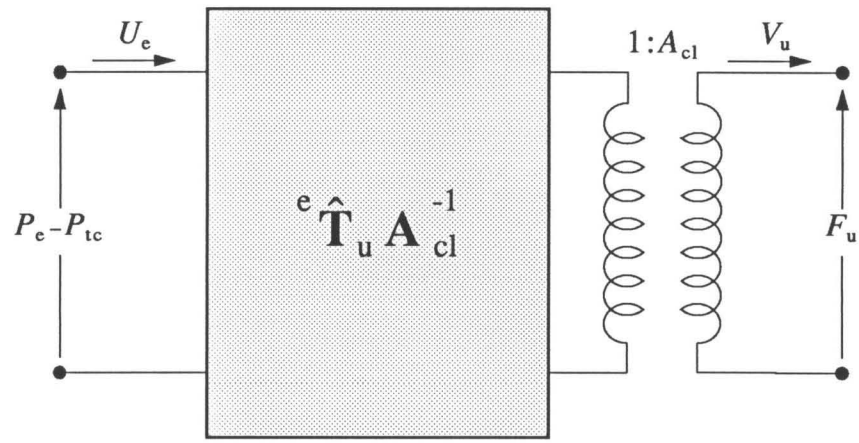

Figure 2b. A factored representation of the two-port network of Fig. 2a, making explicit the dimensional transformation (transduction) performed by the eardrum. The representation consists of the transfer matrix product $\hat{\mathbf{T}}_u^e \mathbf{A}_{cl}{}^{-1}$ in cascade with an ideal transformer of turns ratio A_{cl} whose function is to provide a change of dimension. The ideal transformer is represented by the transfer matrix $\mathbf{A}_{cl}$, defined by

$$\mathbf{A}_{cl} \equiv \begin{pmatrix} A_{cl}^{-1} & 0 \\ 0 & A_{cl} \end{pmatrix} .$$

The unit of area A_{cl} was chosen to be the "classical effective area" of the eardrum (see Sec. I).

the matrix characterizes both "forward" and "reverse" transduction; the same elements characterize eardrum transduction whether it is driven by pressure variations in the ear canal or by the autonomous motion of the organ of Corti. The transfer matrix thus allows a convenient separation between the boundary, or loading, conditions as represented by the input and output vectors and the dynamics of the eardrum as described by the matrix $\widehat{\mathbf{T}}_{\mathrm{u}}^{\mathrm{e}}$.

The simple 2×2 transfer-matrix description of the eardrum is appropriate when the four variables comprising the input and output vectors suffice to determine the eardrum transformation. For example, although sound propagation in the human ear canal is one-dimensional at frequencies less than the cutoff frequency for higher-order modes—which for a typical human ear canal is approximately 19 kHz (Stevens et al. 1987)—the pressure may be nonuniform close to the eardrum due to the presence of evanescent waves; the acoustic force driving the eardrum might not then be accurately approximated by the pressure difference $\widehat{P}_{\mathrm{e}}$. The effects of those non-propagating modes appear to be small, however, at frequencies less than ~ 6 kHz (Stinson 1985).

Although the motion of the malleus may be quite complex at high frequencies (e.g., Decraemer et al. 1989)—consisting, for example, of both rotational and translational components (Donahue 1989)—the one-dimensional variables F_{u} and V_{u} suffice to describe the "output" of the eardrum transformation so long as the effective mechanical input to the middle ear is well approximated by a single force and velocity coordinate,[2] as it appears to be at low frequencies (the precise region of validity, however, has yet to be established). In the simplest picture of eardrum dynamics, those coordinates are naturally associated with the force applied to the manubrium and the velocity of the umbo. If the action of the eardrum is more complicated, other definitions for those coordinates may be more useful.[3]

---

[2] Although at some frequencies the malleus may vibrate in all three spatial dimensions—suggesting that a simple transfer-matrix description is not possible—it may be that the effective input to the middle ear may still be one-dimensional. For example, vibration in the plane of the displacement of the stapes may be most significant for coupling energy into the inner ear.

[3] Although presumably concentrated at the umbo—the malleus is most firmly attached to the eardrum at the umbo (Graham et al. 1978; Schuknecht and Gulya 1986)—the total force F_{u} on the manubrium results from forces distributed all along the tympanic membrane-malleus attachment and can thus be expressed as an integral over the area of contact between the eardrum and the malleus (cf. Tonndorf and Khanna 1970; Khanna and Tonndorf 1972). If mallear motion is predominantly rotational the force F_{u}

A. Measurement and interpretation of the matrix elements

Determination of the matrix $\widehat{\mathbf{T}}_{\mathrm{u}}^{\mathrm{e}}(\omega)$ and its (species-dependent) region of validity constitutes a fundamental problem in eardrum phenomenology. The elements of the transfer matrix

$$\widehat{\mathbf{T}}_{\mathrm{u}}^{\mathrm{e}} \equiv \begin{pmatrix} \widehat{A}_{\mathrm{F}}^{-1} & \widehat{Z}_{\mathrm{e}} \\ \widehat{Y}_{\mathrm{e}} & \widehat{A}_{\mathrm{V}} \end{pmatrix} \tag{4}$$

can be measured by manipulating the middle-ear ossicles. (The diacritical hats indicate that the matrix elements are measured with the cavities opened widely.) For example, if the malleus is immobilized so that $V_{\mathrm{u}} = 0$, the element $\widehat{A}_{\mathrm{F}}^{-1}$ is given by the ratio

$$\widehat{A}_{\mathrm{F}}^{-1} = \left.\frac{\widehat{P}_{\mathrm{e}}}{F_{\mathrm{u}}}\right|_{V_{\mathrm{u}}=0 \text{ (malleus held fixed)}} . \tag{5}$$

Note that $\widehat{A}_{\mathrm{F}}(\omega)$ has the dimensions of an area. When the malleus is immobilized, the "effective area for force" represents that area by which the pressure difference $\widehat{P}_{\mathrm{e}}$ must by multiplied to obtain the force on the malleus.

The matrix element $\widehat{A}_{\mathrm{V}}$ provides another effective area, but in this case associated with the transformation of velocity coordinates by the eardrum:

$$\widehat{A}_{\mathrm{V}} = \left.\frac{U_{\mathrm{e}}}{V_{\mathrm{u}}}\right|_{F_{\mathrm{u}}=0 \text{ (ossicular load removed)}} . \tag{6}$$

When loading due to the ossicular chain has been removed,[4] the "effective area for velocity" provides the proportionality factor between the velocity of the umbo and the

---

can be considered an effective force, acting at the mallear moment arm l_{m} and defined in terms of the total torque by the equation

$$F_{\mathrm{u}} \equiv T l_{\mathrm{m}}^{-1} . \tag{3.1}$$

If, in addition, the malleus does not rotate as a rigid body, but, for example, flexes near the tip of the manubrium, it may be more useful to define V_{u} to be the "effective velocity" of the umbo, defined in terms of the angular velocity $\dot{\theta}_{\mathrm{h}}$ of the head of the malleus (measured at the axis of rotation) and the mallear moment arm l_{m} by

$$V_{\mathrm{u}} = \dot{\theta}_{\mathrm{h}} l_{\mathrm{m}} . \tag{3.2}$$

[4] Note that the force F_{u} is measured relative to the static force on the malleus (normally counterbalanced by forces from the ligaments of the middle-ear ossicles) present when the middle ear is quiescent and which helps to maintain the configuration of the eardrum. Because static forces from the ligaments help maintain the equilibrium position about which the eardrum vibrates, one cannot establish a no-load condition on the eardrum by simply removing the malleus altogether. One can, however, establish a no-load condition by employing a feedback loop and null-detector: in addition to driving the eardrum acoustically, one applies an additional force directly to the malleus so that the total measured force F_{u} is always zero.

total volume velocity of the eardrum. If the eardrum were a rigid piston, both effective areas would be real constants equal to the area of the piston. In general, however, the two areas $\widehat{A}_V(\omega)$ and $\widehat{A}_F(\omega)$

The remaining elements of the matrix $\widehat{\mathbf{T}}_u^e$ may be determined by similar measurements. The element $\widehat{Z}_e$ represents the no-load transfer impedance of the eardrum found by removing the ossicular load and measuring, as a function of frequency, the velocity of the umbo produced by a known driving pressure:

$$\widehat{Z}_e = \left.\frac{\widehat{P}_e}{V_u}\right|_{F_u=0 \text{ (ossicular load removed)}} . \tag{7}$$

Similarly, the element $\widehat{Y}_e$ can be found from the relation

$$\widehat{Y}_e = \left.\frac{U_e}{F_u}\right|_{V_u=0 \text{ (malleus held fixed)}} . \tag{8}$$

Were the eardrum a rigid plate, fixing the malleus would prevent the umbo and the rest of the eardrum from moving; the matrix element $\widehat{Y}_e$ would then be zero.

Note that $\widehat{\mathbf{T}}_u^e$ cannot be found from measurements of surface-displacement patterns. Such experiments do not, for example, measure the pressure in the tympanic cavity or the force transmitted to the ossicles. In addition, whereas surface-displacement patterns depend on the loading of the eardrum, the matrix $\widehat{\mathbf{T}}_u^e$ does not. Although surface-displacement patterns are not directly related to the functional role of the eardrum in the process of hearing, they can be helpful in establishing an understanding of the internal dynamics of the eardrum (Funnell et al. 1987; Rabbitt and Holmes 1986). For example, examination of displacement patterns can aid in determining which of a family of models that accurately predict the transfer-matrix elements provides the most realistic description of the eardrum.

B. Constraints on the matrix elements

Study of a complex system such as the eardrum often best proceeds by first identifying the analyticity and symmetry conditions that constrain the dynamics. At every angular frequency ω the matrix $\widehat{\mathbf{T}}_u^e$ has four elements, each of which has both a real and an imaginary part. Those eight functions of frequency, however, are not all independent. Two classes of constraints provide relations among the matrix elements. First are those that follow from general physical principles such as causality. Second are those, such as reciprocity, that, although not binding in general, might apply to the eardrum because of certain qualitative characteristics of its dynamics.

1. Causality

All physical systems are constrained by causality; a system cannot respond before it is driven. For a linear system characterized in the frequency domain, causality requires that the real and imaginary parts of each transfer-matrix element $T_{ij}(\omega)$ be Hilbert transforms of one another (Bode 1945):

$$\mathrm{Re}[T_{ij}(\omega)] = -\frac{1}{\pi} \mathrm{P}\!\!\int_{-\infty}^{\infty} \frac{\mathrm{Im}[T_{ij}(\omega')]}{\omega' - \omega} d\omega' \tag{9}$$

and

$$\mathrm{Im}[T_{ij}(\omega)] = \frac{1}{\pi} \mathrm{P}\!\!\int_{-\infty}^{\infty} \frac{\mathrm{Re}[T_{ij}(\omega')]}{\omega' - \omega} d\omega' \ . \tag{10}$$

Here $\mathrm{P}\!\!\int$ represents a Cauchy principal-value integral. Equations (9) and (10) are equivalent to the statement that considered as a function of complex frequency the matrix elements $T_{ij}(\omega)$ are analytic in the lower half of the frequency plane. Causality thus provides analytic constraints on the matrix elements.[5] Those constraints may be used to check measurements of the T_{ij} for internal consistency, reduce measurement uncertainty, and determine functional values at frequencies for which measurements are not available (Zweig 1976; Zweig and Konishi 1987).

2. Minimum-phase behavior

In addition to causality, the transfer-matrix elements may satisfy the stronger minimum-phase constraint, which requires that the real and imaginary parts of $\ln T_{ij}(\omega)$ be Hilbert transforms of one another. The responses described by each matrix element would then be produced by a mechanical system that responds as rapidly as possible consistent with its amplitude characteristic and the constraint of causality (Bode 1945). The matrix elements of the example model (see Sec. II) are such minimum-phase functions. Although certain combinations of matrix elements, such as the umbo transfer function, might be expected to have evolved "optimal" minimum-phase characteristics, such teleological arguments do not apply to the matrix elements individually.

---

[5] The dispersion relations (9) and (10) are valid when the matrix element $T_{ij}(\omega) \to 0$ as $\omega \to \infty$. When that is not the case, modified, or subtracted, dispersion relations exist (Bode 1945). In addition, the subtracted form of the dispersion relations may be computationally more convenient if, for example, the low-frequency behavior of the element $T_{ij}(\omega)$ is known but the high-frequency behavior poorly determined (Zweig and Konishi 1987).

3. Reciprocity

Linear passive mechanical systems obey the principle of reciprocity (Helmholtz 1860; Maxwell 1864; Rayleigh 1896; Foldy and Primakoff 1945). A two-port system is said to be reciprocal if it is not possible, given the transfer function $F_{\text{out}}/V_{\text{in}}$—where F_{out} is the generalized force produced at the output port by a generalized velocity V_{in} at the input—to identify which of the two ports served as the input port for obtaining the given transfer function. A necessary and sufficient condition for a system to be reciprocal is that its transfer-matrix elements satisfy the algebraic relation

$$\det \mathbf{T} = +1 \, . \tag{11}$$

All linear two-port systems that contain only capacitors, resistors, and inductors—or their mechanical analogs—and no sources of generalized force or velocity are reciprocal[6] (Friedland et al. 1961). For small input signals the eardrum appears to be a linear, passive mechanical system and can thus be expected to be reciprocal. If satisfied, reciprocity would allow determination of one matrix element from measurements of the others:

$$\frac{\widehat{A}_{\text{V}}}{\widehat{A}_{\text{F}}} - \widehat{Z}_{\text{e}}\widehat{Y}_{\text{e}} = +1 \, . \tag{12}$$

The eardrum models discussed in Secs. II and III are all reciprocal. It is possible, however, that eardrums in some animals may in the process of transduction actively amplify (or diminish) the energy in incoming sounds. Were they to be realized in nature, such as yet hypothetical eardrums might not be reciprocal.

C. The effective areas $\widehat{A}_{\text{F}}$ and $\widehat{A}_{\text{V}}$

Discussions of the contribution of the eardrum to the "transformer action" of the middle ear often make reference to the "effective area" of the eardrum (von Békésy 1941; Wever et al. 1948; Zwislocki 1975). As demonstrated above, however, there are two such effective areas, one associated with each of the two principal effects of eardrum motion: transmission of a force to the middle-ear ossicles and a change in the volume of the tympanic cavity. The areas associated with those two actions of the eardrum (i.e., transformation

[6] McMillan (1946) demonstrates violation of reciprocity in a linear passive electromechanical system containing somewhat more exotic components.

of pressure into both force and volume velocity) are not necessarily equal. Indeed, the constraint of reciprocity (12) implies, assuming $\widehat{Z}_e \neq 0$, that the two areas could be equal if and only if $\widehat{Y}_e = 0$ (that is, only if the eardrum were perfectly rigid).

The classical concept of the effective area confuses those two actions of the eardrum. For example, the classical effective area A_{cl} has been defined to be the area of the plate that, if moved through a distance equal to that traversed by the umbo, would sweep out the same total volume as the eardrum (Wever and Lawrence 1954). A_{cl} has been estimated—taking into account the conical geometry of the membrane—to be roughly two-thirds the anatomical area of the eardrum (von Békésy 1941; Wever and Lawrence 1954). Defined with reference to eardrum volume displacement, the area A_{cl} is often inappropriately applied to the transformation of pressure between the eardrum and the oval window (e.g., Zwislocki 1975). In addition, since loading conditions on the eardrum are not specified, the classical definition of the effective area is ill-defined. Nevertheless, A_{cl} provides a useful reference area with which the amplitudes of the two effective areas $\widehat{A}_V(\omega)$ and $\widehat{A}_F(\omega)$ appearing in $\widehat{\mathbf{T}}_u^e$ may be compared. The next paper in this series (Shera and Zweig 1992a) discusses the relative importance of the two areas $\widehat{A}_V(\omega)$ and $\widehat{A}_F(\omega)$ for middle-ear and cochlear mechanics.

A simple argument based on reciprocity gives the relative size of the two effective areas at low frequencies. The displacement of the umbo X_u is then expected to be in phase with the driving pressure $\widehat{P}_e$ when the ossicular load is removed. The element $\widehat{Z}_e$ is thus proportional to $1/i\omega$:

$$\widehat{Z}_e \underset{\omega\to 0}{\longrightarrow} \frac{K_e}{i\omega} \qquad (K_e > 0). \tag{13}$$

Analogous arguments suggest that at low frequencies $\widehat{Y}_e$ is proportional to $i\omega$,

$$\widehat{Y}_e \underset{\omega\to 0}{\longrightarrow} \frac{i\omega}{K_d} \qquad (K_d > 0), \tag{14}$$

and that the effective areas $\widehat{A}_V$ and $\widehat{A}_F$ are both positive and real. Reciprocity requires that

$$\lim_{\omega\to 0} \frac{\widehat{A}_F}{\widehat{A}_V} = \lim_{\omega\to 0} \frac{1}{1+\widehat{Z}_e\widehat{Y}_e} = \frac{1}{1+K_e/K_d} < 1\,. \tag{15}$$

Note that $\widehat{A}_V$ and $\widehat{A}_F$ have similar values at low frequencies if and only if $K_e/K_d \ll 1$.

II. Oscillator Model for Eardrum Transduction Characteristics

To illustrate the formalism, this section presents a simple phenomenological model—the "oscillator model"—for the transduction characteristics of the eardrum defined completely in terms of measurable quantities. As such, the model differs from other lumped-element models of the eardrum, which contain impedances that would be difficult to measure on a real eardrum.[7] In contrast with other models, no attempt will be made to model the internal dynamics or complex oscillations of the eardrum. Rather, a different approach is adopted based on the assumption that three of the elements of the transfer matrix $\widehat{\mathbf{T}}_{\mathrm{u}}^{\mathrm{e}}$ of the eardrum are "simple" at low frequencies (i.e., are either constant or have Laurent expansions in $i\omega$ dominated by the first three terms). The remaining matrix element is determined by assuming reciprocity. Those assumptions, although perhaps plausible, have no firm empirical basis and are adopted solely for purposes of illustration.

For clarity of exposition the discussion proceeds by first considering, and then extending, the transfer-matrix elements of a simple plate model of the eardrum. The model is thus ultimately defined by its transfer matrix, without reference to a particular physical model of the eardrum. Section II–A demonstrates, however, that the mechanical two-piston model introduced by Shaw (1977; Shaw and Stinson 1981) provides, in the limit implied by his parameter values, a mechanical realization of the model transfer matrix proposed here. The matrix elements for alternative mechanical models proposed by other authors are discussed in the final section.

A. Matrix elements of the oscillator model

Measurements indicate that at low frequencies most of the eardrum vibrates in phase as a unit, much like a simple piston. For example, Tonndorf and Khanna (1970; 1972) have measured the surface displacement of eardrums in human cadavers in response to tones of several frequencies. They found that the eardrum remains in its lowest mode of oscillation at frequencies less than 3–4 kHz. At higher frequencies the eardrum of the cadaver ear breaks up into complex oscillations. Although transition frequencies were higher, Khanna

[7] For example, Kringlebotn (1988) provides no prescription for measuring (and no equations defining) the impedance associated with the structures suspending the eardrum in the ear canal. In addition, since the equations defining the plate and coupling impedances have no obvious analogs for an actual eardrum, it would be difficult—without comparing matrix elements—to determine the extent to which two- or three-piston models (Shaw and Stinson 1986) accurately describe eardrum transduction.

and Tonndorf (1972) and Decraemer et al. (1989) found qualitatively similar vibration patterns in anesthetized cats. Their findings are consistent with those of others based on human temporal bone preparations (von Bally 1976) and living subjects (Løkberg et al. 1980).

A first approximation to the transfer matrix of the eardrum might thus be found by imagining the eardrum as a rigid plate (e.g., Peake and Guinan 1967; Dallos 1973; Geisler and Hubbard 1975) with an area A_p held in the ear canal by springs and dampers representing the annular ring. Such a model should be a fair approximation at low frequencies where the eardrum vibrates in its lowest mode of oscillation. The transfer matrix $\widehat{\mathbf{T}}_u^e \equiv \begin{pmatrix} \widehat{A}_F^{-1} & \widehat{Z}_e \\ \widehat{Y}_e & \widehat{A}_V \end{pmatrix}$ representing the eardrum would then have the form

$$\widehat{\mathbf{T}}_u^e = \begin{pmatrix} A_p^{-1} & Z_p \\ 0 & A_p \end{pmatrix} . \tag{16}$$

The impedance

$$Z_p \equiv i\omega M_p + R_p + K_p/i\omega \tag{17}$$

contains parameters representing the effective mass, damping, and compliance (per unit area) of the plate and the structures holding it in place.

In the plate approximation the two effective areas $\widehat{A}_F$ and $\widehat{A}_V$ are identical and equal to the area of the plate. Since reciprocity implies that

$$\frac{\widehat{A}_F}{\widehat{A}_V} = \frac{1}{1 + \widehat{Z}_e \widehat{Y}_e} , \tag{18}$$

the plate approximation remains approximately valid—in the sense that the areas $\widehat{A}_F$ and $\widehat{A}_V$ have similar values—at frequencies for which $|\widehat{Z}_e \widehat{Y}_e| \ll 1$. If that inequality is satisfied, eardrum transduction can be considered effectively "piston-like" even in the presence of complex surface-displacement patterns.

The plate approximation may be extended by examining the transfer-matrix elements individually. Note that in the plate model the matrix element

$$\widehat{Y}_e \equiv \left. \frac{U_e}{F_u} \right|_{\text{malleus held fixed}} = 0 , \tag{19}$$

reflecting the fact that the plate was assumed to be rigid. However, measurements in the cat made with the ossicles immobilized by gluing them to the cavity walls (Lynch

1981) indicate that $\widehat{Y}_e$ is nonzero and probably compliant at low frequencies,[8] as suggested by Eq. (14). More generally, we assume that at higher frequencies this element has the form of a simple resonator:

$$\widehat{Y}_e \approx Y_d \equiv \left\{ i\omega M_d + R_d + K_d/i\omega \right\}^{-1} . \tag{20}$$

Writing $\widehat{Y}_e(\omega)$ in that form is equivalent to representing $1/\widehat{Y}_e$ by the first three terms in a Laurent expansion in $i\omega$.

With the ossicular load removed, the eardrum might be expected to remain in its lowest mode of oscillation at frequencies higher than those observed by Tonndorf and Khanna. In the lowest mode the volume velocity of the eardrum and the velocity of the umbo should be roughly in phase and proportional. The effective area for velocity is thus approximated, as in the plate model, by a real positive constant:

$$\begin{aligned} \widehat{A}_V &= \left. \frac{U_e}{V_u} \right|_{\text{ossicular load removed}} \\ &\approx \text{real positive constant} \equiv A_e . \end{aligned} \tag{21}$$

The element $\widehat{Z}_e$ is taken, again as in the plate model, to have the form of a harmonic oscillator:

$$\widehat{Z}_e \approx Z_e \equiv i\omega M_e + R_e + K_e/i\omega . \tag{22}$$

Note that the parameters of the model provide phenomenological characterizations of the dynamics; they do not correspond directly to particular anatomical structures, but summarize their collective behavior.

With those assumptions, the effective area for force $\widehat{A}_F$, which relates the pressure across the membrane to the force on the malleus at the umbo, may be determined from the other elements by assuming reciprocity:

$$\det \widehat{\mathbf{T}}_u^e = +1 \quad \Longrightarrow \quad \widehat{A}_F^{-1} = \left. \frac{\widehat{P}_e}{F_u} \right|_{\text{malleus held fixed}} = \frac{1 + \widehat{Z}_e \widehat{Y}_e}{\widehat{A}_V} . \tag{23}$$

---

[8] Lynch (1981) measured the input admittance $Y_{in} \equiv U_e/P_e$ at the eardrum with the malleus "blocked" (so that $V_u = 0$) and found

$$Y_{in} \approx i\omega C \qquad (V_u = 0) \tag{8.1}$$

at low frequencies. Since the middle-ear cavities were widely open, $P_e = \widehat{P}_e$. Hence $Y_{in} = \widehat{Y}_e \widehat{A}_F$. If the plate approximation is correct to first order, then

$$\lim_{\omega \to 0} \frac{\widehat{A}_F}{\widehat{A}_V} = O(1) , \tag{8.2}$$

and the measured frequency variation is primarily that of $\widehat{Y}_e$, which is therefore compliant at low frequencies.

Thus, although $\widehat{A}_V$ is constant in the model, $\widehat{A}_F$ can vary substantially in regions where $\widehat{Z}_e\widehat{Y}_e$ is not constant. The model transfer matrix then has the form

$$\widehat{\mathbf{T}}_u^e \approx \begin{pmatrix} 1 + Z_e Y_d & Z_e A_e^{-1} \\ Y_d A_e & 1 \end{pmatrix} \begin{pmatrix} A_e^{-1} & 0 \\ 0 & A_e \end{pmatrix} , \tag{24}$$

where the factorization, which separates the dimensional and dynamical transformations effected by the eardrum, corresponds to the representation of Fig. 2b. The transfer matrix can be factored further to allow the topology of the corresponding equivalent circuit to be obtained by inspection (see, for example, Table I of Lampton 1978):

$$\widehat{\mathbf{T}}_u^e \approx \begin{pmatrix} 1 & Z_e A_e^{-1} \\ 0 & 1 \end{pmatrix} \begin{pmatrix} 1 & 0 \\ Y_d A_e & 1 \end{pmatrix} \begin{pmatrix} A_e^{-1} & 0 \\ 0 & A_e \end{pmatrix} . \tag{25}$$

The model of Eq. (24) can be thus represented (see Fig. 3) by a series impedance $Z_e A_e^{-1}$ and an ideal transformer (of turns ratio A_e) separated by a shunt admittance $A_e Y_d$. Factorization in that form follows immediately from the assumed constancy of the area $\widehat{A}_V$: were the first two matrices in the product to be interchanged, the area $\widehat{A}_F$, and not $\widehat{A}_V$ would have the constant value A_e.

Simple, qualitative arguments give relations among several of the parameters. First note that the area of the eardrum that moves is presumably greater when the ossicular loading is removed than when the malleus is fixed:

$$\Big(A_0 \equiv \text{Area in motion}\Big)\Big|_{\text{ossicular load removed}} > \Big(A_\infty \equiv \text{Area in motion}\Big)\Big|_{\text{malleus held fixed}} . \tag{26}$$

The subscripts "0" and "∞" denote the no-load and infinite-load conditions, respectively. To the extent, however, that the total mass in motion is proportional to the corresponding area one expects

$$\left(M_e \sim \frac{\text{Mass}_0}{A_0}\right) \approx \left(M_d \sim \frac{\text{Mass}_\infty}{A_\infty}\right) . \tag{27}$$

Consistent with the model's origin as an extension of the plate model, one requires that the areas $\widehat{A}_F$ and $\widehat{A}_V$ be approximately equal at low frequencies. Equation (15) then implies that

$$K_e \ll K_d . \tag{28}$$

Measurement of the matrix elements would allow these relations to be tested experimentally.

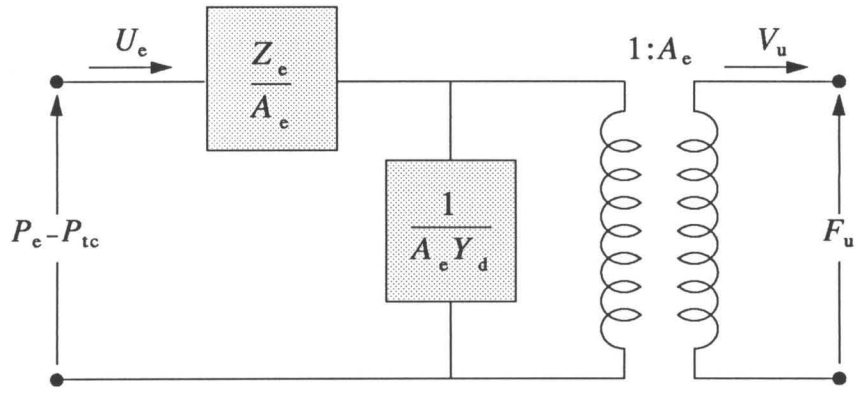

Figure 3. Network representation of the oscillator model defined by Eq. (24).

B. Comparison with simple mechanical models

Further insight into the interpretation of the oscillator model can be gained by comparison with the transfer matrices of simple mechanical models of the eardrum. Recall that the oscillator model reduces to the rigid-plate (single-piston) model when the matrix element $\widehat{Y}_e$ is zero. A more complicated "two-piston" model has been introduced by Shaw (1977; Shaw and Stinson 1981) in an attempt to account for measured membrane surface-displacement patterns. Two limiting forms of the two-piston model, distinguished primarily by the strength of the coupling between the pistons, are discussed below. When the coupling is strong, the transfer characteristics of the two-piston model are shown to reduce to an equation of the form (24). The system then provides a mechanical realization of the model transfer matrix given above. When the coupling is weak, however, the two-piston model has transfer characteristics similar to other simple eardrum models proposed in the literature (e.g., Matthews 1980; Neely 1981).

The compound-eardrum model, illustrated in Fig. 4, represents the eardrum by two coupled plates held in the ear canal with springs and dampers. The malleus is rigidly attached to the center plate. The pressure difference $\widehat{P}_e$ between the ear canal and tympanic cavity drives the motion of the plates and produces a force F_u on the malleus, which is displaced a distance X_u. The motion of the plates also changes the volume of and hence the pressure in the tympanic cavity. If the equations of motion are written in terms of the pressure difference $\widehat{P}_e$, those two effects of plate motion are uncoupled.

The transfer matrix $\widehat{\mathbf{T}}_u^e(\omega)$ for the compound eardrum follows immediately from the equations of motion (the matrix is written most succinctly as a product of factors):

$$\widehat{\mathbf{T}}_u^e = \frac{1}{Z_o + (1+\kappa)Z_c} \begin{pmatrix} Z_o + Z_c & \kappa Z_o Z_c \\ 1 & (2+\kappa)Z_c + \kappa^{-1}(Z_o + Z_c) \end{pmatrix} \begin{pmatrix} 1 & \kappa^{-1} Z_m \\ 0 & 1 \end{pmatrix} \begin{pmatrix} A_m^{-1} & 0 \\ 0 & A_o \end{pmatrix} . \tag{29}$$

Here, Z_m represents the impedance of the plate attached to the malleus and Z_o the impedance of the other plate:

$$Z_m \equiv \left. \frac{\widehat{P}_e}{A_m V_u} \right|_{Z_c=0; F_u=0} \quad \text{and} \quad Z_o \equiv \left. \frac{\widehat{P}_e}{A_o V_o} \right|_{Z_c=0} . \tag{30}$$

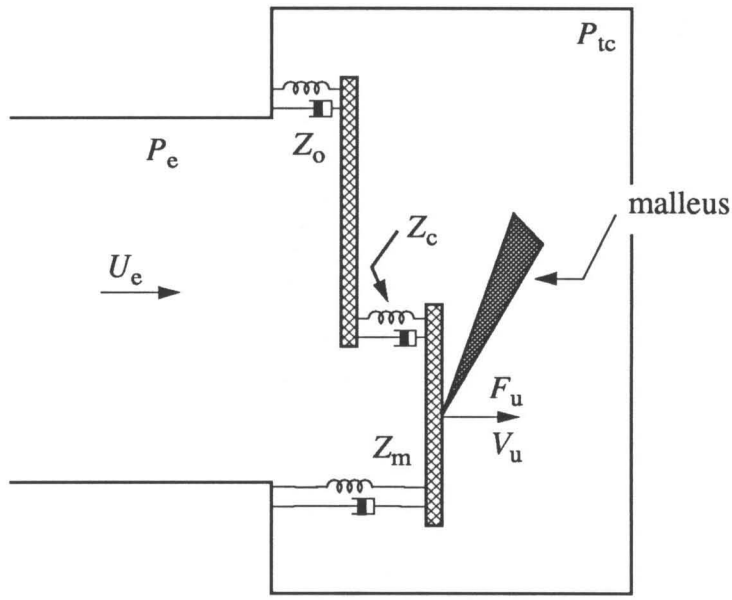

Figure 4. Schematic illustration of the compound-eardrum model in which the eardrum is represented by two coupled plates one of which is attached to the malleus. Following Shaw (1977; 1981), the impedances Z_m and Z_o are shown as harmonic oscillators and the coupling impedance Z_c as a spring-damper combination.

Z_c represents the coupling impedance between the plates and κ the ratio of the plate areas:

$$\kappa \equiv \frac{A_o}{A_m} . \tag{31}$$

In Shaw's model Z_m and Z_o have the form of harmonic oscillators and the interplate coupling impedance Z_c consists of a spring-damper combination.[9] A straightforward calculation gives $\det \hat{\mathbf{T}}_u^e = +1$; as expected, the system is reciprocal.

The transfer-matrix elements of the compound-eardrum model are, in general, complicated combinations of the impedances Z_m, Z_o, and Z_c that define the model. In the limit implied by Shaw and Stinson's (1981) parameter values, however, the matrix elements are, as shown below, considerably simplified. Although the matrix elements themselves can be readily compared with experiment, because definitions (30) require that determination of the impedances Z_m and Z_o be made in the limit $Z_c \to 0$, those quantities would be difficult to measure on a real eardrum.

1. A mechanical realization: Models with strong coupling

To find a mechanical realization for the oscillator model, it is instructive to examine the structure of the transfer-matrix elements (29) in the limit in which the area of the plate coupled directly to the malleus is only a small fraction of the total area of the eardrum (i.e., $\kappa \gg 1$). Note that if the coupling between the umbo and the adjacent membrane (i.e., between the inner and outer plates) is strong relative to the stiffness of the majority of the membrane, then $|Z_o| \ll |Z_c|$. Assume then that

$$\left.\begin{aligned} |Z_m| &\ll \kappa |Z_c| \\ |Z_o| &\ll \kappa |Z_c| \end{aligned}\right\} \qquad (\kappa \gg 1) . \tag{32}$$

In essence, these assumptions imply that the two resonant normal modes of the unloaded compound eardrum are widely separated in frequency so that at low and intermediate frequencies the higher mode may be neglected. In addition, since $\kappa \gg 1$ the motion of the plate attached to the malleus makes little contribution to the total volume velocity of the

---

[9] To recover Shaw's notation use the rules

$$Z_c \longmapsto Z_{do}, \quad Z_o \longmapsto Z_d, \quad \text{and} \quad Z_m \longmapsto Z_o, \tag{9.1}$$

where (this paper) $\longmapsto$ (Shaw and Stinson 1981). Note that the impedances Z_m, Z_o, and Z_c have dimensions different from the impedances Z_e and $1/Y_d$ discussed in the oscillator model.

eardrum. The limiting model outlined here is essentially that implied by the parameters values used by Shaw and Stinson (1981).[10]

Under assumptions (32), the transfer matrix $\widehat{\mathbf{T}}_{\mathrm{u}}^{\mathrm{e}}$ for the compound eardrum reduces to an especially simple form:

$$\lim_{\substack{\text{strong}\\ \text{coupling}}} \widehat{\mathbf{T}}_{\mathrm{u}}^{\mathrm{e}} \approx \begin{pmatrix} 1 & Z_{\mathrm{o}} \\ 0 & 1 \end{pmatrix} \begin{pmatrix} 1 & 0 \\ Z_{\mathrm{c}}^{-1} & 1 \end{pmatrix} \begin{pmatrix} A_{\mathrm{o}}^{-1} & 0 \\ 0 & A_{\mathrm{o}} \end{pmatrix} , \tag{33}$$

as given by the oscillator model [Eq. (25)]. The strong mechanical coupling between the plates ensures that they move together when the ossicular load is removed. Hence, $\widehat{A}_{\mathrm{V}}$ is approximately constant. The coupling—which is not so strong that it prevents *both* plates from moving when motion of the malleus is blocked—allows the moving plate to apply a force to the malleus, thereby giving rise to a frequency variation in the area $\widehat{A}_{\mathrm{F}}$.

2. Another limit: Models with weak coupling

Another class of eardrum models—those with constant $\widehat{A}_{\mathrm{F}}$—arises when the mechanical coupling between the plates is weak and the plates move independently.[11] The transfer matrix then reduces to

$$\lim_{\substack{\text{weak}\\ \text{coupling}}} \widehat{\mathbf{T}}_{\mathrm{u}}^{\mathrm{e}} \approx \begin{pmatrix} 1 & 0 \\ Z_{\mathrm{o}}^{-1} & 1 \end{pmatrix} \begin{pmatrix} 1 & Z_{\mathrm{m}} \\ 0 & 1 \end{pmatrix} \begin{pmatrix} A_{\mathrm{m}}^{-1} & 0 \\ 0 & A_{\mathrm{m}} \end{pmatrix} . \tag{34}$$

Note that relative to the oscillator model, and its realization as a pair of strongly coupled plates, the positions of the matrices corresponding to series and shunt impedances are interchanged. Since only a single plate contributes to the force on the malleus, compound-eardrum models with weak coupling between the plates have $\widehat{A}_{\mathrm{F}}$ approximately constant (e.g., Matthews 1980; Neely 1981).

---

[10] For example, Shaw and Stinson's (1981) parameter values imply that

$$\kappa = 9 \quad \text{and} \quad \kappa \left| \frac{Z_{\mathrm{c}}}{Z_{\mathrm{o}}} \right|_{\omega/2\pi \sim 3\ \mathrm{kHz}} \approx 14 . \tag{10.1}$$

As noted below, however, Shaw's model presents some ambiguity with regard to the composition of the impedance Z_{m}.

[11] The coupling is weak when

$$\left.\begin{aligned} |Z_{\mathrm{m}}| &\gg \kappa |Z_{\mathrm{c}}| \\ |Z_{\mathrm{o}}| &\gg \kappa |Z_{\mathrm{c}}| \end{aligned}\right\} \text{ if } \kappa \geq 1 ; \quad \text{or} \quad \left.\begin{aligned} |Z_{\mathrm{m}}| &\gg |Z_{\mathrm{c}}| \\ |Z_{\mathrm{o}}| &\gg |Z_{\mathrm{c}}| \end{aligned}\right\} \text{ if } \kappa \leq 1 . \tag{11.1}$$

III. Predictions of the Oscillator Model

To illustrate how the transfer matrix provides a common ground for comparing theory and experiment, this section discusses predictions concerning the areas $\widehat{A}_{\mathrm{F}}$ and $\widehat{A}_{\mathrm{V}}$, first for the oscillator model and then for several other models that make definite, testable predictions about the transduction effected by the eardrum.

A. The ratio of the areas

The deviation of the ratio $\widehat{A}_{\mathrm{F}}/\widehat{A}_{\mathrm{V}}$ from unity provides a measure of the extent to which eardrum transduction cannot be characterized as resulting from the action of a single piston. For the oscillator model

$$\xi(\omega) \equiv \frac{\widehat{A}_{\mathrm{F}}}{\widehat{A}_{\mathrm{V}}} = \left[1 + \frac{K_{\mathrm{e}}}{K_{\mathrm{d}}}\left(\frac{1 - \omega^2/\omega_{\mathrm{e}}^2 + i\delta_{\mathrm{e}}\omega/\omega_{\mathrm{e}}}{1 - \omega^2/\omega_{\mathrm{d}}^2 + i\delta_{\mathrm{d}}\omega/\omega_{\mathrm{d}}}\right)\right]^{-1} , \tag{35}$$

where, for example, $\omega_{\mathrm{e}} \equiv \sqrt{K_{\mathrm{e}}/M_{\mathrm{e}}}$ and $\delta_{\mathrm{e}} \equiv \omega_{\mathrm{e}} R_{\mathrm{e}}/K_{\mathrm{e}}$. At low frequencies this ratio approaches

$$\xi_0 \equiv \lim_{\omega \to 0} \frac{\widehat{A}_{\mathrm{F}}}{\widehat{A}_{\mathrm{V}}} = \frac{1}{1 + K_{\mathrm{e}}/K_{\mathrm{d}}} , \tag{36}$$

as given by Eq. (15). Note that if $K_{\mathrm{e}} < K_{\mathrm{d}}$ as argued above, then $\frac{1}{2} < \xi_0 < 1$, in agreement with Eq. (15). Combining Eqs. (27) and (28) yields the further inequality

$$\omega_{\mathrm{e}} < \omega_{\mathrm{d}} . \tag{37}$$

Although $\widehat{A}_{\mathrm{V}}$ is constant, a local maximum in $|\widehat{A}_{\mathrm{F}}(\omega)|$ occurs at roughly $\omega_{\mathrm{peak}} \sim \sqrt{K_{\mathrm{d}}/M_{\mathrm{e}}}$ when $|1 - \xi_0| \ll 1$ and $\omega_{\mathrm{e}}/\omega_{\mathrm{d}} \ll 1$.

Figure 5 shows the ratio of the effective areas $\xi(\omega)$ as a function of frequency for the oscillator model. Shown for comparison are the predictions of other lumped-parameter models of the eardrum for which $\xi(\omega)$ is well defined (Kringlebotn 1988; Matthews 1980; Neely 1981). Each of the models predicts that $|\xi(\omega)|$ is essentially constant and of $O(1)$ at low frequencies but rises to a maximum at frequencies above 1 kHz. (With the given parameter values, the oscillator model predicts a $|\xi(\omega)|$ closest to unity; that model is thus the most "plate-like" at low frequencies.) The position, magnitude, and sharpness of the peak, however, vary dramatically between the models. In the model of Kringlebotn $\widehat{A}_{\mathrm{V}}$ is constant; the peak in $|\widehat{A}_{\mathrm{F}}(\omega)|$ results primarily from a sharp resonance in the

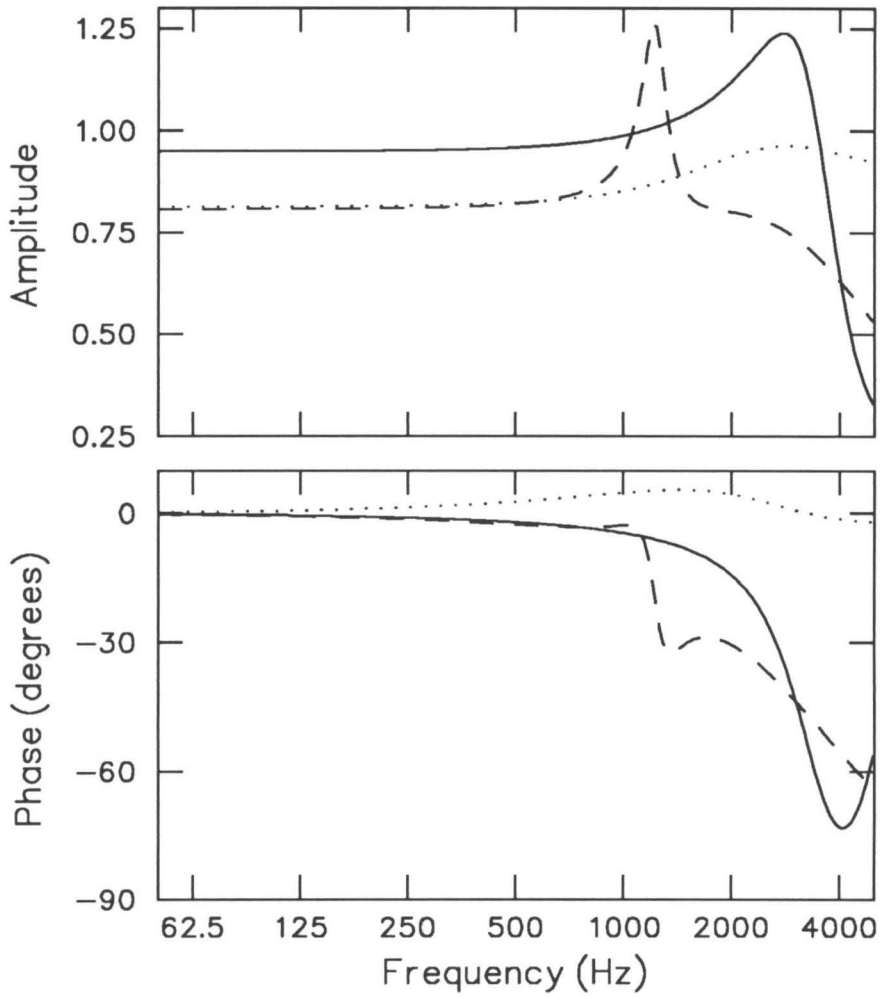

Figure 5. Amplitude and phase of the ratio $\xi(\omega) \equiv \widehat{A}_{\mathrm{F}}/\widehat{A}_{\mathrm{V}}$ for three models of the eardrum: (———) the oscillator model of Sec. II using the parameter values

Name	Value
$\omega_{\mathrm{e}}/2\pi$	1 kHz
$\omega_{\mathrm{d}}/2\pi$	5 kHz
δ_{e}	1.5
δ_{d}	0.5
ξ_0	0.95

; (— — —) the model of Kringlebotn (1988) for the human eardrum; (·····) the model of Matthews (1980) for the cat eardrum with parameter values from Neely (1981). The parameter values used for the oscillator model are typical of those found by fitting measurements of the input impedance in cadavers (Merchant et al. 1988; Rosowski et al. 1990) to a model of the human middle ear (Shera and Zweig 1992d). The model of Matthews–Neely does not explicitly specify the mass of the piston attached to the malleus; it was taken to be proportional to the piston area. Note that since the models are reciprocal,

$$\widehat{A}_{\mathrm{V}}/\widehat{A}_{\mathrm{F}} = 1 + \widehat{Z}_{\mathrm{e}}\widehat{Y}_{\mathrm{e}} \; .$$

In the first two models $\widehat{A}_{\mathrm{V}}$ is constant; in the third, $\widehat{A}_{\mathrm{F}}$.

impedance representing the structures, principally the annular ring, that suspend the eardrum in the ear canal. The model of Matthews-Neely predicts that the area $\widehat{A}_F$ is constant but that $|\widehat{A}_V(\omega)|$ has a broad, shallow minimum—producing a maximum in $|\xi(\omega)|$—at frequencies where the two (mechanically uncoupled) plates representing the eardrum move with opposite phase.

In many eardrum models (e.g., Onchi 1961; Zwislocki 1962; Shaw and Stinson 1981) the matrix elements are not determined because some eardrum impedances are either incompletely specified or lumped together with parameters describing the middle-ear ossicles. Although no quantitative comparison is possible, the ratio $|\xi(\omega)|$ predicted by Shaw and Stinson's (1981) two-piston model can be expected to resemble that found for the oscillator model.

B. Assumptions of other models

Although other authors do not give explicit expressions for the elements of the transfer matrix $\widehat{\mathbf{T}}_u^e$ of the eardrum, the implicit assumptions underlying their work can sometimes be inferred from the topologies of their middle-ear networks. Most authors (e.g., Zwislocki 1962; Lutman and Martin 1979; Matthews 1980; Lynch 1981) implicitly assume that the effective area for force $\widehat{A}_F(\omega)$ is a real constant independent of frequency. Onchi (1961) and Kringlebotn (1988), by contrast, make the implicit assumption that the area for velocity $\widehat{A}_V(\omega)$ is a real constant. For the reasons outlined above, that approximation was explicitly adopted in the oscillator model outlined in Sec. II. In his two-piston model Shaw (1977) effectively assumes that $\widehat{A}_V(\omega)$ and $\widehat{A}_F(\omega)$ are complex functions with a frequency variation dependent on the detailed interaction of the pistons. As shown above, however, Shaw and Stinson's (1981) parameter values imply that $\widehat{A}_V(\omega)$ is approximately constant. The transfer-matrix elements for more detailed theoretical descriptions of the eardrum (e.g., Funnell et al. 1987; Rabbitt and Holmes 1986) are not available.

IV. Summary

The paper presents a framework, based on the matrix $\widehat{\mathbf{T}}_u^e$, for the phenomenological description of eardrum transduction. Measurements determining the matrix elements are defined. The measurements are invasive and involve manipulation of the middle-ear

ossicles to vary the load on the eardrum. (Measurements of eardrum surface-displacement patterns do not determine the transfer-matrix elements.) Within its region of validity, the transfer matrix of the eardrum constitutes a common ground where theory and experiment may be systematically compared. In addition:

- Analyticity and symmetry conditions that may place constraints on the measurements of the matrix elements are identified. Those constraints may be used either to reduce the number of measurements necessary to characterize the eardrum or to check the consistency of measurements that overdetermine the system. Causality constrains the analytic structure of the transfer-matrix elements individually. Reciprocity and minimum-phase behavior are constraints whose applicability to the eardrum depends on the nature of its dynamics. The principle of reciprocity, if found to be applicable, provides algebraic constraints among the elements.
- Two complex effective areas, $\widehat{A}_{\mathrm{F}}(\omega)$ and $\widehat{A}_{\mathrm{V}}(\omega)$, comprise two of the matrix elements. Those two areas are associated, respectively, with the transmission of force to the middle-ear ossicles and with the change in volume of the tympanic cavity resulting from motion of the eardrum. Reciprocity implies that those two areas cannot be equal.
- For purposes of illustration an oscillator model of the transfer characteristics of the eardrum is presented. The oscillator model uses reciprocity, and the assumed constancy of the area $\widehat{A}_{\mathrm{V}}(\omega)$, to determine the element $\widehat{A}_{\mathrm{F}}(\omega)$ in terms of others whose form can be approximated by a Laurent expansion in $i\omega$. The model matrix elements are minimum-phase functions.

Acknowledgments

The authors thank William Peake and John Rosowski for their comments on an earlier version of the manuscript. This work was supported by the Theoretical Division of Los Alamos National Laboratory and a National Science Foundation Graduate Fellowship to C. A. S.

References

von Bally, G. (1976). "Holographic analysis of tympanic membrane vibrations in human temporal bone preparations using a double pulsed ruby laser system," in *Applications of Holography and Optical Data Processing*, edited by E. Maron et al., 593–602. Oxford: Pergamon Press.

von Békésy, G. (1941). "Über die Messung der Schwingungsamplitude der Gehörknochelchen mittels einer kapazitiven Sonde," *Akust. Zeits.* **6**, 1–16.

von Békésy, G. (1960). *Experiments in Hearing.*New York: McGraw-Hill.

Bode, H. (1945). *Network Analysis and Feedback Amplifier Design.*Princeton: Van Nostrand Reinhold.

Brillouin, L. (1946). *Wave Propagation in Periodic Structures.*New York: McGraw-Hill.

Buunen, T. J. F. and M. S. M. G. Vlaming (1981). "Laser-Doppler velocity meter applied to tympanic membrane vibrations in cat," *J. Acoust. Soc. Am.* **69**, 744–750.

Dallos, P. (1973). *The Auditory Periphery: Biophysics and Physiology.*New York: Academic Press.

Decraemer, W. F., S. M. Khanna, and W. R. J. Funnell (1989). "Interferometric measurement of the amplitude and phase of tympanic membrane vibrations in cat," *Hearing Res.* **38**, 1–18.

Donahue, K. M. (1989). "Human middle-ear mallear motion: Models and measurements," M.S. thesis, Massachusetts Institute of Technology.

Esser, M. H. (1947). "The mechanism of the middle ear: Part II. The drum," *Bull. Math. Biophysics* **9**, 75–91.

Foldy, L. L. and H. Primakoff (1945). "A general theory of passive linear electroacoustic transducers and the electroacoustic reciprocity theorem. I," *J. Acoust. Soc. Am.* **17**, 109–120.

Friedland, B., O. Wing, and R. Ash (1961). *Principles of Linear Networks.*New York: McGraw-Hill.

Funnell, W. R. J., W. F. Decraemer, and S. M. Khanna (1987). "On the damped frequency response of a finite-element model of the cat eardrum," *J. Acoust. Soc. Am.* **81**, 1851–1859.

Geisler, C. D. and A. E. Hubbard (1975). "The compatibility of various measurements on the ear as related by a simple model," *Acustica* **33**, 220–222.

Graham, M. D., C. Reams, and R. Perkins (1978). "Human tympanic membrane-malleus attachment," *Ann. Otol. Rhinol. Laryngol.* **87**, 426–431.

Guinan, J. J. and W. T. Peake (1967). "Middle-ear characteristics of anesthetized cats," *J. Acoust. Soc. Am.* **41**, 1237–1261.

Helmholtz, H. L. F (1860). "Theorie des Luftschalls in Rohren mit offenen Enden," *Crelle J.* **57**, 1.

Helmholtz, H. L. F. (1868). "*Die Mechanik der Gehörknöchelchen und des Trommelfells*," *Pflüg. Arch. ges. Physiol.* **1**, 1–60. Trans. by A. H. Buck and N. Smith, "The mechanism of the ossicles of the ear and the membrana tympani," 1873.

Khanna, S. M. and J. Tonndorf (1972). "Tympanic membrane vibrations in cats studied by time-averaged holography," *J. Acoust. Soc. Am.* **51**, 1904–1920.

Kringlebotn, M. (1988). "Network model for the human middle ear," *Scand. Audiol.* **17**, 75–85.

Lampton, M. (1978). "Transmission matrices in electroacoustics," *Acustica* **39**, 239–251.

Løkberg, O.J, K. Høgmoen, and T. Gundersen (1980). "Vibration measurement in the human tympanic membrane — in vivo," *Acta Otolaryngol.* **89**, 37–42.

Lutman, M. E. and A. M. Martin (1979). "Development of an electroacoustic analogue model of the middle ear and acoustic reflex," *J. Sound Vib.* **64**, 133–157.

Lynch, T. J. (1981). "Signal processing by the cat middle ear: Admittance and transmission, measurements and models," Ph.D. thesis, Massachusetts Institute of Technology.

Matthews, J. W. (1980). "Mechanical modeling of nonlinear phenomena observed in the peripheral auditory system," Ph.D. thesis, Washington University, St. Louis.

Maxwell, J. C. (1864). "On the calculations of the equilibrium and stiffness of frames," *Phil. Mag.* **27**, 294–299.

McMillan, E. M. (1946). "Violation of the reciprocity theorem in linear passive electromechanical systems," *J. Acoust. Soc. Am.* **18**, 344–347.

Merchant, S. N., P. J. Davis, J. J. Rosowski, and M. D. Coltrara (1988). "Normality of the input immittance of middle ears from human cadavers," Abstracts of the 11th ARO Midwinter Research Meeting.

Neely, S. T. (1981). "Fourth-order partition dynamics for a two-dimensional model of the cochlea," D.Sc. thesis, Sever Institute of Technology, Washington University, St. Louis.

Onchi, Y. (1961). "Mechanism of the middle ear," *J. Acoust. Soc. Am.* **33**, 794–805.

Peake, W. T. and J. J. Guinan (1967). "Circuit model for the cat's middle ear," *MIT Quart. Prog. Rep.* **84**, 320–326.

Rabbitt, R. D. and M. H. Holmes (1986). "A fibrous dynamic continuum model of the tympanic membrane," *J. Acoust. Soc. Am.* **80**, 1716–1728.

Rayleigh, J. W. (1896). *Theory of Sound.*New York: Dover.

Rosowski, J. J., P. J. Davis, S. N. Merchant, K. M. Donahue, and M. D. Coltrara (1990). "Cadaver middle ears as models for living ears: Comparisons of middle-ear input immittance," *Ann. Otol. Rhinol. Laryngol.* , .

Schuknecht, H. F. and A. J. Gulya (1986). *Anatomy of the Temporal Bone with Surgical Implications.*Philadelphia: Lea and Febiger.

Shaw, E. A. G. (1977). "Eardrum representation in middle-ear acoustical networks," *J. Acoust. Soc. Am.* **62** Suppl. 1, S102.

Shaw, E. A. G. and M. R. Stinson (1981). "Network concepts and energy flow in the human middle ear," *J. Acoust. Soc. Am.* **69** Suppl. 1, S43.

Shaw, E. A. G. and M. R. Stinson (1986). "Eardrum dynamics, middle-ear transmission and the human hearing threshold curve," in *Proceedings of the 12th International Congress on Acoustics*, Toronto.

Shera, C. A. and G. Zweig (1991c). "Phenomenological characterization of eardrum transduction," *J. Acoust. Soc. Am.* **90**, 253–262.

Shera, C. A. and G. Zweig (1992a). "Middle-ear phenomenology: The view from the three windows," submitted to *J. Acoust. Soc. Am.*

Shera, C. A. and G. Zweig (1992d). "Noninvasive estimation of middle-ear transfer characteristics in human cadavers," in preparation.

Stevens, K. N., R. Berkovitz, G. Kidd, Jr., and D. M. Green (1987). "Calibration of ear canals for audiometry at high frequencies," *J. Acoust. Soc. Am.* **81**, 470–484.

Stinson, M. R. (1985). "The spatial distribution of sound pressure within scaled replicas of the human ear canal," *J. Acoust. Soc. Am.* **78**, 1596–1602.

Tonndorf, J. and S. M. Khanna (1970). "The role of the tympanic membrane in middle ear transmission," *Ann. Otol. Rhinol. Laryngol.* **79**, 743–753.

Tonndorf, J. and S. M. Khanna (1972). "Tympanic-membrane vibrations in human cadaver ears studied by time-averaged holography," *J. Acoust. Soc. Am.* **52**, 1221–1233.

Wever, E. G., M. Lawrence, and K. R. Smith (1948). "The middle ear in sound conduction," *Arch. Otolaryngol.* **48**, 19–35.

Wever, E. G. and M. Lawrence (1954). *Physiological Acoustics.*Princeton: Princeton University Press.

Zweig, G. (1976). "Basilar membrane motion," in *Cold Spring Harbor Symposia on Quantitative Biology, volume XL, 1975*, 619–633. Cold Spring Harbor: Cold Spring Harbor Laboratory.

Zweig, G. and S. Konishi (1987). "Constraints on measurements of causal or minimum-phase systems," accepted for publication in *J. Acoust. Soc. Am.*

Zwislocki, J. (1962). "Analysis of the middle-ear function. Part I: Input impedance," *J. Acoust. Soc. Am.* **34**, 1514–1523.

Zwislocki, J. J. (1975). "The role of the external and middle ear in sound transmission," in *The Nervous System, Vol. 3: Human Communication and Its Disorders*, edited by D. B. Tower, 45–55. New York: Raven Press.

Middle-Ear Phenomenology: The View from the Three Windows

Christopher A. Shera and George Zweig

Theoretical Division
Los Alamos National Laboratory
Los Alamos, New Mexico 87545

and

Physics Department
California Institute of Technology
Pasadena, California 91125

ABSTRACT

To provide a common ground for the comparison between theory and experiment, this paper presents a framework for the phenomenological description of middle-ear mechanics. The framework defines those measurements sufficient to characterize the transduction properties of the middle ear and its components. Phenomenological equations are represented in the form of an equivalent electrical circuit that can be used to deduce testable relations among measurable quantities. Two applications are then discussed. First, the classical concept of the middle-ear transformer ratio is generalized to include any effects of eardrum flexion or nonrotational ossicular motion. Middle-ear models predict that the resulting transformer ratios vary considerably with frequency. Second, the conditions under which the topology of existing circuit analogs satisfactorily approximates middle-ear mechanics are given. Most middle-ear models cannot be used to correctly predict the absolute pressures in the cochlea.

Contents

Appendix A: Phenomenology of the Feline Middle Ear

A. The round window

B. The cavities

C. Equivalent circuit

Introduction

The middle ear converts air-borne sound waves into hydromechanical waves that travel along the fluid-filled chambers of the cochlea. Many models of the middle ear have been proposed to describe that transduction, a number of which correctly represent the middle-ear input impedance of an "average" ear. Yet even at low frequencies those models, most consisting of lumped-parameter circuit analogues, remain incompletely tested. For example, models predict both "forward-" and "reverse-transmission" characteristics, but the latter have never been compared with experiment. In addition, the models often include circuit elements that are not defined by equations relating measurable quantities in the middle ear. Finally, comprehensive measurements in a single animal, necessary for a rigorous comparison between model predictions and experiment, are lacking.

Since measurements are incomplete and middle-ear transduction not well understood, the need exists for a framework within which theory and experiment may be systematically compared. This paper presents such a framework—analogous to that proposed earlier for the eardrum (Shera and Zweig 1991c)—for the phenomenological description of mammalian middle-ear mechanics. The goals of the framework are

- to indicate those experiments sufficient to characterize the transfer characteristics of the middle ear and of its components;
- to show how to prove what is believed known about the system (i.e., its analyticity and symmetry properties) and, once proven, to remove the effects of those constraints from measurements;
- to make explicit the (often incompletely tested) assumptions underlying circuit models of the middle ear;
- to indicate the conditions under which existing circuit models accurately predict the pressures in the cochlea;
- to show how the forward and reverse transduction characteristics of the middle ear can be found from characterizations of its constituent parts, and, conversely, how measurements of those transduction characteristics can be "inverted" to describe the components; and thus
- to provide a common ground for comparing theory and experiment on the middle ear.

The description is obtained by writing down the minimum number of equations that suffice

to describe the action of the middle ear as viewed from the "outside"—that is, from behind the three "windows" (i.e., the eardrum and the oval and round windows) that face onto the tympanic cavity. Those equations are independent of the boundary conditions at any of the three windows. For example, no assumptions about the nature of the cochlear load (e.g., its compressibility) are made. The form of the resulting equations depends only on the linearity of middle-ear mechanics, an assumption that holds throughout the intensity range of normal hearing below the threshold for activation of the acoustic reflex.

This paper is the second in a series (Shera and Zweig 1991c, 1992a-d) devoted to middle-ear mechanics. The two companion papers (Shera and Zweig 1992bc) apply the phenomenology outlined here to address problems of middle-ear and cochlear mechanics. The final paper in the pentalogy (Shera and Zweig 1992d) proposes a simple model of the human middle ear and uses it to "invert" measurements of the middle-ear input impedance in individual subjects and obtain noninvasive estimates of the mechanical properties of the components of the middle ear.

A. Overview

This paper extends the phenomenological framework applied previously to the eardrum (Shera and Zweig 1991c) to encompass the entire middle ear. Middle-ear mechanics is first reviewed and linearity shown to guarantee the existence of simple matrix relations among the pressures and volume velocities at the three windows (Sec. I). A phenomenological description of middle-ear mechanics independent of the boundary conditions at the windows is then presented (Sec. II), including characterizations of the eardrum (Shera and Zweig 1991c) and the ossicular chain. The description of middle-ear mechanics—written in terms of measurable impedances describing the mechanical and acoustic properties of the membranes, bones, ligaments, and cavities of the middle ear—is summarized in a block-diagram equivalent circuit (Sec. III). The structure of the equations is then explored, their representation and solution for various stimulus configurations outlined, and testable consistency relations given. The paper concludes (Sec. IV) with an examination of two issues important for middle-ear mechanics: 1) the generalization of the classical concept of the middle-ear transformer ratio to include the effects of eardrum flexion and any nonrotational oscillation or bending of the ossicles; and 2) the conditions under which existing circuit models accurately predict the pressures in the cochlea.

I. The Structure of the Middle Ear

The human middle ear consists of those structures within and facing onto the tympanic cavity. The tympanic cavity is an irregularly shaped, room-like enclosure in the temporal bone bounded by six walls. (In many mammals, such as cats and rodents, the middle ear is surrounded not by the temporal bone but instead by a bony compartment known as the auditory bulla.) The walls, lined with a thin, ciliated mucosa, face one another in roughly paired opposition. The lateral wall of the cavity is formed by the eardrum, which moves in response to incident sound. Suspended from ligaments and muscles attached to the cavity walls, the three bones of the ossicular chain span the cavity like an arch and transmit the motion of the eardrum to the oval window on the medial wall, where the vibration of the stapes sets the cochlear fluids into motion. Volume displacements of the stapes footplate are relieved by displacement of the round window located in a membrane-covered niche on the medial wall. The posterior wall of the cavity opens through the aditus into the mastoid antrum, whose walls are lined with a labyrinth of mastoid air cells reminiscent of a miniature swiss cheese. That cancellate mastoid meshwork greatly increases the surface area of the cavity. The anterior wall opens into the Eustachian tube, which connects the tympanic cavity with the pharynx. Closed during normal hearing, the Eustachian tube opens during swallowing to permit equalization of pressure in the tympanic cavity. The superior wall, or roof, of the cavity separates the tympanic cavity from the brain, whereas the floor separates the middle ear from the carotid artery and the jugular bulb.

The arrival of a sound wave at the eardrum triggers a series of events in the middle ear. In brief, the eardrum oscillates, changing the pressure in the tympanic cavity and moving the malleus. The vibration of the malleus is transmitted bone by bone through the ossicular chain to the oval window, where the vibration of the stapes footplate sets the cochlear fluids into motion, generating waves that travel down the organ of Corti. Although coupling through the ossicular chain is stronger, pressure variations in the tympanic cavity also affect the motion of both the stapes and the round window. The middle ear can, of course, be driven "in reverse" by the arrival at the stapes and round window of waves generated within the cochlea.

A. Linearity of the middle ear

The measurements of Guinan and Peake (1967) and Buunen and Vlaming (1981) on the cat indicate that the middle ear responds linearly throughout the intensity range of normal hearing up to the threshold for activation of the acoustic reflex. Working on cadavers, Rubinstein et al. (1966) found a linear variation in stapes displacement with sound pressure level (SPL) below $\sim$ 100 dB SPL. Correspondingly, linearity for humans will be assumed. Linearity implies that the middle ear can be completely characterized in terms of its response to pure tones; all variables in this paper have therefore been written as complex quantities describing those responses.

B. Middle-ear geometry: A room with three views

Figure 1 provides a schematic illustration of a generic mammalian middle ear. Three flexible membranes face onto the tympanic cavity, the ossicular chain connecting the eardrum with the oval window. (Complications arising in mammals, such as the cat, in which the oval and round windows face onto separate cavities are addressed in Appendix A.) Associated with each of the three "windows" is a corresponding pressure P—representing an average over the membrane surface—and net volume velocity U. The linearity of middle-ear mechanics implies that the middle ear can be regarded as a "black box" and characterized by its frequency response without detailed knowledge of its internal dynamics. Phenomenological equations provide relations among the seven variables—a pressure and volume velocity outside each of three windows and the pressure within the tympanic cavity—illustrated in the figure. The equations describe the response of the middle ear when it is driven from any of the three windows or from the cavity onto which they face. The form of those equations is independent of specific details of cavity geometry and the precise mode of motion of the bones of the middle ear.

Four phenomenological equations relate the seven variables in the figure.[1] Those four equations provide a complete phenomenological description of middle-ear mechanics. The three additional equations necessary to complete the system specify the boundary conditions, one at each of the three windows.

[1] More generally, $n - n_w$ equations (where n_w is the number of windows) relate n unknowns. In the cat, for example, $n = 9$ and $n_w = 3$ (see Appendix A).

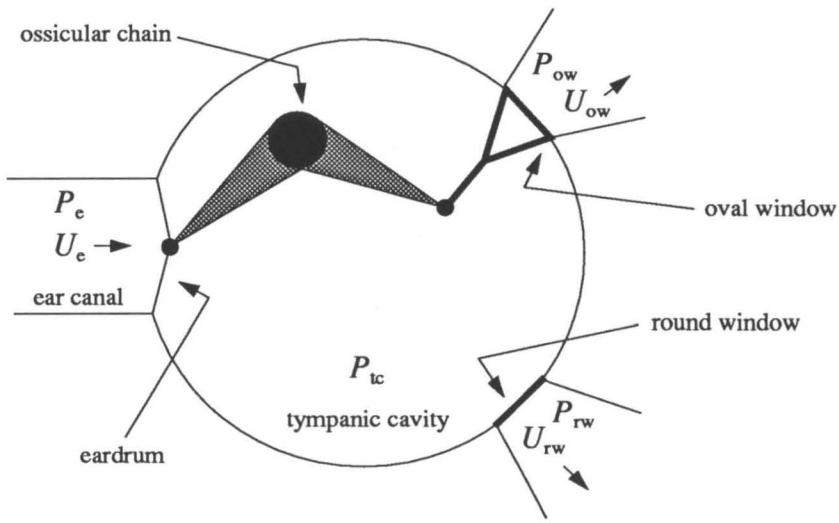

Figure 1. Schematic representation of a typical mammalian middle ear illustrating the "room with three views (windows)." Associated with each window is a corresponding pressure P and volume velocity U. This simple picture must be extended in animals, such as the cat, in which the round window faces onto the bulla.

Linearity implies that the middle-ear equations can be summarized by matrix relations in which three (i.e., the number of windows) of the variables are regarded as "independent" (that is, they are determined not by middle-ear mechanics but by boundary conditions at the windows) and the other variables expressed in terms of them. Which three of the seven variables are chosen as independent may depend, for example, on how the system is driven.

As a simple illustration, note that the structure and linearity of the middle ear guarantee that the four pressures P are linear, homogeneous functions of the three volume velocities U; that is, there exists a matrix $\mathbf{Z}$ such that

$$\begin{pmatrix} P_{\mathrm{e}} \\ P_{\mathrm{ow}} \\ P_{\mathrm{rw}} \\ P_{\mathrm{tc}} \end{pmatrix} = \mathbf{Z} \begin{pmatrix} U_{\mathrm{e}} \\ U_{\mathrm{ow}} \\ U_{\mathrm{rw}} \end{pmatrix} , \tag{1}$$

where $\mathbf{Z}$ is a 4×3 matrix of impedance coefficients determined (solely) by middle-ear mechanics. The homogeneity of the equations follows from the assumption that the middle-ear contains no independent internal sources of motion. There are, of course, $\binom{7}{3} = 35$ such matrices, one for each choice of the three independent variables.

The four equations that constitute Eq. (1)—or, equivalently, the four simpler equations obtained below—summarize middle-ear mechanics in a manner independent of the boundary conditions at the three windows. Specification of those boundary conditions provides the three additional equations that complete the system. In a typical application, that specification would include characterizations of the cochlear load and a source term in the ear canal that determines, for example, the volume velocity U_{e} delivered by an earphone.

The equations obtained in the next section—which summarize the mechanical and acoustical properties of the membranes, bones, ligaments, and cavities of the middle ear by a few independent, measurable impedance functions (five, if eardrum/ossicular transduction is reciprocal)—permit determination of all twelve matrix elements of $\mathbf{Z}$ (or the corresponding elements of any of the other possible matrices). Subsequent sections discuss the representation of those equations as equivalent circuits, examine the nature of the boundary conditions, and provide examples in which the formalism is applied to problems of middle-ear mechanics.

II. Phenomenological Deconstruction of Middle-Ear Mechanics

This section examines each of the major functional components of the middle ear and obtains equations describing the motion of the three windows and the ossicular chain. Obtaining equations that are independent of the cochlear load is facilitated by noting that the effects of the cavities and the ossicular chain can be uncoupled. Such uncoupling permits the definition of a "transfer matrix" that describes the combined action of the eardrum and the bones of the middle ear. Under certain conditions, that matrix can be factored into components representing the separate contributions of the eardrum and the ossicular chain. If the motion of the stapes is sufficiently simple, the matrix representing the middle-ear ossicles can itself be factored. When those factorizations are valid, middle-ear transduction characteristics can be systematically "deconstructed" in a manner that permits convenient comparison between theory and experiment.

A. Characterization of the eardrum and ossicular chain

1. Uncoupling the cavities

Motion of the eardrum has two effects on the middle ear: it both vibrates the middle-ear bones and changes the pressure in the middle-ear cavities. A discussion of the mechanics of the middle ear is simplified if those two effects of eardrum motion are separated.

The eardrum and the oval window both face onto the tympanic cavity; each moves in response to a pressure difference across its surface. The motion of each membrane is therefore naturally described in terms of a pressure difference $\widehat{P}$ defined by

$$\widehat{P} \equiv P - P_{\mathrm{tc}} \ , \tag{2}$$

where P_{tc} is the pressure in the tympanic cavity. Pressure differences $\widehat{P}$ signified by the diacritical hat are simply pressures measured relative to a reference in the tympanic cavity. Note that if the middle-ear cavities were surgically exposed and opened widely to the atmosphere, the pressure in the tympanic cavity would become a constant atmospheric, and P_{tc} would, by definition, vanish; the two pressures $\widehat{P}$ and P would then become equivalent.[2] With the cavities exposed in that manner, the eardrum remains coupled to the

[2] Here we assume that the cavities are opened widely enough that the radiation impedances of any holes in the cavities can be neglected at the low and intermediate frequencies (i.e., less than roughly 10 kHz) for which the framework is valid.

inner ear only through the motion of the ossicular chain. The cavities thus affect middle-ear transduction by providing a frequency-dependent pressure offset from the atmospheric pressure surrounding the head.

2. The eardrum and ossicular chain: ${}^{e}\hat{\mathbf{T}}_{ow}$

When pressures are measured relative to the cavity reference, the effects of the cavities are uncoupled from those of the ossicular chain. Such uncoupling permits the introduction of a transfer matrix, ${}^{e}\hat{\mathbf{T}}_{ow}$, that characterizes the eardrum/ossicular contribution to coupling between the ear canal and the oval window (see Fig. 2a). Consider the transformation from the pressure and volume velocity at the eardrum to the pressure and volume velocity at the oval window in the inner ear. Since the transformation is linear, those four quantities are related by an equation of the form

$$\begin{pmatrix} \hat{P}_e \\ U_e \end{pmatrix} = {}^{e}\hat{\mathbf{T}}_{ow} \begin{pmatrix} \hat{P}_{ow} \\ U_{ow} \end{pmatrix} ; \tag{3}$$

where the matrix,

$${}^{e}\hat{\mathbf{T}}_{ow} \equiv \begin{pmatrix} \hat{N}_P^{-1} & \hat{Z} \\ \hat{Y} & \hat{N}_U \end{pmatrix} , \tag{4}$$

is a 2×2 matrix of complex, frequency-dependent transfer coefficients. (The diacritical hats indicate that the matrix elements are measured with the cavities opened widely.) The matrix ${}^{e}\hat{\mathbf{T}}_{ow}$ thus characterizes the generation of force by the eardrum and its subsequent transmission to the cochlea by the bones and ligaments of the middle ear in a manner independent of any sources or loads presented to it. The same matrix elements characterize the system whether it is driven from the free field or "in reverse" from within the inner ear.

The matrix elements of ${}^{e}\hat{\mathbf{T}}_{ow}$ have simple physical interpretations as ratios of "input" to "output" variables under specific loading conditions. For example, reference to Eq. (3) yields

$$\hat{Z} = \left. \frac{\hat{P}_e}{U_{ow}} \right|_{\hat{P}_{ow}=0} . \tag{5}$$

The element $\hat{Z}(\omega)$ may therefore be interpreted as the "no-load" transfer impedance. In practice, the pressure P_{ow} may be set to zero by draining the cochlear fluids and removing the organ of Corti. The other matrix element have similar interpretations: $\hat{N}_P^{-1}$ is the

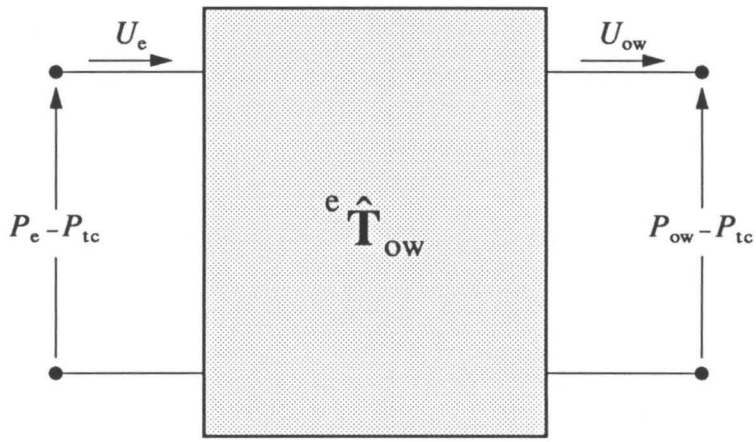

Figure 2a. Schematic illustration of the transformation performed by the combined action of the eardrum and ossicular chain.

"infinite-load" pressure ratio, $\hat{Y}$ the infinite-load transfer admittance, and $\hat{N}_U$ the no-load velocity ratio. In the language of electrical circuits, the no- and infinite-load conditions correspond, respectively, to short and open circuits. The interpretation of $\hat{N}_P$ and $\hat{N}_U$ as generalized middle-ear transformer ratios is discussed in Sec. IV-A.

The matrix elements are not all independent; constraints on the elements—which may be used either to reduce the number of measurements necessary to characterize eardrum/ossicular transduction or to check the consistency of measurements that overdetermine the system—are discussed in the first paper of the series (Shera and Zweig 1991c). Examples of such constraints include causality, which requires that the real and imaginary parts of each matrix element be Hilbert transforms of one another, and reciprocity, which requires that $\det {}^{e}\hat{\mathbf{T}}_{ow} = +1$.[3]

Note that the matrix ${}^{e}\hat{\mathbf{T}}_{ow}$ provides a meaningful description of the open-cavity middle ear whenever the four variables defining the transformation constitute the effective input and output of the system. The vibration of the eardrum and ossicles can be arbitrarily complicated, involving complex oscillations in all three spatial dimensions, so long as the input and output are effectively one-dimensional. On the "input" side, the pressure in the human ear canal near the eardrum is uniform in any cross-section at frequencies at least as high as 6 kHz (Stinson 1985). And on the output side, measurements near the oval window in the basal turn of the cat cochlea are consistent with the "long-wavelength approximation," indicating that the pressure is essentially uniform across the stapes footplate, at least for frequencies much less than the local characteristic frequency (Nedzelnitsky 1980).

3. Approximate factorization of ${}^{e}\hat{\mathbf{T}}_{ow}$

When the input to the ossicular chain (i.e., the output of the eardrum) can itself be summarized by two variables—representing, for example, the effective force F_u produced by the eardrum at the umbo and the umbo velocity V_u—the matrix ${}^{e}\hat{\mathbf{T}}_{ow}$ can be factored into two component matrices, the first, ${}^{e}\hat{\mathbf{T}}_{u}$, describing the transduction of the eardrum (Shera and Zweig 1991c) and the second, ${}^{u}\hat{\mathbf{T}}_{ow}$, describing the action of the ossicular chain (see Fig. 2b):

$$ {}^{e}\hat{\mathbf{T}}_{ow} \approx {}^{e}\hat{\mathbf{T}}_{u}\,{}^{u}\hat{\mathbf{T}}_{ow} \,. \tag{6}$$

[3] Although the middle ear is expected to be reciprocal, it is conceivable that some as yet unrecognized aspect of its dynamics could render the system nonreciprocal (e.g., were the eardrum or ossicular chain actively to amplify signal energy during transduction).

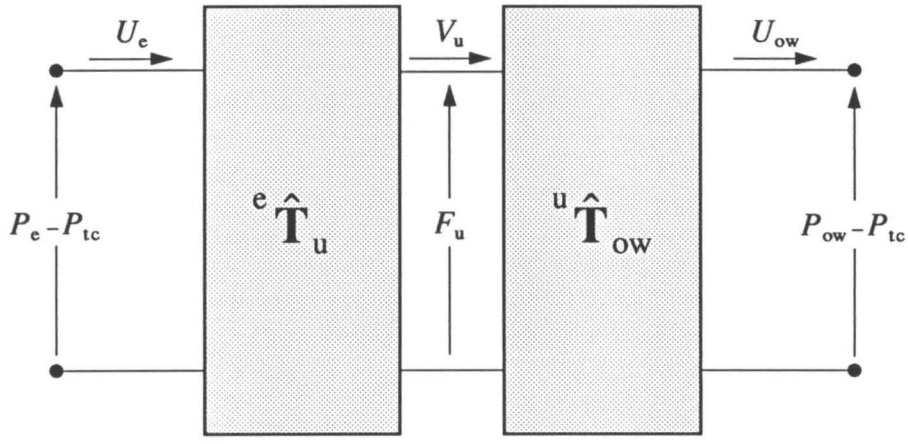

Figure 2b. Network representation of the eardrum/ossicular transformation based on the approximate factorization of the matrix ${}^{e}\hat{\mathbf{T}}_{ow}$ into a product of matrices describing the eardrum and ossicular transformations individually.

The component matrices satisfy the equations

$$\begin{pmatrix} \hat{P}_e \\ U_e \end{pmatrix} = {}^{e}\hat{\mathbf{T}}_u \begin{pmatrix} F_u \\ V_u \end{pmatrix} , \tag{7}$$

and

$$\begin{pmatrix} F_u \\ V_u \end{pmatrix} = {}^{u}\hat{\mathbf{T}}_{ow} \begin{pmatrix} \hat{P}_{ow} \\ U_{ow} \end{pmatrix} . \tag{8}$$

Note that the two equations (7) and (8) can be combined and written in an abbreviated symbolic form, analogous to the representation in Fig. 2b, in which each matrix is flanked by the input and output vectors it transforms:

$$\begin{pmatrix} \hat{P}_e \\ U_e \end{pmatrix} {}^{e}\hat{\mathbf{T}}_u \begin{pmatrix} F_u \\ V_u \end{pmatrix} {}^{u}\hat{\mathbf{T}}_{ow} \begin{pmatrix} \hat{P}_{ow} \\ U_{ow} \end{pmatrix} . \tag{9}$$

This more compact notation is used again in Sec. II-A-3-b-2 when discussing an approximate factorization of the the matrix ${}^{u}\hat{\mathbf{T}}_{ow}$.

The regions of validity for this factorization are not known with any certainty (Shera and Zweig 1991c); presumably the factorization applies at least at low frequencies where the vibration of the ossicles is sufficiently simple (Donahue 1989; Donahue et al. 1991; Decraemer and Khanna 1991).

a) The eardrum: ${}^{e}\hat{\mathbf{T}}_u$

Motion of the eardrum both exerts a force on the malleus and drives pressure variations in the tympanic cavity. A phenomenological description of eardrum mechanics is provided by the transfer matrix ${}^{e}\hat{\mathbf{T}}_u$ of the eardrum, defined by Eq. (7). Measurement and interpretation of the matrix elements,

$${}^{e}\hat{\mathbf{T}}_u = \begin{pmatrix} \hat{A}_F^{-1} & \hat{Z}_e \\ \hat{Y}_e & \hat{A}_V \end{pmatrix} , \tag{10}$$

are discussed elsewhere (Shera and Zweig 1991c). Note, however, that the characterization includes two effective areas of the eardrum. The first, the "effective area for force" $\hat{A}_F$, provides the force on the malleus due to the pressure difference $\hat{P}_e$ across the eardrum when the malleus is immobilized. When loading due to the ossicular chain has been removed, the second, the "effective area for velocity" $\hat{A}_V$, relates the volume displacement of the eardrum to the displacement of the umbo. If the eardrum were a rigid piston, both effective areas would be real constants equal to the area of the piston. In general, however, the two areas $\hat{A}_V(\omega)$ and $\hat{A}_F(\omega)$ are different complex functions of frequency.

b) The ossicular chain: ${}^{u}\hat{\mathbf{T}}_{ow}$

The eardrum exerts a force on the malleus that is then transmitted, bone by bone, to the stapes footplate in the oval window. Although the precise mode of motion of the middle-ear ossicles remains somewhat controversial (e.g., Khanna and Tonndorf 1972; Gundersen and Høgmoen 1976; Brenkman et al. 1986; Gyo et al. 1987; Donahue 1989; Donahue et al. 1991; Decraemer and Khanna 1991), a phenomenological description of ossicular mechanics is provided by the transfer matrix ${}^{u}\hat{\mathbf{T}}_{ow}$ of the ossicular chain.

The elements of the matrix

$$ {}^{u}\hat{\mathbf{T}}_{ow} = \begin{pmatrix} \hat{A}_P & \hat{Z}_{oc} \\ \hat{Y}_{oc} & \hat{A}_U^{-1} \end{pmatrix} \tag{11} $$

can be measured by manipulating the cochlear load. For example, if the oval window is blocked so that $U_{ow} = 0$ the element $\hat{A}_P$ is given by the ratio

$$ \hat{A}_P = \left. \frac{F_u}{\hat{P}_{ow}} \right|_{U_{ow}=0 \text{ (oval window blocked)}} . \tag{12} $$

If the cochlear contents are incompressible, the oval window can be blocked by blocking the round window. (It might seem that an easier way to block the oval window would simply be to cement the stapes in place. To the extent, however, that such gluing alters the impedance of the stapes, it modifies the mechanical system one is trying to characterize.) Note that $\hat{A}_P(\omega)$ has the dimensions of an area. When the oval window is blocked, the "effective area for pressure" provides the pressure difference $\hat{P}_{ow}$ across the stapes footplate due to the force on the malleus. The matrix element $\hat{A}_U^{-1}$ provides another effective area associated with the ossicular chain:

$$ \hat{A}_U^{-1} = \left. \frac{V_u}{U_{ow}} \right|_{\hat{P}_{ow}=0 \text{ (cochlear load removed)}} . \tag{13} $$

When loading due to the inner ear has been removed, the "effective area for volume velocity" relates the velocity of the umbo to the volume velocity of the stapes footplate. The remaining elements of the matrix ${}^{u}\hat{\mathbf{T}}_{ow}$ may be determined by similar measurements. Like ${}^{e}\hat{\mathbf{T}}_{u}$, the transfer matrix ${}^{u}\hat{\mathbf{T}}_{ow}$ of the ossicular chain is expected to be reciprocal.

(1) Comparison with the eardrum

Note that the ossicular chain converts a force and velocity into a pressure and volume velocity and is thus analogous to an eardrum driven in reverse. The principal transduction of the middle ear, described by the matrix ${}^{e}\widehat{\mathbf{T}}_{ow} \approx {}^{e}\widehat{\mathbf{T}}_{u}\,{}^{u}\widehat{\mathbf{T}}_{ow}$, can thus be viewed as being generated by two "eardrums" connected back-to-back at the umbo.

Both "eardrums" have two effective areas, one associated with the transformation of force, the other with the transformation of velocity. Unless the two systems are perfectly "stiff" (i.e., unless the eardrum is inflexible and the ossicular joints rigid so that $\widehat{Y}_{oc} = \widehat{Y}_{e} = 0$), reciprocity implies that those two areas cannot be equal. Indeed, a simple argument based on reciprocity (Shera and Zweig 1991c) yields the inequalities

$$\lim_{\omega\to 0} \frac{\widehat{A}_{F}}{\widehat{A}_{V}} < 1 \quad \text{and} \quad \lim_{\omega\to 0} \frac{\widehat{A}_{P}}{\widehat{A}_{U}} > 1 \,. \tag{14}$$

At low frequencies, the relative magnitudes of the corresponding areas for the two "eardrums" are thus reversed.

As an illustrative example, consider an idealized ossicular chain consisting of a simple lever system in which the malleus and incus are massless, rigidly connected, and rotate freely, connecting firmly to the eardrum and stapes with lever arms of l_m and l_i, respectively. Let the massless stapes, with footplate area A_{sf}, move freely in the oval window. The matrix ${}^{u}\widehat{\mathbf{T}}_{ow}$ then becomes

$${}^{u}\widehat{\mathbf{T}}_{ow} = \begin{pmatrix} 1/l_m & 0 \\ 0 & l_m \end{pmatrix} \begin{pmatrix} l_i & 0 \\ 0 & 1/l_i \end{pmatrix} \begin{pmatrix} A_{sf} & 0 \\ 0 & 1/A_{sf} \end{pmatrix} = \begin{pmatrix} l_i A_{sf}/l_m & 0 \\ 0 & l_m/l_i A_{sf} \end{pmatrix} . \tag{15}$$

Equation (15) represents the ossicular chain as a simple mechanical transformer of turns ratio $l_m/l_i A_{sf}$. A corresponding—although somewhat less idealized—example for the matrix ${}^{e}\widehat{\mathbf{T}}_{u}$, obtained by a simple extension of the transfer matrix of a rigid-plate model of the eardrum, is discussed in the first paper in this series (Shera and Zweig 1991c).

(2) Approximate factorization of ${}^{u}\widehat{\mathbf{T}}_{ow}$

This section presents an approximate factorization of the matrix ${}^{u}\widehat{\mathbf{T}}_{ow}$ into three component matrices representing, respectively, the action of the malleoincudal complex, the incudostapedial joint, and the stapes. The factorization is based on the assumption

that the motion of the stapes is piston-like and can therefore be described by a single spatial degree of freedom.

Each of the three bones of the middle ear presumably moves as a rigid body and each therefore has, in principle, three translational and three rotational degrees of freedom. For example, recent measurements (Brenkman et al. 1986; Gyo et al. 1987; Donahue 1989; Donahue et al. 1991; Decraemer and Khanna 1991) suggest that the mode of vibration of the malleus and incus may be more complicated than the simple rotational motion classically described (Dahmann 1929; Dahmann 1930; Wever and Lawrence 1954; von Békésy 1960; Kobrak 1959; Kirikae 1960; Guinan and Peake 1967). The motion of the stapes is also controversial.

For example, von Békésy (1960) concluded, from observations made on human cadavers at high sound intensities (and in which the cochleae had been drained), that the stapes rotates like a trapdoor about a point on the annular ligament of the stapediovestibular joint. More recently Gyo et al. (1987) observed rotational motion in cadavers with intact cochleae (also at high SPL). Other recent measurements on cadavers and on anesthetized cats and squirrel monkeys, however, contradict that conclusion. Working with cadavers, Dankbaar (1970), and more recently Vlaming and Feenstra (1986), found no evidence for rotational motion at sound intensities up to 130 dB SPL. Rhode (1978) has shown that the motion of the stapes is primarily translational in the squirrel monkey, moving into and out of the inner ear like a piston with little rocking motion. Also, Guinan and Peake (1967) have observed similar, piston-like stapedial motion in the cat. Thus, although the observations on cadavers contradict one another, the measurements on animals suggest that a single spatial coordinate may suffice to characterize the motion of the stapes, at least at low and intermediate frequencies and normal sound intensities. The motion of the stapes would then be completely specified by the translational displacement X_s of its footplate. Although the motion of the malleus and incus may involve both translational and rotational oscillations, the effective "output" of the malleoincudal complex (i.e., the "input" to the stapes) would then be one-dimensional.

With that approximation, the matrix ${}^{u}\widehat{\mathbf{T}}_{ow}$ representing the ossicular chain can be factored into component matrices:[4]

$$ {}^{u}\widehat{\mathbf{T}}_{ow} \approx {}^{u}\mathbf{T}_{lp}\,{}^{lp}\mathbf{T}_{s}\,{}^{s}\widehat{\mathbf{T}}_{ow} \,. \tag{16} $$

The component matrices are defined by the chain of variables

$$ \begin{pmatrix} F_u \\ V_u \end{pmatrix} {}^{u}\mathbf{T}_{lp} \begin{pmatrix} F_{lp} \\ V_{lp} \end{pmatrix} {}^{lp}\mathbf{T}_{s} \begin{pmatrix} F_s \\ V_s \end{pmatrix} {}^{s}\widehat{\mathbf{T}}_{ow} \begin{pmatrix} \widehat{P}_{ow} \\ U_{ow} \end{pmatrix} \,. \tag{17} $$

The symbolic notation introduced in Eq. (9) is used again here for brevity. Equation (17) describes the transformation of a force and velocity at the umbo into a pressure and volume velocity at the oval window: motion of the umbo is transferred through the malleoincudal complex to the lenticular process of the incus, which exerts a force F_s on the head of the stapes through the incudostapedial joint; motion of the stapes footplate then changes the pressure across the oval window.

If the motion of the stapes is indeed sufficiently simple that the factorization outlined above is valid, one can deduce approximate forms for the matrices ${}^{lp}\mathbf{T}_{s}$ and ${}^{s}\widehat{\mathbf{T}}_{ow}$ by considering the forces acting on the head and footplate of the stapes. The impedance Z_s of the stapes is defined by the equation

$$ F_s - \widehat{P}_{ow} A_{sf} \equiv Z_s V_s \,, \tag{18} $$

where A_{sf} is the area of the stapes footplate. The velocity V_s of the stapes produces an oval-window volume velocity

$$ U_{ow} = A_{sf} V_s \,. \tag{19} $$

The force F_s on the head of the stapes results from the motion, mediated by the ligament in the incudostapedial joint, of the lenticular process of the incus:

$$ F_s \equiv Z_{isj} \left(V_{lp} - V_s \right) \,. \tag{20} $$

---

[4] Although presented, for clarity, as a factorization of the matrix ${}^{u}\widehat{\mathbf{T}}_{ow}$, the contributions of the stapes could just as well have been "factored out" from the matrix ${}^{e}\widehat{\mathbf{T}}_{ow}$:

$$ {}^{e}\widehat{\mathbf{T}}_{ow} \approx {}^{e}\widehat{\mathbf{T}}_{lp}\,{}^{lp}\mathbf{T}_{s}\,{}^{s}\widehat{\mathbf{T}}_{ow} \,, \tag{4.1} $$

where ${}^{e}\widehat{\mathbf{T}}_{lp}$ describes the combined action of the eardrum and malleoincudal complex. A similar factorization has been introduced by Peake et al. (1991), who represent the eardrum and malleoincudal complex by a two-port network equivalent to the matrix ${}^{e}\widehat{\mathbf{T}}_{lp}\,{}^{lp}\mathbf{T}_{s}$.

Equations (18)–(20) imply that

$$ {}^{\mathrm{lp}}\mathbf{T}_{\mathrm{s}} \approx \begin{pmatrix} 1 & 0 \\ 1/Z_{\mathrm{isj}} & 1 \end{pmatrix} \tag{21} $$

and

$$ {}^{\mathrm{s}}\widehat{\mathbf{T}}_{\mathrm{ow}} \approx \begin{pmatrix} 1 & Z_{\mathrm{s}} \\ 0 & 1 \end{pmatrix} \begin{pmatrix} A_{\mathrm{sf}} & 0 \\ 0 & 1/A_{\mathrm{sf}} \end{pmatrix} . \tag{22} $$

The approximate factorizations of the matrices ${}^{\mathrm{e}}\widehat{\mathbf{T}}_{\mathrm{ow}}$ and ${}^{\mathrm{u}}\widehat{\mathbf{T}}_{\mathrm{ow}}$ discussed in this section and the representations of the component matrices ${}^{\mathrm{lp}}\mathbf{T}_{\mathrm{s}}$ and ${}^{\mathrm{s}}\widehat{\mathbf{T}}_{\mathrm{ow}}$ given by Eqs. (21) and (22) are adopted in the final paper of this series (Shera and Zweig 1992d), which fits a simple model of the middle ear to measurements of the middle-ear input impedance in humans and cadavers.

B. Characterization of the round window

Khanna and Tonndorf (1971) and Nomura (1984) have shown that the round-window membrane of the cat breaks into complicated modes of oscillation at frequencies as low as 1 kHz. Fortunately, only the net volume velocity of the round window enters the equations of motion for the middle ear. The effects of the complex oscillations of the round window are included in the impedance Z_{rw} defined below.

The motion of the round-window membrane is characterized by the impedance Z_{rw} defined by the equation

$$ P_{\mathrm{rw}} - P_{\mathrm{tc}} \equiv -Z_{\mathrm{rw}} U_{\mathrm{rw}} , \tag{23} $$

The minus sign appears because volume displacements of the round window, like those of the oval window, are defined to be positive *out* of the adjoining cavity.

C. Characterization of the cavities

The pressure in the middle-ear cavities varies in response to the volume displacements of the eardrum and the oval and round windows. When the wavelength of sound is long compared to the characteristic dimensions of the cavities, the pressure in the cavities is nearly uniform and the acoustic properties of the cavities are accurately represented by lumped impedances.

The pressure $P_{\rm tc}$ in the tympanic cavity is related to the volume velocities of the three windows through the equation

$$P_{\rm tc} \equiv Z_{\rm cav}\Big(U_{\rm e} - U_{\rm ow} - U_{\rm rw}\Big) \ , \tag{24}$$

The impedance $Z_{\rm cav}$ represents the effective impedance of the middle-ear cavities and mastoid air cells. The quantity in parentheses represents the rate of change in volume of the tympanic cavity.[5] If that volume decreases, the pressure $P_{\rm tc}$ rises; those volume displacements that increase the total volume of the tympanic cavity thus enter with a minus sign. Equation (24) provides an expression for the reference pressure relative to which pressures $\widehat{P}$ are measured.

Note that if the inner ear is essentially incompressible (Shera and Zweig 1992c),

$$\delta_{\rm eardrum} \equiv \left| \frac{U_{\rm ow} + U_{\rm rw}}{U_{\rm e}} \right| \ll 1 \ . \tag{25}$$

Equation (24) then reduces to

$$P_{\rm tc} \approx Z_{\rm cav} U_{\rm e} \ ; \tag{26}$$

the pressure in the tympanic cavity varies in response only to the motion of the eardrum. Indeed, the companion paper (Shera and Zweig 1992c) demonstrates that because of the large area ratio between the eardrum and oval window, the pressure in the tympanic cavity is determined (regardless of possible cochlear compressibility) principally by the eardrum;[6] the "ossicular eardrum" has little relative effect on the cavity pressure even in those animals, such as the cat, in which the oval and round windows face onto separate cavities.

III. Representation of the Phenomenological Equations

This section discusses the representation—both as equivalent electrical circuits and as matrix equations—of the system of middle-ear equations outlined above in Sec. II, explores assumptions underlying the existence of the conventional "two-port" representation

[5] Variations in volume due to circulation of blood through the mucosa lining the cavities and diffusion of air from the cavities into the blood have not been included. Such variations are small and occur on time scales significantly longer than those important here (Ingelstedt et al. 1967).

[6] At frequencies at which not all sections of the eardrum vibrate in phase, however, the area $\widehat{A}_{\rm V}$ and hence the effective area ratio may decrease considerably.

of middle-ear mechanics, and illustrates how the equations can be completed with boundary conditions at the three windows to obtain solutions (for the pressures and volume velocities) for a variety of stimulus configurations.

A. Equivalent circuit of the middle ear

The equations of motion for the middle ear can be represented in the form of an equivalent "black-box" electrical circuit (Fig. 3). The equivalent circuit is symmetric with respect to its treatment of the three windows: no specification of either the cochlear or external-ear loads are included. Two versions of the circuit are shown. The first, and most general, incorporates the transfer matrix ${}^{e}\widehat{\mathbf{T}}_{ow}$ defined in Sec. II-A; the second adopts the approximate factorization of that matrix into separate eardrum and ossicular contributions discussed in Sec. II-A-3. Throughout the circuit, voltages are analogous to "forces" (e.g., to pressures or torques) and currents to "velocities" (e.g., to volume or angular velocities).

The circuit representation illustrated in Fig. 3 is completely equivalent to the equations given above. The mechanics of the middle ear uniquely determines the topology of the equivalent circuit; the equations of motion can be recovered from the figure using Kirchoff's circuit laws.

Other investigators have proposed circuit models of the human middle ear (Zwislocki 1957; Zwislocki 1962; Møller 1961; Onchi 1961). Those circuits were developed to represent the input impedance of an "average" middle ear and, for this purpose, have proved successful, although middle-ear mechanics has not always been faithfully reflected in the network topology. In contrast to previous circuits all voltages, currents, and impedances in the equivalent circuit shown in Fig. 3 have measurable analogues. The eardrum and ossicular chain, for example, are represented by the matrix ${}^{e}\widehat{\mathbf{T}}_{ow}$, whose elements are defined by, and could be measured using, the equations in Sec. II-A. The correspondence between the equivalent circuit and phenomenological equations guarantees that the circuit elements can, in principle, be measured and that the circuit can be used to obtain defining relationships between measurable quantities.

By contrast, the circuit of Møller (1961), for example, is not based on equations of motion, and the circuit elements can not be measured. Since in most circuit models the correspondence between circuit voltages or currents and measurable quantities in

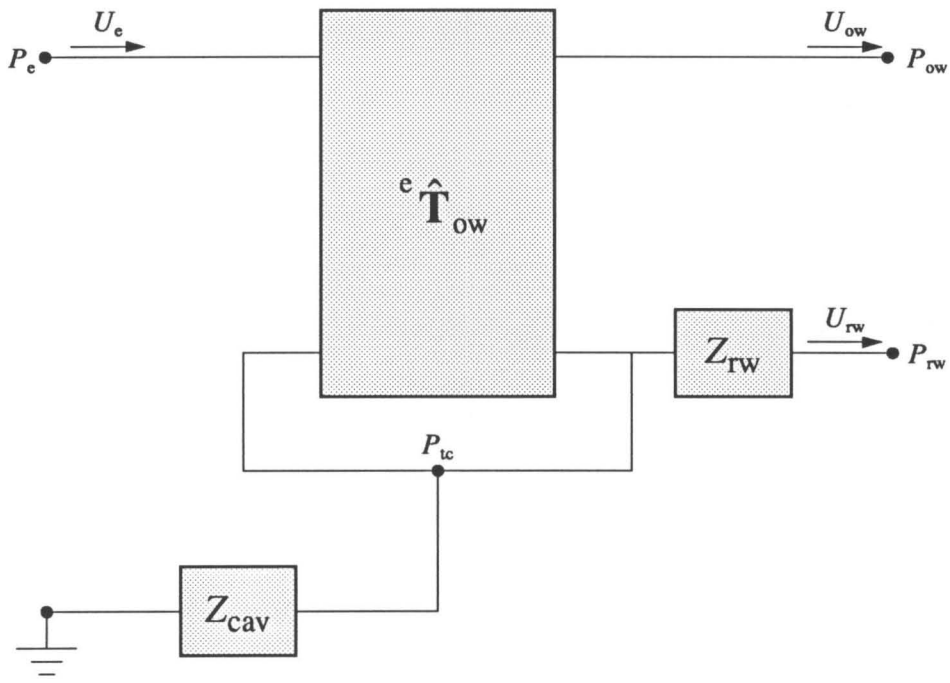

Figure 3a. Equivalent circuit for the human middle ear. The equivalent circuit provides a pictorial representation of the equations of the middle ear, which can be recovered by applying Kirchoff's circuit laws. The atmospheric pressure surrounding the head is indicated by ground.

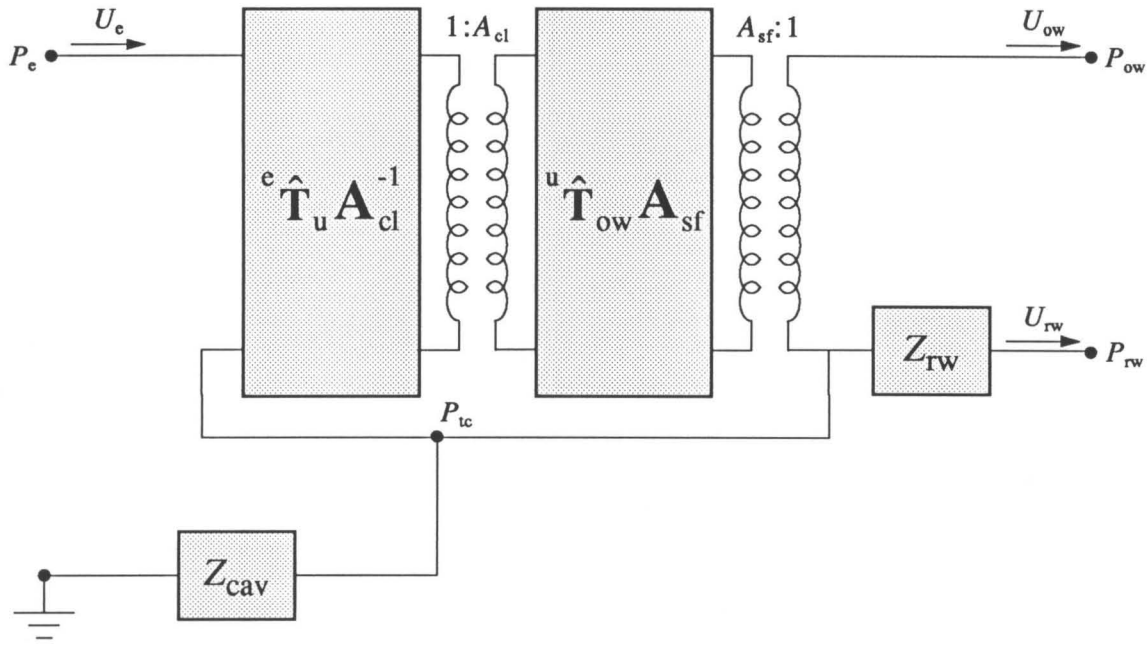

Figure 3b. Equivalent circuit incorporating the approximate factorization of ${}^{e}\widehat{\mathbf{T}}_{ow}$ into separate eardrum and ossicular contributions and making explicit the dimensional transformations (transduction) they perform. The representation of the eardrum consists of the matrix product ${}^{e}\widehat{\mathbf{T}}_{u}\mathbf{A}_{cl}{}^{-1}$ in cascade with an ideal transformer of turns ratio A_{cl}, which provides a change of dimension. The ideal transformer is represented by the transfer matrix $\mathbf{A}_{cl}$, defined by

$$\mathbf{A}_{cl} \equiv \begin{pmatrix} A_{cl}^{-1} & 0 \\ 0 & A_{cl} \end{pmatrix} .$$

The reference area A_{cl} was chosen to be the "classical effective area" of the eardrum (Shera and Zweig 1991c). The ossicular transformation is represented similarly; the matrix $\mathbf{A}_{sf}$ is identical to $\mathbf{A}_{cl}$ with A_{cl} replaced by A_{sf}, the area of the stapes footplate.

the middle ear is seldom made explicit, the underlying equations implicit in the model cannot easily be recovered. It is thus difficult to determine whether those equations accurately describe the mechanics of the middle ear; those circuit models cannot, therefore, conveniently serve as the basis for a comparison between theory and experiment.

Most middle-ear networks in the literature (e.g., Ross 1968; Shaw 1977; Shaw and Stinson 1981; Lutman and Martin 1979; Killion and Clemis 1981; Goode and Killion 1987) are variations and refinements on the circuit of Zwislocki (1957; 1962), which provides a good representation of the input impedance of an "average" ear for frequencies less than 1–2 kHz. The topology of Zwislocki's circuit model differs from the equivalent circuit shown in Fig. 3 principally in the location of the impedances representing the middle-ear cavities. The position of the cavity impedances in the equivalent circuit follows from the requirement that the pressure P_{tc} influence not only the motion of the eardrum but also the motions of the oval and round windows. Correct prediction of absolute intracochlear pressures depends on the placement of the cavity impedances in the equivalent circuit. The effect of incorrect placement of the cavity impedances on quantities such as the middle-ear input impedance and stapes transfer function depends on the nature of the cochlear load (Shera and Zweig 1992c).

B. Matrix representation of middle-ear mechanics

Equations (3), (23), and (24)—four equations relating seven unknowns (P_{e}, U_{e}, P_{ow}, U_{ow}, P_{rw}, U_{rw}, and P_{tc})—provide a complete phenomenological characterization of middle-ear mechanics independent of the loads at any of the three windows. (Here we assume that the matrix elements of ${}^{\mathrm{e}}\widehat{\mathbf{T}}_{\mathrm{ow}}$—of which, assuming reciprocity, only three are independent—and the impedances of the cavities and round window are known.) To solve the equations for a given stimulus configuration, three additional equations, one for each window, are needed: two to complete specification of the loading conditions—for example, to characterize the nature of the cochlear load seen from the oval and round windows—and the third (the inhomogeneous source equation) to specify how the system is driven. If the loads seen by the three windows are linear (as they are, for example, at the cochlear windows in both the low- and high-amplitude limits of cochlear mechanics) the source equation simply determines an overall multiplicative constant in the solution.

Note that nothing has so far been assumed about the cochlear load other than that the pressures $P_{\rm ow}$ and $P_{\rm rw}$ and the volume velocities $U_{\rm ow}$ and $U_{\rm rw}$ suffice, in some combination, to determine the cochlear input. Likewise nothing specific has been assumed about the boundary conditions in the ear canal. Knowledge of the impedance seen "looking out" from the eardrum is needed when the middle ear is driven from one or both of the other windows (e.g., when measuring reverse transfer functions). An example in which the middle ear is driven from an artificial fourth window introduced into the tympanic cavity is discussed in Sec. III-C.

Section I briefly discussed the existence of matrix representations of middle-ear mechanics. A particularly illuminating example can be obtained by noting that rather than working with the port variables given in Fig. 1, adopting certain linear combinations of those variables can simplify specification of the boundary conditions. For example, if the cochlear contents are incompressible, the volume velocities $U_{\rm ow}$ and $U_{\rm rw}$ of the oval and round windows are equal and opposite; the inner ear then responds only to the pressure difference $P_{\rm ow} - P_{\rm rw}$ between the oval and round windows and not the absolute pressure at either window. It is therefore convenient to introduce the quantities

$$P_{\pm} \equiv P_{\rm ow} \pm P_{\rm rw} \ , \tag{27}$$

and

$$U_{\pm} \equiv \left(U_{\rm ow} \pm U_{\rm rw}\right)/2 \ ; \tag{28}$$

representing sums and differences of the average pressures and volume velocities immediately inside the oval and round windows.

A particularly useful representation of the equations is then given by the equation

$$\begin{pmatrix} P_{\rm e} \\ U_{\rm e} \\ P_{+} \end{pmatrix} = \mathbf{M} \begin{pmatrix} P_{-} \\ U_{-} \\ U_{+} \end{pmatrix} \ . \tag{29}$$

Note that $\mathbf{M}$ is defined only in terms of quantities measurable at the windows, or ports, of the middle ear; a fourth equation, for the internal cavity pressure $P_{\rm tc}$, has been omitted [cf. Eq. (1)]. The matrix elements of $\mathbf{M}$, obtained by algebraic manipulation of the middle-ear equations outlined in Sec. II, are given in Table I. The following subsection shows how this general "three-port" representation can be used to obtain the standard "two-port" description of middle-ear mechanics by assuming that the cochlear contents are incompressible.

1. Incompressibility and the "two-port" description

The cochlear contents are approximately incompressible if

$$2\left|\frac{U_{\rm ow}+U_{\rm rw}}{U_{\rm ow}-U_{\rm rw}}\right| = 2\left|\frac{U_+}{U_-}\right| \ll 1\,. \tag{30}$$

A companion paper (Shera and Zweig 1992c) explores cochlear compressibility in more detail and shows that the assumption of incompressibility appears good to within a few percent in the normal ear. In the incompressible limit U_+ vanishes identically, providing a fifth equation (i.e, $U_+ = 0$) among the dynamical variables. Equation (29) for $\mathbf{M}$ implies that there then exists a simple 2×2 transfer matrix that relates the "input" to the "output" of the middle ear:

$$\begin{pmatrix} P_{\rm e} \\ U_{\rm e} \end{pmatrix} = {}^{\rm e}\mathbf{T}_- \begin{pmatrix} P_- \\ U_- \end{pmatrix}\,. \tag{31}$$

Solving the middle-ear equations for the matrix elements yields

$${}^{\rm e}\mathbf{T}_- = \begin{pmatrix} \hat{N}_{\rm P}^{-1} + \hat{Y}Z_{\rm cav} & \hat{Z} + Z_{\rm rw}/\hat{N}_{\rm P} + (\hat{N}_{\rm U} + \hat{Y}Z_{\rm rw})Z_{\rm cav} \\ \hat{Y} & \hat{N}_{\rm U} + \hat{Y}Z_{\rm rw} \end{pmatrix}\,. \tag{32}$$

These four matrix elements constitute the upper left-hand corner of the matrix $\mathbf{M}$ (see Table I). ${}^{\rm e}\mathbf{T}_-$ can be written as the simple matrix product

$${}^{\rm e}\mathbf{T}_- = \begin{pmatrix} 1 & Z_{\rm cav} \\ 0 & 1 \end{pmatrix} {}^{\rm e}\hat{\mathbf{T}}_{\rm ow} \begin{pmatrix} 1 & Z_{\rm rw} \\ 0 & 1 \end{pmatrix}\,. \tag{33}$$

Assuming that the cavities can be "factored out" in this fashion—even in animals, such as the cat, in which the oval and round windows face onto separate cavities—is the basis for the "series approximation" (e.g., Lynch 1981). Note that Eq. (33) implies that the overall middle-ear transformation described by ${}^{\rm e}\mathbf{T}_-$ is reciprocal if and only if the eardrum/ossicular transformation satisfies $\det {}^{\rm e}\hat{\mathbf{T}}_{\rm ow} = +1$.

Existence of this approximate "two-port" description of middle-ear mechanics [i.e, Eq. (32)] depends on the incompressibility of the cochlear load. Note, however, that even in the incompressible limit the two-port description fails when the cochlea is opened and driven "in reverse." For example, if a miniature sound source inserted into the cochlea delivers a volume velocity $U_{\rm s}$ into the scalae, then

$$U_{\rm ow} + U_{\rm rw} = U_{\rm s}\,. \tag{34}$$

Thus, $U_+ = U_s \neq 0$ and the pressure P_e, for example, depends on all three cochlear variables:

$$P_e = \left[\widehat{N}_P^{-1} + \widehat{Y} Z_{cav}\right] P_- + \left[\widehat{Z} + Z_{rw}/\widehat{N}_P + \left(\widehat{N}_U + \widehat{Y} Z_{rw}\right) Z_{cav}\right] U_- + \left[\widehat{Z} - Z_{rw}/\widehat{N}_P + \left(\widehat{N}_U - 2 - \widehat{Y} Z_{rw}\right) Z_{cav}\right] U_+ \ . \tag{35}$$

Despite its convenience, the matrix ${}^e\mathbf{T}_-$ does not—even in the incompressible limit—provide a *complete* description of the middle ear (as viewed, outside looking in, from the three windows): an additional equation (see Table I, row three),

$$P_+ = \left[1 + 2\widehat{Y} Z_{cav}\right] P_- + 2\left[Z_{rw} + \left(\widehat{N}_U + \widehat{Y} Z_{rw}\right) Z_{cav}\right] U_- \ , \tag{36}$$

is needed to determine the absolute pressures within the cochlea.

C. Boundary conditions at the three windows

Complete determination of all seven dynamical variables requires—if U_+ vanishes identically—two additional equations. For example, if the middle ear is driven from the ear canal with an earphone delivering a volume velocity U_s at the eardrum, those equations are

$$U_e = U_s \quad \text{and} \quad P_{ow} - P_{rw} = Z_{ie} U_{ow} \ ; \tag{37}$$

the first constitutes the source equation, the second defines the inner-ear input impedance Z_{ie}, which characterizes the cochlear load in the incompressible limit (Shera and Zweig 1992c).

With knowledge of the loads seen from the three windows, solutions can, of course, be obtained for a variety of stimulus configurations. Those solutions can be used to check the consistency of the framework. For example, imagine driving the middle ear by introducing a volume velocity U_s into the tympanic cavity through an artificial fourth window (the Eustachian tube or a small opening drilled into the cavity, for example). Equation (24) then becomes

$$P_{tc} = Z_{cav}\left(U_e + U_s - U_{ow} - U_{rw}\right) \ . \tag{38}$$

The resulting pressure in the cavity is found to be

$$\frac{P_{tc}}{U_s} = Z_{cav}\left[1 + Z_{cav}\frac{\widehat{N}_U + \widehat{Y}\left(Z_{ie} + Z_{rw}\right)}{\widehat{Z} + \widehat{N}_U Z_{ee} + \left(\widehat{N}_P^{-1} + \widehat{Y} Z_{ee}\right)\left(Z_{ie} + Z_{rw}\right)}\right]^{-1} \ , \tag{39}$$

where Z_{ie} is the lumped impedance of the inner ear (assumed incompressible) and Z_{ee} is the impedance of the external ear seen looking out from the eardrum (Rosowski et al. 1988):

$$Z_{ee} \equiv -\left.\frac{P_e}{U_e}\right|_{\text{ear canal driven from the eardrum}} . \tag{40}$$

The impedance measured in this configuration is simply the cavity impedance Z_{cav} modified by corrections terms arising from motions induced in the three windows and in the ossicular chain.

1. Consistency relations for the elements of ${}^{e}\hat{\mathbf{T}}_{ow}$

Section II-A-2 illustrated how the matrix elements of ${}^{e}\hat{\mathbf{T}}_{ow}$ can be determined by measurements of the pressures and volume velocities at the eardrum and oval window under no- and infinite-load conditions. Alternatively, the matrix elements can be determined by combining measurements, such as those of forward and reverse transfer functions, that do not require artificial manipulation of the loads seen by the three windows (provided, that is, that those loads themselves are measured). Those independent determinations of the matrix elements provide relations that can be used to check the internal consistency of the framework. For example, by assuming reciprocity one can determine the matrix elements from measurements of the middle-ear input impedance $\hat{Z}_{me}$, defined by

$$\hat{Z}_{me} \equiv \left.\frac{\hat{P}_e}{U_e}\right|_{\text{middle ear driven forward}} . \tag{41}$$

and the transfer functions

$$\hat{T}_{ow} \equiv \left.\frac{\hat{P}_{ow}}{\hat{P}_e}\right|_{\text{middle ear driven forward}} , \tag{42}$$

and

$$\hat{T}_{e} \equiv \left.\frac{\hat{P}_{e}}{\hat{P}_{ow}}\right|_{\text{middle ear driven backward}} . \tag{43}$$

In these measurements, made with the cavities opened widely (so that $P = \hat{P}$), the middle-ear might be driven "in reverse" with a miniature sound source inserted into the scala vestibuli near the oval window.

Expressions for the transfer functions follow immediately from the middle-ear equations and the supplemental reciprocity constraint $\det {}^{e}\widehat{\mathbf{T}}_{ow} = +1$; those expressions can then be "inverted" to obtain the matrix elements:

$$\widehat{N}_P^{-1} = \frac{Z_{ie+rw}(Z_{ee} + \widehat{Z}_{me})\widehat{T}_e - Z_{ee}\widehat{Z}_{me}\widehat{T}_{ow}(1 - \widehat{T}_e\widehat{T}_{ow})}{Z_{ie+rw}(Z_{ee} + \widehat{Z}_{me})\widehat{T}_e\widehat{T}_{ow}} ; \tag{44}$$

$$\widehat{Z} = \frac{Z_{ee}\widehat{Z}_{me}\widehat{T}_{ow}(1 - \widehat{T}_e\widehat{T}_{ow})}{(Z_{ee} + \widehat{Z}_{me})\widehat{T}_e} ; \tag{45}$$

$$\widehat{Y} = \frac{Z_{ie+rw}(Z_{ee} + \widehat{Z}_{me})\widehat{T}_e - \widehat{Z}_{me}\widehat{T}_{ow}(Z_{ee} + \widehat{Z}_{me}\widehat{T}_e\widehat{T}_{ow})}{Z_{ie+rw}\widehat{Z}_{me}(Z_{ee} + \widehat{Z}_{me})\widehat{T}_e\widehat{T}_{ow}} ; \tag{46}$$

and

$$\widehat{N}_U = \frac{Z_{ee} + \widehat{Z}_{me}\widehat{T}_e\widehat{T}_{ow}}{(Z_{ee} + \widehat{Z}_{me})\widehat{T}_e} . \tag{47}$$

Z_{ie+rw} is the lumped impedance of the inner ear and round window: $Z_{ie+rw} \equiv Z_{ie} + Z_{rw}$. As discussed before (Sec. II-A-2), the matrix elements obtained from Eqs. (44)–(47) can be checked for consistency with the constraints of causality and minimum-phase behavior.

IV. Views from the Three Windows

This section examines two issues of relevance to middle-ear mechanics. First, the classical, but somewhat ill-defined, concept of the middle-ear transformer ratio is generalized. Second, the conditions under which existing circuit models accurately predict the absolute pressures in the cochlea are considered. The two companion papers (Shera and Zweig 1992b; Shera and Zweig 1992c) illustrate how the framework can be used to address problems of cochlear mechanics.

Unfortunately, existing measurements do not permit a direct quantitative examination of these issues. To provide an indication of the range of existing theoretical predictions, however, each section is illustrated with examples from published models of the human middle ear (Zwislocki 1962; Kringlebotn 1988). Although they provide a good representation of the input impedance of an average ear, the models remain incompletely tested in other respects, even at low frequencies. Thus, the extent to which the models accurately predict the quantities discussed here is not known.

A. Middle-ear transformer ratios

The action of the middle-ear is often characterized as that of a mechanical transformer whose purpose is to provide the well-known partial impedance match between the inner ear and the outside world (Zwislocki 1965; Dallos 1973; Killion and Dallos 1979). The overall "transformer ratio" of the middle ear is conventionally defined in terms of the classical effective area A_e of the eardrum:

$$N_{me} \equiv \frac{A_e l_m}{A_{sf} l_i} \,. \tag{48}$$

Here A_{sf} is the area of the stapes footplate, and l_m and l_i are, respectively, the mallear and incudal moment arms.[7]

Just like the classical effective area of the eardrum, however, the traditional concept of the middle-ear transformer ratio is based on an idealization of middle-ear mechanics with limited operational significance. For example, a better definition would take into account the distinction between the two effective areas of the eardrum and their variation with frequency (Shera and Zweig 1991c). Even more generally, two overall transformer ratios naturally arise:

$$\widehat{N}_P^{-1}(\omega) \equiv \left.\frac{\widehat{P}_e}{\widehat{P}_{ow}}\right|_{U_{ow}=0} = \left({}^e\widehat{\mathbf{T}}_{ow}\right)_{11} , \tag{49}$$

and

$$\widehat{N}_U(\omega) \equiv \left.\frac{U_e}{U_{ow}}\right|_{\widehat{P}_{ow}=0} = \left({}^e\widehat{\mathbf{T}}_{ow}\right)_{22} . \tag{50}$$

The ratio $\widehat{N}_U$ is associated with the transformation of volume velocity between the ear canal and the oval window, whereas the ratio $\widehat{N}_P$ figures in the pressure transformation. Note that the transformer ratios $\widehat{N}_U$ and $\widehat{N}_P$ are neither necessarily equal, constant, nor real. Indeed, reciprocity implies that they cannot be equal unless the eardrum and ossicular chain are perfectly stiff (so that $\widehat{Y} = 0$). A simple argument based on reciprocity (Shera and Zweig 1991c) yields the further relation

$$\lim_{\omega\to 0} \frac{\widehat{N}_P}{\widehat{N}_U} < 1 \,. \tag{51}$$

[7] Measurements (e.g., Wever and Lawrence 1954; von Békésy 1960) imply that $N_{me} \approx 20$ for humans, with A_e/A_{sf} providing the dominant contribution to the ratio.

The ratios $\widehat{N}_{\mathrm{U}}$ and $\widehat{N}_{\mathrm{P}}$ reduce to the classical transformer ratio N_{me} only in the limiting (and unrealistic) case in which the eardrum becomes a rigid plate (of area A_{e}) and the ossicular chain is idealized as a simple lever system as in Eq. (15). In that limit, ${}^{\mathrm{e}}\widehat{\mathbf{T}}_{\mathrm{ow}}$ becomes

$$ {}^{\mathrm{e}}\widehat{\mathbf{T}}_{\mathrm{ow}} \approx {}^{\mathrm{e}}\widehat{\mathbf{T}}_{\mathrm{u}}\,{}^{\mathrm{u}}\widehat{\mathbf{T}}_{\mathrm{ow}} = \begin{pmatrix} A_{\mathrm{e}}^{-1} & Z_{\mathrm{e}} \\ 0 & A_{\mathrm{e}} \end{pmatrix} \begin{pmatrix} l_{\mathrm{i}} A_{\mathrm{sf}}/l_{\mathrm{m}} & 0 \\ 0 & l_{\mathrm{m}}/l_{\mathrm{i}} A_{\mathrm{sf}} \end{pmatrix} = \begin{pmatrix} N_{\mathrm{me}}^{-1} & N_{\mathrm{me}} Z_{\mathrm{e}}/A_{\mathrm{e}} \\ 0 & N_{\mathrm{me}} \end{pmatrix} . \quad (52) $$

In contrast to the classical transformer ratio N_{me}, the complex ratios $\widehat{N}_{\mathrm{P}}$ and $\widehat{N}_{\mathrm{U}}$ are directly measurable and include any effects due to the curvature of the eardrum (Helmholtz 1868; Tonndorf and Khanna 1970) or to frequency-dependent variations in the ossicular lever-arms. For example, measurements suggest that at higher frequencies the mode of vibration of the malleus and incus becomes more complicated than a simple rotation (Brenkman et al. 1986; Gyo et al. 1987; Donahue 1989; Donahue et al. 1991; Decraemer and Khanna 1991). Those effects are included in the transformer ratios defined above.

1. Predicted human transformer ratios

Figure 4 plots the transformer ratios $\widehat{N}_{\mathrm{U}}$ and $\widehat{N}_{\mathrm{P}}$ predicted by the middle-ear models of Zwislocki (1962) and Kringlebotn (1988).[8] Although qualitatively similar overall, the model predictions differ in detail. Both models predict that the transformer ratios are real below 1 kHz but at higher frequencies become largely imaginary and have nearly opposite sign. Whereas $|\widehat{N}_{\mathrm{P}}|$ is roughly constant below 5 kHz, $|\widehat{N}_{\mathrm{U}}|$ decreases to a minimum near 2 kHz before increasing abruptly at higher frequencies. In both models the ratios $\widehat{N}_{\mathrm{U}}$ and $\widehat{N}_{\mathrm{P}}$ are thus quite different and show substantial frequency dependence, even at low frequencies, where $|\widehat{N}_{\mathrm{U}}| > |\widehat{N}_{\mathrm{P}}|$, as given by Eq. (51).

---

[8] Unfortunately, Zwislocki (1962) and Kringlebotn (1988) lump the impedances Z_{ow} and Z_{rw} together with impedances describing the inner ear. To "unlump" those impedances, the impedance Z_{ow} of the stapes, annular ligament, and oval window was assumed to have the form of an harmonic oscillator:

$$ Z_{\mathrm{ow}} \approx i\omega M_{\mathrm{s}} + R_{\mathrm{ow}} + 1/i\omega C_{\mathrm{al}} . \quad (8.1) $$

The parameter M_{s} represents the acoustic mass of the stapes

$$ M_{\mathrm{s}} = m_{\mathrm{s}}/A_{\mathrm{sf}}^2 , \quad (8.2) $$

where $m_{\mathrm{s}} \approx 2.5$ mg (Schuknecht 1974) and $A_{\mathrm{sf}} \approx 3.6$ mm^2 (Nomura 1984). The compliance of the annular ligament C_{al} and the impedance Z_{rw} were determined as discussed in footnote 9. The damping constant R_{ow} was taken, in accordance with the measurements of Lynch et al. (1982) in cat, to be $1/7$ of the total series resistance allocated to the stapes and inner ear in the model [the Qs of the impedance Z_{ow} are then of $O(1)$]. None of the issues discussed here depend on the precise values of the parameters.

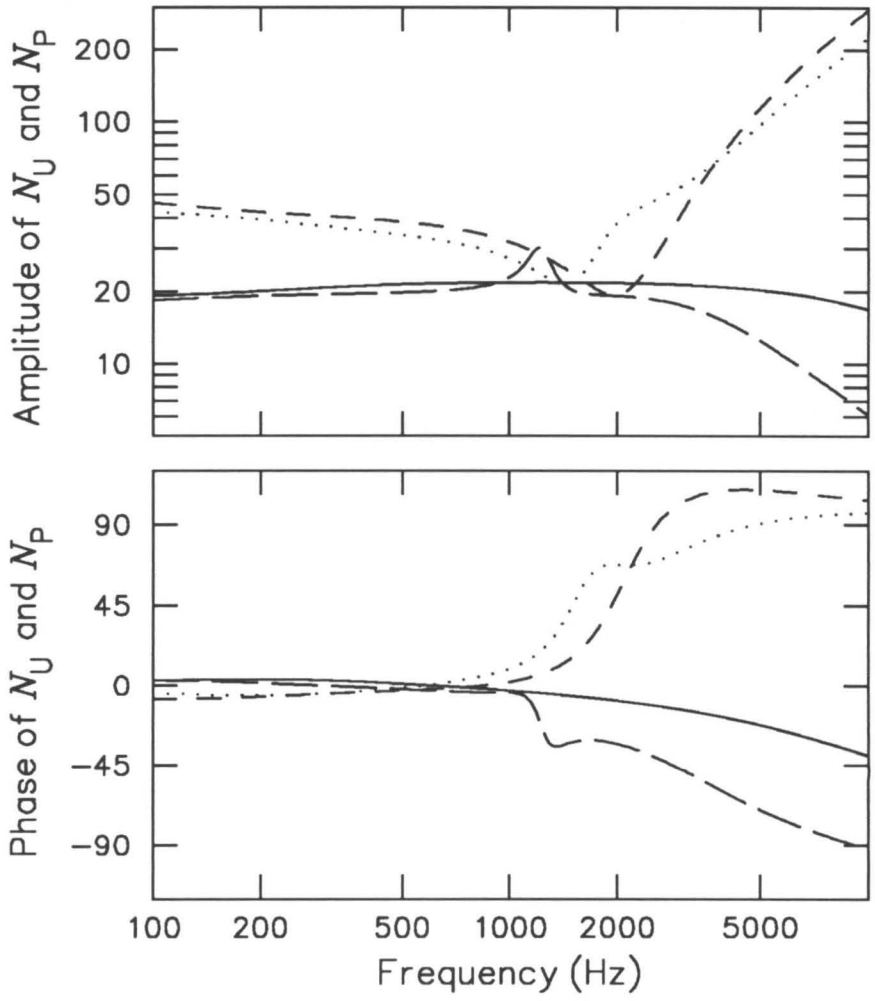

Figure 4. The transformer ratios $\widehat{N}_P$ and $\widehat{N}_U$ predicted by the models of Zwislocki (1962) and Kringlebotn (1988) for the human middle ear. Zwislocki's predictions for $\widehat{N}_P$ and $\widehat{N}_U$ are represented by solid (———) and dotted (·····) lines, respectively; Kringlebotn's by long- (— —) and short-dashed (— — —) lines. Both transformer ratios considerably with frequency.

B. Circuit topology

The pressure in the tympanic cavity affects not only the motion of the eardrum, but also that of the oval and round windows. In most middle-ear networks, (e.g., Zwislocki 1962; Ross 1968; Lutman and Martin 1979; Shaw and Stinson 1981; Goode and Killion 1987; Kringlebotn 1988) that secondary effect of the cavities is ignored. As discussed below, correct positioning of the cavities in the model is essential for exploring the effects of direct acoustic coupling to the oval and round windows (see also Peake et al. 1991). For example, most middle-ear networks cannot be used to correctly compute the absolute pressures within the cochlea. Even such quantities as the middle-ear input impedance depend on correct placement of the cavities unless the cochlear contents are incompressible. The companion paper (Shera and Zweig 1992c) demonstrates, however, that the effects of cochlear compressibility are small, at least in the normal human ear.

To illustrate these remarks, consider, for example, the transfer function $P_{\rm rw}/U_{\rm e}$, which, in humans, is given by

$$T_{\rm rw} \equiv \frac{P_{\rm rw}}{U_{\rm e}} = \frac{Z_{\rm rw}\left(1+\widehat{Y}Z_{\rm cav}\right)+Z_{\rm cav}\left(\widehat{N}_{\rm U}+\widehat{Y}Z_{\rm ie}\right)}{\widehat{N}_{\rm U}+\widehat{Y}\left(Z_{\rm ie}+Z_{\rm rw}\right)} \ . \tag{53}$$

Here, $Z_{\rm ie}$ is the lumped impedance of the inner ear (for simplicity, this section assumes that the cochlear contents are incompressible). The network topology of Zwislocki and others, in which the cavity pressure effects only the eardrum, predicts, however, that

$$T_{\rm rw} = \frac{Z_{\rm rw}}{\widehat{N}_{\rm U}+\widehat{Y}\left(Z_{\rm ie}+Z_{\rm rw}\right)} \qquad \text{(Zwislocki topology)}, \tag{54}$$

which can be obtained simply by taking the limit $Z_{\rm cav} \to 0$ in Eq. (53). The Zwislocki topology therefore makes no distinction, even in principle, between middle-ear transfer functions T and $\widehat{T}$. Equation (53) reduces to the approximation implicit in Zwislocki's circuit, Eq. (54), if and only if

$$\delta_{\rm topology} \equiv \left| Z_{\rm cav}\left[\widehat{Y}+\left(\widehat{N}_{\rm U}+\widehat{Y}Z_{\rm ie}\right)/Z_{\rm rw}\right]\right| \ll 1 \ . \tag{55}$$

When inequality (55) is satisfied the cavities affect the absolute cochlear pressures primarily by modifying the motion of the eardrum, rather than through any direct action of the cavity pressure on the oval and round windows.

As an example of what models predict for the human ear, Fig. 5 evaluates δ_{topology} using the middle-ear models of Zwislocki (1962) and Kringlebotn (1988). Like most existing middle-ear models, those models place the cavities in a position in which they have no direct effect upon the absolute pressures in the cochlea. Since the parameter values were chosen to provide a good representation of the input impedance of an "average" middle ear—for which, since cochlear compressibility appears small (Shera and Zweig 1992c), the position of the cavities is not important—and were not constrained by measurements of intracochlear pressure, their values have not been distorted by an incorrect network topology.[9] Both models predict that inequality (55) is violated at frequencies greater than $\sim$ 1 kHz (note, however, that in their fine structure the predictions are quite different). The figure shows that because of their incorrect circuit topology, such models cannot be used to predict the absolute pressure P_{rw} at high frequencies. (Because the cochlear input impedance is large, $|P_{\text{ow}}| \gg |P_{\text{rw}}|$, and the effects of incorrect cavity placement are small for the pressure P_{ow}.)

V. Summary

The paper has presented a phenomenological description of the middle ear and its constituent structures valid for both forward and reverse transmission during the normal

---

[9] Inequality (55) depends on the impedance Z_{rw} of the round window, which is not defined in the models but rather lumped together with the impedances of the stapes and cochlea. The calculations shown assume that Z_{rw} is compliant throughout the frequency range of the figure. Similar results are obtained, however, so long as the impedance of the round window constitutes only a small fraction of the lumped impedance of the stapes and inner ear.

To estimate Z_{rw}, note that Lynch et al. (1982) have shown that the lumped compliance of the stapes and inner ear in cat has the approximate form

$$1/C_{\text{lumped}} \approx 1/C_{\text{al}} + 1/C_{\text{rw}} \,, \tag{9.1}$$

where C_{al} and C_{rw} are the compliances of the annular ligament and round window, respectively. Their measurements, and those of Nedzelnitsky (1980), indicate that $C_{\text{al}} \ll C_{\text{rw}}$ (their ratio in the cat is approximately $1/25$) so that $C_{\text{lumped}} \approx C_{\text{al}}$. The model calculations presented in this paper assume that similar results hold for the human as well. The compliance C_{lumped} in the models of Zwislocki (1962) and Kringlebotn (1988)—which is known in both as C_{c}—has therefore been "unlumped" according to the formulae:

$$C_{\text{al}} \approx 25 C_{\text{lumped}}/24 \qquad \text{and} \qquad C_{\text{rw}} \approx 25 C_{\text{lumped}} \,. \tag{9.2}$$

None of the qualitative results discussed in this paper depend on the precise values of these parameters.

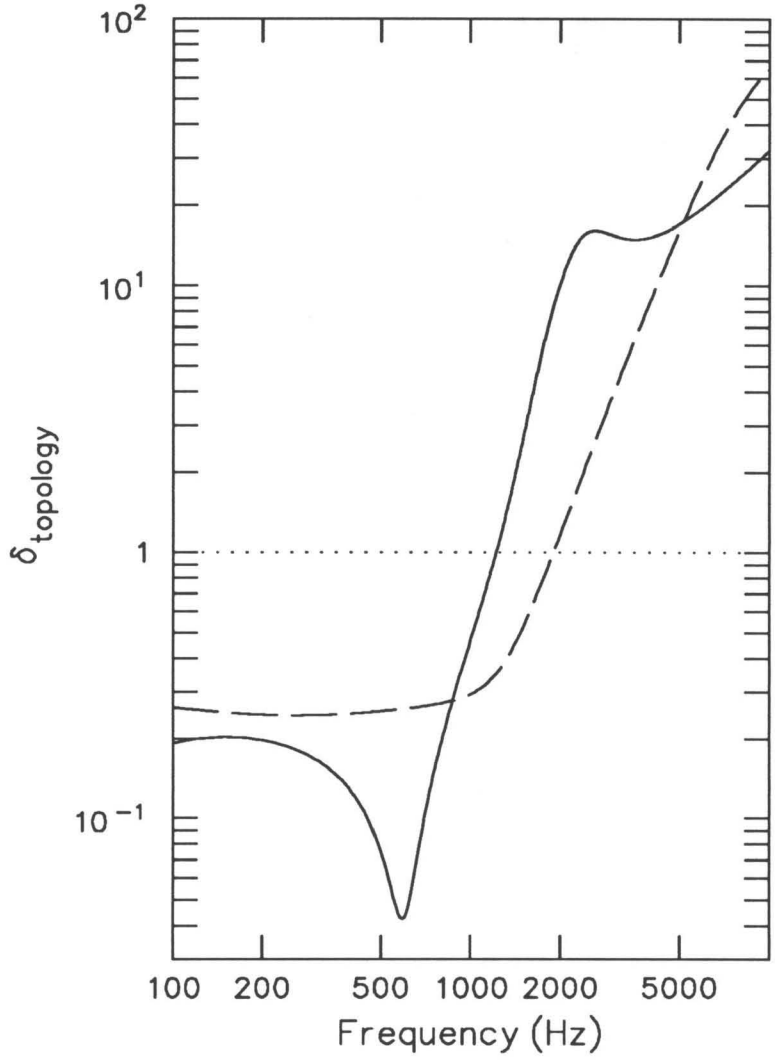

Figure 5. The function $\delta_{\text{topology}}(\omega)$ defined by inequality (55) evaluated using the the middle-ear models of Zwislocki (———) and Kringlebotn (— —). The right-hand side of the inequality (i.e., the line $\delta_{\text{topology}} = 1$) is indicated with a dotted line (· · · ·). Both models predict that the inequality is violated above $\sim$ 1 kHz and therefore that models with their circuit topology can not accurately predict the intracochlear pressure P_{rw} at high frequencies.

course of hearing (< 80 dB SPL). The framework defines those experiments sufficient to characterize the transduction characteristics of the middle ear and its components, and thus constitutes a common ground where theory and experiment may be systematically compared. The constraint of causality (and, if found to be applicable, those of reciprocity and minimum-phase behavior) may be used either to reduce the number of measurements necessary to characterize the middle ear or to check the consistency of measurements that overdetermine the system (Shera and Zweig 1991c). The phenomenology may be used to characterize the middle ears of cats (see Appendix A) and other vertebrates.

The framework has been used to generalize the classical transformer ratio to include effects of eardrum flexion or nonrotational vibration of the bones of the middle ear. Middle-ear models predict that the generalized transformer ratios $\widehat{N}_{\mathrm{U}}$ and $\widehat{N}_{\mathrm{P}}$ vary considerably with frequency. The conditions under which the topology of existing circuit analogs satisfactorily approximates middle-ear mechanics have been given and used to demonstrate that most models cannot correctly predict absolute intracochlear pressures.

Acknowledgments

The authors thank Jeffrey Carr for many helpful conversations and William Peake and John Rosowski for their useful comments on an earlier version of the manuscript. This work was supported by the Theoretical Division of Los Alamos National Laboratory and a National Science Foundation Graduate Fellowship to C. A. S.

Appendix A: Phenomenology of the Feline Middle Ear

This Appendix extends the phenomenological description of human middle-ear mechanics to address complications that arise in mammals, such as the cat, in which the oval and round window face onto different cavities. Although the description of eardrum/ossicular transduction carries over from the human, the variation in topology of the three windows modifies the equations characterizing the round window and the middle-ear cavities. The equations for the feline middle ear are represented in the form of an equivalent circuit.

A. The round window

Since the round window faces onto the bulla cavity in the cat, its motion is characterized by the equation [cf. Eq. (23)]

$$P_{\rm rw} - P_{\rm bc} \equiv -Z_{\rm rw} U_{\rm rw} \ , \tag{A1}$$

where $P_{\rm bc}$ is the pressure in the bulla cavity. Equations relating $P_{\rm tc}$ and $P_{\rm bc}$ are given in the following section.

B. The cavities

Because the oval and round windows face onto separate cavities in the cat, an equation for the pressure in each cavity must be obtained; representation of the effects of the divided middle-ear cavities by a single lumped impedance (i.e., $Z_{\rm cav}$) is not, in general, possible.

The pressure $P_{\rm tc}$ in the tympanic cavity is given by

$$P_{\rm tc} \equiv Z_{\rm tc}\Big(U_{\rm e} - U_{\rm ow} - U_{\rm f}\Big) \ , \tag{A2}$$

where $Z_{\rm tc}$ is the impedance of the tympanic cavity and $U_{\rm f}$ is the volume velocity of air moving between the tympanic cavity and the bulla through the hole in the bony septum known as the foramen.

Likewise, the pressure in the bulla is given by

$$P_{\rm bc} \equiv Z_{\rm bc}\Big(U_{\rm f} - U_{\rm rw}\Big) \ . \tag{A3}$$

The volume velocity U_f is determined by the impedance Z_f of the foramen:

$$P_{tc} - P_{bc} \equiv Z_f U_f \ . \tag{A4}$$

C. Equivalent circuit

In the cat six equations—i.e., Eqs. (3), (A1), (A2), (A3), and (A4)—relate nine unknowns (P_e, U_e, P_{ow}, U_{ow}, P_{rw}, U_{rw}, P_{tc}, U_f, and P_{bc}); as before, three boundary-condition equations complete specification of the solution.

A "black-box" equivalent circuit corresponding to the equations for the cat is given in Fig. A1. Note that the pressure outside the round window is P_{bc}. In this respect the circuit topology shown here (Carr and Zweig 1984) differs from traditional representations of the cat middle-ear (Møller 1965; Peake and Guinan 1967; Lynch 1981) in which either the cavities affect only the eardrum or the round window is approximated as facing onto the tympanic cavity. [A similar network topology has, however, recently been proposed by Peake et al. (1991).] Traditional representations are based on the "series approximation," so-called because the middle-ear input impedance Z_{me} is approximated by the sum (i.e., the "series combination") of the effective cavity impedance Z_{cav} and the equivalent impedance of other middle-ear structures measured with the cavities exposed widely to the atmosphere (e.g., Lynch 1981):

$$Z_{me} \approx Z_{cav} + \widehat{Z}_{me} \ , \tag{A5}$$

where $\widehat{Z}_{me}$ is defined by Eq. (41).

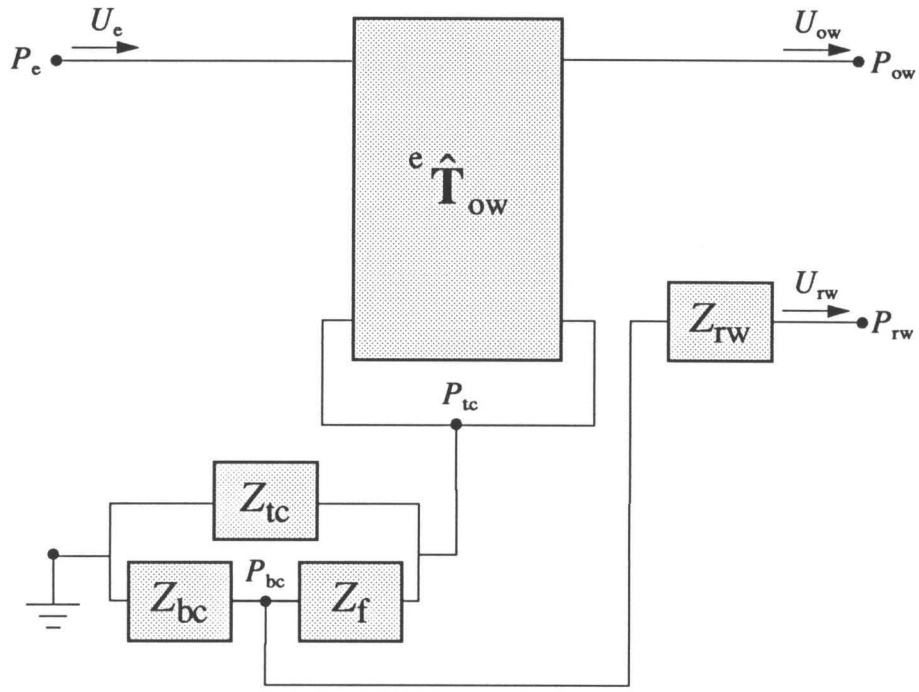

Figure A1. Equivalent circuit for the middle ear of the cat and other mammals in which the round window faces onto the bulla.

References

von Békésy, G. (1960). *Experiments in Hearing.*New York: McGraw-Hill.

Brenkman, C. J., W. L. C. Rutten, and J. J. Grote (1986). "Middle ear research using a SQUID magnetometer II. Transfer characteristics of human middle ears," in *Peripheral Auditory Mechanisms*, edited by J. B. Allen, J. L. Hall, A. Hubbard, S. T. Neely, and A. Tubis, 56–59. Berlin: Springer–Verlag.

Buunen, T. J. F. and M. S. M. G. Vlaming (1981). "Laser-Doppler velocity meter applied to tympanic membrane vibrations in cat," *J. Acoust. Soc. Am.* **69**, 744–750.

Carr, J. N. and G. Zweig (1984). "A mechanical model of the middle ear of anesthetized cats," unpublished report.

Dahmann, H. (1929). "Zur Physiologie des Hörens," *Zeits. Hals- Nasen- Ohrenheilk.* **24**, 462–497.

Dahmann, H. (1930). "Zur Physiologie des Hörens," *Zeits. Hals- Nasen- Ohrenheilk.* **27**, 329–368.

Dallos, P. (1973). *The Auditory Periphery: Biophysics and Physiology.*New York: Academic Press.

Dankbaar, W. A. (1970). "The pattern of stapedial vibration," *J. Acoust. Soc. Am.* **48**, 1021–1022.

Decraemer, W. F. and S. M. Khanna (1991). "Changes in the mode of malleus vibration with frequency," Abstracts of the 14th ARO Midwinter Research Meeting.

Donahue, K. M. (1989). "Human middle-ear mallear motion: Models and measurements," M.S. thesis, Massachusetts Institute of Technology.

Donahue, K. M., J. J. Rosowski, and W. T. Peake (1991). "Can the motion of the human malleus be described as pure rotation?" Abstracts of the 14th ARO Midwinter Research Meeting.

Goode, R. L. and M. C. Killion (1987). "The middle ear from the standpoint of the surgeon and the acoustician," paper presented at the 113th meeting of the Acoustical Society of America, Indianapolis, Indiana.

Guinan, J. J. and W. T. Peake (1967). "Middle-ear characteristics of anesthetized cats," *J. Acoust. Soc. Am.* **41**, 1237–1261.

Gundersen, T. and K. Høgmoen (1976). "Holographic vibration analysis of the ossicular chain," *Acta Otolaryngol.* **82**, 16–25.

Gyo, K., H. Aritomo, and R. L. Goode (1987). "Measurement of the ossicular vibration ratio in human temporal bones by use of a video measuring system," *Acta Otolaryngol.* **103**, 87–95.

Helmholtz, H. L. F. (1868). "*Die Mechanik der Gehörknöchelchen und des Trommelfells*," *Pflüg. Arch. ges. Physiol.* **1**, 1–60. Trans. by A. H. Buck and N. Smith, "The mechanism of the ossicles of the ear and the membrana tympani," 1873.

Ingelstedt, S., A. Ivarsson, and B. Jonson (1967). "Mechanics of the human middle ear," *Acta Otolaryngol.* Suppl. **228**, 3–58.

Khanna, S. M. and J. Tonndorf (1971). "The vibratory pattern of the round window in cats," *J. Acoust. Soc. Am.* **50**, 1475–1483.

Khanna, S. M. and J. Tonndorf (1972). "Tympanic membrane vibrations in cats studied by time-averaged holography," *J. Acoust. Soc. Am.* **51**, 1904–1920.

Killion, M. C. and P. Dallos (1979). "Impedance matching by the combined effects of the outer and middle ear," *J. Acoust. Soc. Am.* **66**, 599–602.

Killion, M. C. and J. D. Clemis (1981). "An engineering view of middle ear surgery," *J. Acoust. Soc. Am.* **69** Suppl. 1, A544.

Kirikae, I. (1960). *The Structure and Function of the Middle Ear.*Tokyo: University of Tokyo Press.

Kobrak, H. (1959). *The Middle Ear.*Chicago: University of Chicage Press.

Kringlebotn, M. (1988). "Network model for the human middle ear," *Scand. Audiol.* **17**, 75–85.

Lutman, M. E. and A. M. Martin (1979). "Development of an electroacoustic analogue model of the middle ear and acoustic reflex," *J. Sound Vib.* **64**, 133–157.

Lynch, T. J. (1981). "Signal processing by the cat middle ear: Admittance and transmission, measurements and models," Ph.D. thesis, Massachusetts Institute of Technology.

Lynch, T. J., V. Nedzelnitsky, and W. T. Peake (1982). "Input impedance of the cochlea in cat," *J. Acoust. Soc. Am.* **72**, 108–130.

Møller, A. R. (1961). "Network model of the middle ear," *J. Acoust. Soc. Am.* **33**, 168–176.

Møller, A. R. (1965). "An experimental study of the acoustic impedance of the middle ear and its transmission properties," *Acta. Otolaryngol.* **60**, 129–149.

Nedzelnitsky, V. (1980). "Sound pressures in the basal turn of the cat cochlea," *J. Acoust. Soc. Am.* **68**, 1676–1689.

Nomura, Y. (1984). *Otological Significance of the Round Window.*Basel: Karger.

Onchi, Y. (1961). "Mechanism of the middle ear," *J. Acoust. Soc. Am.* **33**, 794–805.

Peake, W. T. and J. J. Guinan (1967). "Circuit model for the cat's middle ear," *MIT Quart. Prog. Rep.* **84**, 320–326.

Peake, W. T., J. J. Rosowski, and T. J. Lynch, III (1992). "Middle-ear transmission: Acoustic versus ossicular coupling in cat and human," *Hearing Res.* **57**, 245–268.

Rhode, W. S. (1978). "Some observations on cochlear mechanics," *J. Acoust. Soc. Am.* **64**, 158–176.

Rosowski, J. J., L. H. Carney, and W. T. Peake (1988). "The radiation impedance of the external ear of cat: Measurements and applications," *J. Acoust. Soc. Am.* **84**, 1695–1708.

Ross, S. (1968). "Impedance at the eardrum, middle-ear transmission, and equal loudness," *J. Acoust. Soc. Am.* **43**, 491–505.

Rubinstein, M., B. Feldman, H. Fischler, E. H. Frei, and D. Spira (1966). "Measurement of stapedial-footplate displacements during transmission of sound through the middle ear," *J. Acoust. Soc. Am.* **40**, 1420–1426.

Schuknecht, H. F. (1974). *Pathology of the Ear.*Cambridge: Harvard University Press.

Shaw, E. A. G. (1977). "Eardrum representation in middle-ear acoustical networks," *J. Acoust. Soc. Am.* **62** Suppl. 1, S102.

Shaw, E. A. G. and M. R. Stinson (1981). "Network concepts and energy flow in the human middle ear," *J. Acoust. Soc. Am.* **69** Suppl. 1, S43.

Shera, C. A. and G. Zweig (1991c). "Phenomenological characterization of eardrum transduction," *J. Acoust. Soc. Am.* **90**, 253–262.

Shera, C. A. and G. Zweig (1992a). "Middle-ear phenomenology: The view from the three windows," submitted to *J. Acoust. Soc. Am.*

Shera, C. A. and G. Zweig (1992b). "Analyzing reverse middle-ear transmission: Noninvasive *Gedankenexperiments*," submitted to *J. Acoust. Soc. Am.*

Shera, C. A. and G. Zweig (1992c). "An empirical bound on the compressibility of the cochlea," submitted to *J. Acoust. Soc. Am.*

Shera, C. A. and G. Zweig (1992d). "Noninvasive estimation of middle-ear transfer characteristics in human cadavers," in preparation.

Stinson, M. R. (1985). "The spatial distribution of sound pressure within scaled replicas of the human ear canal," *J. Acoust. Soc. Am.* **78**, 1596–1602.

Tonndorf, J. and S. M. Khanna (1970). "The role of the tympanic membrane in middle ear transmission," *Ann. Otol. Rhinol. Laryngol.* **79**, 743–753.

Vlaming, M. S. M. G. and L. Feenstra (1986). "Studies on the mechanics of the normal human middle ear," *Clin. Otolaryngol.* **11**, 353–363.

Wever, E. G. and M. Lawrence (1954). *Physiological Acoustics.*Princeton: Princeton University Press.

Zwislocki, J. (1957). "Some impedance measurements on normal and pathological ears," *J. Acoust. Soc. Am.* **29**, 1312–1317.

Zwislocki, J. (1962). "Analysis of the middle-ear function. Part I: Input impedance," *J. Acoust. Soc. Am.* **34**, 1514–1523.

Zwislocki, J. (1965). "Analysis of some auditory characteristics," in *Handbook of Mathematical Psychology*, edited by R. D. Luce, R. R. Bush, and E. Galanter, 1–97. New York: John Wiley & Sons.

Analyzing Reverse Middle-Ear Transmission: Noninvasive *Gedankenexperiments*

Christopher A. Shera and George Zweig

Theoretical Division
Los Alamos National Laboratory
Los Alamos, New Mexico 87545

and

Physics Department
California Institute of Technology
Pasadena, California 91125

ABSTRACT

The phenomenological framework outlined in the companion paper (Shera and Zweig 1992a) characterizes both forward and reverse transmission through the middle ear. This paper illustrates its use in the analysis of noninvasive measurements of middle-ear and cochlear mechanics. It is shown how cochlear nonlinearities can be exploited to measure middle-ear scattering coefficients, and a noninvasive experiment is proposed to test the common assumption that the middle ear can be idealized as a simple mechanical transformer. A cochlear scattering framework is developed for the analysis of combination-tone and other experiments in which acoustic distortion products are used to drive the middle ear "in reverse." The framework is illustrated with a simple psychophysical *Gedankenexperiment* analogous to the neurophysiological experiments of Fahey and Allen (1985).

Contents

Introduction

Otoacoustic emissions offer a promising acoustic window on the mechanics of the cochlea. That window is clouded, however, by an incomplete knowledge of the transmission properties of the middle ear. The potential for using otoacoustic emissions as a noninvasive probe of cochlear mechanics is nicely illustrated by the work of Allen and Fahey, who have recently proposed using measurements of acoustic distortion products to measure the gain of the "cochlear amplifier" (Allen and Fahey 1992; Fahey and Allen 1985). Cogent analysis of that and other combination-tone experiments depends critically, however, on understanding the reflection and transmission of retrograde waves by the middle ear. Models for otoacoustic emissions often ignore the considerable interference effects arising from middle-ear reflection, making it difficult to compare their predictions with experiment.

The framework outlined in the companion paper (Shera and Zweig 1992a) characterizes both forward and reverse transmission through the middle ear. This paper—the third in a series (Shera and Zweig 1991c, 1992a–d) devoted to problems of middle-ear mechanics—illustrates, largely by means of concrete example, how that framework can be applied to address problems of cochlear and middle-ear mechanics involving the reflection and transmission of cochlear waves by and through the middle ear.

The paper consists of three parts. In the first, the phenomenological framework outlined in the companion paper (Shera and Zweig 1992a) is reexpressed in the equivalent language of middle-ear scattering coefficients. In the second, the framework is used to demonstrate how measurements of otoacoustic emissions can be exploited to measure middle-ear reflection and transmission coefficients and thereby to test certain common assumptions about the operation of the middle ear. In the third, a cochlear scattering formalism suited to the analysis of combination- and cancellation-tone experiments is developed within the context of a simple psychophysical *Gedankenexperiment* similar to the neurophysiological experiments of Fahey and Allen (1985). Finally, examples are provided that illustrate the considerable interference effects that arise due to the reflection of retrograde waves from the stapes. It is shown, for example, that the ear can generate tones that are considerably louder outside the cochlea than they are within it.

I. Scattering Representation of the Middle Ear

Earlier papers (Shera and Zweig 1991c; Shera and Zweig 1992a) adopted the transfer-matrix formalism as a natural framework for the systematic "deconstruction" of middle-ear transduction characteristics into a product of separately-measurable component transformations. The overall middle-ear transformation can, however, also be described using another representation of two-port networks suited to the analysis of wave reflection and transmission on either side of the middle ear: the scattering matrix (e.g., Carlin 1956; Kuo 1962). With separate knowledge of the wave impedances at the two ports, the two representations are equivalent and interconvertible. Although not as computationally convenient as transfer matrices for the description of cascades of systems, scattering matrices provide a more intuitive framework for the analysis of wave reflection and interference effects.

The middle ear converts air-borne sound waves into hydromechanical waves that travel along the organ of Corti. Let P_e^+ and P_e^- be the pressure waves at the eardrum propagating in directions, respectively, towards and away from the drum. On the other side of the middle ear, let the forward- and backward-traveling waves at the basal end of the organ of Corti near the stapes be denoted P_0^+ and P_0^-, respectively. The scattering matrix for the middle ear ${}^{e}\mathbf{S}_0$ is then defined by the equation

$$\begin{pmatrix} P_e^- \\ P_0^+ \end{pmatrix} \equiv {}^{e}\mathbf{S}_0 \begin{pmatrix} P_e^+ \\ P_0^- \end{pmatrix} , \tag{1}$$

which characterizes the middle-ear transformation by expressing the two outgoing waves (i.e., the two waves propagating *away* from the middle ear) as linear combinations of the two incoming waves. The four matrix elements of ${}^{e}\mathbf{S}_0$, denoted

$${}^{e}\mathbf{S}_0 \equiv \begin{pmatrix} r^+ & t^- \\ t^+ & r^- \end{pmatrix} , \tag{2}$$

are thus the forward and reverse transmission and reflection coefficients for the middle ear (defined here as that part of the ear lying between the end of the ear canal and the beginning of the organ of Corti).[1]

---

[1] In the notation of the companion paper (Shera and Zweig 1992a), which was concerned only with the sum and difference pressures just inside the cochlear windows, the two-port ${}^{e}\blacksquare_0$ would be written as the cascade ${}^{e}\blacksquare_- \otimes {}^{-}\blacksquare_0$, where ${}^{-}\blacksquare_0$ represents the vestibular space between the cochlear windows and the beginning of the organ of Corti.

The waves traveling in the two directions are related to the total pressure and volume velocity through the wave impedances $Z_{\pm}$, which generalize the concept of characteristic impedance to nonuniform media (Shera and Zweig 1991b). For example, so long as the cross-sectional area of the ear canal does not vary too rapidly, the wave impedances for the ear canal are independent of direction and equal to the local value of the characteristic impedance Z_0. Thus,

$$P_e^{\pm} = \tfrac{1}{2}(P_e \pm Z_0 U_e) \; . \tag{3}$$

To find the cochlear waves $P_0^{\pm}$, recall that the cochlea of the cat manifests a tapering symmetry (Shera and Zweig 1991a) that guarantees that the wavelength or characteristic impedance λ changes slowly with position χ in the basal turns of the cochlea. The cochlear wave impedances are therefore also approximately independent of direction (despite the rapid variation of scalae area in the basal turn), and

$$P^{\pm} = \tfrac{1}{2}(P \pm \lambda U) \; . \tag{4}$$

When evaluated at the basal end of the organ of Corti near the stapes (i.e., at $\chi = 0$), the wavelength λ_0 is simply the cochlear input impedance (Shera and Zweig 1991a).

Appendix A summarizes the formulae for obtaining the scattering matrix of a system given its transfer matrix and the wave impedances at its ports. In addition, Appendix A shows how to combine scattering matrices representing the individual networks in a cascade to find the matrix representing the cascaded system.

II. Noninvasive Measurement of Middle-Ear Scattering Coefficients

Otoacoustic emissions demonstrate that the ear emits sound as well as receiving it. When evoked by an external tone, such emissions can be produced by the reflection of forward-traveling waves from mechanical inhomogeneities in the organ of Corti (Shera and Zweig 1992f). This section shows how evoked emissions and their nonlinear growth with stimulus amplitude A can be exploited to measure middle-ear scattering coefficients.

In the ear canal, evoked otoacoustic emissions manifest themselves through the eardrum reflection coefficient $R_e^{\triangleright}(\omega; A)$. The cascading formulae in Appendix A imply that

$$R_e^{\triangleright} = \frac{r^+ - R \det {}^e\mathbf{S}_0}{1 - Rr^-} \; , \tag{5}$$

where $R \equiv R_0^{\triangleright}$ is the traveling-wave ratio evaluated at the basal end of the cochlear spiral (Shera and Zweig 1992e).

At sufficiently low intensities the cochlear traveling-wave ratio R becomes independent of A:

$$R(\omega; A) = R(\omega) \qquad (A < A_1) \,. \tag{6}$$

At high stimulus intensities the relative amplitude of any reflected waves becomes small, and R becomes negligible. Thus,

$$R(\omega; A) = 0 \qquad (A > A^1) \,, \tag{7}$$

and, consequently,

$$R_e^{\triangleright}(\omega; A) = r^+(\omega) \qquad (A > A^1) \,. \tag{8}$$

In humans, the stimulus amplitudes A_1 and A^1 correspond to roughly 20 dB and 60 dB above threshold, respectively (Zwicker and Schloth 1984).

Were it possible to determine the cochlear traveling-wave ratio $R(\omega; A)$ independently, measurements of $R_e^{\triangleright}$ at three stimulus intensities would provide three independent equations that could be solved for the two middle-ear reflection coefficients $r^{\pm}$ and the determinant $\det {}^e\mathbf{S}_0$ (or, equivalently, the product of transmission coefficients t^+t^-). In the following, the three stimulus amplitudes are assumed to be A_1, A^1, and A (with $A_1 < A < A^1$; a reasonable choice for A might be $\sqrt{A_1 A^1}$). Then,

$$r^+ = R_e(A^1) \,; \tag{9}$$

$$r^- = \frac{R(A)\left[R_e(A_1) - r^+\right] - R(A_1)\left[R_e(A) - r^+\right]}{R(A_1)R(A)\left[R_e(A_1) - R_e(A)\right]} \,; \tag{10}$$

and

$$t^+t^- = \frac{\left[R(A_1) - R(A)\right]\left[R_e(A_1) - r^+\right]\left[R_e(A) - r^+\right]}{R(A_1)R(A)\left[R_e(A_1) - R_e(A)\right]} \,; \tag{11}$$

where $R_e \equiv R_e^{\triangleright}$. For simplicity, the frequency dependence has been suppressed.

Although Eqs. (9)–(11) require independent determination of the cochlear traveling-wave ratio $R(\omega; A)$, considerable information about middle-ear scattering coefficients can be obtained with less complete knowledge of R. For example, consider the ratio of scattering coefficients Γ defined by

$$\Gamma \equiv \frac{t^+t^-}{r^-} \,. \tag{12}$$

Eqs. (10) and (11) imply that Γ can be written

$$\Gamma(\omega) = \frac{[1 - \Lambda][R_e(A_1) - r^+][R_e(A) - r^+]}{\Lambda[R_e(A_1) - r^+] - [R_e(A) - r^+]} , \tag{13}$$

where

$$\Lambda \equiv R(A)/R(A_1) . \tag{14}$$

Since the unknown function cancels in the ratio, measurement of Λ only requires determination of $R(\omega; A)$ to within an unknown multiplicative function of frequency independent of A. Equation (13) thus permits determination of $\Gamma \equiv t^+t^-/r^-$ from measurements of Λ and r^+.

Noninvasive measurements of the form and frequency variation of $R(\omega; A)$, including determinations to within an unknown function independent of A, are discussed elsewhere (Shera and Zweig 1992e). The following section shows how measurement of Γ can be used to test a common assumption about the operation of the middle ear.

A. The middle ear as transformer: An experimental test

To simplify calculations of middle-ear transmission, the middle ear is often idealized and regarded as a mechanical transformer, albeit with a possibly complex and frequency-dependent transformer ratio N_{me} (e.g., Allen and Fahey 1992). No direct test of this assumption, however, has ever been performed. This section shows how measurements of otoacoustic emissions can be used to test that assumption noninvasively.

The action of the middle ear is that of a transformer if its transfer matrix has the form (e.g., Shera and Zweig 1992a)

$${}^e\mathbf{T}_0 \approx \begin{pmatrix} 1/N_{me} & 0 \\ 0 & N_{me} \end{pmatrix} . \tag{15}$$

The interconversion formulae in Appendix A imply that the elements of ${}^e\mathbf{S}_0$ then satisfy the equations

$$r^- = -r^+ , \tag{16}$$

and

$$\det {}^e\mathbf{S}_0 = -1 . \tag{17}$$

If the transformer assumption is valid, the function Γ can be simplied to the form

$$\Gamma = r^+ - 1/r^+ . \tag{18}$$

Equation (9) indicates that the forward reflection coefficient r^+ is easily measured (e.g., Puria and Allen 1991). Both r^+ and Γ can therefore be measured noninvasively in the ear canal. Those measurements can then be combined to test the transformer assumption, as represented by Eq. (18).

III. Analyzing Combination-Tone Experiments

This section develops, largely by means of concrete example, a framework for the analysis of combination-tone and similar experiments in which cochlear nonlinearities create distortion products that propagate in both directions along the organ of Corti. The effects of the middle ear are explicitly included. The framework allows the convenient incorporation of cochlear reflection and interference phenomena into analytic approximations of the responses of cochlear models to multiple pure-tone stimuli.

Although the techniques outlined here are useful for the analysis of a number of experiments (e.g., Furst et al. 1988), the discussion uses as its principle example an experiment similar to that of Fahey and Allen (1985). That experiment uses distortion-product otoacoustic emissions to drive the middle ear "in reverse," and compares the amplitude of the combination tone measured in the ear canal at threshold (defined, for example, by a constant basilar membrane velocity at CF) with the pressure recorded when a tone at the distortion-product frequency—its loudness also adjusted to threshold—is played directly.

More specifically, the experiment consists of measuring the ratio ρ of ear-canal pressures P_{ec} defined by

$$\rho \equiv P_{ec}^{\dagger}\big|_{\text{intracochlear source}} \,/\, P_{ec}^{\dagger}\big|_{\text{external source}} , \tag{19}$$

where the superscripted † indicates that the pressure is measured at psychophysical or neurophysiological threshold.[2] The pressures P_{ec} represent the complex Fourier components of the ear-canal pressure p_{ec} at the distortion-product frequency. The qualifier

[2] As a useful mnemonic, note the resemblance between the † and the recording electrodes used to determine the neurophysiological threshold.

"intracochlear source" denotes a stimulus condition in which the measured tone is generated within the cochlea as a distortion product; "external source" indicates that the tone is produced in the ear canal with an earphone.

A. Assumptions and analysis

Figure 1 provides a schematic diagram of the peripheral auditory system for each of the two stimulus conditions. An earpiece containing a miniature earphone and microphone is sealed into the ear canal; its Norton-equivalent source impedance is denoted Z_s. The residual ear-canal space and the middle ear are represented, respectively, by the two-port networks ${}^{ec}\blacksquare_e$ and ${}^{e}\blacksquare_0$. Appendix A shows how the matrix ${}^{ec}\mathbf{S}_0$, with elements denoted

$$ {}^{ec}\mathbf{S}_0 \equiv \begin{pmatrix} R^+ & T^- \\ T^+ & R^- \end{pmatrix} , \tag{20} $$

can be obtained by combining the elements of ${}^{ec}\mathbf{S}_e$ and ${}^{e}\mathbf{S}_0$.[3]

The generation of distortion products by the nonlinear interaction of primary tones at frequencies f_1 and f_2 (with $f_2 > f_1$) is assumed to occur within some region $[a,b]$ of the cochlea, presumably near the f_2 place where the product of the envelopes of the responses to the two primaries is large. The "source region" $[a,b]$ is defined so that outside its boundaries the primaries are small enough that the cochlear response to those tones is linear. Outside the region $[a,b]$ the response to the combination tone (e.g., at a frequency $f_{ct} = 2f_1 - f_2$) is therefore assumed to superpose linearly with the responses to the primaries; any nonlinear interactions—either between the primaries themselves (e.g., those generating the combination tone) or, subsequently, between the combination tone and its primaries (e.g., two-tone suppression)—thus occur, by definition, entirely within $[a,b]$. The details of those nonlinear interactions, however, are unimportant for the phenomenological analysis presented here.

The source region is regarded as a nonlinear "glass box" (denoted ${}^{a}\widetilde{\square}_{b}$) described by level-dependent boundary conditions at its borders. The box is glass, its walls transparent,

[3] If the residual ear-canal space between the transducers and the eardrum is made small enough, the matrices ${}^{ec}\mathbf{S}_0$ and ${}^{e}\mathbf{S}_0$ become equivalent. The residual ear-canal space is negligible if $2\omega L/c \ll 1$, where L is the length of the residual space and c is the speed of sound (see Appendix C). The factor of two arises because phase differences due to round-trip travel are important here. As an example, the inequality requires $L \ll 3$ cm at a frequency of 1 kHz. The residual ear-canal space is therefore *not* negligible in the examples shown in Figs. 2 and 3.

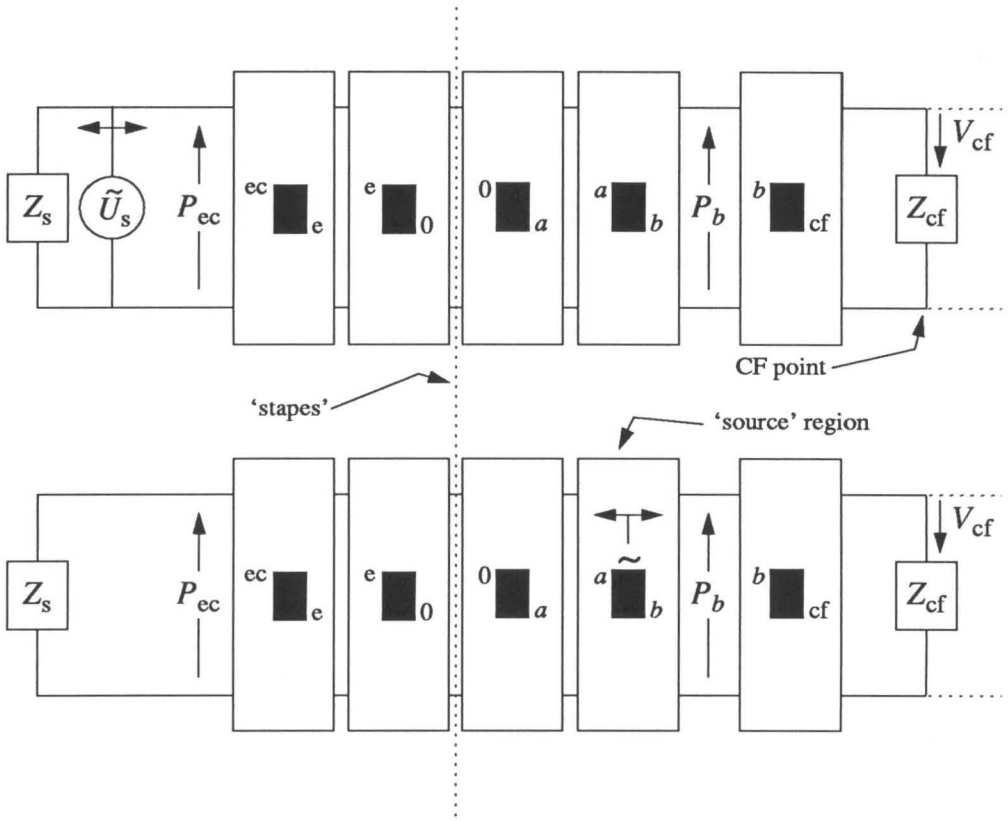

Figure 1. Schematic diagrams of the peripheral auditory system for the external (top) and intracochlear (bottom) stimulus conditions described in the text. Z_s represents the Norton-equivalent source impedance of the stimulus-delivery and recording system sealed into the ear canal. The networks ${}^{ec}\blacksquare_{e}$, ${}^{e}\blacksquare_{0}$, and ${}^{0}\blacksquare_{a}$ represent, respectively, the residual ear-canal space, the middle ear and vestibular space, and the basal portion of the cochlea. The vertical dotted line indicates the position of the basal end of the organ of Corti near the stapes. The generation of distortion products is assumed to occur within the region $[a, b]$, represented by the nonlinear "glass box" ${}^{a}\tilde{\square}_{b}$, presumably located near the f_2 place. The source region generates waves that travel away from their site of generation in both directions. Forward-traveling waves of frequency f_{ct} travel through the apical turns of the cochlea (represented by the network ${}^{b}\blacksquare_{cf}$) and deposit their energy near the f_2 place, denoted x_{cf}.

because its behavior, unlike that of a linear system, cannot be characterized completely in the frequency domain without detailed knowledge of its components. The following analysis focuses exclusively on wave propagation at the combination-tone frequency f_{ct}, regarding the primaries simply as parametric "knobs" controlling the amplitude and phase of the distortion products generated within $[a, b]$. Unless otherwise noted, all equations are therefore tacitly understood to apply only at the frequency f_{ct}.

1. The basal region $[0, a]$

The basal region of the cochlea $[0, a]$ is assumed analogous to a linear, one-dimensional hydromechanical transmission-line (Peterson and Bogert 1950; Zweig et al. 1976; Zweig 1991). That is, the analysis assumes that the wavelengths of the waves in the basal turns of the cochlea (i.e., within and basal to the source region) are long relative to the heights of the scalae and, hence, that wave propagation is one-dimensional. This so-called "long-wavelength approximation," while valid for the lower-frequency combination tone, is presumably violated within $[a, b]$ for the primaries. At the combination-tone frequency the region $[0, a]$ can thus be represented by a two-port network ${}^0\blacksquare_a$ and has a corresponding scattering-matrix description ${}^0\mathbf{S}_a$.

Throughout this paper the elements of the cochlear scattering matrix ${}^x\mathbf{S}_y$ representing the interval $[x, y]$ are denoted

$$ {}^x\mathbf{S}_y \equiv \begin{pmatrix} r^+_{xy} & t^-_{xy} \\ t^+_{xy} & r^-_{xy} \end{pmatrix} , \tag{21} $$

For simplicity, and in accord with measurements of the cochlear input impedance in cat (Shera and Zweig 1991a), waves are assumed to propagate without reflection through the basal turn, despite the rapid secular variation of the stiffness of the basilar membrane (see also Shera and Zweig 1991b). The reflection coefficients are therefore assumed negligible:

$$ r^{\pm}_{xy} = 0 \qquad (x, y < a) . \tag{22} $$

As an example, the cochlear transmission-line equations in Appendix C imply that the matrix ${}^x\mathbf{S}_y$ has the approximate form

$$ {}^x\mathbf{S}_y \approx \begin{pmatrix} 0 & \sqrt{\lambda_x/\lambda_y}\, e^{-i\phi} \\ \sqrt{\lambda_y/\lambda_x}\, e^{-i\phi} & 0 \end{pmatrix} , \tag{23} $$

where

$$ \phi = \int_x^y d\chi/\lambda . \tag{24} $$

The subscripts "x" and "y" indicate that the wavelengths λ have been evaluated at the corresponding "port" or boundary.

2. The source region $[a,b]$

At the combination-tone frequency, the source region $[a,b]$ has two effects: first, it acts as a source of wave energy and, second, it transmits from one boundary to the other waves originating outside the region.

Consider first its role as a source of energy at the combination-tone frequency. Imagine for the moment the region $[a,b]$ embedded in an infinite, reflectionless cochlea without other combination-tone sources. Two waves then propagate away from the source region. At the apical border one measures a net forward-traveling wave $\tilde{P}_b^+$, and at the basal boundary a net backward-traveling wave $\tilde{P}_a^-$. Those wave amplitudes are, of course, functions of the primaries:

$$\tilde{P}_b^+ = \tilde{P}_b^+[\mathcal{P}_1, \mathcal{P}_2] \quad \text{and} \quad \tilde{P}_a^- = \tilde{P}_a^-[\mathcal{P}_1, \mathcal{P}_2]\,, \tag{25}$$

where $\mathcal{P}_1$ and $\mathcal{P}_2$ represent the complex amplitudes of the primaries at some reference location (e.g., the stapes). The primaries are written in a calligraphic font, rather than the standard italic, to remind the reader that they represent complex amplitudes at frequencies, namely f_1 and f_2, other than the combination-tone frequency f_{ct} for which the response is sought.

Cochlear waves created outside the source region are transmitted or reflected as they propagate through $[a,b]$. In the absence of the primaries, that propagation would be described by a standard scattering matrix ${}^a\mathbf{S}_b$. When the primaries are present, however, possible nonlinear interactions between the primaries and waves at the combination-tone frequency may make things more complicated. A useful phenomenological approach is to regard the primaries as modifying the effective scattering matrix for the region. This approach enables one to obtain an approximate initial solution to the nonlinear problem. The procedure can then be iterated, if necessary, and, with the help of this bootstrap, higher accuracy obtained.

At the frequency f_{ct} wave propagation through the region is then described by the matrix ${}^a\tilde{\mathbf{S}}_b$, whose elements—the reflection and transmission coefficients at f_{ct} in the presence of the primaries—are, in general, functions of the primaries. When wave propagation

at f_{ct} is linear and unaffected by the presence of the primaries (e.g., when the primaries are sufficiently higher in frequency), the matrix ${}^a\tilde{\mathbf{S}}_b$ reduces to ${}^a\mathbf{S}_b$.

Descriptions of the region's wave-generation and wave-transmission characteristics can now be combined. As viewed from its boundaries, the source region is assumed to be described, at the combination-tone frequency, by the equation

$$\begin{pmatrix} P_a^- \\ P_b^+ \end{pmatrix} = {}^a\tilde{\mathbf{S}}_b \begin{pmatrix} P_a^+ \\ P_b^- \end{pmatrix} + \begin{pmatrix} \tilde{P}_a^- \\ \tilde{P}_b^+ \end{pmatrix} , \tag{26}$$

where the matrix ${}^a\tilde{\mathbf{S}}_b$ and source waves $\tilde{P}_a^-$ and $\tilde{P}_b^+$ are functions of the primaries $\mathcal{P}_1$ and $\mathcal{P}_2$ (and, in general, of the incoming and outgoing wave amplitudes $P_a^\pm$ and $P_b^\pm$):

$${}^a\tilde{\mathbf{S}}_b = {}^a\tilde{\mathbf{S}}_b[\mathcal{P}_1, \mathcal{P}_2, P_a^\pm, P_b^\pm] . \tag{27}$$

The first term in Eq. (26) describes wave propagation across the region; the second, wave generation within it. In the infinite, reflectionless cochlea described above, the vector $\left(\begin{smallmatrix} P_a^+ \\ P_b^- \end{smallmatrix}\right)$ vanishes, and the region acts only as a source:

$$\begin{pmatrix} P_a^- \\ P_b^+ \end{pmatrix} = \begin{pmatrix} \tilde{P}_a^- \\ \tilde{P}_b^+ \end{pmatrix} . \tag{28}$$

3. The apical region $[b, \text{“}\infty\text{”}]$

As seen from the boundary b, the apical region of the cochlea can be characterized by an equivalent reflection coefficient $R_b^\triangleright$ for waves of frequency f_{ct}. (The superscripted $\triangleright$ indicates that the reflection coefficient is defined with the primary wave traveling apically to the right.)[4] A nonzero reflection coefficient can arise, for example, from scattering of the forward-traveling wave by mechanical inhomogeneities in the organ of Corti near the f_{ct} place. Reflected wavelets combine and propagate back toward the stapes, ultimately giving rise to stimulus-frequency emissions measurable in the ear canal (Shera and Zweig 1992f). Since the amplitude of stimulus-frequency emissions varies with stimulus level, the reflection coefficient $R_b^\triangleright$ depends on the amplitude of the combination tone. In the experiment analyzed here, however, the combination tone is held at threshold where the response is assumed linear; $R_b^\triangleright$ is therefore independent of $\tilde{P}_b^+$ (see Sec. I).

[4] This notation differs from that of an earlier paper (Shera and Zweig 1991b), which represents the same information using a diacritical arrow.

Detection of the tone at f_{ct}—whether that tone is generated externally or within the cochlea—is assumed to occur when the velocity of the basilar membrane at the f_{ct} place (denoted x_{cf}, the characteristic-frequency point) reaches some threshold value $V_{cf}^{\dagger}$, or, equivalently, when the forward-traveling pressure wave at the point b reaches the threshold value $P_b^{+\dagger}$. Note, however, that because the pressures $P_b^{+\dagger}$ (or, equivalently, the velocities $V_{cf}^{\dagger}$) cancel when forming the ratio, ρ, given by Eq. (19), the measurement remains independent of the assumed detection criterion.

4. Iterating for self-consistency

Because of the nonlinearities, the properties of the source region (summarized at its boundaries, for the frequency f_{ct}, by the amplitudes $\tilde{P}_b^{+}$ and $\tilde{P}_a^{-}$ and the matrix ${}^{a}\tilde{\mathbf{S}}_b$) depend, in general, on all characteristics of the system (e.g., on boundary conditions in the ear canal). For example, the original source waves $\tilde{P}_b^{+}$ and $\tilde{P}_a^{-}$ are partially reflected by the cochlear boundary with the middle ear. Some fraction of their energy therefore returns to the source region, where it may interact with the primaries, perhaps changing, in turn, the amplitudes of the outgoing source waves. In general, the region $[a, b]$ cannot, therefore, be isolated and characterized independently, with exact solutions for the cochlear response at f_{ct} obtained simply by superposition.

Such solutions can, however, be obtained by iteration. One assumes some reasonable initial values for $\tilde{P}_b^{+}$, $\tilde{P}_a^{-}$, and ${}^{a}\tilde{\mathbf{S}}_b$ and "solves" the system assuming superposition at the frequency f_{ct} (see below). The resulting approximate solution is then used to adjust the characteristics of the source region (according to equations determined by the underlying model of cochlear mechanics), and the procedure iterated until a self-consistent solution is obtained. A sample iteration algorithm is given in Appendix B.

B. Solutions assuming superposition

This section solves for the ear canal pressures $P_{ec}^{\dagger}$ for the two stimulus conditions by assuming that the principle of superposition holds throughout the cochlea for waves at the distortion-product frequency. Superposition implies that the cochlear response at f_{ct} can be obtained simply by summing contributions from all combination-tone wavelets (e.g., those originating in the ear canal, within the source region, or by reflection). Depending

on the nature of the cochlear nonlinearities, additional iteration may then be required to accurately approximate the behavior of the system.

Many of the equations obtained in this section represent variations on the cascading formulae derived in Appendix A. Familiarity with those derivations may be helpful in understanding the physical content of equations whose origin may otherwise appear somewhat obscure.

1. External source

To solve for the ear canal pressure $P_{\rm ec}$ in terms of the pressure P_b^+, note that

$$P_{\rm ec} = P_{\rm ec}^+ + P_{\rm ec}^- \equiv P_{\rm ec}^+\left(1 + R_{\rm ec}^{\triangleright}\right) . \tag{29}$$

Similarly,

$$P_b = P_b^+ + P_b^- \equiv P_b^+\left(1 + R_b^{\triangleright}\right) . \tag{30}$$

When the source $\widetilde{U}_{\rm s}$ is used to generate the tone externally (Fig. 1, top),

$$P_b^+ = \frac{t_{0b}^+ T^+ P_{\rm ec}^+}{1 - R_b^{\triangleright} t_{0b}^+ t_{0b}^- R^-} . \tag{31}$$

The numerator represents the wave produced by direct transmission of the forward-traveling wave $P_{\rm ec}^+$ in the ear canal; that wave is then multiply reflected (with reflection coefficient $R_b^{\triangleright}$ in the forward direction and $t_{0b}^+ t_{0b}^- R^-$ in the backward).[5] Summing those multiple reflections introduces an overall multiplicative factor, given by the reciprocal of the denominator (see Appendix A), and yields Eq. (31) for the net forward-traveling wave at b.

Combining Eqs. (29) and (31) yields the relation

$$P_{\rm ec}^{\dagger} / P_b^{+\dagger} = \frac{\left(1 + R_{\rm ec}^{\triangleright}\right)\left(1 - R_b^{\triangleright} t_{0b}^+ t_{0b}^- R^-\right)}{t_{0b}^+ T^+} . \tag{32}$$

The cascading formulae in Appendix A imply that

$$R_{\rm ec}^{\triangleright} = \frac{R^+ - R \det {}^{\rm ec}\mathbf{S}_0}{1 - R R^-} , \tag{33}$$

---

[5] The operative retrograde reflection coefficient is not

$$R_b^{\triangleleft} = t_{0b}^+ t_{0b}^- \frac{R^- - R_{\rm s} \det {}^{\rm ec}\mathbf{S}_0}{1 - R_{\rm s} R^+} , \tag{5.1}$$

as might be expected, because $R_b^{\triangleleft}$ contains contributions from the boundary conditions in the ear canal that are already included in the transmitted wave $P_{\rm ec}^+$.

where R is the cochlear traveling-wave ratio discussed in Sec. I. Since waves are assumed to propagate through the basal region $[0, b]$ without reflection, R and $R_b^{\triangleright}$ are related by

$$R = t_{0b}^{+} t_{0b}^{-} R_b^{\triangleright} \, . \tag{34}$$

Equation (32) can therefore be simplified to yield

$$P_{\mathrm{ec}}^{\dagger} / P_b^{+\dagger} = \frac{\left(1 + R_{\mathrm{ec}}^{\triangleright}\right)\left(1 - RR^{-}\right)}{t_{0b}^{+} T^{+}} \, . \tag{35}$$

2. Intracochlear source

When the tone is generated within the cochlea as a distortion product (Fig. 1, bottom), the total forward-traveling wave at b is

$$P_b^{+} = \frac{\tilde{P}_b^{+} + \tilde{P}_a^{-} R_a^{\triangleleft} \tilde{t}_{ab}^{+}}{1 - R_b^{\triangleright} R_b^{\triangleleft}} \, . \tag{36}$$

In this case, the numerator contains contributions from both source waves $\tilde{P}_b^{+}$ and $\tilde{P}_a^{-}$; the latter, after partial reflection at a, propagates across $[a, b]$ as a forward-traveling wave before joining with $\tilde{P}_b^{+}$. As before, the net forward-traveling wave is obtained by summing the effects of multiple reflection. Note that we assume $\tilde{r}_{ab}^{\pm} = 0$, for simplicity.

Similarly, the total backward-traveling wave at a is

$$P_a^{-} = \frac{\tilde{P}_a^{-} + \tilde{P}_b^{+} R_b^{\triangleright} \tilde{t}_{ab}^{-}}{1 - R_a^{\triangleright} R_a^{\triangleleft}} \, . \tag{37}$$

For future reference, note that the relations

$$R_a^{\triangleright} = \tilde{t}_{ab}^{+} \tilde{t}_{ab}^{-} R_b^{\triangleright} \quad \text{and} \quad R_b^{\triangleleft} = \tilde{t}_{ab}^{-} \tilde{t}_{ab}^{+} R_a^{\triangleleft} \tag{38}$$

imply that

$$R_a^{\triangleright} R_a^{\triangleleft} = R_b^{\triangleright} R_b^{\triangleleft} \, . \tag{39}$$

Waves traveling outwards from the eardrum are reflected by the transducer assembly with reflection coefficient R_{s}, given in terms of the Norton-equivalent source impedance by the equation

$$R_{\mathrm{s}} = \frac{Z_{\mathrm{s}} - Z_0}{Z_{\mathrm{s}} + Z_0} \, , \tag{40}$$

where Z_0 is the characteristic impedance of the ear canal. Consequently, the total ear-canal pressure can be written

$$P_{ec} = P_{ec}^{-}(1 + R_s) , \tag{41}$$

where the outward-traveling wave

$$P_{ec}^{-} = \frac{t_{0a}^{-} T^{-} P_a^{-}}{1 - R_s R^{+}} . \tag{42}$$

Combining Eqs. (36)–(42), one obtains

$$P_{ec}^{\dagger}/P_b^{+\dagger} = \frac{t_{0a}^{-} T^{-}(1 + R_s)}{1 - R_s R^{+}} \frac{\tilde{\alpha} + \tilde{t}_{ab}^{-} R_b^{\triangleright}}{1 + \tilde{\alpha} R_b^{\triangleleft}/\tilde{t}_{ab}^{-}} , \tag{43}$$

where $\tilde{\alpha}$ is the ratio of source-wave amplitudes:[6]

$$\tilde{\alpha} \equiv \tilde{P}_a^{-}/\tilde{P}_b^{+} . \tag{44}$$

3. The pressure ratio ρ

Combining the two pressure ratios [Eqs. (35) and (43)] yields

$$\rho = \frac{t_{0a}^{-} t_{0b}^{+} T^{+} T^{-}(1 + R_s)}{(1 + R_{ec}^{\triangleright})(1 - R_s R^{+})(1 - R R^{-})} \frac{\tilde{\alpha} + \tilde{t}_{ab}^{-} R_b^{\triangleright}}{1 + \tilde{\alpha} \tilde{t}_{ab}^{+} R_a^{\triangleleft}} . \tag{45}$$

Note that the pressures $P_b^{+\dagger}$ have cancelled in the ratio; ρ is therefore independent of the assumed detection criterion.[7] Section III-C evaluates Eq. (45) in several simple limiting cases.

C. Some simple examples

This section illustrates the formalism by calculating the ratio of ear-canal pressures ρ for the simple case in which the distortion product is assumed to originate from a distribution of ideal point sources and the middle ear is regarded as a simple mechanical transformer.

---

[6] In this case R and $R_b^{\triangleright}$ are related by

$$R = \tilde{t}_{0b}^{+} \tilde{t}_{0b}^{-} R_b^{\triangleright} , \tag{6.1}$$

where

$$\tilde{t}_{0b}^{\pm} \equiv t_{0a}^{\pm} \tilde{t}_{ab}^{\pm} . \tag{6.2}$$

[7] The simple cancellation of pressures $P_b^{+\dagger}$ in the ratio ρ may not occur if threshold detection of the combination tone is nonlocal (i.e., depends on the cochlear response at locations other than the combination-tone place).

1. A distribution of ideal sources

For this example, assume that ${}^a\tilde{\mathbf{S}}_b = {}^a\mathbf{S}_b$ and let the generation of distortion products in $[a,b]$ be modeled by a distribution of ideal "current" sources (each with negligible Norton-equivalent source admittance) operating at the distortion product frequency. Each source is assumed to launch waves of equal amplitude in the two directions. Although cochlear nonlinearities are responsible for creating the combination tone (i.e., for introducing the sources), once created the source wavelets are assumed, in this example, to superpose linearly with the primaries and with each other.

Sources at difference locations may interfere with one another in complicated ways. The assumed superposition of source wavelets implies, however, that the waves $\tilde{P}_b^+$ and $\tilde{P}_a^-$ measured at the boundaries can be written as an integral over the source region. The relative amplitude $\tilde{\alpha} \equiv \tilde{P}_a^-/\tilde{P}_b^+$ of the waves generated by the distribution of sources is then summarized by the simple formula

$$\tilde{\alpha} = \int_a^b \sigma(\chi)\tilde{t}^-(a,\chi)d\chi \Big/ \int_a^b \sigma(\chi)\tilde{t}^+(\chi,b)d\chi \,, \tag{46}$$

where $\tilde{t}^{\pm}(x,y) \equiv \tilde{t}^{\pm}_{xy} = t^{\pm}_{xy}$ and the complex source density function $\sigma(\chi)$ represents the source strength per unit length $d\chi$. The transmission coefficients $\tilde{t}^-(a,\chi)$ and $\tilde{t}^+(\chi,b)$ simply propagate wavelets from their site of generation to the appropriate boundary.

In this simple model, the source density function σ can be expected to depend, for example, on the amplitude of the primaries, particularly that of f_2. As f_2 increases in amplitude, the region of overlap between the two primaries increases and σ broadens. Consider, however, the limiting case of a single ideal point source located at p:

$$\sigma(\chi) = \sigma_0\delta(\chi - p) \,, \tag{47}$$

where δ is the Dirac δ-function. Then,

$$\tilde{\alpha} = t^-_{ap}/t^+_{pb} \,. \tag{48}$$

2. A transformer middle ear

To simplify the calculation of middle-ear transmission, let the residual ear-canal space be negligible (so that ${}^{ec}\mathbf{S}_0 = {}^{e}\mathbf{S}_0$—see note 3) and imagine that the middle ear acts

like a mechanical transformer, albeit with a possibly complex and frequency-dependent transformer ratio $N_{\rm me}$ (e.g., Allen and Fahey 1992). The action of the middle ear is that of a transformer if its transfer matrix has the form (e.g., Shera and Zweig 1992a)

$$ {}^{\rm e}\mathbf{T}_0 \approx \begin{pmatrix} 1/N_{\rm me} & 0 \\ 0 & N_{\rm me} \end{pmatrix} . \tag{49} $$

The interconversion formulae in Appendix A imply that the elements of ${}^{\rm e}\mathbf{S}_0$ then satisfy the equations

$$ r^- = -r^+ , \tag{50} $$

and

$$ \det {}^{\rm e}\mathbf{S}_0 = -1 . \tag{51} $$

3. The pressure ratio

If evoked emissions are ignored (so that $R_b^{\triangleright} = 0$), Eq. (45) for ρ then reduces to

$$ \rho = \frac{\gamma_p^2 (1 + r^-)(1 + R_{\rm s})}{1 + R_{\rm s} r^- + \gamma_p^2 (r^- + R_{\rm s})} , \tag{52} $$

where

$$ \gamma_p^2 \equiv t_{0p}^- t_{0p}^+ . \tag{53} $$

Equation (23) implies that

$$ \gamma_p^2 \approx \exp\left(-2i \int_0^p d\chi/\lambda \right) . \tag{54} $$

a) Limiting special cases

Two special cases are of interest. If the transducer source impedance $Z_{\rm s}$ is perfectly matched to the characteristic impedance of the ear canal, then $R_{\rm s} = 0$, and

$$ \rho = \frac{\gamma_p^2 (1 + r^-)}{1 + \gamma_p^2 r^-} \qquad (R_{\rm s} = 0) . \tag{55} $$

An equation equivalent to Eq. (55) has been obtained independently by Allen and Fahey (1992), who use it to estimate the gain of the "cochlear amplifier" (i.e., $|\gamma_p|$). Note that when the gain is large (i.e., $|\gamma_p|^2 \gg 1$), the ratio ρ, in this example, depends only on the basal reflection coefficient r^-:

$$ \lim_{|\gamma_p| \to \infty} \rho = (1 + r^-)/r^- . \tag{56} $$

If the source impedance Z_s is infinite, then $R_s = 1$, and

$$\rho = \frac{2\gamma_p^2}{1+\gamma_p^2} \qquad (R_s = 1)\ . \tag{57}$$

In this case, ρ is, remarkably, independent of the middle ear, with

$$\lim_{|\gamma_p|\to\infty} \rho = 2\ . \tag{58}$$

D. An illustrated example

This section illustrates the considerable, and often underappreciated, effects that can arise due to cochlear reflection and interference phenomena by computing the ratio ρ using a more realistic model of the middle ear. The generation of distortion products is modeled by a single, ideal point source located at $p \in [a,b]$, with ${}^a\tilde{\mathbf{S}}_b = {}^a\mathbf{S}_b$, neglecting the concomitant generation of stimulus-frequency emissions at the distortion-product frequency (i.e., $R_b^{\triangleright}$ is assumed zero). These simplifying assumptions are adopted purely for the purposes of illustration; the situation in the real cochlea (or any nonlinear model) will presumably be more complicated. Middle-ear scattering coefficients are computed using published models of the human middle ear. This simple *Gedankenexperiment* is first analyzed heuristically and then with the help of the cochlear scattering formalism outlined above.

Figure 2a plots $|\rho_1(f_{ct})|$ computed using the middle-ear models of Zwislocki (1962) and Kringlebotn (1988). [The subscript "1" denotes the value of R_s and indicates that the calculations assume that the Norton-equivalent source impedance Z_s of the transducer is infinite and hence that the ear-canal reflection coefficient is $+1$.] Shown for comparison in Fig. 2b are corresponding calculations for the cat (with cavities opened) computed using the feline middle-ear models of Carr and Zweig (1984) and Puria (1991). Parameter values and matrix characterizations for the networks ${}^{ec}\blacksquare_e$ and ${}^{0}\blacksquare_p$ are given in Appendix C. In each case, the frequency of the primary f_2 is fixed and f_1 varied as necessary to produce the distortion-product frequency indicated along the abscissa. [This paradigm, chosen for the simplicity of its analysis, differs from that of Fahey and Allen (1985), who held f_{ct} fixed and varied the primaries.] The figures indicate that $|\rho|$ has considerable structure, including the presence of "resonance peaks" due to interference effects within the cochlea (see below). Although details of the predictions such as the locations and widths of the peaks depend on characteristics of the middle and inner ears not known with certainty, the qualitative features of the curves are robust.

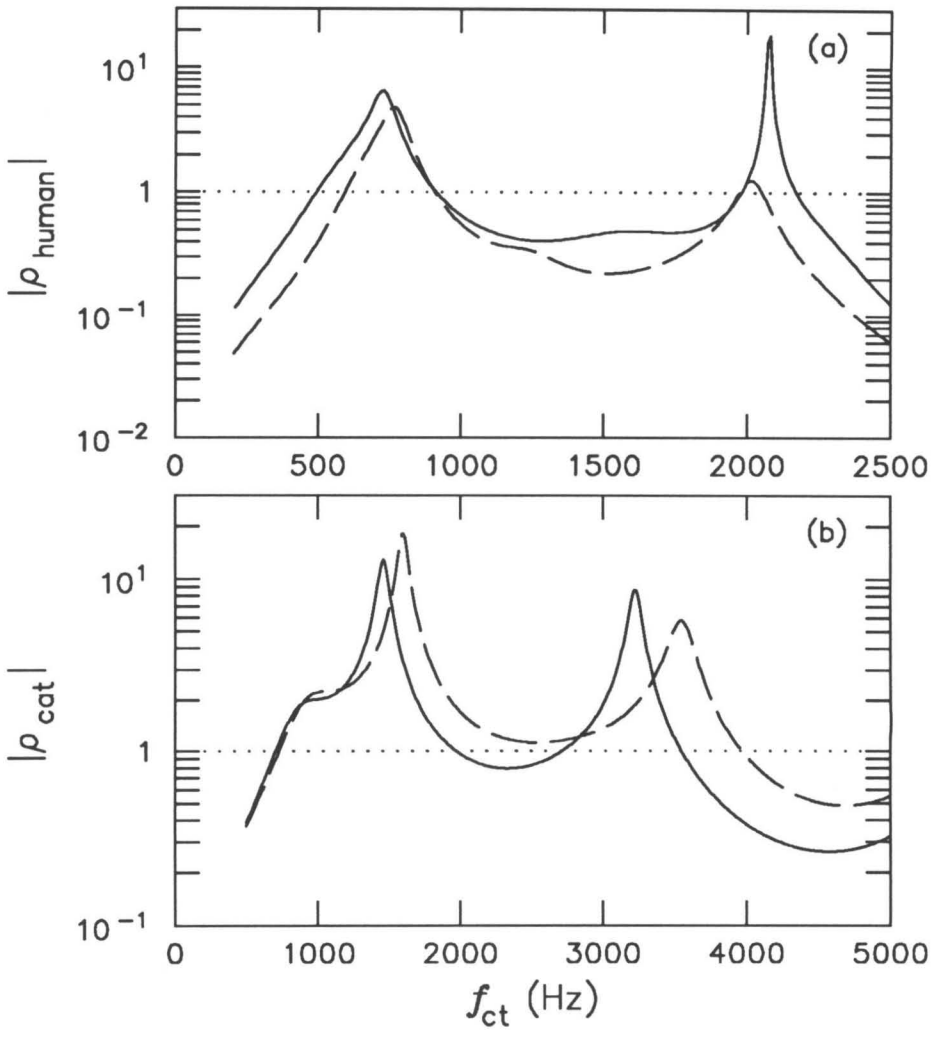

Figure 2. Amplitude of the pressure ratio $\rho_1(f_{ct})$ for the human (panel a) and feline (panel b) ears. In this idealized example, distortion products at the frequency f_{ct} are produced a single, ideal point source located at p. For the human, the predictions use the middle-ear models of Zwislocki (———) and Kringlebotn (— —); for the cat, they use the models of Carr and Zweig (———) and Puria (— —) in which the cavity impedances have been set to zero to simulate open-cavity recording conditions. Note that the scales along the axes differ in the two panels. The frequency f_2 was fixed at 10 kHz in the human and at 20 kHz in the cat. Other parameter values and matrix representations for $^{ec}\blacksquare_e$ and $^{0}\blacksquare_p$ are given in Appendix B. The calculations assume that the Norton-equivalent source impedance Z_s is *infinite*. Note that $|\rho|$ can become much greater than unity (·····) when wave cancellation occurs within the cochlea.

1. Interpretation as an interference phenomenon

Although one might naively expect $|\rho|$ always to be less than unity—the idea being that because all measurements are performed at the f_{ct} threshold, a supra-threshold pressure can never appear in the ear canal (Fahey and Allen 1985)—no such constraint is apparent in Eq. (45) for ρ. Indeed, Fig. 2 clearly indicates that $|\rho|$ can become quite large. To understand this (and the origin of the "resonance peaks"), note that the distortion-product source generates two waves: a wave that travels apically towards its characteristic place and another that travels basally towards the stapes, where it undergoes partial reflection (cf. Shera and Zweig 1991b). Large values of $|\rho|$ occur when the two forward-traveling waves (i.e., the forward-traveling wave originally produced by the source and that subsequently generated from the backward-traveling wave by reflection off the stapes) interfere with one another and nearly cancel at the site of detection. The total phase difference between the waves, which determines the extent to which cancellation occurs, depends both on propagation delays in traveling to and from the stapes and on the phase of the stapes reflection coefficient.

Figure 3 illustrates how phase shifts due to propagation and reflection sum to yield the total phase difference by plotting the ratio of the two forward-traveling waves at the f_2 place p:

$$\psi \equiv P_p^+\big|_{\text{reflected}} \,/\, P_p^+\big|_{\text{generated}} \,. \tag{59}$$

The $P^{\pm}$ denote the wave components and the subscripts $\pm$ indicate the direction of travel (the $+$ indicates that the wave is traveling towards the helicotrema). The qualifiers "generated" and "reflected" indicate, respectively, that the corresponding wave has either been generated directly by the distortion product source at p or created by reflection of the retrograde wave $P_p^-\big|_{\text{generated}}$ from the cochlear boundary with the middle ear. The ratio ψ, computed at p, is maintained as both waves propagate towards their common characteristic place.

An approximate expression for ψ can be obtained by noting that measurements of the cochlear input impedance in cat (Lynch et al. 1982) imply that the wavelength λ of the traveling wave (or, equivalently, the characteristic impedance of the transmission line) changes slowly in the basal turns of the cochlea (Shera and Zweig 1991a). Since

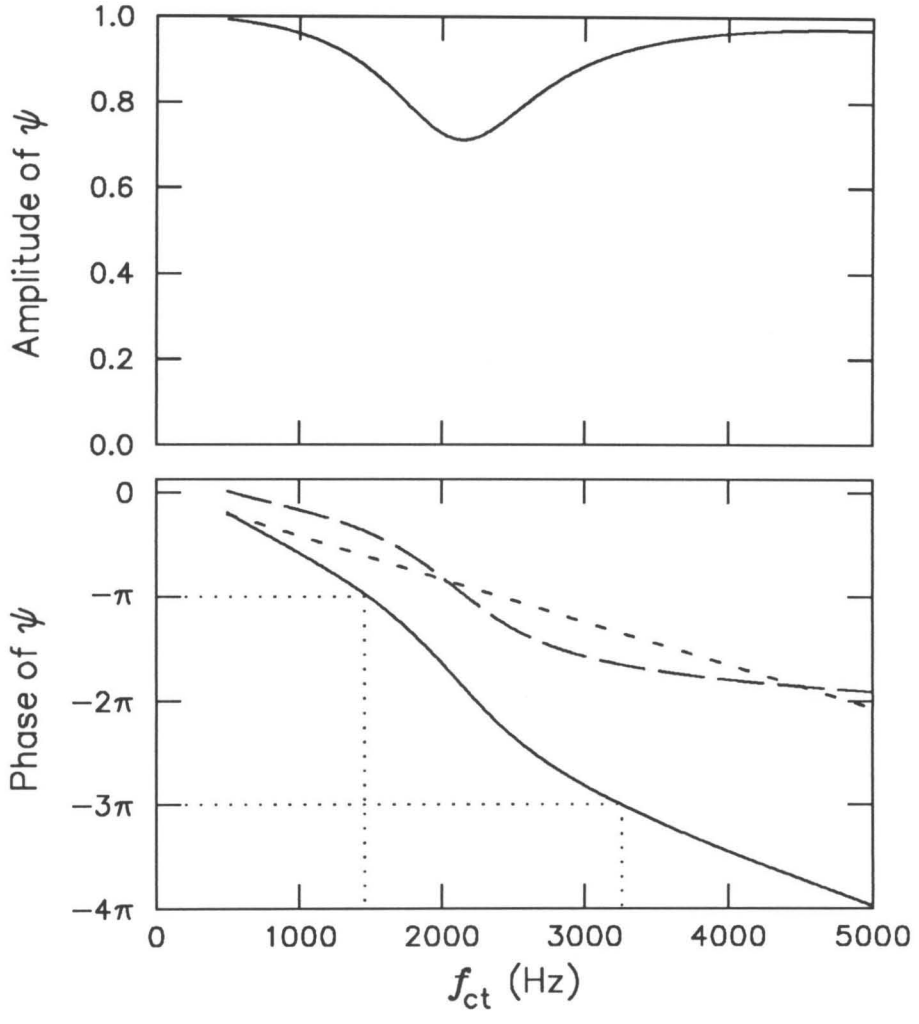

Figure 3. Amplitude and phase (———) of the ratio ψ of the two forward-traveling waves at the point p computed for the cat under simulated recording conditions using the middle-ear model of Carr and Zweig (1984). The phase $\angle\psi$ is the sum of two contributions [see Eq. (63)]: a phase shift $-8N(\beta_p - \beta_0)$ due to propagation delays (- - - -) and a shift $\angle\overleftarrow{R_0}$ due to reflection from the stapes (—— ——). The dotted lines (· · · · ·) indicate those frequencies at which the two waves are out of phase; that destructive interference produces a peak in the magnitude of the pressure ratio ρ (cf. Fig. 2).

$|\lambda'| \ll 1$,[8] the wave impedances $Z_\pm$ seen by the source $\tilde{U}_{ct}$ are approximately equal in the two directions (Shera and Zweig 1991b):

$$Z_- \approx Z_+ \,. \tag{60}$$

Hence, the backward- and forward-traveling waves produced by the source are nearly equal at p:

$$P_p^- \big|_{\text{generated}} \approx P_p^+ \big|_{\text{generated}} \,. \tag{61}$$

Consequently, ψ can be reexpressed as

$$\psi \approx R_p^{\triangleleft} \equiv P_p^+ \big|_{\text{reflected}} \,/\, P_p^- \big|_{\text{generated}} \,. \tag{62}$$

The ratio ψ of the two forward-traveling waves is thus approximately equal to the traveling-wave ratio $R_p^{\triangleleft}$, measured at p, when the cochlea is driven "in reverse." The magnitude of that traveling-wave ratio is determined principally by any impedance mismatch at the cochlear boundary with the middle ear. Were that boundary not present, but the cochlea instead extended infinitely in the negative-x direction, the traveling-wave ratio $R_p^{\triangleleft}$ would be zero (cf. Shera and Zweig 1991b).

The traveling-wave ratio $R_p^{\triangleleft}$ measured at p will differ from of its value $R_0^{\triangleleft}$ at $x = 0$ principally because of phase shifts introduced by traveling to and from the stapes. Those phase changes can be computed using the WKB approximation to solve for the wave components $P^\pm$. The resulting WKB waves—which constitute accurate approximate solutions to the transmission-line equations describing the basal turn of the cat cochlea at low frequencies (Shera and Zweig 1991a)—are defined in Shera and Zweig (1991b). That paper also computes the basal reflection coefficient $R_0^{\triangleleft}$ for the cat (with intact cavities), under both normal, physiological conditions and the simulated recording conditions used here.

Equation (62) therefore implies that ψ has the approximate value (see Appendix C)

$$\psi \approx R_0^{\triangleleft} e^{-8Ni(\beta_p - \beta_0)} \qquad (\beta_p \ll 1), \tag{63}$$

[8] The prime denotes differentiation with respect to the "spatial" variable χ, in terms of which the distance between two points is given by $-i$ times the total series impedance between them (Shera and Zweig 1991a).

where

$$\beta_p \equiv f_{ct}/f_2 \quad \text{and} \quad \beta_0 \equiv f_{ct}/f_{c_0} \,. \tag{64}$$

The frequency f_{c_0} represents the maximum frequency of hearing, and N represents the approximate number of wavelengths of the pressure wave in the cochlea in response to sinusoidal stimulation. Thus, ψ is simply the product of two factors: the basal reflection coefficient $R_0^{\triangleleft}$ and a phase shift $e^{-8Ni(\beta_p-\beta_0)}$ due to round-trip wave propagation through the basal turn. Peaks in $|\rho|$ occur at frequencies f_{peak} for which

$$\angle\psi(f_{\mathrm{peak}}) = -(2n+1)\pi \qquad (n = 0, 1, \ldots) \,; \tag{65}$$

that is, when the two waves are out of phase at the f_{ct} place.

The results and interpretation presented heuristically above can be obtained directly from the cochlear scattering formalism outlined in Sec. III-B. In the idealized case considered here (i.e., point source at p; superposition at f_{ct}; $R_p^{\triangleright} = 0$; and $R_s = +1$), Eq. (45) for ρ reduces to

$$\rho_1 = \frac{2\gamma_p^2 T^+ T^-}{\left(1 - R^+ R^+\right)\left(1 + R_p^{\triangleleft}\right)} \,. \tag{66}$$

Poles in ρ_1 occur at zeroes of the denominator. In our case $|R^+|^2 \ll 1$ (e.g., Puria and Allen 1991), and the second factor in the denominator dominates the behavior. Thus, ρ_1 has a pole whenever

$$R_p^{\triangleleft} = -1. \tag{67}$$

Since $\psi \approx R_p^{\triangleleft}$ [Eq. (62)], peaks in $|\rho_1|$ occur whenever

$$\angle R_p^{\triangleleft} \approx \angle\psi = -(2n+1)\pi \qquad (n = 0, 1, \ldots) \,, \tag{68}$$

in agreement with Eq. (65) derived above.

Note that $R_p^{\triangleleft}$ can be written

$$R_p^{\triangleleft} = \gamma_p^2 R_0^{\triangleleft} \,, \tag{69}$$

where

$$R_0^{\triangleleft} = \frac{R^- - R_s \det{}^{\mathrm{ec}}\mathbf{S}_0}{1 - R_s R^+} \,, \tag{70}$$

with, in this case, $R_s = +1$. Comparison with Eq. (63) for ψ shows the round-trip phase shift $e^{-8Ni(\beta_p - \beta_0)}$ is simply γ_p^2, the product of the one-way transmission coefficients t_{0p}^- and t_{0p}^+.

Note that at frequencies for which $|\rho| \gg 1$, the intracochlear source is producing a sound that is, by this measure, much louder outside the cochlea than it is within it. The interference effects seen here differ from those that may underly the microstructure observed in the threshold hearing curve (Elliot 1958; Thomas 1975; Kemp 1980; Zweig 1991). Recall that, for simplicity in the example, the scattering of traveling waves and their possible amplification at low levels by the "lasing" action of the cochlea (Zweig 1991) have here been ignored (i.e., $R_p^{\triangleright} = 0$). In the more realistic case—or an actual measurement—one expects an additional fine structure, cognate to the microstructure in the threshold hearing curve, superimposed on the features found here.

IV. Summary

This paper has shown how the phenomenological framework outlined in the companion paper (Shera and Zweig 1992a) can be employed in the analysis of noninvasive measurements of middle-ear and cochlear mechanics. For example, the framework has been used to demonstrate how cochlear nonlinearities can be exploited to measure middle-ear scattering coefficients. In addition, a noninvasive experiment has been devised that tests the assumption that the middle ear can be idealized as a simple mechanical transformer. A cochlear scattering framework has been developed for the analysis of combination-tone experiments in which acoustic distortion products are used to drive the middle ear "in reverse." The framework—applied to the analysis of a simple noninvasive *Gedankenexperiment*—was used to demonstrate that the ear can generate sounds that are considerably louder outside the cochlea than they are within it.

Acknowledgments

This work was supported by the Theoretical Division of Los Alamos National Laboratory and a National Science Foundation Graduate Fellowship to C. A. S.

Appendix A: Transfer and Scattering Matrices

This Appendix provides a succinct outline of basic properties of transfer and scattering matrices, including rules for their mutual interconversion. In addition, formulae for computing the overall transfer or scattering matrix characterizing a cascade of networks each individually so characterized are given.

A. Definitions and interconversion

Consider a two-port network ${}^1\blacksquare_2$ with ports labeled "1" and "2." Let V_i and I_i be, respectively, the Fourier transforms of the total "voltage" and the total "current" (positive flowing to the right) at the two ports. The transfer matrix, ${}^1\mathbf{T}_2 \equiv \left(\begin{smallmatrix} A & B \\ C & D \end{smallmatrix}\right)$, for the system is defined by

$$\begin{pmatrix} V_1 \\ I_1 \end{pmatrix} \equiv {}^1\mathbf{T}_2 \begin{pmatrix} V_2 \\ I_2 \end{pmatrix} . \tag{A1}$$

Define right- and leftward traveling waves (denoted V^+ and V^-, respectively) by the equations[9]

$$V_i^{\pm} \equiv \tfrac{1}{2}(V_i \pm Z_i I_i) , \tag{A2}$$

where Z_1 and Z_2 are the wave (or characteristic) impedances at the two ports (assumed to be independent of the direction of wave propagation). The corresponding scattering matrix,

$${}^1\mathbf{S}_2 \equiv \begin{pmatrix} R^+ & T^- \\ T^+ & R^- \end{pmatrix} , \tag{A3}$$

is then defined by the equation

$$\begin{pmatrix} V_1^- \\ V_2^+ \end{pmatrix} \equiv {}^1\mathbf{S}_2 \begin{pmatrix} V_1^+ \\ V_2^- \end{pmatrix} . \tag{A4}$$

Simple algebraic manipulation allows the matrix elements of ${}^1\mathbf{S}_2$ to be found from the elements of ${}^1\mathbf{T}_2$, and vice versa. In terms of the elements of ${}^1\mathbf{T}_2$,

$${}^1\mathbf{S}_2 = Y_{12} \begin{pmatrix} B - DZ_1 + AZ_2 - CZ_1Z_2 & 2Z_1 \det {}^1\mathbf{T}_2 \\ 2Z_2 & B + DZ_1 - AZ_2 - CZ_1Z_2 \end{pmatrix} , \tag{A5}$$

---

[9] Note that these definitions differ from those conventional in the circuit theory of scattering matrices, in which the impedances Z_i are assumed to be positive real and the forward and reverse waves (conventionally denoted a_i and b_i) defined so that their product has the dimensions of a power (e.g., Kuo 1962). In the latter respect, the waves defined here are similar to the conventions of the theory of wave digital filters (e.g., Fettweis 1986; Strube 1986; Friedman 1990).

where

$$1/Y_{12} \equiv B + DZ_1 + AZ_2 + CZ_1Z_2 \ . \tag{A6}$$

And in terms of the elements of ${}^1\mathbf{S}_2$, the elements of ${}^1\mathbf{T}_2$ are found to be:

$$A = \left(1 + R^+ - R^- - \det {}^1\mathbf{S}_2\right)/2T^+ \ ; \tag{A7}$$

$$B = \left(1 + R^+ + R^- + \det {}^1\mathbf{S}_2\right)Z_2/2T^+ \ ; \tag{A8}$$

$$C = \left(1 - R^+ - R^- + \det {}^1\mathbf{S}_2\right)/2Z_1T^+ \ ; \tag{A9}$$

and

$$D = \left(1 - R^+ + R^- - \det {}^1\mathbf{S}_2\right)Z_2/2Z_1T^+ \ . \tag{A10}$$

If the network ${}^1\blacksquare_2$ is reciprocal,

$$\det {}^1\mathbf{T}_2 = +1 \quad \text{and} \quad Z_1T^+ = Z_2T^- \ . \tag{A11}$$

B. Cascades

Consider a cascade ($\otimes$) of two networks:

$${}^1\blacksquare_3 = {}^1\blacksquare_2 \otimes {}^2\blacksquare_3 \ . \tag{A12}$$

The transfer matrix ${}^1\mathbf{T}_3$ for the cascade is simply the product of the corresponding matrices:

$${}^1\mathbf{T}_3 = {}^1\mathbf{T}_2 {}^2\mathbf{T}_3 \ . \tag{A13}$$

The rules for cascading scattering matrices are more elaborate. Let the two scattering matrices have elements

$${}^1\mathbf{S}_2 \equiv \begin{pmatrix} r^+ & t^- \\ t^+ & r^- \end{pmatrix} \quad \text{and} \quad {}^2\mathbf{S}_3 \equiv \begin{pmatrix} R^+ & T^- \\ T^+ & R^- \end{pmatrix} \ . \tag{A14}$$

Then,

$${}^1\mathbf{S}_3 = \frac{1}{1 - r^-R^+} \begin{pmatrix} r^+ - R^+ \det {}^1\mathbf{S}_2 & t^-T^- \\ t^+T^+ & R^- - r^- \det {}^2\mathbf{S}_3 \end{pmatrix} \ . \tag{A15}$$

Although Eq. (A15) can be tediously proved by algebra, a more physically illuminating derivation goes as follows. Let a rightward-traveling wave of unit amplitude be incident from the left on ${}^1\blacksquare_3$. The matrix element $({}^1\mathbf{S}_3)_{11}$ is then simply equal to the amplitude

of the net reflected wave, which is easily obtained by superposition; that is, by summing that fraction r^+ of the incident wave initially reflected by ${}^1\blacksquare_2$ with the series of wavelets that "rattle around," (i.e., are reflected back and forth between the two systems ${}^1\blacksquare_2$ and ${}^2\blacksquare_3$ all possible number of times) before "escaping" and contributing to the sum:

$$\begin{aligned}
({}^1\mathbf{S}_3)_{11} &= r^+ + t^+R^+t^- + t^+R^+r^-R^+t^- + t^+R^+r^-R^+r^-R^+t^- + \cdots \\
&= r^+ + t^+R^+t^- \sum_{n=0}^{\infty} (r^-R^+)^n \\
&= r^+ + \frac{t^+R^+t^-}{1 - r^-R^+} \qquad (|r^-R^+| < 1) \\
&= \frac{r^+ - R^+ \det {}^1\mathbf{S}_2}{1 - r^-R^+} .
\end{aligned} \tag{A16}$$

Analogous arguments yields expressions for the other matrix elements.

The net reflection coefficient for a two-port terminated with a one-port (e.g., an impedance) follows trivially from Eq. (A16). Let ${}^1\blacksquare_2$ be terminated at port 2 in a one-port characterized by the reflection coefficient R. The reflection coefficient r measured at port 1 is then

$$r = \frac{r^+ - R \det {}^1\mathbf{S}_2}{1 - Rr^-} . \tag{A17}$$

When the termination is attached to port 1 and r measured at port 2, symmetry implies that

$$r = \frac{r^- - R \det {}^1\mathbf{S}_2}{1 - Rr^+} . \tag{A18}$$

Appendix B: An Iteration Algorithm

This Appendix illustrates the use of the equations derived in Sec. II by providing an example algorithm for obtaining a self-consistent solution for the pressure ratio P_b/P_{ec} by iteration. For simplicity, we assume that forward-traveling waves passing the apical boundary of the source region are not subsequently reflected (i.e., that $R_b^{\triangleright} = 0$). The steps in the algorithm are as follows.

1. Fix the values of the primaries, $\mathcal{P}_1$ and $\mathcal{P}_2$, at the stapes.
2. Assume, initially, that the cochlear response at the frequency f_{ct} is zero (i.e., that $P_a^{\pm} = 0$ and $P_b^{\pm} = 0$).
3. Determine the source characteristics (that is, find the waves $\tilde{P}_b^{-}[\mathcal{P}_1, \mathcal{P}_2, P_a^{\pm}, P_b^{\pm}]$ and $\tilde{P}_a^{+}[\mathcal{P}_1, \mathcal{P}_2, P_a^{\pm}, P_b^{\pm}]$, and the matrix ${}^{a}\tilde{\mathbf{S}}_b[\mathcal{P}_1, \mathcal{P}_2, P_a^{\pm}, P_b^{\pm}]$) using the equations defining the cochlear model and the current values of $P_a^{\pm}$ and $P_b^{\pm}$.
4. Assume superposition and compute the distortion-product pressures $P_a^{\pm}$ and $P_b^{\pm}$ using the following equations:

$$P_b^{+} = \tilde{P}_b^{+} + \tilde{P}_a^{-} R_a^{\triangleleft} \tilde{t}_{ab}^{+} \qquad \text{[from Eq. (36)]};$$

$$P_b^{-} = 0 \qquad \text{[from Eq. (30)]};$$

$$P_a^{-} = \tilde{P}_a^{-} \qquad \text{[from Eq. (37)]};$$

and

$$P_a^{+} = \tilde{P}_a^{-} R_a^{\triangleleft} \qquad \text{[inferred from Eq. (36)]}.$$

Recall that $R_b^{\triangleright}$ and $\tilde{r}_{ab}^{\pm}$ have all been assumed zero.

5. Repeat steps #3 and #4 until satisfactory convergence for P_a and P_b is obtained.
6. Compute P_b/P_{ec} using Eq. (43).

Appendix C: Representations of the Ear Canal and Cochlea

This Appendix presents simple scattering-matrix descriptions of the two-ports ${}^{ec}\blacksquare_e$ and ${}^{0}\blacksquare_p$ representing, respectively, the residual ear-canal space and the basal portion of the cochlea. The corresponding transfer matrices can be found using the interconversion formulae summarized in Appendix A.

A. The ear canal

The residual ear-canal space between the transducers and the eardrum is modeled as a rigid-walled cylindrical tube of constant cross-section. At frequencies low enough that the pressure is uniform in any cross-section, the scattering matrix ${}^{ec}\mathbf{S}_e$ then has the approximate form (e.g., Pierce 1981)

$$ {}^{ec}\mathbf{S}_e \approx \begin{pmatrix} 0 & e^{-ikL} \\ e^{-ikL} & 0 \end{pmatrix} , \tag{C1} $$

where the wavenumber $k = \omega/c$, and L is the length of the tube. The characteristic acoustic impedance of the tube is given by

$$ Z_0 = \rho_0 c/S , \tag{C2} $$

where ρ_0 is the density of air, c the speed of sound, and S the cross-sectional area of the tube. At 34° C the constants have the approximate values: $\rho_0 \approx 1.15 \times 10^{-3}\mathrm{g/cm}^3$; $c \approx 3.52 \times 10^4\mathrm{cm/s}$. The parameter values used in the calculations are $L = 1.5$ cm and $S = 0.4$ cm^2 for the human; and $L = 1.5$ cm and $S = 0.2$ cm^2 for the cat. The parameter values for the cat are the same as those used to compute the stapes reflection coefficient under simulated recording conditions (Shera and Zweig 1991b).

B. The cochlea

The basal portion of the cochlea (i.e., between the stapes and the distortion-product source) is modeled as a linear, one-dimensional, hydromechanical transmission line of the type used in an earlier paper to discuss the reflection of retrograde waves (Shera and Zweig 1991b). The model is assumed scaling-symmetric, in accord with measurements of the cochlear input impedance (Shera and Zweig 1991a). For the purposes of the examples, the wavelength (or characteristic impedance) λ was taken to have the form

$$ \lambda = \lambda_0 \sqrt{1 - \beta^2 + i\delta\beta} , \tag{C3} $$

where $\beta = f/f_c$ and $f_c(x)$ is the cochlear frequency-position map. The real constant λ_0 was set equal to the value R_c of the cochlear input impedance (resistance) adopted by the middle-ear model used for the calculation. [For the feline middle-ear model of Puria (1991), the resistance measured by Lynch et al. (1982) was used.] Note that when the distance χ between two points along the cochlear transmission line is defined to be $-i$ times the total series impedance between them, then λ is simply $1/2\pi$ times the wavelength of the traveling pressure wave.

Solving the transmission-line equations using the WKB approximation yields an expression for the wave components $P^{\pm}$ (Zweig et al. 1976):

$$P^{\pm} \approx \sqrt{\lambda} e^{\mp i \int_0^x d\chi/\lambda} . \tag{C4}$$

The scattering matrix ${}^0\mathbf{S}_p$ follows immediately:

$${}^0\mathbf{S}_p \approx \begin{pmatrix} 0 & \sqrt{\lambda_0/\lambda_p}\, e^{-i\phi} \\ \sqrt{\lambda_p/\lambda_0}\, e^{-i\phi} & 0 \end{pmatrix} , \tag{C5}$$

where

$$\phi \equiv \int_0^p d\chi/\lambda . \tag{C6}$$

Since the integrals cover only the basal, small-β region of the cochlea, λ is essentially real, and (Zweig et al. 1976)

$$\int_0^p d\chi/\lambda \approx 4N(\beta_p - \beta_0) \qquad (\beta_p \ll 1). \tag{C7}$$

Here, the variables $\beta_0 = f_{ct}/f_{c_0}$ and $\beta_p = f_{ct}/f_2$, assuming that $f_c(p) = f_2$. For the human, $f_{c_0} \approx 20$ kHz; for the cat, $f_{c_0} \approx 57$ kHz (Liberman 1982). The constant N represents the approximate number of wavelengths of the traveling wave in the cochlea in response to sinusoidal stimulation. The value $N = 5$ was assumed in all calculations.

For simplicity, the calculations shown in Figs. 2 and 3 assume that the Norton-equivalent source impedance Z_s is infinite. The input impedance of the apical portion of the cochlea seen from p is approximated as

$$Z_{ac} \approx \lambda_p . \tag{C8}$$

Note that Z_{ac} is a smooth function of frequency and does not include oscillations arising from the interference of wavelets reflected from mechanical inhomogeneities expected in the more realistic case.

References

Allen, J. B. and Fahey, P. F. (1992). "Using acoustic distortion products to measure the cochlear amplifier gain on the basilar membrane," accepted for publication in *J. Acoust. Soc. Am.*

Carlin, H. J. (1956). "The scattering matrix in network theory," *Trans. IRE* **CT-3,** No. 2, 88–96.

Carr, J. N. and Zweig, G. (1984). "A mechanical model of the middle ear of anesthetized cats," unpublished report.

Elliot, E. (1958). "A ripple effect in the audiogram," *Nature* **181**, 1076.

Fahey, P. F. and Allen, J. B. (1985). "Nonlinear phenomena as observed in the ear canal and at the auditory nerve," *J. Acoust. Soc. Am.* **77**, 599–612.

Fettweis, A. (1986). "Wave digital filters: Theory and practice," *Proc. IEEE* **74**(2), 270–327.

Friedman, D. H. (1990). "Implementation of a nonlinear wave-digital-filter cochlear model," in *Mechanics and Biophysics of Hearing*, edited by P. Dallos, C. D. Geisler, J. W. Matthews, M. A. Ruggero, and C. R. Steele, 372–379. New York: Springer–Verlag.

Furst, M., Rabinowitz, W. M., and Zurek, P. M. (1988). "Ear canal acoustic distortion at $2f_1 - f_2$ from human ears: Relation to other emissions and perceived combinations tones," *J. Acoust. Soc. Am.* **84**, 215–221.

Kemp, D. T. (1980). "Towards a model for the origin of cochlear echoes," *Hearing Res.* **2**, 533–548.

Kringlebotn, M. (1988). "Network model for the human middle ear," *Scand. Audiol.* **17**, 75–85.

Kuo, F. F. (1962). *Network Analysis and Synthesis.*New York: John Wiley & Sons.

Liberman, M. C. (1982). "The cochlear frequency map for the cat: Labeling auditory-nerve fibers of known characteristic frequency," *J. Acoust. Soc. Am.* **72**, 1441–1449.

Lynch, T. J., Nedzelnitsky, V., and Peake, W. T. (1982). "Input impedance of the cochlea in cat," *J. Acoust. Soc. Am.* **72**, 108–130.

Peterson, L. C. and Bogert, B. P. (1950). "A dynamical theory of the cochlea," *J. Acoust. Soc. Am.* **22**, 369–381.

Pierce, A. D. (1981). *Acoustics: An Introduction to its Physical Principles and Applications.*New York: McGraw-Hill.

Puria, S. and Allen, J. B. (1991). "Modelling the surgically-modified middle ear," in preparation.

Puria, S. (1991). "A theory of cochlear input impedance and middle-ear parameter estimation," Ph.D. thesis, City University of New York.

Shera, C. A. and Zweig, G. (1991a). "A symmetry suppresses the cochlear catastrophe," *J. Acoust. Soc. Am.* **89**, 1276–1289.

Shera, C. A. and Zweig, G. (1991b). "Reflection of retrograde waves within the cochlea and at the stapes," *J. Acoust. Soc. Am.* **89**, 1290–1305.

Shera, C. A. and Zweig, G. (1991c). "Phenomenological characterization of eardrum transduction," *J. Acoust. Soc. Am.* **90**, 253–262.

Shera, C. A. and Zweig, G. (1992a). "Middle-ear phenomenology: The view from the three windows," submitted to *J. Acoust. Soc. Am.*

Shera, C. A. and Zweig, G. (1992b). "Analyzing reverse middle-ear transmission: Noninvasive *Gedankenexperiments*," submitted to *J. Acoust. Soc. Am.*

Shera, C. A. and Zweig, G. (1992c). "An empirical bound on the compressibility of the cochlea," submitted to *J. Acoust. Soc. Am.*

Shera, C. A. and Zweig, G. (1992d). "Noninvasive estimation of middle-ear transfer characteristics in human cadavers," in preparation.

Shera, C. A. and Zweig, G. (1992e). "Noninvasive measurement of the cochlear traveling-wave ratio," submitted to *J. Acoust. Soc. Am.*

Shera, C. A. and Zweig, G. (1992f). "Spectral periodicity without spatial corrugation: On the origin of evoked otoacoustic emission," in preparation.

Strube, H. W. (1985). "A computationally efficient basilar-membrane model," *Acustica* **58**, 207–214.

Thomas, I. B. (1975). "Microstructure of the pure-tone threshold," *J. Acoust. Soc. Am.* **57** Suppl. 1, S26–S27.

Zweig, G., Lipes, R., and Pierce, J. R. (1976). "The cochlear compromise," *J. Acoust. Soc. Am.* **59**, 975–982.

Zweig, G. (1991). "Finding the impedance of the organ of Corti," *J. Acoust. Soc. Am.* **89**, 1229–1254.

Zwicker, E. and Schloth, E. (1984). "Interrelation of different oto-acoustic emissions," *J. Acoust. Soc. Am.* **75**, 1148–1154.

Zwislocki, J. (1962). "Analysis of the middle-ear function. Part I: Input impedance," *J. Acoust. Soc. Am.* **34**, 1514–1523.

An Empirical Bound on the Compressibility of the Cochlea

Christopher A. Shera and George Zweig

Theoretical Division
Los Alamos National Laboratory
Los Alamos, New Mexico 87545

and

Physics Department
California Institute of Technology
Pasadena, California 91125

ABSTRACT

Effects of a possible inner-ear compressibility on middle-ear transfer functions are explored and a small upper bound on the magnitude of that compressibility established. Consequently, the traditional two-port representation of middle-ear mechanics remains valid to within a few percent. If the compressibility of the cochlea is small but finite, a simple phenomenological model of that compressibility correctly predicts hearing thresholds in the "middleless" ear at low frequencies. Experiments to establish the value of cochlear compressibility and to explore further its possible contributions to residual hearing in patients with missing or disarticulated middle-ear ossicles are suggested.

Contents

Introduction

The representation of middle-ear mechanics simplifies considerably if the cochlear contents are incompressible at auditory frequencies. In that limit the volume displacements of the cochlear windows are equal and opposite, and the phenomenological framework outlined in the companion paper (Shera and Zweig 1992a) implies that the middle ear can then be represented as a two-port network and characterized with standard transfer or scattering matrices. Although such a representation is almost universally assumed, its validity has never been experimentally established.

For example, direct measurements of cochlear compressibility made by comparing the volume velocities of the oval and round windows are few and have been largely inconclusive.[1] Nedzelnitsky (1974ab) conservatively concludes, based on the measurements of Moxon (1971), that the ratio of oval- to round-window volume displacements is -1, but only to within an uncertainty perhaps as large as ± 10 dB in the amplitude.

Although the fluids in the cochlea should be effectively incompressible for all but the highest frequencies (e.g., Viergever 1980), the compressibility of the scala media is not known. For example, von Békésy (1936; 1960) has suggested that pressure applied to the cochlear windows may change the total fluid volume of the inner ear by inducing flow in blood vessels or through the cochlear and vestibular aqueducts. In addition, a nonzero cochlear compressibility might arise as the result of cochlear pathology or trauma, or during invasive surgery (e.g., through the introduction of transitory air bubbles into the scalae).

This paper presents a phenomenological characterization of cochlear compressibility—analogous to those presented earlier for the eardrum (Shera and Zweig 1991c) and the middle ear (Shera and Zweig 1992a)—and uses it to explore its effects on middle-ear and cochlear measurements. The results are applied to obtain an upper bound on the magnitude of cochlear compressibility considerably tighter than the limits provided by existing measurements. If that upper bound is realized, cochlear compressibility may provide an important mechanism for stimulating the ear in patients with missing or disarticulated middle ear bones.

[1] For a review of measurements on cochlear compressibility see Appendix VII of the doctoral thesis by Nedzelnitsky (1974a).

I. Characterization of Cochlear Compressibility

Consequences of cochlear compressibility for middle-ear and cochlear mechanics can be explored by regarding the inner ear as a two-port network and defining the matrix ${}^{\mathrm{ow}}\mathbf{T}_{\mathrm{rw}}$, which relates the pressures and volume velocities just inside the two windows (Fig. 1):

$$\begin{pmatrix} P_{\mathrm{ow}} \\ U_{\mathrm{ow}} \end{pmatrix} = {}^{\mathrm{ow}}\mathbf{T}_{\mathrm{rw}} \begin{pmatrix} P_{\mathrm{rw}} \\ U_{\mathrm{rw}} \end{pmatrix} . \tag{1}$$

[This paper adopts the notation of its companion (Shera and Zweig 1992a).] The matrix ${}^{\mathrm{ow}}\mathbf{T}_{\mathrm{rw}}$ exists when nonlinearities in cochlear mechanics have little effect on the response of the cochlea at its basal end near the boundary with the middle ear. At moderate intensities, nonlinearities in cochlear mechanics contribute significantly to the loading of the middle ear (Kemp 1979; Zwicker and Schloth 1984); characterization of the cochlear load by transfer matrices or impedances is not then appropriate. As seen from the basal end, cochlear mechanics is linear, however, at both low and at high sound intensities (Kemp and Chum 1980; Zwicker and Schloth 1984).

The transfer-matrix description of cochlear compressibility is represented in Fig. 1. The connections to ground illustrate that the volume velocity of the oval window is not necessarily equal and opposite to that of the round window. The sum of the "currents" flowing to or from those ground connections represents the sum U_+ of the volume velocities of the oval and round windows (both are defined positive *into* the inner ear).

A. The incompressible limit

All existing models of the middle ear assume that the inner ear is incompressible. Incompressibility requires that the volume velocity U_{ow} of the stapes footplate be canceled by the volume velocity U_{rw} of the round window:

$$\delta_{\mathrm{windows}} \equiv 2\left|\frac{U_{\mathrm{ow}} + U_{\mathrm{rw}}}{U_{\mathrm{ow}} - U_{\mathrm{rw}}}\right| = 2\left|\frac{U_+}{U_-}\right| \ll 1 . \tag{2}$$

The inner ear may then be represented by an equivalent lumped impedance $Z_{\mathrm{ie}}(\omega)$, defined by

$$Z_{\mathrm{ie}} \equiv \frac{P_{\mathrm{ow}} - P_{\mathrm{rw}}}{U_{\mathrm{ow}}} , \tag{3}$$

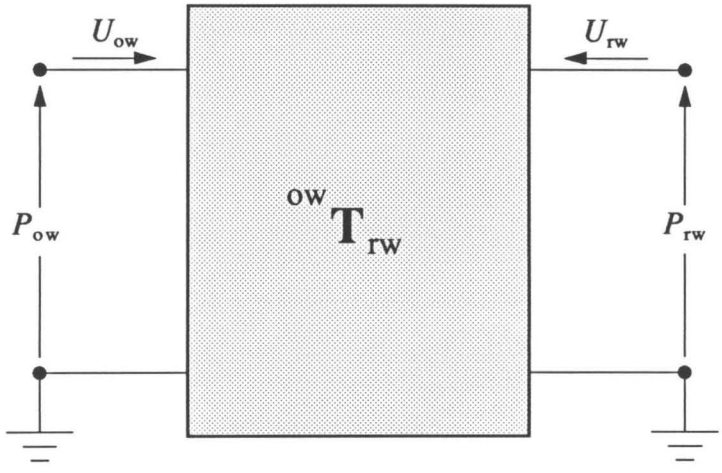

Figure 1. Schematic representation of the inner ear as a two-port network. The ground connections imply that the volume velocity of the oval window is not necessarily equal and opposite to that of the round window. (The sign convention is such that both U_{ow} and U_{rw} flow *into* the inner ear.)

and the matrix ${}^{\mathrm{ow}}\mathbf{T}_{\mathrm{rw}}$ assumes the form

$$ {}^{\mathrm{ow}}\mathbf{T}_{\mathrm{rw}} \approx \begin{pmatrix} 1 & -Z_{\mathrm{ie}} \\ 0 & -1 \end{pmatrix} . \tag{4} $$

In the incompressible limit the volume velocities of the oval and round windows are equal and opposite, no current flows to the ground connections of Fig. 1, and the four-terminal transfer-matrix description of the inner ear reduces to a two-terminal lumped impedance. In that limit the matrix element

$$ \left({}^{\mathrm{ow}}\mathbf{T}_{\mathrm{rw}}\right)_{21} \equiv \left.\frac{U_{\mathrm{ow}}}{P_{\mathrm{rw}}}\right|_{U_{\mathrm{rw}}=0} = 0 , \tag{5} $$

indicating that blocking the round window prevents motion of the stapes. ${}^{\mathrm{ow}}\mathbf{T}_{\mathrm{rw}}$ is antireciprocal (i.e., $\det {}^{\mathrm{ow}}\mathbf{T}_{\mathrm{rw}} = -1$) because of the sign convention for the volume velocity U_{rw}.

Note that for incompressibility to hold within the context of middle-ear mechanics, the volume velocities U_{ow} and U_{rw} must satisfy the less restrictive relation (Shera and Zweig 1992a),

$$ \delta_{\mathrm{eardrum}} \equiv \left| \frac{U_{\mathrm{ow}} + U_{\mathrm{rw}}}{U_{\mathrm{e}}} \right| \ll 1 . \tag{6} $$

When this equation is valid, the pressure P_{tc} in the tympanic cavity is driven only by the motion of the eardrum.

The companion paper (Shera and Zweig 1992a) shows that the representation of middle-ear mechanics simplifies in the incompressible limit, the more general three-port description reducing to the standard two-port.

II. Effects of a Finite Compressibility

Measurement of the matrix elements

$$ {}^{\mathrm{ow}}\mathbf{T}_{\mathrm{rw}} \equiv \begin{pmatrix} a & b \\ c & d \end{pmatrix} \tag{7} $$

would permit determination of the validity of the assumption of incompressibility, both for middle-ear and cochlear mechanics. For example, consider the idealized ossicular chain introduced in the companion paper (Shera and Zweig 1992a) and approximate the eardrum as a rigid piston. Then $\left({}^{\mathrm{e}}\widehat{\mathbf{T}}_{\mathrm{ow}}\right)_{21} = 0$, and the two middle-ear transformer ratios

$\widehat{N}_{\mathrm{U}}$ and $\widehat{N}_{\mathrm{P}}$ reduce to their traditional value N_{me}. Rewriting Eq. (6) in terms of the matrix elements then yields[2]

$$\delta_{\mathrm{eardrum}} = \frac{1}{2N_{\mathrm{me}}} \left| \frac{1 + d - c(Z_{\mathrm{rw}} + N_{\mathrm{me}} Z_{\mathrm{cav}})}{d - c(Z_{\mathrm{rw}} + Z_{\mathrm{cav}})} \right| \ll 1 \,. \tag{8}$$

In this simple example, a large value of N_{me} (e.g., a large area ratio between the eardrum and stapes footplate) helps guarantee that even a significant cochlear compressibility remains unimportant for middle-ear mechanics (provided, that is, that N_{me} is not so large that the term $cN_{\mathrm{me}}Z_{\mathrm{cav}}$ makes the dominant contribution to the numerator). The situation in the real middle ear, in which the transformer ratios $\widehat{N}_{\mathrm{U}}$ and $\widehat{N}_{\mathrm{P}}$ may vary significantly at higher frequencies, is, of course, more complicated.

For cochlear compressibility to be unimportant within the context of cochlear mechanics requires, however, the more restrictive condition Eq. (2):

$$\delta_{\mathrm{windows}} = 2 \left| \frac{1 + d - c\big(Z_{\mathrm{rw}} + N_{\mathrm{me}} Z_{\mathrm{cav}}\big)}{1 - d + c\big(Z_{\mathrm{rw}} + (2 - N_{\mathrm{me}}) Z_{\mathrm{cav}}\big)} \right| \ll 1 \,. \tag{9}$$

Not surprisingly, effects of cochlear compressibility are not here suppressed by large values of N_{me}.

Any finite cochlear compressibility can thus have significant effects, for example, on the interpretation of measurements of the inner-ear input impedance, defined by the right-hand side of Eq. (3). Calculation of the impedance yields the expression

$$\frac{P_{\mathrm{ow}} - P_{\mathrm{rw}}}{U_{\mathrm{ow}}} = \frac{b + (1 - a)(Z_{\mathrm{rw}} + Z_{\mathrm{cav}} + \widehat{Y} Z_{\mathrm{cav}} Z_{\mathrm{rw}}) + (1 + d)(1 - N_{\mathrm{me}}) Z_{\mathrm{cav}}}{d - c(Z_{\mathrm{rw}} + Z_{\mathrm{cav}}) + \widehat{Y} Z_{\mathrm{cav}} (1 + d - c Z_{\mathrm{rw}})} \,, \tag{10}$$

which reduces to the value $-b = Z_{\mathrm{ie}}$ in the incompressible limit. Note that the measured impedance depends not only on properties of the inner ear but also on those of the

---

[2] If no simplifying assumptions (other than that $\det {}^{\mathrm{ow}}\mathbf{T}_{\mathrm{rw}} = -1$) about the eardrum and ossicular chain are made, inequalities (8) and (9) become, respectively,

$$\delta_{\mathrm{eardrum}} = \frac{1}{2} \left| \frac{1 + d - c(Z_{\mathrm{rw}} + \widehat{N}_{\mathrm{U}} Z_{\mathrm{cav}}) + \widehat{Y} Z_{\mathrm{cav}} (2 - a + d - c Z_{\mathrm{rw}})}{\widehat{N}_{\mathrm{U}} \big[d + c(Z_{\mathrm{rw}} + Z_{\mathrm{cav}})\big] + \widehat{Y} \Big\{ b - a Z_{\mathrm{rw}} + Z_{\mathrm{cav}} \big[2 - a + d - c Z_{\mathrm{rw}}\big] \Big\}} \right| \ll 1 \,, \tag{2.1}$$

and

$$\delta_{\mathrm{windows}} = 2 \left| \frac{1 + d - c\big(Z_{\mathrm{rw}} + \widehat{N}_{\mathrm{U}} Z_{\mathrm{cav}}\big) + \widehat{Y} Z_{\mathrm{cav}} \big(2 - a + d - c Z_{\mathrm{rw}}\big)}{1 - d + c\big(Z_{\mathrm{rw}} + (2 - \widehat{N}_{\mathrm{U}}) Z_{\mathrm{cav}}\big) - \widehat{Y} Z_{\mathrm{cav}} \big(a + d - c Z_{\mathrm{rw}}\big)} \right| \ll 1 \,. \tag{2.2}$$

eardrum, ossicular chain, round window, and middle-ear cavities. Since the cochlear input impedance is typically measured with the cavities opened and exposed to the atmosphere (so that $Z_{\rm cav} \approx 0$), the measured impedance has the value

$$\frac{P_{\rm ow} - P_{\rm rw}}{U_{\rm ow}} = \frac{b + (1-a)Z_{\rm rw}}{d - cZ_{\rm rw}} \,. \tag{11}$$

To the extent that the cochlea is compressible—or may, accidentally, have been made compressible during the measurement, say by the introduction of air bubbles into the scalae—the measured impedance does not therefore necessarily reflect its value in an intact animal.

Should the cochlear contents prove to have a nonzero compressibility, placement of the cavities in circuit models of the middle ear affects not only the predicted cochlear pressures (Shera and Zweig 1992a) but also such quantities as the middle-ear input impedance and stapes transfer function, whose values are often assumed not to depend on cavity position: those quantities are independent of cavity placement only in the incompressible limit. The next section demonstrates that consistency with measurements of hearing thresholds in individuals without a middle ear requires that the compressibility of the normal human inner ear be small.

III. Hearing with a Middleless Ear

As noted by von Békésy (1936; 1960), a finite cochlear compressibility provides one mechanism for direct acoustic stimulation of the cochlea. That mechanism may be especially important in ears lacking the eardrum or having an interrupted or missing ossicular chain. Although individuals with such impairments can, in fact, hear—albeit with considerably elevated thresholds—cochlear mechanics in the incompressible limit predicts that no pressure difference across the organ of Corti (i.e., no traveling wave) can be produced at stimulus frequencies low enough that the cavity pressures driving the oval and round windows are equal in magnitude and phase. (Stimulation of the cochlea via bone conduction is not considered here.) By allowing compression of the cochlear contents, however, a nonzero compressibility would permit motion of the two windows. Indeed, calculation of the volume velocity U_- resulting from a pressure $P_{\rm e}$ at the eardrum yields

$$\frac{U_-}{P_{\rm e}} = \frac{1}{2}\frac{a + d + c\left(Z_{\rm ow} - Z_{\rm rw}\right)}{b + dZ_{\rm ow} - aZ_{\rm rw} - cZ_{\rm ow}Z_{\rm rw}} \tag{12}$$

in individuals missing their eardrum, malleus, and incus.[3] Here, Z_{ow} is the combined impedance of the stapes, annular ligament, and oval window; and, in the absence of the eardrum, $P_e = P_{tc}$. Thus, if the cochlea is compressible, traveling waves are generated even without an ossicular chain to break the symmetry between the windows.

A. An upper bound on the compressibility of the cochlea

Measurements of hearing thresholds in subjects without ossicular input to the inner ear (i.e., in the middle-earless) enable one—by assuming that near threshold any residual hearing results principally from traveling waves generated as a result of cochlear compressibility—to constrain a simple phenomenological model of cochlear compressibility and thereby obtain an approximate upper bound on the value of a dimensionless parameter whose difference from zero characterizes the compressibility of the cochlear contents. The limit is only an upper bound because other mechanisms that may make contributions to stimulating the cochlea—bone conduction or pressure differences between the cochlear windows (Peake et al. 1992), for example—are not included.

The Appendix outlines a simple "squeezable sandwich" model of the organ of Corti in which the scala media can change its volume in response to the sum of the pressures in the adjoining scalae. The degree of compressibility of the cochlear contents is characterized by the dimensionless parameter ϵ, defined in terms of the ratio of the translational stiffness of the organ of Corti and basilar membrane to the compressional stiffness of the scala media. The model predicts that for frequencies $\omega \ll \omega_{c0}$, where ω_{c0} is 2π times the maximum characteristic frequency represented along the organ of Corti, ϵ is a positive real constant. The Appendix shows that the matrix ${}^{ow}\mathbf{T}_{rw}$ then has the form

$$ {}^{ow}\mathbf{T}_{rw} = \frac{1}{1-\epsilon} \begin{pmatrix} 1+\epsilon & -Z_{ie} \\ 4\epsilon/Z_{ie} & -(1+\epsilon) \end{pmatrix} . \tag{13} $$

---

[3] The equations describing the middleless ear are

$$ \widehat{P}_e = 0 ; \tag{3.1} $$

$$ \widehat{P}_{ow} = -Z_{ow} U_{ow} ; \tag{3.2} $$

and

$$ \widehat{P}_{rw} = -Z_{rw} U_{rw} . \tag{3.3} $$

In obtaining Eq. (12), the matrix ${}^{ow}\mathbf{T}_{rw}$ was assumed antireciprocal. Substitution of the matrix elements from Eq. (4) verifies that the transfer function U_{-}/P_e in the impaired ear vanishes in the incompressible limit.

Note that the incompressible limit [Eq. (4)] is defined as the limit $\epsilon \to 0$. The "squeezable sandwich" model provides, of course, only one simple mechanism, among many, that yields a transfer matrix of approximately that form.

Substitution of the matrix elements into Eq. (12) yields

$$\frac{U_-}{P_e} = -\frac{2\epsilon(Z_{ow} - Z_{rw})}{Z_{ie}\left[Z_{ie} + (1+\epsilon)(Z_{ow} + Z_{rw})\right] + 4\epsilon Z_{ow} Z_{rw}} . \tag{14}$$

Note for later comparison that the transfer function in a normal ear has the value

$$\frac{U_-}{P_e} = \frac{1 + O(\epsilon)}{\widehat{Z} + \widehat{N}_U Z_{cav} + (1/\widehat{N}_P + \widehat{Y} Z_{cav})(Z_{ie} + Z_{rw})} . \tag{15}$$

Since the transfer function in a middleless ear depends on the difference between the impedances Z_{ow} and Z_{rw}, Eq. (14) predicts that blocking the oval window and preventing the stapes from moving (so that $|Z_{ow}|$ becomes effectively infinite) should actually improve hearing at low frequencies.[4] In that limit the transfer function becomes

$$\lim_{|Z_{ow}| \to \infty} \frac{U_-}{P_e} = -\frac{2\epsilon}{(1+\epsilon) Z_{ie} + 4\epsilon Z_{rw}} . \tag{16}$$

1. Comparison between theory and experiment

To make that prediction more explicit and obtain a bound on the value of ϵ, note that the ratio of transfer functions in normal and middleless ears provides a measure of the resulting hearing loss:[5]

$$\text{Hearing loss in dB} \approx -20 \log_{10} \left(\left| \frac{U_-}{P_e} \right|_{\text{middleless ear}} \Big/ \left| \frac{U_-}{P_e} \right|_{\text{normal}} \right) . \tag{17}$$

Figure 2 compares that ratio computed[6] from the middle-ear models of Zwislocki (1962) and Kringlebotn (1988) with the threshold measurements of von Békésy (1936; 1960). Since

---

[4] By noting that at low frequencies Z_{ow} and Z_{rw} are both expected to be negative imaginary (i.e., proportional to $1/i\omega$) and Z_{ie} positive real [or, if tapering symmetry is broken (Shera and Zweig 1991a), positive imaginary at the very lowest frequencies], one can show that

$$\lim_{\substack{\omega \to 0 \\ |Z_{ow}| \to \infty}} |T_-| > |T_-|_{\text{normal}} , \tag{4.1}$$

where T_- denotes the transfer function U_-/P_e in a middleless ear with normal stapes.

[5] Here we assume that the operative detection threshold (e.g., a constant basilar-membrane velocity at CF) is proportional to the volume velocity U_-. Because P_- and U_- are proportional in the model, identical results are obtained if the transfer functions P_-/P_e are used to predict the hearing loss.

[6] Details of the calculations can be found in footnotes 8 and 9 of the companion paper (Shera and Zweig 1992a).

the mobility of the stapes in von Békésy's subjects is not known (they may have suffered from otosclerosis or other fixation of the stapes), predictions are shown for both the normal and fixed-stapes conditions. The actual mobility of the stapes in these subjects presumably falls somewhere between. Note, however, that at low frequencies the differences between the two cases are small.

The overall agreement between theory and experiment is unexpected. The agreement at low frequencies depends, of course, on the approximate constancy of the parameter ϵ, as given by the simple model outlined in the Appendix. Since pressure differences outside the oval and round windows have been ignored, the relative contribution of any compressibility to the residual hearing should be largest at low frequencies, where those pressure differences are smallest (von Békésy 1960; Peake et al. 1992). The best upper bound on the value of ϵ can therefore be obtained by comparing with measurements at low frequencies: the value $\epsilon = 1/100$ was used in the calculations. Predictions for different values of ϵ can be obtained, for $\epsilon \ll 1$, simply by translating the theoretical curves along the ordinate. For example, decreasing ϵ by a factor of two shifts the curves upwards (in the direction of greater hearing loss) by 6 dB. The figure suggests that cochlear compressibility, as parametrized by ϵ, must be small and less than a few percent at low frequencies:

$$\epsilon < O(1/100) \qquad (\omega \ll \omega_{c_0}) \,. \tag{18}$$

If ϵ were any larger, the theory predicts that von Békésy's subjects would have had more sensitive hearing than the measurements indicate. That upper bound is significantly tighter than limits obtained by the more direct measurements of cochlear compressibility mentioned above (cf. Nedzelnitsky 1974a).

The bound on ϵ obtained above can be used to determine the importance of compressibility for normal middle-ear and cochlear mechanics [cf. inequalities (6) and (2)]. Figure 3 plots δ_{eardrum} and δ_{windows} evaluated using the middle-ear models of Zwislocki (1962) and Kringlebotn (1988). As expected [cf. inequalities (8) and (9)],

$$\delta_{\text{windows}} = O(\epsilon) \qquad \text{and} \qquad \delta_{\text{eardrum}} = O(\epsilon/|\widehat{N}_{\text{U}}|) \ll \delta_{\text{windows}} \,. \tag{19}$$

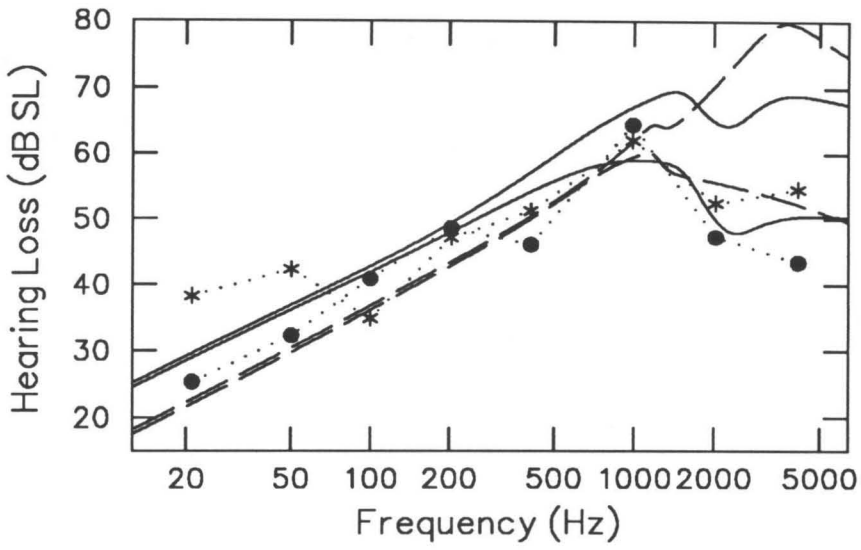

Figure 2. Predicted hearing loss for impaired middle ears (i.e., ears lacking the eardrum, malleus, or incus) computed by incorporating a simple phenomenological model of cochlear compressibility (with $\epsilon = 0.01$) into the middle-ear models of Zwislocki (———) and Kringlebotn (— — —). Predictions are shown for both a normal and a fixed stapes; the theory predicts that fixation of the stapes should actually improve hearing in these subjects (the curve corresponding to the immobilized stapes is in each case the lower of the two curves for a particular model). Shown for comparison are measurements of the hearing loss in impaired subjects ($\bullet$ and $*$) obtained from threshold measurements by von Békésy (1960; Fig. 5-10). The two curves correspond to different determinations of the normal threshold: ($\bullet$) average audiogram from measurements in five subjects with unilateral impairment relative to the mean audiogram for the other, normal ear; ($*$) average audiogram for the same impaired ears relative to normal audiograms obtained in another study. The calculations provide an approximate upper limit on the value of the dimensionless parameter ϵ; that is, $\epsilon < O(1/100)$ at low frequencies, indicating that *cochlear compressibility* must be small.

Consequently, the effects of any compressibility on cochlear or middle-ear mechanics are expected to be small in the normal ear.[7] The traditional two-port representation of middle-ear mechanics thus appears valid to within a few percent.

Remarkably, the measurements in Fig. 2 follow the theoretical curves predicted for a compressible cochlea in the fixed-stapes limit. The subjects thus behave in their threshold responses as if their cochleae had a small, frequency-independent compressibility ϵ and suffered from at least partial fixation of the stapes. Given the existence of other mechanisms (e.g., bone conduction or pressure differences between the windows) that may contribute to the residual hearing—especially above $\sim$ 1 kHz, both because of potentially larger stimulus phase differences between the windows and the increasing intensities needed to reach threshold at high frequencies—the agreement at high frequencies is difficult to interpret. The agreement at lower frequencies, however, is more conclusive. Although Peake et al. (1991) argue that pressure differences alone can explain all residual hearing above 500 Hz, they note that those differences cannot account for the measured decrease in relative hearing loss at lower frequencies. That improved sensitivity is predicted, however, by the phenomenological model of inner-ear compressibility presented here, suggesting that hearing in middleless ears can be explained, at least at low frequencies, by a small but finite compressibility of the cochlear contents.

Equation (14) can be used to make other predictions to test whether the residual hearing actually originates in a slight compressibility of the cochlear contents. For example, the prediction that immobilizing the stapes may actually improve hearing in these subjects, especially at higher frequencies, can be tested in cats or other animals where measurements of auditory-nerve fiber thresholds could replace psychophysical determination of the hearing threshold. To minimize pressure differences between the oval and round windows, which can drive the cochlea and complicate the interpretation, the experiments should ideally be performed in animals in which the two windows face onto the same cavity or in preparations in which the cavities have been opened widely. Similarly, residual hearing due to compressibility can be expected to decrease if the impedances of the oval

[7] The conclusion, quantified by inequality (9), that the effects of compressibility in cochlear mechanics are small applies only at frequencies much less than the local characteristic frequency. The possible contributions of compressibility to the "micromechanics" of the organ of Corti at frequencies near CF are not known.

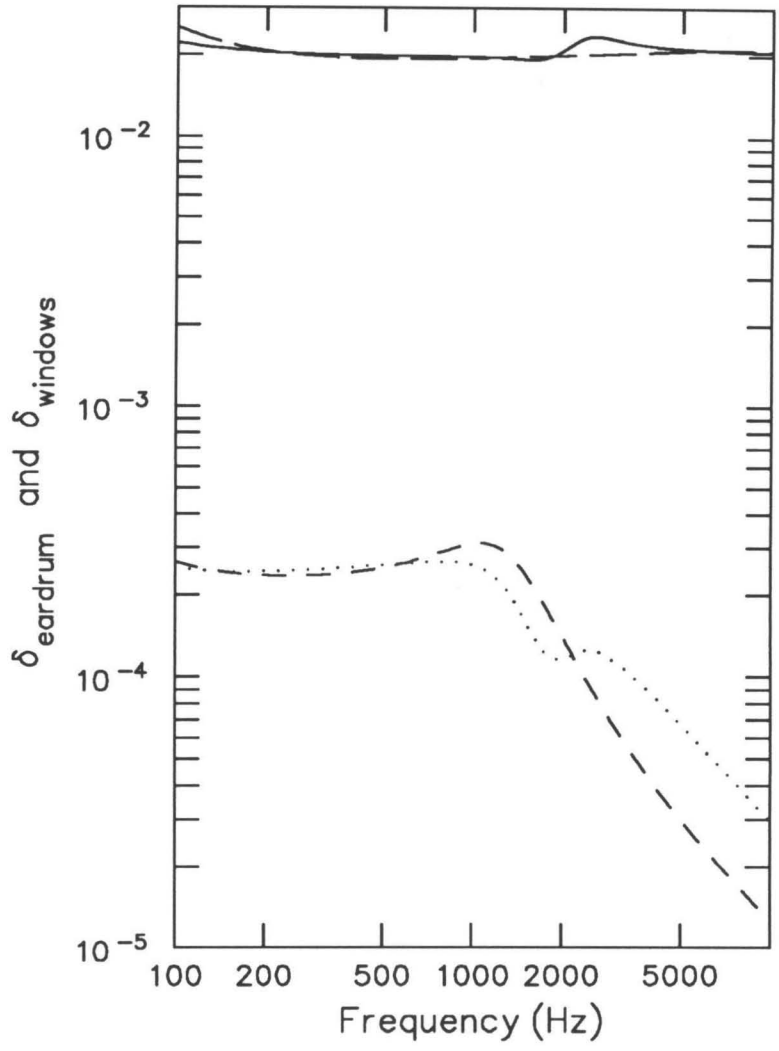

Figure 3. The functions δ_{eardrum} and δ_{windows}, defined by inequalities (6) and (2), evaluated—without any simplifying assumptions about the eardrum or ossicular chain (see footnote 3)—using the the middle-ear models of Zwislocki and Kringlebotn. Zwislocki's predictions for δ_{eardrum} and δ_{windows} are represented by dotted (·····) and solid (———) lines, respectively; Kringlebotn's by short- (— — —) and long-dashed (—— ——) lines. The value $\epsilon = 0.01$ was used in the calculations. The figure indicates that the effects of compressibility on cochlear and *middle-ear* mechanics are expected to be small in the normal ear.

and round windows are made more comparable. For example, removing the stapes while retaining the oval window membrane, which presumably increases the symmetry between the windows, should result in an elevation of hearing thresholds at low frequencies.

IV. Summary

The effects of a possible inner-ear compressibility on middle-ear and cochlear measurements have been examined. A consideration of hearing thresholds in the middleless ear is used to obtain an upper bound on the magnitude of cochlear compressibility. That bound, considerably more stringent than that obtained from direct measurements, suggests that effects of cochlear compressibility are small in normal hearing. Consequently, the traditional two-port representation of middle-ear mechanics is valid to within a few percent.

In the middleless ear, however, a small but finite cochlear compressibility may provide the dominant mechanism for stimulating the cochlea at low frequencies. Experiments are suggested to establish the magnitude of that compressibility and to explore further its contributions to hearing in patients with missing or interrupted ossicular chains.

Acknowledgments

This work was supported by the Theoretical Division of Los Alamos National Laboratory and a National Science Foundation Graduate Fellowship to C. A. S.

Appendix A: A Simple Model for a Compressible Scala Media

This Appendix extends a simple transmission-line model of cochlear mechanics to include a finite compressibility for the scala media. Solving the resulting equations for the transfer matrix ${}^{ow}\mathbf{T}_{rw}$ yields an expression of the form assumed in the text.

A. The "squeezable sandwich" model

Consider the "squeezable sandwich" model of the scala media shown in Fig. A1. A finite stiffness K_{comp} allows the scala media to change its total volume in response to pressures in the two scalae. Adjacent sections are coupled only by motion of the cochlear fluids; compression of one section of the sandwich squeezes its contents—as if, for example, the scala media contained bubbles of air—and does not result in its contents oozing out to expand other sections.

The equations describing the motion of the upper and lower surfaces of the scala media (which adjoin, respectively, the scala vestibuli and scala tympani) are

$$M\ddot{y}_{\text{v}}/2 + R\dot{y}_{\text{v}}/2 + \left(K/2 + K_{\text{comp}}\right)y_{\text{v}} - K_{\text{comp}}y_{\text{t}} = bp_{\text{v}} \ ; \tag{A1}$$

and

$$M\ddot{y}_{\text{t}}/2 + R\dot{y}_{\text{t}}/2 + \left(K/2 + K_{\text{comp}}\right)y_{\text{t}} - K_{\text{comp}}y_{\text{v}} = -bp_{\text{t}} \ . \tag{A2}$$

The parameters M, R, and K are, respectively, the effective mass, damping, and stiffness (per unit length) of the organ of Corti. The pressures in the two scalae (assumed uniform in the yz-plane) are represented by p_{v} and p_{t}. The width of the basilar membrane is denoted by b. A small compressibility of the cochlear contents implies that $K_{\text{comp}} \gg K$.

The equations can be uncoupled by defining two new coordinates $y_{\pm}$ by

$$y_{\pm} \equiv \tfrac{1}{2}\left(y_{\text{v}} \pm y_{\text{t}}\right) \ . \tag{A3}$$

Substitution and forming sums and differences yields

$$M\ddot{y}_{+} + R\dot{y}_{+} + Ky_{+} = bp_{-} \ ; \tag{A4}$$

and

$$M\ddot{y}_{-} + R\dot{y}_{-} + \left(K + 4K_{\text{comp}}\right)y_{-} = bp_{+} \ , \tag{A5}$$

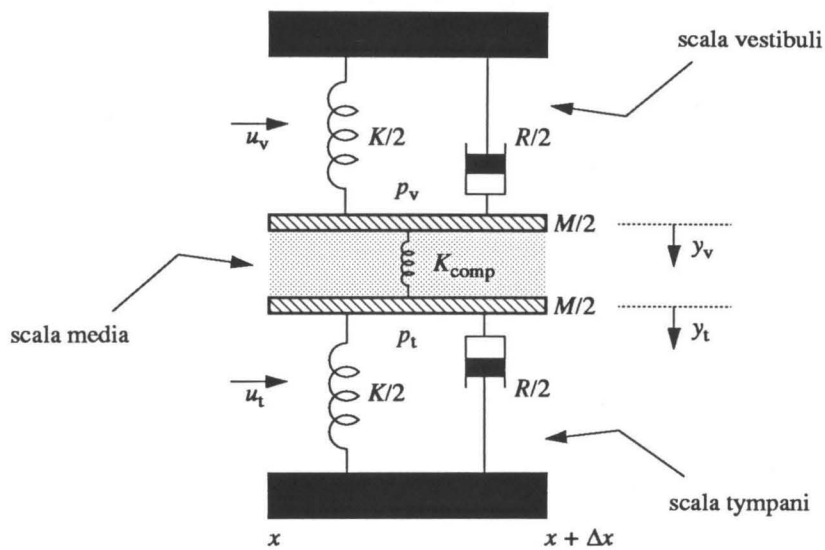

Figure A1. Schematic diagram of a section Δx of the cochlea in which the scala media is represented phenomenologically as a "squeezable sandwich." The finite stiffness K_{comp} permits the scala media to change its total volume in response to the sum of the pressures p_v and p_t in the adjoining scalae.

where

$$p_{\pm} \equiv p_{\mathrm{v}} \pm p_{\mathrm{t}} \, . \tag{A6}$$

Note that Eqs. (A4) and (A5) are uncoupled and describe symmetric and antisymmetric modes of vibration driven, respectively, by the difference and sum of the applied forces.

The motion of the cochlear fluids is described by Newton's second law:

$$\frac{\partial p_{\mathrm{v}}}{\partial x} + \rho \frac{\partial v_{\mathrm{v}}}{\partial t} = 0 \, ; \tag{A7}$$

and

$$\frac{\partial p_{\mathrm{t}}}{\partial x} + \rho \frac{\partial v_{\mathrm{t}}}{\partial t} = 0 \, , \tag{A8}$$

where v_{v} and v_{t} are the particle velocities in the x-direction. Terms nonlinear in the particle velocity are small and have been neglected. Since the fluid volume velocities u_{v} and u_{t} are, by definition, the product of particle velocity and cross-sectional area, Eqs. (A7) and (A8) can be combined to yield

$$\frac{\partial p_{\pm}}{\partial x} + \frac{\partial}{\partial t}\left(\bar{M}_{+} u_{\pm} - \bar{M}_{-} u_{\mp} \right) = 0 \, , \tag{A9}$$

where

$$u_{\pm} \equiv \tfrac{1}{2}\left(u_{\mathrm{v}} \pm u_{\mathrm{t}} \right) . \tag{A10}$$

The acoustic inertances

$$\bar{M}_{\pm} \equiv \rho \frac{S_{\mathrm{v}} \pm S_{\mathrm{t}}}{S_{\mathrm{v}} S_{\mathrm{t}}} \, , \tag{A11}$$

where ρ is the density of the cochlear fluids and S_{v} and S_{t} are the scalae cross-sectional areas. $\bar{M}_{\pm}$ are proportional to the symmetric and antisymmetric parallel additions of the areas of the scalae. If the scalae were completely symmetric, as is often assumed (and will, for simplicity, be assumed here), then $\bar{M}_{-} = 0$.

Motion of the cochlear fluid couples the oscillations of adjoining regions of the organ of Corti. The fluid volume velocities satisfy equations of continuity of the form

$$\frac{\partial u_{\mathrm{v}}}{\partial x} + b \dot{y}_{\mathrm{v}} = 0 \, ; \tag{A12}$$

and

$$\frac{\partial u_{\mathrm{t}}}{\partial x} - b \dot{y}_{\mathrm{t}} = 0 \, . \tag{A13}$$

Adding and subtracting these equations yields

$$\frac{\partial u_{\pm}}{\partial x} + b y_{\mp} = 0 \, . \tag{A14}$$

Taking Fourier transforms of these partial differential equations yields two pair of coupled ordinary differential equations describing the motion of the organ of Corti:

$$\frac{dP_-}{dx} = -\bar{Z} U_- \; ; \tag{A15}$$

$$\frac{dU_-}{dx} = -Y P_- \; ; \tag{A16}$$

and

$$\frac{dP_+}{dx} = -\bar{Z} U_+ \; ; \tag{A17}$$

$$\frac{dU_+}{dx} = -Y_{\rm comp} P_+ \, . \tag{A18}$$

The impedances and admittances are defined by

$$\bar{Z} \equiv i\omega \bar{M}_+ \; ; \tag{A19}$$

$$Y \equiv \frac{b^2}{i\omega M + R + K/i\omega} \; ; \tag{A20}$$

and

$$Y_{\rm comp} \equiv \frac{b^2}{i\omega M + R + \left(K + 4K_{\rm comp}\right)/i\omega} \, . \tag{A21}$$

Equations (A15)–(A18) describe two uncoupled hydromechanical transmission lines (the first, driven by P_-, with series impedance $\bar{Z}$ and shunt admittance Y per unit length; the second, driven by P_+, with series and shunt elements $\bar{Z}$ and $Y_{\rm comp}$, respectively).

B. The matrix ${}^{\rm ow}\mathbf{T}_{\rm rw}$ and the dimensionless parameter ϵ

At every point the pressures and volume velocities in each of the two transmission lines are proportional (i.e., the transmission lines are linear). If waves travel in only a single direction along the lines and the spatial variation of parameters is appropriate—e.g., if the circuit elements "scale" within the basal turns of the cochlea (Shera and Zweig 1991a)—the proportionality constant is simply the corresponding characteristic impedance. Hence

$$P_- = Z_c U_- \; ; \tag{A22}$$

and

$$P_+ = Z_{\rm comp} U_+ \ , \tag{A23}$$

where

$$Z_{\rm c} \equiv \sqrt{\frac{\bar{Z}}{Y}} \qquad \text{and} \qquad Z_{\rm comp} \equiv \sqrt{\frac{\bar{Z}}{Y_{\rm comp}}} \ . \tag{A24}$$

Evaluating the equations at the basal end of the cochlea yields an expression for the transfer matrix ${}^{\rm ow}\mathbf{T}_{\rm rw}$:

$$\begin{pmatrix} P_{\rm ow} \\ U_{\rm ow} \end{pmatrix} = \frac{1}{1-\epsilon} \begin{pmatrix} 1+\epsilon & -Z_{\rm c} \\ 4\epsilon/Z_{\rm c} & -(1+\epsilon) \end{pmatrix} \begin{pmatrix} P_{\rm rw} \\ U_{\rm rw} \end{pmatrix} \ , \tag{A25}$$

where

$$\epsilon \equiv \frac{Z_{\rm c}}{Z_{\rm comp}} = \sqrt{\frac{Y_{\rm comp}}{Y}} \ . \tag{A26}$$

Note that $\det {}^{\rm ow}\mathbf{T}_{\rm rw} = -1$ (the matrix is antireciprocal because of the sign conventions for $U_{\rm ow}$ and $U_{\rm rw}$). At frequencies $\omega \ll \omega_{\rm c_0}$, where $\omega_{\rm c_0}$ is 2π times the maximum characteristic frequency represented along the organ of Corti, both Y and $Y_{\rm comp}$ are stiffness-dominated. Hence,

$$\epsilon \approx 1/\sqrt{1 + 4K_{\rm comp}/K} = \text{positive real constant} \qquad (\omega \ll \omega_{\rm c_0}). \tag{A27}$$

Section III adopts a transfer matrix of the form (A25) to demonstrate that $\epsilon \ll 1$ in the human ear.

References

von Békésy, G. (1936). "Zur Physik des Mittelohres und über das Hören bei fehlerhaftem Trommelfell," *Akust. Zeits.* **1**, 13–23.

von Békésy, G. (1960). *Experiments in Hearing.*New York: McGraw-Hill.

Kemp, D. T. (1979). "The evoked cochlear mechanical response and the auditory microstructure — Evidence for a new element in cochlear mechanics," *Scand. Audiol. Suppl.* **9**, 35–47.

Kemp, D. T. and Chum, R. A. (1980). "Observations on the generator mechanism of stimulus frequency acoustic emissions — Two tone suppression," in *Psychophysical Physiological and Behavioural Studies in Hearing*, edited by G. Van Den Brink and F. A. Bilsen, 34–42. Delft: Delft University Press.

Kringlebotn, M. (1988). "Network model for the human middle ear," *Scand. Audiol.* **17**, 75–85.

Moxon, E. C. (1971). "Neural and mechanical responses to electric stimulation of the cat's inner ear," Ph.D. thesis, Massachusetts Institute of Technology.

Nedzelnitsky, V. (1974a). "Measurements of sound pressure in the cochleae of anesthetized cats," Ph.D. thesis, Massachusetts Institute of Technology.

Nedzelnitsky, V. (1974b). "Measurements of sound pressure in the cochleae of anesthetized cats," in *Facts and Models of Hearing*, edited by E. Zwicker and E. Terhardt, 45–55. Berlin: Springer–Verlag.

Peake, W. T., Rosowski, J. J., and Lynch, T. J. III (1992). "Middle-ear transmission: Acoustic versus ossicular coupling in cat and human," *Hearing Res.* **57**, 245–268.

Shera, C. A. and Zweig, G. (1991a). "A symmetry suppresses the cochlear catastrophe," *J. Acoust. Soc. Am.* **89**, 1276–1289.

Shera, C. A. and Zweig, G. (1991c). "Phenomenological characterization of eardrum transduction," *J. Acoust. Soc. Am.* **90**, 253–262.

Shera, C. A. and Zweig, G. (1992a). "Middle-ear phenomenology: The view from the three windows," submitted to *J. Acoust. Soc. Am.*

Viergever, M. A. (1980). *Mechanics of the Inner Ear: A Mathematical Approach.*Delft: Delft University Press.

Zwicker, E. and Schloth, E. (1984). "Interrelation of different oto-acoustic emissions," *J. Acoust. Soc. Am.* **75**, 1148–1154.

Zwislocki, J. (1962). "Analysis of the middle-ear function. Part I: Input impedance," *J. Acoust. Soc. Am.* **34**, 1514–1523.

Noninvasive Measurement of the Cochlear Traveling-Wave Ratio

Christopher A. Shera and George Zweig

Hearing Research Laboratory
Signition, Inc.
P.O. Box 1020
Los Alamos, New Mexico 87544

Theoretical Division
Los Alamos National Laboratory
Los Alamos, New Mexico 87545

and

Physics Department
California Institute of Technology
Pasadena, California 91125

ABSTRACT

Threshold hearing curves and the spectra of evoked otoacoustic emissions both display a roughly periodic sequence of maxima and minima as a function of frequency. Since the cochlea maps frequency into position, many current models for the generation of otoacoustic emissions (e.g., Strube 1985; Peisl 1988; Strube 1989) explain the observed periodicity by supposing that it mirrors a spatial oscillation in the mechanics of the organ of Corti. Emissions are generated when forward-traveling waves reflect from these corrugations in the mechanics, suggesting that the amplitude of the cochlear traveling-wave ratio should manifest pronounced maxima and minima with a corresponding periodicity. This paper describes measurements of stimulus-frequency emissions, establishes their analyticity properties, and uses them to explore the spatial distribution of mechanical inhomogeneities in the human cochlea. The approximate form and frequency dependence of the cochlear traveling-wave ratio are determined noninvasively. The amplitude of the traveling-wave ratio found empirically is a slowly-varying, nonperiodic function of frequency, suggesting that the distribution of inhomogeneities is uncorrelated with the periodicity found in the threshold microstructure. The observed periodicities arise predominantly from the sinusoidal variation in relative phase between the forward- and backward-traveling waves at the stapes.

Contents

Introduction

The study of cochlear mechanics began with Helmholtz (Helmholtz 1863) who viewed the organ of Corti as a miniature harp connected string by string to neural fibers. Sensations of tone were created as sound waves induced the strings to resonate in sympathetic vibration, exciting corresponding fibers which sent electrical signals to the brain. This view of cochlear mechanics was overturned by the experiments of von Békésy (von Békésy 1960) who showed that structures within the organ of Corti are not under tension. By directly observing the motion of the basilar membrane in cadavers, von Békésy demonstrated that a pure tone generates a forward-traveling wave that propagates through the cochlea to a place of maximal membrane displacement beyond which it is strongly attenuated. The point of maximal displacement varies monotonically with the frequency of the tone. Low-frequency tones stimulate regions near the apex of the cochlea; higher-frequency tones excite regions closer to the stapes. This "textbook" picture of traveling-wave excitation in the cochlea was, until recently, believed correct at all stimulus levels.[1]

It is now known, however, that the ear creates sound while listening to sound (Kemp 1978). For example, a recent model of cochlear mechanics deduced from measurements of basilar-membrane motion (Zweig 1991) predicts that cellular force generators in the cochlea—presumably the outer hair cells—amplify traveling waves somewhat as a laser amplifies light. Consequently, small backward-traveling waves, originating from forward-traveling waves by reflection from spatial inhomogeneities in the mechanics of the organ of Corti (Manley 1983; Lonsbury-Martin et al. 1988; Shera and Zweig 1992f), are amplified as they travel backwards to the stapes, from which they are partially reflected. Unreflected waves vibrate the middle-ear bones and ultimately appear in the ear canal as sound ("otoacoustic emissions"). The generation of large backward-traveling waves radically changes our view of wave motion in the cochlea at low sound-pressure levels. The superposition of forward- and backward-traveling waves leads to a standing-wave component in the cochlear response. Active elements amplify the forward and backward waves, thereby increasing the sensitivity of hearing.

[1] See, however, the work of LePage (LePage 1987; LePage 1990), who describes experiments identifying another possible component—a "summating baseline shift"—in the response of the organ of Corti and suggests that they provide evidence for the dynamic control of cochlear tuning, achieved by varying the tension in the radial fibers of the pars pectinata. The outer hair cells then serve—returning to Helmholtz—much like the pedals on an orchestral harp.

The threshold hearing curve shows periodic minima (Elliot 1958) at frequencies that correlate strongly with maxima in the spectra of otoacoustic emissions (Horst et al. 1983; Zwicker and Schloth 1984). The ear emits most loudly at those frequencies for which it is most sensitive. Since the cellular force generators are limited in the energy they can emit, cochlear excitation patterns produced when the ear listens to quiet sounds are qualitatively different from those produced in response to louder sounds.

Otoacoustic emissions and the threshold hearing curve may be controlled from the central nervous system. Experiments have shown, for example, that contralateral tones (Mott et al. 1989) can alter both the amplitude and frequency of spontaneous and evoked emissions. Whitehead (1991) has described similar, centrally-mediated variations in emission characteristics. In addition, careful measurements of stimulus-frequency emissions (Zwicker and Schloth 1984) have an analytic structure inconsistent with that of a causal system (Shera and Zweig 1986, unpublished observation), raising the intriguing possibility that feedback from the brain plays a major role in controlling evoked emission. Since the stimuli used in the measurements are periodic and predictable, the brain may actually be anticipating its input and altering the mechanical state of the cochlea accordingly. As seen from the ear canal, the cochlea would then appear acausal in its response.[2]

This paper describes measurements of otoacoustic emissions performed with accuracy sufficient to test this apparent acausality and to determine the frequency dependence of the complex-valued traveling-wave ratio. Determination of the traveling-wave ratio enables one to explore the nature of the mechanical spatial inhomogeneities from which backward-traveling waves originate. (The traveling-wave ratio, denoted R, is defined to be the ratio of the backward- to the forward-traveling wave measured at the basal end of the cochlea near the stapes.) The inhomogeneities cannot be determined from measurements of basilar-membrane motion because those measurements are made at a single point. A

[2] Although a physiological mechanism capable of generating the sort of cycle-by-cycle feedback necessary to produce the apparent acausality observed by Zwicker and Schloth may be difficult to imagine, one might be wise to remember that

> "There are more things in heaven and earth, Horatio,
> Than are dreamt of in your philosophy."
> —Shakespeare, *Hamlet* (act I, scene v).

quantitative analysis of otoacoustic emissions, however, makes an exploration of the spatial variation of mechanical properties possible.

Two simple spatial distributions of the inhomogeneities are consistent with current experiments. Since the cochlea maps frequency into position, one possibility is that the spatial variation of mechanical characteristics correlates strongly with the periodicities observed in otoacoustic emissions and the threshold microstructure (e.g., Strube 1985; Peisl 1988; Strube 1989). For example, the effective damping of the organ of Corti could be made to mirror the threshold hearing curve, with smaller damping (greater sensitivity) occurring at points corresponding to minima in the threshold curve (where quieter sounds can be detected).

Another possibility is that the spatial variation of mechanical characteristics is uncorrelated with the periodic variation in frequency of the spectral peaks in otoacoustic emissions and the corresponding minima in the threshold hearing curve (Shera and Zweig 1992f). In this case the inhomogeneities could, for example, be randomly distributed along the cochlea and the periodic variations due entirely to the frequency dependence of the relative phase at the stapes of the forward- and backward-traveling waves, leading to an alternation of constructive and destructive interference as the frequency of the stimulus is varied monotonically. A mechanism explaining the emergence of such striking spectral order through the scattering of cochlear waves by what may be essentially random spatial inhomogeneities is presented in a companion paper (Shera and Zweig 1992f).

Evidence for or against these two possibilities, both capable of explaining the oscillatory structure of the measured ear-canal pressure P_{ec} and the correlated threshold microstructure, is provided by the form of the traveling-wave ratio R, which contains information, carried back to the stapes by the reflected wave, about possible spatial inhomogeneities in apical regions of the cochlea. A traveling-wave ratio whose amplitude $|R|$ manifests correlated, periodic variations—displaying, for example, pronounced maxima at the "dip" frequencies of the hearing threshold curve and the corresponding peaks of $|P_{ec}|$—strongly suggests a spatial variation of parameters that mirrors the hearing threshold curve. Alternatively, a traveling-wave ratio whose amplitude varies relatively slowly and nonperiodically suggests that the underlying spatial distribution of inhomogeneities

is more probably irregular or random (Shera and Zweig 1992f). The oscillations in ear-canal pressure P_{ec} then arise because the phase of R varies monotonically with increasing frequency, alternately passing through plus and minus one. The existence of these two possibilities is evident from the limiting case in which the middle-ear is idealized as a simple mechanical transformer. The ear canal pressure $P_{ec}(\omega; R)$ then has the form (Shera and Zweig 1992b)

$$P_{ec}(\omega; R)/P_{ec}(\omega; 0) = \frac{1+R}{1-R} \,. \tag{1}$$

Although R cannot be determined from measurements of otoacoustic emissions without detailed knowledge of middle-ear transfer coefficients (Shera and Zweig 1992b), certain characteristics of its frequency variation can be found by exploiting a property of those emissions that enable one to "divide out" many of the the unknown effects of the stimulus-delivery system and the middle ear. The oscillations in the ear-canal pressure P_{ec} are superimposed on a smooth, slowly-varying "background," whose form is determined by the transfer characteristics of the measuring apparatus, the external and middle ears, and cochlear mechanics and geometry near the stapes. Those two components of the pressure can be separated by filtering. The assumption that the unknown transfer characteristics are slowly varying then enables one to determine the principal frequency variation of R.

I. The Measurement

A. Equipment and methods

Otoacoustic emissions were measured in the human ear canal using a setup whose block diagram is illustrated in Fig. 1. Acoustic stimuli were delivered and the response recorded using miniature transducers sealed in the ear canal (the Etymōtic Research ER-2 earphone and ER-10 microphone and preamp). Stimulus-frequency emissions were recorded using the two-channel Hewlett-Packard HP-3562A signal analyzer operating in swept-sine mode (Blackham et al. 1987). The output of the HP-3562A sinusoidal voltage oscillator was fed to channel A of the analyzer, which adjusted the source to maintain a constant amplitude, and then attenuated (Wavetek 5080.1) before being delivered to the ER-2 earphone. With a constant input voltage, the ER-2 is designed to produce an approximately constant sound pressure at the eardrum. After amplification (Brüel &

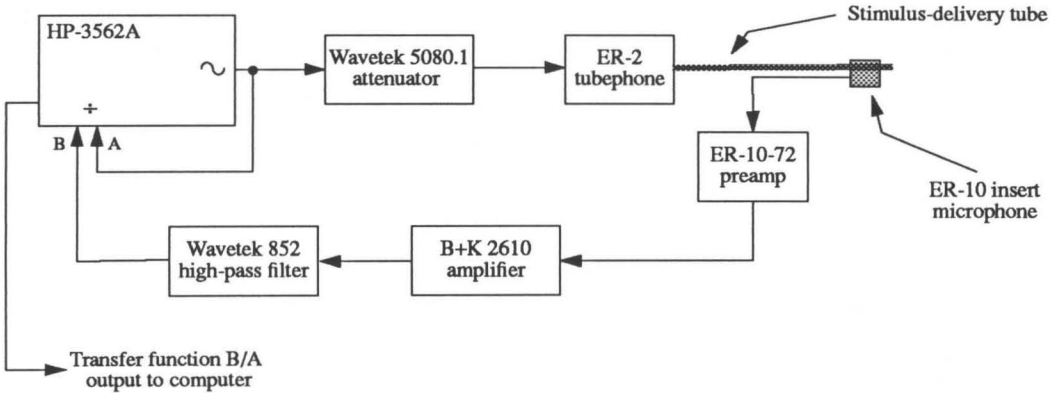

Figure 1. Schematic diagram of the stimulus-delivery and recording system.

Kjær 2610), the microphone signal from the ER-10 was filtered (Wavetek/Rockland 852, 4th-order Butterworth high-pass filter with a cutoff frequency of 600 Hz) and returned to the signal analyzer (channel B), which measured the complex ratio of the voltage signals at its two input ports. Stimulus frequencies were stepped discretely in a phase-continuous manner from the highest measured frequency to the lowest.[3] To ensure a steady-state response the analyzer allows a settling time of 20 ms after stepping to a new frequency. In addition, the response at each frequency was measured for an integration time ΔT (with $\Delta T \geq 200$ ms) chosen to be much greater than reported latencies of click-evoked echoes, which are typically less than 20 ms for all frequencies greater than 800 Hz (e.g., Neely et al. 1988; Zweig et al. 1992).

Subjects were seated comfortably in a reclining chair in a double-walled sound booth (Industrial Acoustics). All were between 20 and 40 years of age and had audiometrically normal hearing.

B. Equivalent circuit

In Fig. 2 the acoustic properties of the stimulus delivery and recording system are represented by their Norton-equivalent source $\bar{U}_s$ and source admittance Y_s. The volume velocity $\bar{U}_s$ is related to the voltage V_i delivered by the voltage source (and sent, via an attenuator, to the earphone) through the transfer-function K_i; that is,

$$\bar{U}_s = K_i V_i \, . \tag{2}$$

Similarly, the transfer-function K_o relates the ear-canal pressure P_{ec} and the measured microphone output voltage V_o:

$$P_{ec} = K_o V_o \, . \tag{3}$$

The measurement thus consists of determining the dimensionless ratio

$$\rho^+(\omega; A) \equiv \frac{V_o}{V_i} \, . \tag{4}$$

[3] Because high frequencies are mapped closer to the stapes than lower frequencies, sweeping from high to low advances the traveling-wave envelope into previously unstimulated regions of the cochlea. In practice, the direction of the sweep appears to make little difference, except perhaps at frequencies near a spontaneous emission.

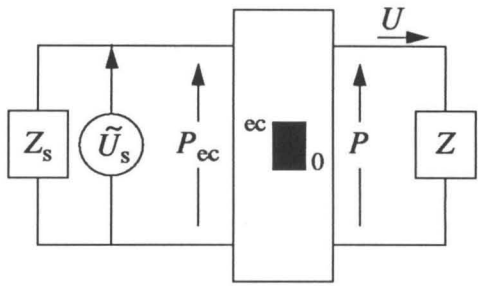

Figure 2. Equivalent circuit for the stimulus-delivery and recording system, represented by its Norton-equivalent source amplitude $\widetilde{U}_{\mathrm{s}}$ and source impedance $Z_{\mathrm{s}} \equiv 1/Y_{\mathrm{s}}$. The residual ear-canal space, middle ear, and vestibular space are represented by an equivalent two-port network ${}^{\mathrm{ec}}\blacksquare_0$, with transfer matrix ${}^{\mathrm{ec}}\mathbf{T}_0 \equiv \left(\begin{smallmatrix} a & b \\ c & d \end{smallmatrix}\right)$. Seen from the basal end of the organ of Corti, the cochlear response at the driving frequency is characterized by the input impedance $Z(\omega; A)$.

When the ratio ρ^+ is independent of stimulus amplitude A, the circuit illustrated in Fig. 2 implies that

$$\rho^+(\omega) = \frac{Y^+ Z_{ec}}{1 + Y_s Z_{ec}} \; ; \tag{5}$$

where

$$Y^+ \equiv K_i / K_o \; , \tag{6}$$

and $Z_{ec}(\omega)$ represents the ear-canal load impedance seen from the tip of the earphone assembly. The residual ear-canal space and middle-ear (including the vestibular space) are represented as a reciprocal two-port network ${}^{ec}\blacksquare_0$ (e.g., Shera and Zweig 1992a), with transfer matrix ${}^{ec}\mathbf{T}_0 \equiv \left(\begin{smallmatrix} a & b \\ c & d \end{smallmatrix}\right)$. The load impedance Z_{ec} therefore has the value

$$Z_{ec}(\omega) = \frac{aZ + b}{cZ + d} \; , \tag{7}$$

where $Z(\omega)$ is the cochlear input impedance. Z_{ec} thus depends on the mechanics of the ear canal, the middle ear, and the cochlea.

As a control and check of the linearity of the measurement system, the ratio ρ^+ was measured with the probe assembly inserted into a rigid-walled cylindrical cavity. The resulting measurements of ρ^+_{cav}, performed at sound pressure levels corresponding to sensation levels (SL) of 20 dB and 40 dB above threshold, are shown in Fig. 3. Except for differences in the noise level near the impedance minimum (arising from the zero in the reactance at the cavity resonance), the two data sets are indistinguishable.

Chiefly because of delays introduced by the stimulus delivery tubes, the phase of K_i, and hence of ρ^+, is dominated by a delay $e^{-i\omega T}$, where the delay time T falls in the range 1–2 ms. Rather than working with ρ^+, it thus convenient to define the quantity

$$\rho \equiv \rho^+ e^{i\omega T} \; , \tag{8}$$

in which that delay has been removed. With the delay subtracted, ρ^+_{cav} becomes a minimum-phase function, as expected for measurements proportional to a driving-point impedance (Bode 1945). In all measurements that follow, the delay time T, determined individually for each measurement using a least-squares linear fit to the phase of ρ^+, has been removed in this way.

The qualitative features of ρ for the human ear are described in Sec. II, where two components of the response are identified. Those components are separated in Sec. III. Sections IV and V then show how contributions to ρ arising from the reflection of cochlear waves can be extracted from the measured response.

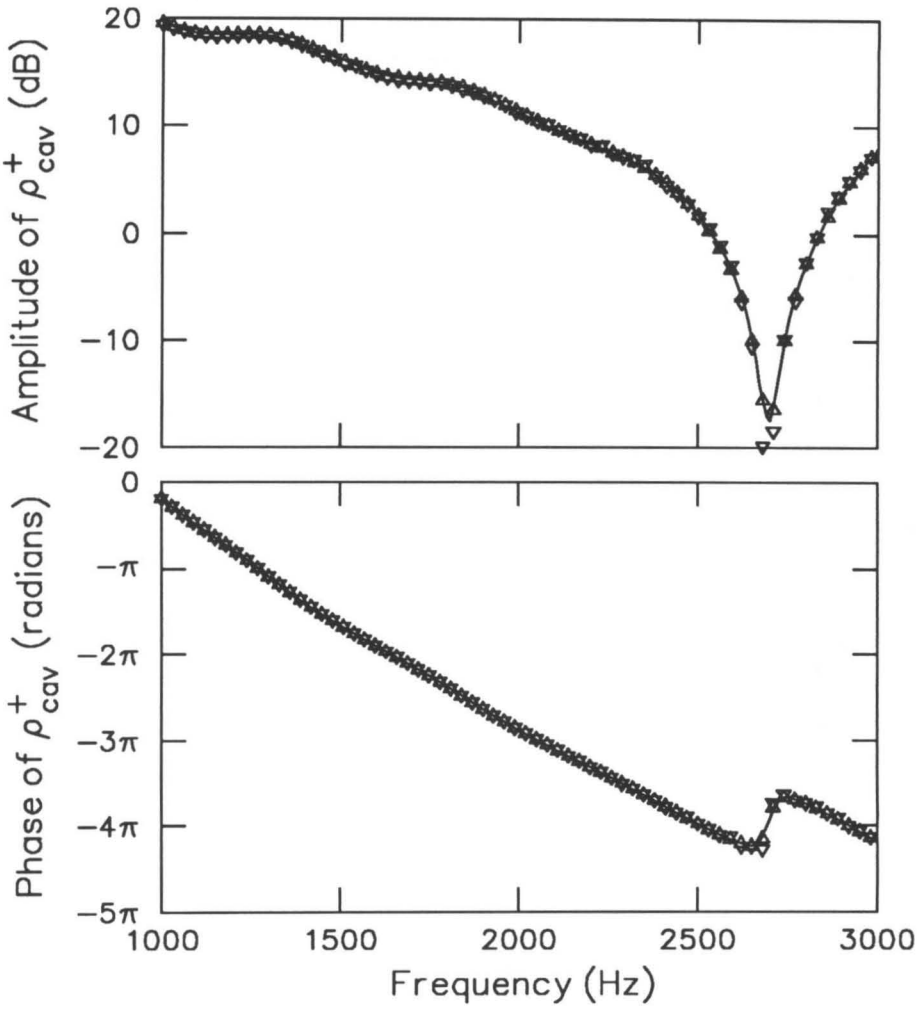

Figure 3. The function $\rho^+_{cav}(\omega; A)$ measured in a rigid-walled cylindrical cavity (consisting of a hole of approximate length 3.1 cm and volume 1.6 cm^3 drilled in a block of plexiglass) at two-different stimulus levels: ($\triangle$) measurements at 40 dB SL; ($\triangledown$) measurements at 20 dB SL. The measurement integration time was one second. Except for increased noise at the lower level (especially noticeable about the impedance minimum near 2700 Hz, a value in close agreement with the resonant frequency, $f_1 = c/4l$, expected for a closed tube of length l), ρ^+_{cav} is, as expected, independent of A (note that the point symbols superpose to form a six-pointed star). The phase of ρ^+_{cav} is dominated by a delay originating primarily in the stimulus-delivery tubes. With that delay subtracted, ρ^+_{cav} is a minimum-phase function, as indicated by the solid line (———), which represents a smoothed, minimum-phase fit to the measurements at 40 dB SL (Zweig and Konishi 1987; Konishi and Zweig 1989).

II. Features and Analyticity of $\rho(\omega; A)$

Figure 4 shows the results of a series of measurements performed at varying sound-pressure levels (subject JEM-R). Two components are identifiable, distinguished by their behavior with stimulus level. At the highest levels, ρ is a smooth and slowly-varying function of frequency. As the stimulus level is reduced, however, an oscillatory component, with a period of roughly 90 Hz, appears superimposed on that smooth background, which may itself vary with stimulus level. The observations suggest that at low levels (where, as shown below, the response is linear) the function $\rho(\omega; A)$ can be viewed as the sum of two components: a slowly-varying background component arising predominantly from the middle and external ears, and an oscillatory component, presumably arising from "stimulus re-emission" within the cochlea. In Sec. III those two components of the response are separated, focusing on the region between the two spontaneous emissions at approximately 1200 and 1660 Hz (cf. Fig. 5).

A. Linearity at low levels

Figure 6 demonstrates the existence of a linear regime by overlaying measurements made at 0 and 5 dB relative to threshold (SL). The measurements superpose over much of the frequency range, although a frequency-dependent temporal shift in the background component is apparent, especially above 1500 Hz.[4] A technique for estimating the background not subject to artifacts introduced by such shifts is introduced in Sec. III. Subsequent sections then focus on finding the form of the traveling-wave ratio in the linear regime.

B. Analyticity properties at low levels

Among the most careful published measurements of stimulus-frequency emissions are those of Zwicker and Schloth (1984). Their data, however, have an analytic structure inconsistent with that of a causal system (Shera and Zweig 1986, unpublished observation). Figure 7 reproduces their measurements of the pressure in the ear canal (data from Fig. 2 recorded from subject A.S.l in the low-level linear regime at 10 dB SL). Causality requires

[4] Similar changes in the background component are apparent when consecutive measurements are made at the same stimulus level, indicating that the variation is due principally, if not entirely, to temporal drift, rather than to a frequency-dependent nonlinearity in the mechanics responsible for the background.

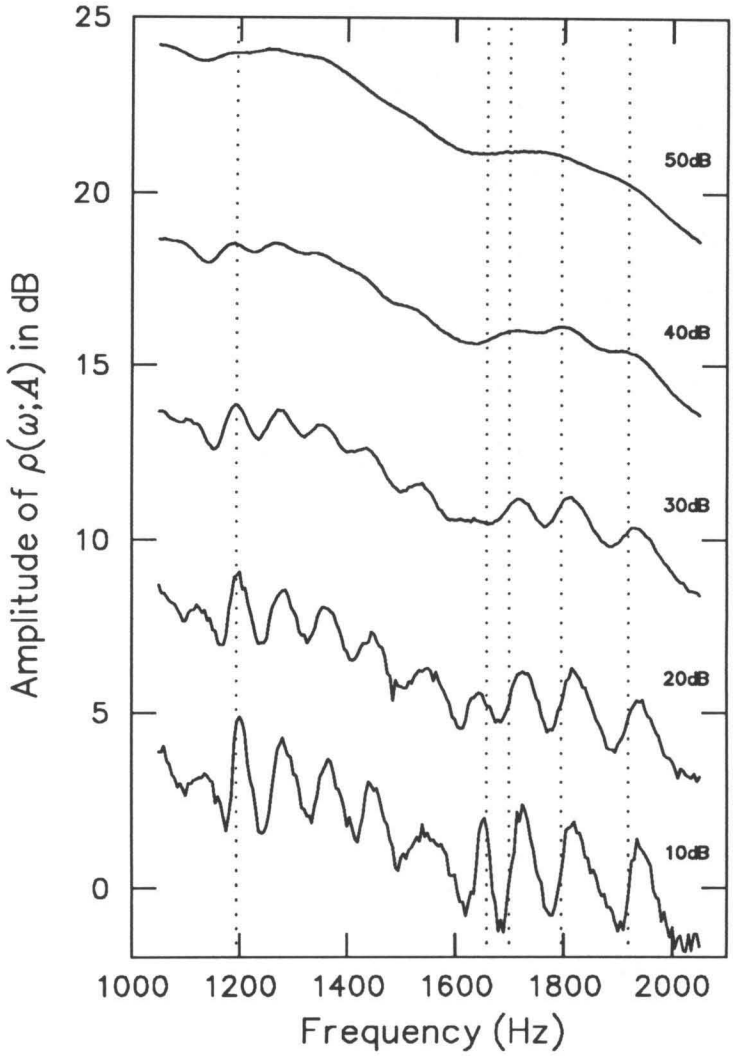

Figure 4. The function $\rho(\omega; A)$ measured in subject JEM-R at stimulus levels A indicated on the right in dB relative to threshold (SL). The average values of the curves approximately superpose but have been offset by 5 dB for clarity. The vertical dotted lines (·····) indicate the frequencies of the subject's known spontaneous emissions in this frequency range (cf. Fig. 5). At the highest level, $\rho(\omega; A)$ is a smooth, slowly-varying function of frequency. As the stimulus level is reduced, oscillations with a period of roughly 100 Hz appear superimposed on that smooth background. Note the increased noise at lower stimulus levels. In the data discussed below, the signal-to-noise ratio was substantially improved by increasing the measurement integration time from the 200 ms used here.

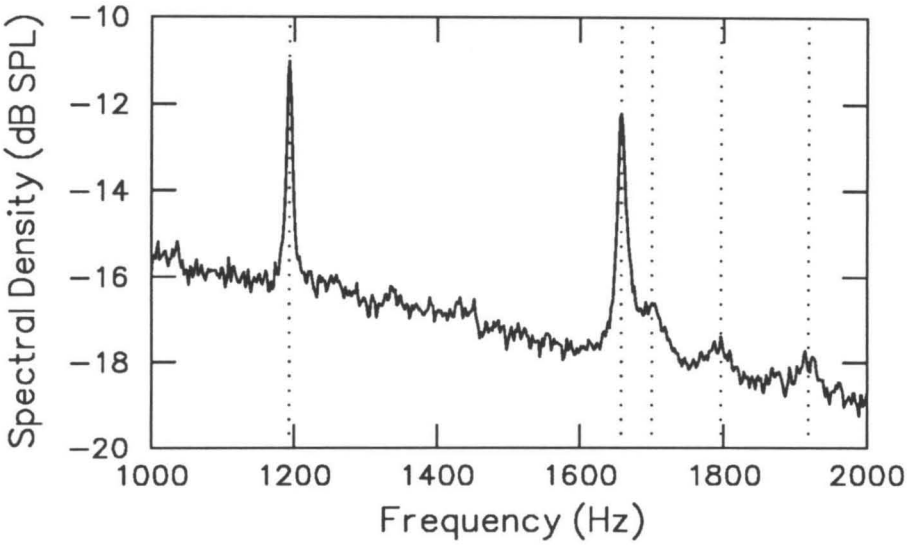

Figure 5. Spectral density of the ear-canal pressure measured without external stimulation in subject JEM-R (average of 800 spectra). The vertical dotted lines (· · · ·), positioned at reproducible spectral peaks, indicate the known spontaneous emissions in this frequency range. Subsequent analysis focuses on the region between the two spontaneous emissions near 1200 and 1660 Hz.

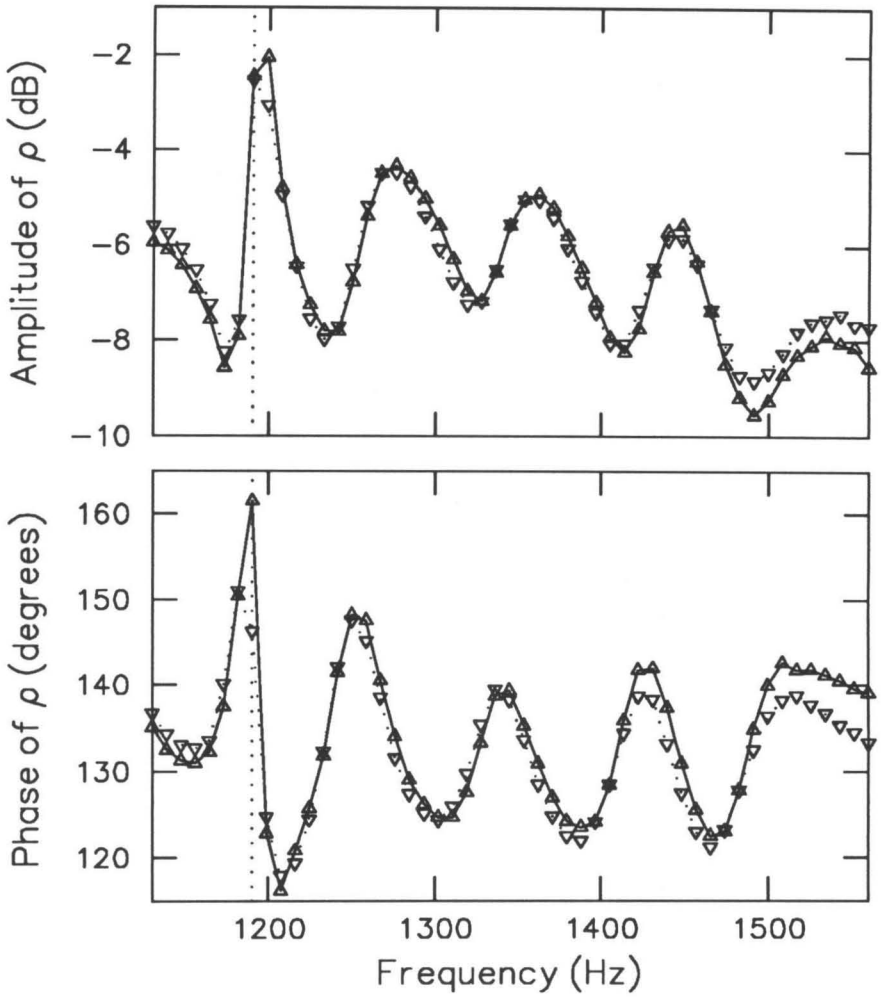

Figure 6. The function $\rho(\omega; A)$ measured (with an 8 second integration time) in subject JEM-R at stimulus levels 0 dB SL ($\triangledown$ connected by $\cdots\cdots$) and 5 dB SL ($\triangle$ connected by ———). As in Fig. 4, the vertical dotted line indicates a known spontaneous emission. Aside from a low-frequency drift in the background—most probably due to static pressure changes in the middle-ear cavities and/or temperature variations in the recording microphone—the two functions nearly superpose, indicating that the response is linear at these levels.

that the real and imaginary parts of the measured pressure be Hilbert transforms of one another (Bode 1945):[5]

$$\mathrm{Re}\{P(\omega)\} = -\frac{1}{\pi} \mathrm{P}\!\!\int_{-\infty}^{\infty} \frac{\mathrm{Im}\{P(\omega')\}}{\omega' - \omega} d\omega' \,, \tag{9}$$

and

$$\mathrm{Im}\{P(\omega)\} = \frac{1}{\pi} \mathrm{P}\!\!\int_{-\infty}^{\infty} \frac{\mathrm{Re}\{P(\omega')\}}{\omega' - \omega} d\omega' \,. \tag{10}$$

Here $\mathrm{P}\!\!\int$ represents a Cauchy principal-value integral.

In addition, measurement of the pressure under the conditions they report is equivalent to determining the driving-point impedance of the ear canal. Driving-point impedances are minimum-phase functions (Bode 1945). Consequently, the measured pressure must also be minimum-phase—that is, $\ln P$ must be causal—unless there are other, unaccounted-for inputs to the ear modifying the response (e.g., signals coming from the central nervous system). As measured from the ear canal, the ear might then appear acausal in its response.

Shown in the figure for comparison are the corresponding Hilbert-transforms pairs, in which the measurements of the amplitude were used to predict the phase, and vice versa. Unless the measurement errors are much larger than suggested by the apparent noise level, the expected analyticity properties would normally require that the measured and predicted curves superpose.

To explore, however, whether the apparent acausality reflects changes in the mechanical state of the ear induced by feedback from the brain, Fig. 8 plots the real and imaginary parts of $\ln \rho$ at 5 dB SL (subject JEM-R), together with smoothed, minimum-phase fits to the measurements (Zweig and Konishi 1987; Konishi and Zweig 1989). The plotted error bars—estimated by comparison with the minimum-phase fit—correspond to 0.125 dB in the amplitude and 0.8° in the phase. The fit is everywhere excellent, except within the immediate neighborhood of the known spontaneous emission.[6] Everywhere

[5] Dispersion relations (9) and (10) are valid when the measured pressure vanishes as $\omega \to \infty$. When that is not the case, modified, or subtracted, dispersion relations exist (Bode 1945). In addition, the subtracted form of the dispersion relations may be computationally more convenient if the low-frequency behavior of the pressure is known but the high-frequency behavior poorly determined (Zweig 1976; Zweig and Konishi 1987).

[6] Zwicker and Schloth (1984) report their subject (A.S.l) as having no measurable spontaneous emission.

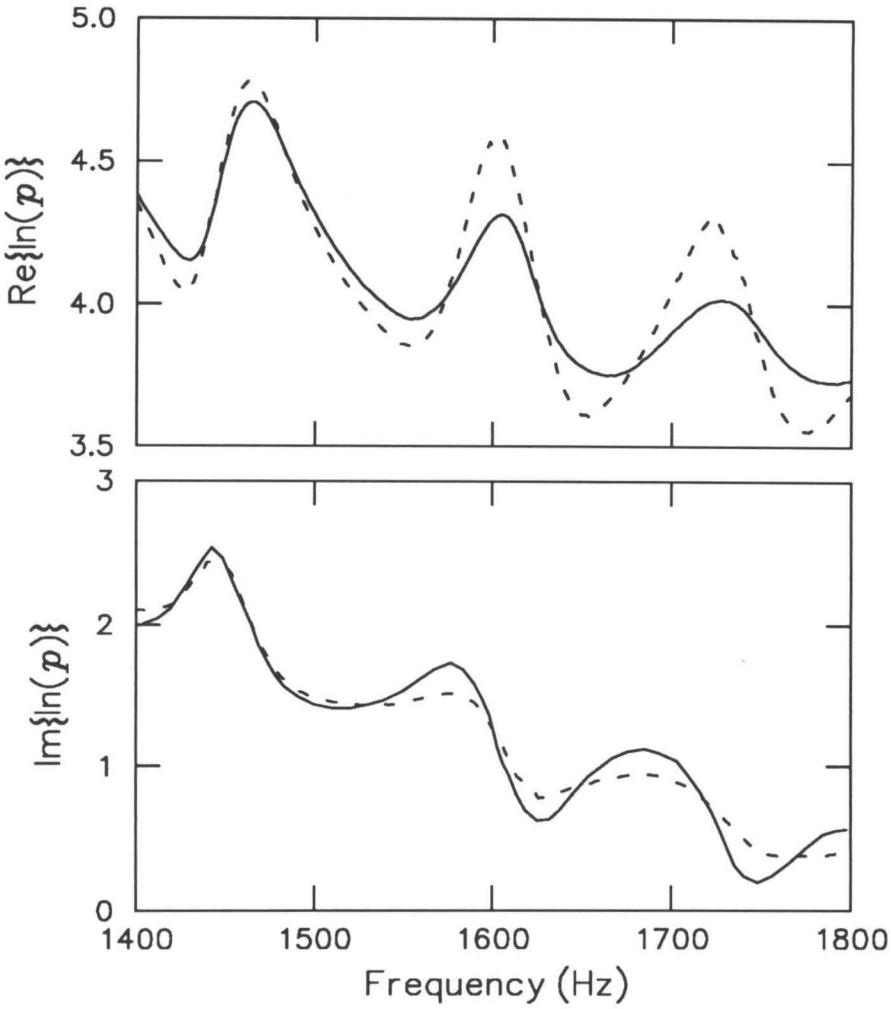

Figure 7. Measurements of ear-canal pressure at 10 dB SL (———) from Fig. 2 of Zwicker and Schloth (1984). The dashed line (- - - -) in the upper (lower) panel represents the Hilbert transform of the data in the lower (upper) panel. Were the measurements minimum-phase (as driving-point impedances must be), the solid and dashed lines would everywhere superpose. Note that measurement errors are not given in the paper, but the smoothness of the curves suggests that the random errors are small. A Hilbert-transform analysis of the real and imaginary parts of the pressure indicates that unless their errors are substantially greater than implied, the measurements could not have originated in a causal system.

else, however, ρ satisfies not only the constraints of causality but also the more stringent analyticity requirements of minimum-phase behavior (Bode 1945). Demonstrated here in the linear regime in one subject, these analyticity properties hold at all stimulus levels and are universal among subjects we have examined.[7]

Although the origin of the peculiar analyticity properties of the measurements of Zwicker and Schloth is not known, their apparent acausality appears unlikely to reflect a general involvement of the central nervous system in the generation or control of otoacoustic emissions.

III. Separating the Crooked from the Straight

Understanding the origin of the oscillatory component in $\rho(\omega)$ is facilitated by subtracting the smooth background and working with the quantity $\Delta(\omega)$, defined by

$$\Delta(\omega) \equiv \rho(\omega)/\rho_0(\omega) \; - \; 1 \; , \tag{11}$$

where ρ_0 is the background. (Since the analysis focuses on measurements in the linear regime, the dependence on stimulus amplitude A has been omitted.) Defining Δ in this manner, rather than as the simple difference $\rho - \rho_0$, guarantees that the extracted oscillatory component will be independent of the absolute scale of ρ.

The two components of $\rho(\omega)$—namely the smooth background $\rho_0(\omega)$ and the oscillations $\Delta(\omega)$—can be separated by filtering, thereby allowing each measurement of $\rho(\omega)$ to serve as its own control against possible variations in the background that occur during the course of the measurement. The oscillatory component occurs in the frequency response and can be removed by passing ρ through a low-pass filter, just as if the measured signal had been recorded in the time domain. Details of the filtering and a discussion of the systematic errors it may introduce are given in the Appendix, which demonstrates that the conclusions of this paper are not especially sensitive to the choice of smooth background.[8]

---

[7] We have systematically investigated the analyticity properties of ρ in seven ears (four subjects).

[8] It is interesting to note that if the temporal shift can be eliminated or controlled for (using, for example, an *A-B-A* measurement sequence that permits "before" and "after" comparisons), then ρ_0 may be measurable at low levels—thereby providing a consistency check on the background extracted by smoothing—if the limit $R \rightarrow 0$ can be reversibly induced with aspirin or other drugs without affecting the mechanics of the middle ear.

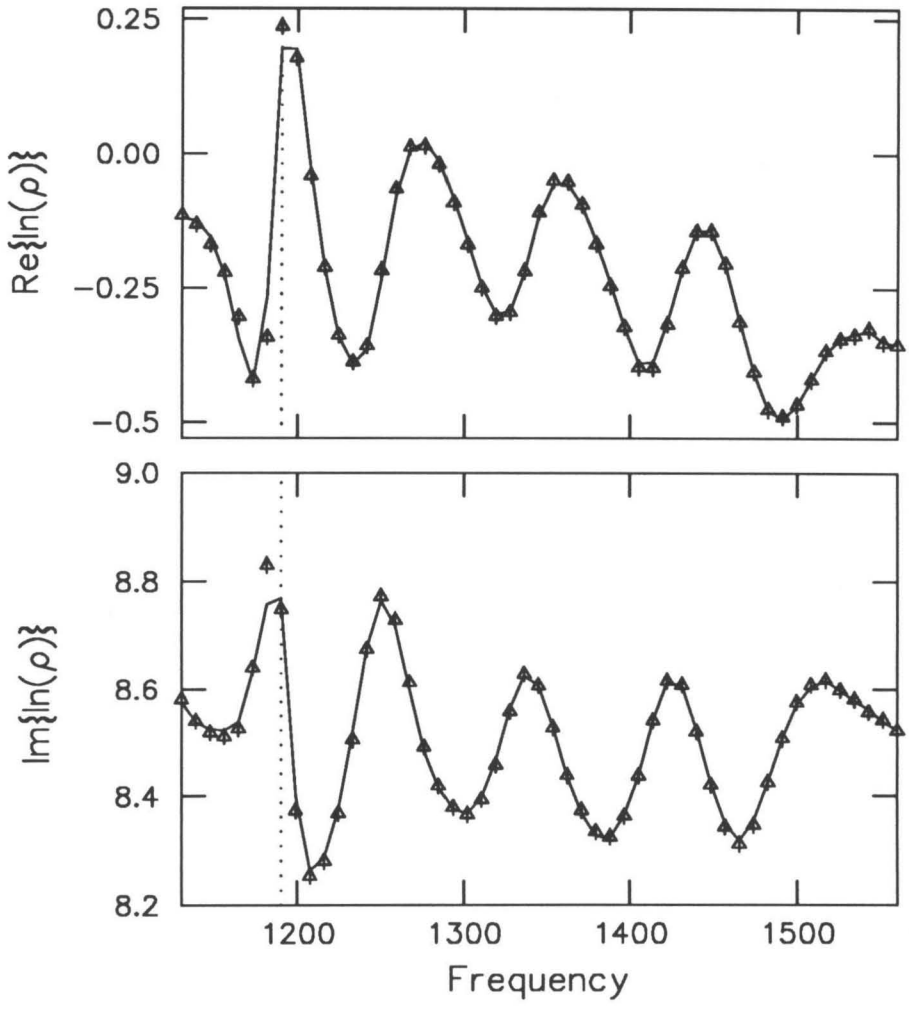

Figure 8. The function $\ln \rho$ at 5 dB SL (data from Fig. 6) together with smoothed, minimum-phase fits (———) to the measurements (Zweig and Konishi 1987; Konishi and Zweig 1989). The error bars—estimated by comparison with the fits—correspond to 0.125 dB in the amplitude and 0.8° in the phase. Except near the spontaneous emission (· · · ·), the fit is excellent. Unlike the measurements of Zwicker and Schloth (1984), which, if accurate, could not have originated in a causal system, the measurements of stimulus-frequency emissions reported here are both causal and minimum-phase.

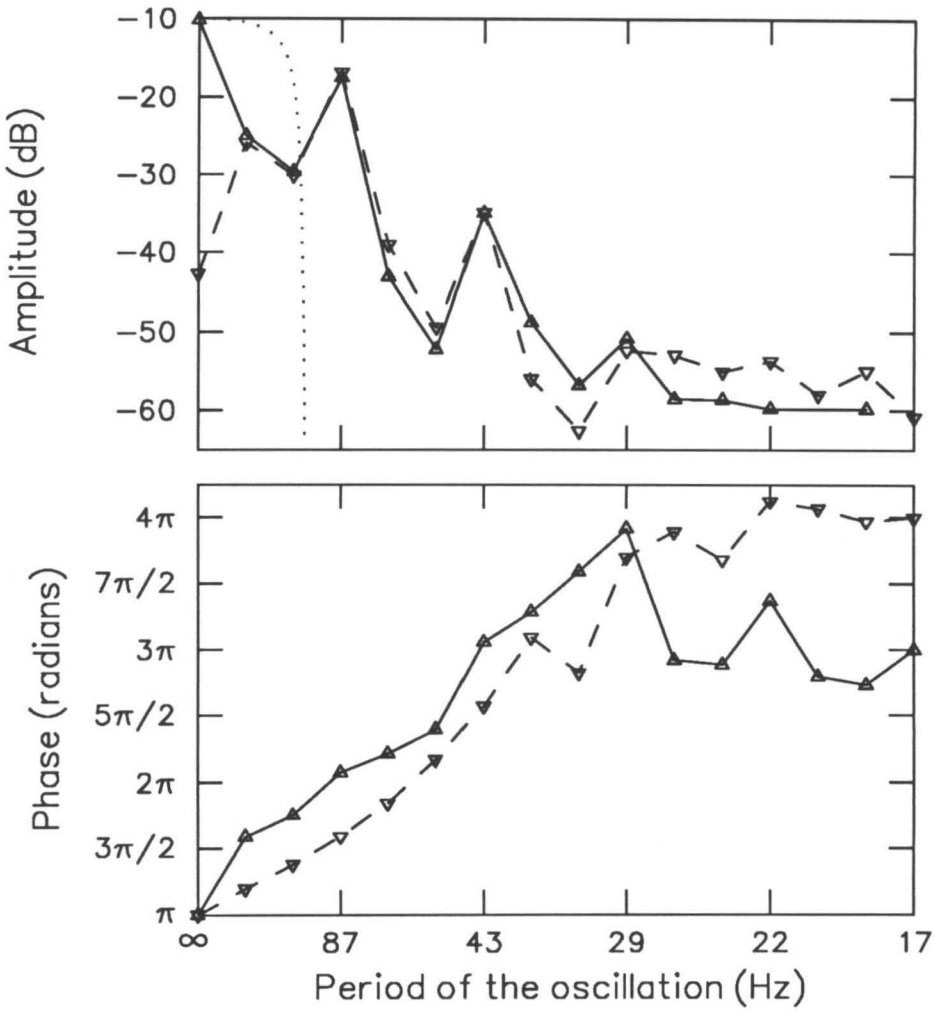

Figure 9. Inverse Fourier transforms $\widehat{F}^{-1}\{\mathrm{Re}\rho(\omega)\}$ ($\triangle$ connected by ———) and $\widehat{F}^{-1}\{\mathrm{Im}\rho(\omega)\}$ ($\triangledown$ connected by — — —) for the data in the frequency interval [1215, 1475]—chosen to make the data nearly periodic—from Fig. 8. Before applying the operator $\widehat{F}^{-1}$, the data were unramped and interpolated to 2^{10} points using bandlimited $\sin(f)/f$ interpolation (e.g., Papoulis 1977). Shown for comparison is the low-pass filter L_{10} (with cutoff set at an oscillation period of 130 Hz) used to extract the slowly-varying background (·····). None of the subsequent analysis is sensitive to the precise value of the cutoff (see the Appendix).

Figure 9 shows the spectrum of $\rho(\omega)$—denoted $F^{-1}\{\rho(\omega)\}$, where $F\{\cdot\}$ represents the operation of Fourier transformation—for a section of the data shown in Fig. 8 (data near the spontaneous emission have not been included). Note that at least two, and perhaps three, spectral peaks are visible at fractional values $1/1$, $1/2$, and $1/3$ of the fundamental oscillation period (approximately 90 Hz). Shown for comparison is the spectrum of the low-pass filter through which $\rho(\omega)$ is passed to remove the oscillatory component. The result of that filtering is shown in Fig. 10, which plots both the original data and the background ρ_0 obtained by smoothing. Finally, by subtracting ρ_0 from ρ according to Eq. (11) one obtains the oscillatory component Δ shown in Fig. 11.

An estimate of the oscillation period Δf can be obtained by fitting a sinusoid to the data. A least-squares fit yields

$$\Delta f = 85.2 \pm 0.3 \text{ Hz}, \tag{12}$$

where the period has been assumed constant over the interval.

The next section shows how the oscillatory component Δ can be understood as arising from wave reflection in the cochlea. The measurements are then used to explore the frequency variation of the traveling-wave ratio.

IV. The Traveling-Wave Ratio

This section presents an interpretive framework within which to continue analysis of the measurements. The oscillatory component in the response is viewed as originating through the production of backward-traveling waves, presumably by the partial reflection of the forward-traveling wave. That reflection is likely to occur predominantly near the characteristic place in the apical turns of the cochlea, where the response to the forward-traveling wave is largest. By changing the pressure and volume velocity near the stapes, backward-traveling waves modify the effective value of the cochlear input impedance.

A. The cochlear input impedance

At stimulus amplitudes A for which the mechanics are linear, the cochlear response seen from the basal end of the organ of Corti can be characterized by the cochlear input

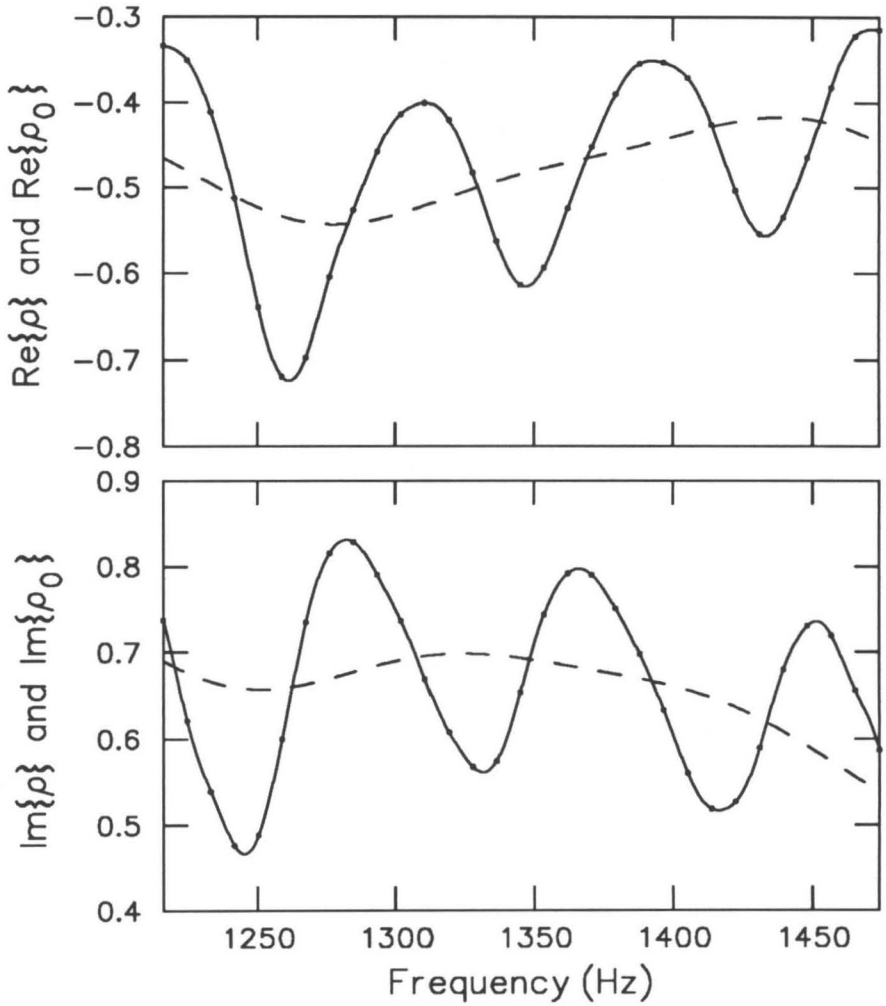

Figure 10. The functions $\rho(\omega)$ (•) and the background $\rho_0(\omega)$ (— — —) obtained by smoothing the data segment described in Fig. 9. The bandlimited interpolant is given by the solid line (———).

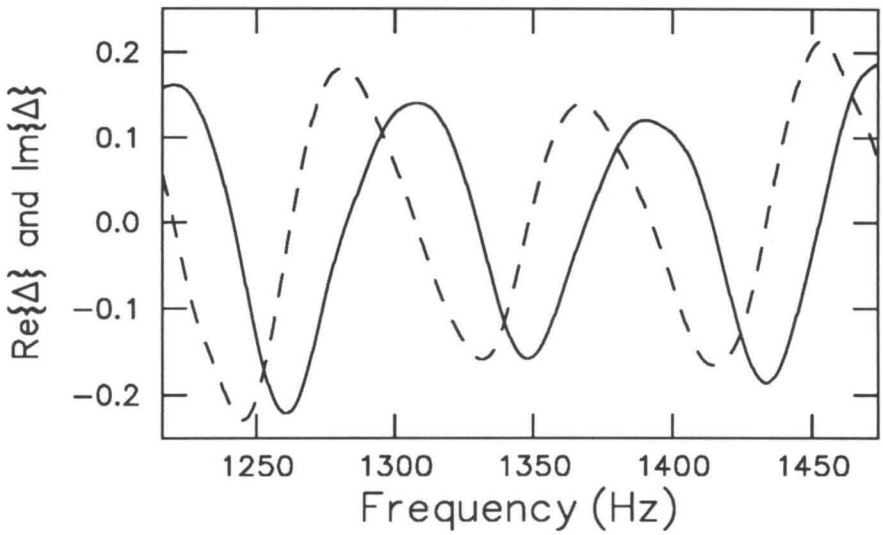

Figure 11. The function $\Delta(\omega) \equiv \rho/\rho_0 - 1$ obtained using the bandlimited interpolants from Fig. 10. The real and imaginary parts are represented, respectively, by solid (———) and dashed (— — —) lines. Note that the amplitude and frequency of the oscillations are nearly constant and the real and imaginary parts approximately 90° out of phase.

impedance,[9] defined as the ratio of the pressure difference $P(x,\omega)$ across the organ of Corti to the volume velocity $U(x,\omega)$ of the cochlear fluids in the scala vestibuli:

$$Z(\omega) \equiv \left.\frac{P}{U}\right|_{x=0;\ \text{cochlea driven forward}} . \tag{13}$$

The position $x = 0$ corresponds to the basal end of the organ of Corti. At moderate intensities, the cochlear response varies strongly with A (Kemp 1979); at high intensities ($A > A^{\mathrm{I}}$), however, the relative amplitude of those nonlinear contributions is always small (Kemp and Chum 1980; Zwicker and Schloth 1984), and the ratio P/U becomes independent of the amplitude of the stimulating tone.

Thus, at stimulus amplitudes $A > A^{\mathrm{I}}$ and frequencies $\omega \ll \omega_{c_0}$, where ω_{c_0} is the characteristic angular frequency at the beginning of the organ of Corti ($x = 0$), the basal turn of the cochlea is analogous to a linear, one-dimensional mechanical transmission line (Zwislocki-Mościcki 1948; Peterson and Bogert 1950; Zweig 1991) with an input impedance,

$$Z(\omega) \equiv Z_{\mathrm{c}}(\omega), \quad \text{for } A > A^{\mathrm{I}} , \tag{14}$$

depending principally on mechanical characteristics and cochlear geometry near the stapes (Shera and Zweig 1991a). The stimulus amplitude A^{I} corresponds to roughly 60 dB above threshold (Zwicker and Schloth 1984).

At lower intensities, however, the response near the stapes contains significant contributions from more apical regions of the cochlea. Measurements of evoked otoacoustic emissions (e.g., Zwicker and Schloth 1984) indicate that their amplitude varies linearly with the stimulus at low sound-pressure levels (see also Sec. II.A). In this low-amplitude linear regime, the input impedance has the form

$$Z(\omega) = Z_{\mathrm{c}}\frac{1 + R(\omega)}{1 - R(\omega)} , \quad \text{for } A < A_{\mathrm{l}}, \tag{15}$$

familiar from transmission-line theory (e.g., Slater 1942). The amplitude A_{l} corresponds to roughly 5–10 dB above threshold in humans.

---

[9] Here we assume that the cochlear contents are essentially incompressible (Shera and Zweig 1992c).

Equation (15) follows (Shera and Zweig 1991b) from the observation that measurements of the cochlear input impedance in cat (Lynch et al. 1982) imply that the wavelength of the traveling pressure wave—or, equivalently, the characteristic impedance $Z_c(\omega)$ of the transmission line—changes slowly in the basal turn (Shera and Zweig 1991a). The tapering symmetry that guarantees a slowly-changing wavelength is assumed applicable to the human cochlea as well.[10]

The function $R(\omega)$, for which Eq. (15) constitutes a definition, is the traveling-wave ratio evaluated at the basal end of the cochlear spiral. Note that the high-amplitude input impedance $Z_c(\omega)$ is recovered in the limit $R \to 0$; reflections are negligible at those intensities. The following section focuses on finding the form of R in the low-level linear regime.

V. Finding the Form of R

A. A series representation for ρ

The expectation of finding $|R|$ less than unity suggests expanding ρ in a power series about $R = 0$. Equation (7) implies that Z_{ec} constitutes a bilinear transform of Z, which, according to Eq. (15), is but a bilinear transform of R. When combined with Eq. (5) for ρ, those sequential bilinear transforms imply that the power series has the form

$$\rho/\rho_0 = 1 \; + \; pR\big(1 \; + \; qR \; + \; q^2R^2 \; + \; \cdots\big) \; , \tag{16}$$

where the smooth background is recovered as the limit

$$\rho_0 = \lim_{R\to 0} \rho \; . \tag{17}$$

The coefficients have the values

$$\rho_0 = \frac{Y Z^0_{ec}}{1 + Y_s Z^0_{ec}} \; ; \tag{18}$$

$$p = \frac{2Z_c/Z^0_{ec}}{\big(d + cZ_c\big)^2\big(1 + Y_s Z^0_{ec}\big)} \; ; \tag{19}$$

and

[10] Relaxing the assumption of tapering symmetry and adopting the more general expression for the input impedance valid when the cochlear wave impedances depend on the direction of propagation (Shera and Zweig 1991b) changes only the values of the coefficients and not the form of the power series for ρ obtained as Eq. (16) below.

$$q = 1 - \frac{2Z_c(aY_s + c)}{(d + cZ_c)(1 + Y_s Z_{ec}^0)} \,. \tag{20}$$

In these expressions,

$$Y \equiv Y^+ e^{i\omega T} \,, \tag{21}$$

and

$$Z_{ec}^0 \equiv \frac{aZ_c + b}{cZ_c + d} \,. \tag{22}$$

Note that the coefficients ρ_0, p, and q are determined by the characteristics of the measurement equipment, ear canal and middle-ear, and the basal region of the cochlea near the stapes. By contrast, the traveling-wave ratio R provides information about mechanical characteristics and possible spatial inhomogeneities in more apical regions of the cochlea close to the characteristic-frequency point (Shera and Zweig 1992f).

B. Interpreting the power series

Convergence of the power series requires $|qR| < 1$. By reexpressing the power series in the equivalent language of middle-ear scattering coefficients (Shera and Zweig 1992b), one can show that the coefficient q represents the net reflection coefficient for retrograde cochlear waves measured at the stapes. Assuming the middle ear to be a passive mechanical system therefore yields the constraint $|q| \leq 1$. Note that q is close to one at frequencies for which the source admittance Y_s is small and the middle-ear "stiff" (so that $|cZ_c| \ll 1$).

The function qR therefore represents the product of two reflection coefficients, both evaluated at the stapes but measured by driving the system in opposite directions. Note that terms in the power series proportional to R^2 or higher vanish in the limit that the stapes represents a perfectly reflectionless boundary (i.e., in the limit $|q| \to 0$). That observation suggests that those terms arise from multiple reflection within the cochlea.

The series expansion (16) for ρ obtained above is consistent with the spectrum illustrated in Fig. 9. Adjacent spectral peaks correspond to terms in ρ proportional to R, R^2, and R^3. The progressive decrease in peak amplitude provides ex-post-facto justification for the series expansion (16) performed above. Inspection shows that the peaks are approximately colinear, implying that their amplitudes occur in geometric progression, as predicted by Eq. (16).

In terms of the power-series expansion, the oscillatory component assumes the form

$$\Delta = pR(1 + qR + q^2R^2 + \cdots) . \tag{23}$$

Note for future reference that

$$\ln \Delta = \ln p + \ln R + \ln(1 + qR + q^2R^2 + \cdots) \tag{24}$$

$$\approx \ln p + \ln R + qR \quad (|qR| \ll 1) ; \tag{25}$$

as shown later, the inequality for $|qR|$ is valid for the measurements reported here.

C. An approximate form for R

The real and imaginary parts of Δ are plotted against one another in Fig. 12. The roughly circular trajectory traced out clockwise about the origin in the complex plane indicates that the oscillations in the real and imaginary parts of Δ are roughly 90° out of phase and of nearly constant amplitude and frequency. As shown above, Δ is, to leading order, equal to pR, where the coefficient p—determined by characteristics of the recording system, middle-ear, and cochlea near the stapes—is likely to vary slowly with frequency compared to $R(\omega)$.[11]

To first approximation, therefore, $\Delta \propto R$. The traveling-wave ratio then has the form of a circular path of slowly-varying radius centered on the origin in the complex plane and traced out with nearly constant angular velocity as the frequency is varied uniformly. In the language of mathematics, [12]

$$R \approx \bar{R} e^{-i[(\omega-\omega_0)\tau+\phi_0]} , \tag{26}$$

---

[11] In this context, a function $y(f)$ varies slowly with frequency if its fractional change over a typical period of oscillation Δf is small; that is, if

$$\Delta f \left| \frac{d \ln y}{df} \right| \ll 1 . \tag{11.1}$$

For the frequency region near 1 kHz, $\Delta f \approx 90$ Hz.

[12] Globally, $R(\omega; A)$ has the form

$$R(\omega; A) = |R|(\omega; A) e^{i\theta(\omega;A)} , \tag{12.1}$$

where $|R|$ and θ are, respectively, the real-valued amplitude and phase. The requirement that the Fourier transform of $Z(\omega; A)$ be real imposes the symmetry

$$R^*(-\omega; A) = R(\omega; A) , \tag{12.2}$$

and, consequently, $|R|$ and θ are even and odd functions of frequency, respectively.

where the radius $\bar{R}(\epsilon\omega)$ and "velocity" $\tau(\epsilon\omega)$ are both real, slowly-varying functions of frequency ($\epsilon \ll 1$); the phase shift ϕ_0 is a real constant. The reference frequency ω_0 emphasizes the local nature of the approximation.[13] Note that $1/\tau$ is simply the oscillation period Δf. A phenomenological model for evoked emissions incorporating a traveling-wave ratio with constant amplitude and linear phase has been proposed by Kemp (1980).

Note that the procedure used to extract the background ρ_0 may have filtered out any slowly-varying DC component R_0 in the traveling-wave ratio, which (if that component is large) might therefore be more appropriately written

$$R \approx R_0 + \bar{R}e^{-i[(\omega-\omega_0)\tau+\phi_0]} , \tag{27}$$

where $R_0(\epsilon\omega)$ is a slowly-varying complex function of frequency. Geometrically, R_0 reflects a possible offset of the circular trajectories from their apparent center about the origin.

Although the experiments reported here do not constrain the magnitude of such a component, other observations suggest that it is small. For example, measurements of stimulus-frequency emissions (e.g., Zwicker and Schloth 1984) indicate that low-level emission curves oscillate about an "average" given by the corresponding emission curve, appropriately rescaled, measured at high levels. (Our own measurements at higher levels, when controlled for temporal shifts in the background, corroborate those findings.) No significant DC-offset connected with R_0 is apparent. In addition, since R_0 is slowly-varying, the corresponding group velocity—given by $d(\angle R_0)/d\omega$—is, by hypothesis, much shorter than τ. Any component R_0 in the traveling-wave ratio would therefore contribute a short-latency response to measurements of click- or tone-burst-evoked otoacoustic emissions. No such component is observed in human ears (e.g., Kemp and Brown 1983).[14] Thus, if those measurements are correct (and the coefficients ρ_0, p, and q are, as expected, essentially independent of stimulus amplitude),

$$|R_0/\bar{R}| \ll 1 ; \tag{28}$$

the procedure employed here then captures the dominant contributions to R.

---

[13] When fitting the data, the reference frequency ω_0 also serves to decrease the sensitivity of the phase shift ϕ_0 to changes in the parameter τ.

[14] A short-latency component has, however, been identified in the gerbil (Kemp and Brown 1983).

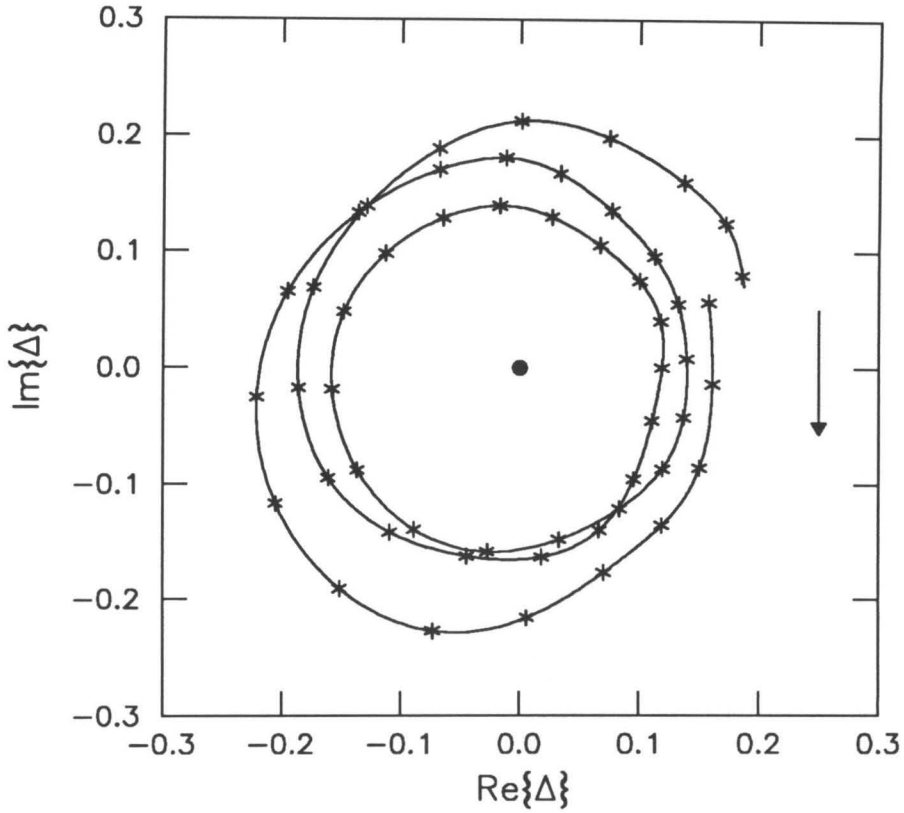

Figure 12. The real versus the imaginary part of $\Delta(\omega)$ for varying ω obtained by replotting the data of Fig. 11. The roughly circular trajectory, traversed clockwise about the origin (arrow), is marked with an asterisk ($*$) at intervals of approximately 5 Hz.

D. Consequences of the approximate form for R

To explore the predictions of the approximate form (26) for R, it is helpful to substitute it into Eq. (25) for $\ln \Delta$:

$$\mathrm{Re}\{\ln \Delta\} = \mathrm{Re}\{\ln p\} \; + \; \bar{R} \; + \; |q|\bar{R}\cos[(\omega - \omega_0)\tau + \phi] \; + \; \cdots \, , \tag{29}$$

and

$$\mathrm{Im}\{\ln \Delta\} = \mathrm{Im}\{\ln p\} \; - \; [(\omega - \omega_0)\tau + \phi_0] \; - \; |q|\bar{R}\sin[(\omega - \omega_0\tau) + \phi] \; + \; \cdots \, , \tag{30}$$

where

$$\phi = \phi_0 - \angle q \, . \tag{31}$$

For comparison, the empirical determination of $\ln \Delta$ is plotted in Fig. 13. If the functions $\ln p$, $\bar{R}$, and q are slowly-varying, $\mathrm{Re}\{\ln \Delta\}$ consists of a nearly constant background upon which oscillations of amplitude $|q|\bar{R}$ and approximate period $1/\tau$ are superposed. Such oscillations, shifted 90° in phase, appear also in $\mathrm{Im}\{\ln \Delta\}$, but in this case superposed on a line of slope $-\tau$.

Equations (29) and (30) for the real and imaginary parts of $\ln \Delta$ suggest that an especially convenient representation of the data can be obtained by differentiating, which also serves to remove much of the unknown, but slowly-varying background. We therefore define the dimensionless function

$$\eta \equiv \frac{d \ln \Delta}{d\Omega} \approx \frac{d \ln R}{d\Omega} \; + \; q\frac{dR}{d\Omega} \, , \tag{32}$$

where the dimensionless frequency Ω is defined by

$$\Omega \equiv \tau\omega \, . \tag{33}$$

By using the approximate form (26) for R and the assumption that $\bar{R}$ and τ are slowly varying one finds

$$\eta \approx \underbrace{|q|\bar{R}\cos[(\omega - \omega_0)\tau + \phi]}_{\mathrm{Re}\{\eta\}} \; - \; i \underbrace{\left[1 + |q|\bar{R}\sin[(\omega - \omega_0)\tau + \phi]\right]}_{\mathrm{Im}\{\eta\}} \, , \tag{34}$$

Thus, if the approximate form (26) is correct, η is a causal function whose real and imaginary parts oscillate with a period of $1/\tau$ Hz and with an amplitude $|q|\bar{R}$. Note that

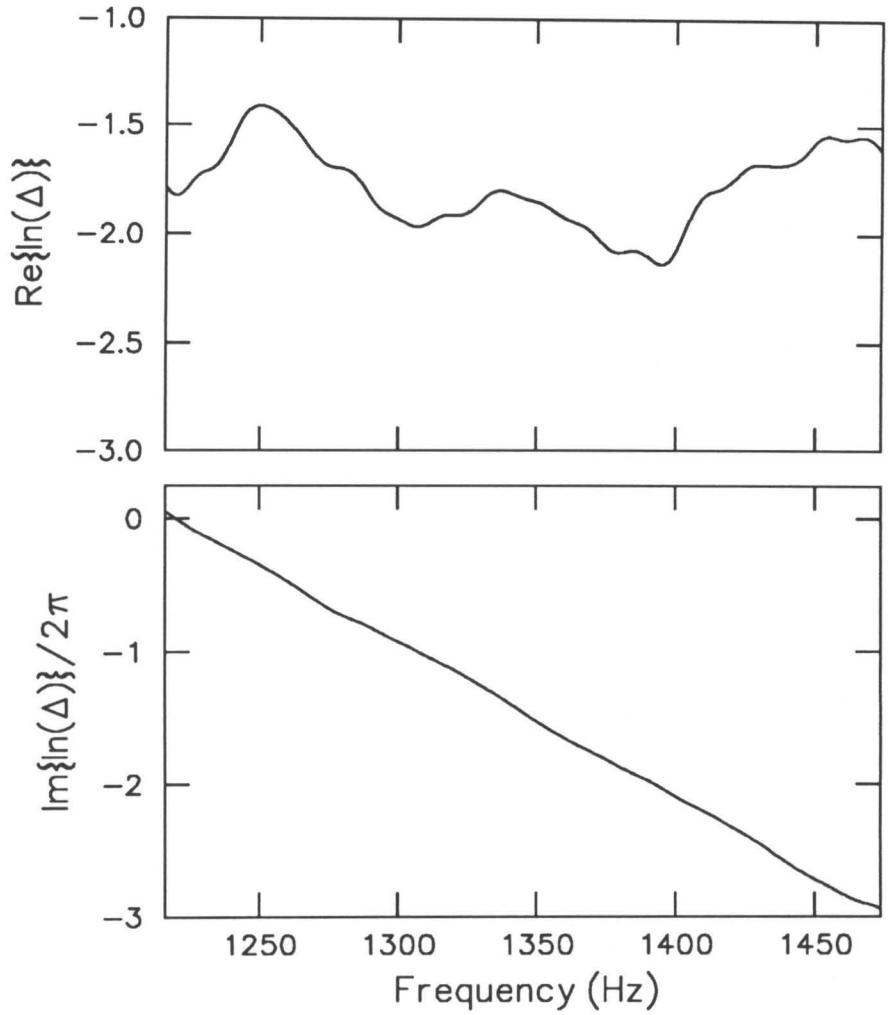

Figure 13. The function $\ln \Delta(\omega)$ computed using $\Delta(\omega)$ from Fig. 11. The real part (———) consists of oscillations superimposed upon a nearly constant background. Similar oscillations, shifted 90° in phase, appear in the imaginary part (— — —), but superimposed upon a line of nearly constant slope $-\tau$. The straight line in the phase indicates the presence of a delay.

the model predicts that $\mathrm{Im}\{\eta\}$ oscillates about the average value -1. These predictions can be compared with experiment by computing η from the empirical determination of Δ.

Figure 14 plots the function η obtained by differentiating the data of Fig. 13. The dimensionless frequency Ω was defined using the value $\tau = 11.73 \pm 0.05$ ms obtained from the estimate (12) for the oscillation period Δf. Since differentiation amplifies high-frequency noise components, the function shown has, for clarity, been low-pass filtered to suppress higher-order terms in η (e.g., those proportional to R^2 or higher[15]). Note that $\mathrm{Im}\{\eta\}$ oscillates about the value -1, as predicted by Eq. (34) using the approximate form (26) for R.

Shown for comparison are the predictions of Eq. (34), where the parameters $\bar{R}$, τ and q were assumed constant over the interval before fitting the data (parameter values are given in the figure caption). The agreement between the empirical η and the model result implies that the foregoing analysis, including the approximate local form for R, is essentially correct.

E. Errors and averages

An indication of the errors in the analysis is provided by Fig. 15, which overlays Fig. 14 with the function η computed from the other data set illustrated in Fig. 6. The small differences between the curves originate principally with changes induced in the background by the low-frequency temporal shifts discussed in Sec. II. The Appendix discusses the magnitude of the systematic errors introduced by the choice of filter used to extract the smooth background ρ_0.

Figure 16 overlays Fig. 15 with functions η computed from measurements on the same subject made several months later. Figure 17 plots the average and its standard deviation computed from Fig. 16. Averaging model fits to the data yields the parameter estimates: $|q|\bar{R} = 0.124 \pm 0.01$, $\tau = 11.67 \pm 0.1$ ms, and $\phi = 2.17 \pm 0.2$ radians. Note that no explicit model for the effects of the background is included in Eq. (34). The background provides a slowly-varying, secular variation in the average value of the curves and thus affects, for example, the optimal choice of the amplitude $|q|R_0$.

[15] Note that terms in η of order R^2 correspond to terms in Δ of order R^3.

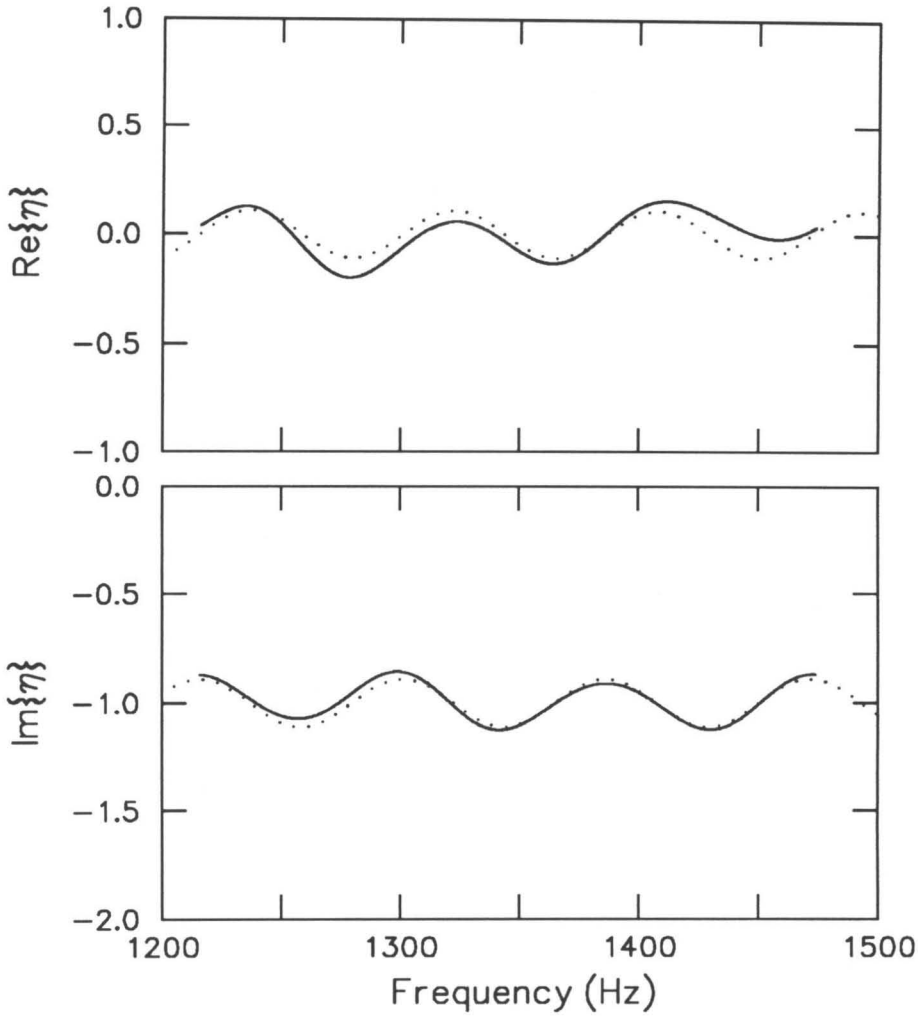

Figure 14. The function $\eta(\omega)$ computed from Eq. (32) and the data of Fig. 13 (———). For clarity, the function was filtered to remove high-frequency noise. Shown for comparison are the predictions of Eq. (34) with parameter values $|q|\bar{R} = 0.11$, $\tau = 11.6$ ms, and $\phi = 2$ radians, determined by a least-squares fit to the data (real and imaginary parts simultaneously). For this data set, the reference frequency ω_0 was taken to have the value $\omega_0/2\pi = 1350$ Hz. Note that Eq. (34) predicts that the imaginary part oscillates about -1, in agreement with the empirical result.

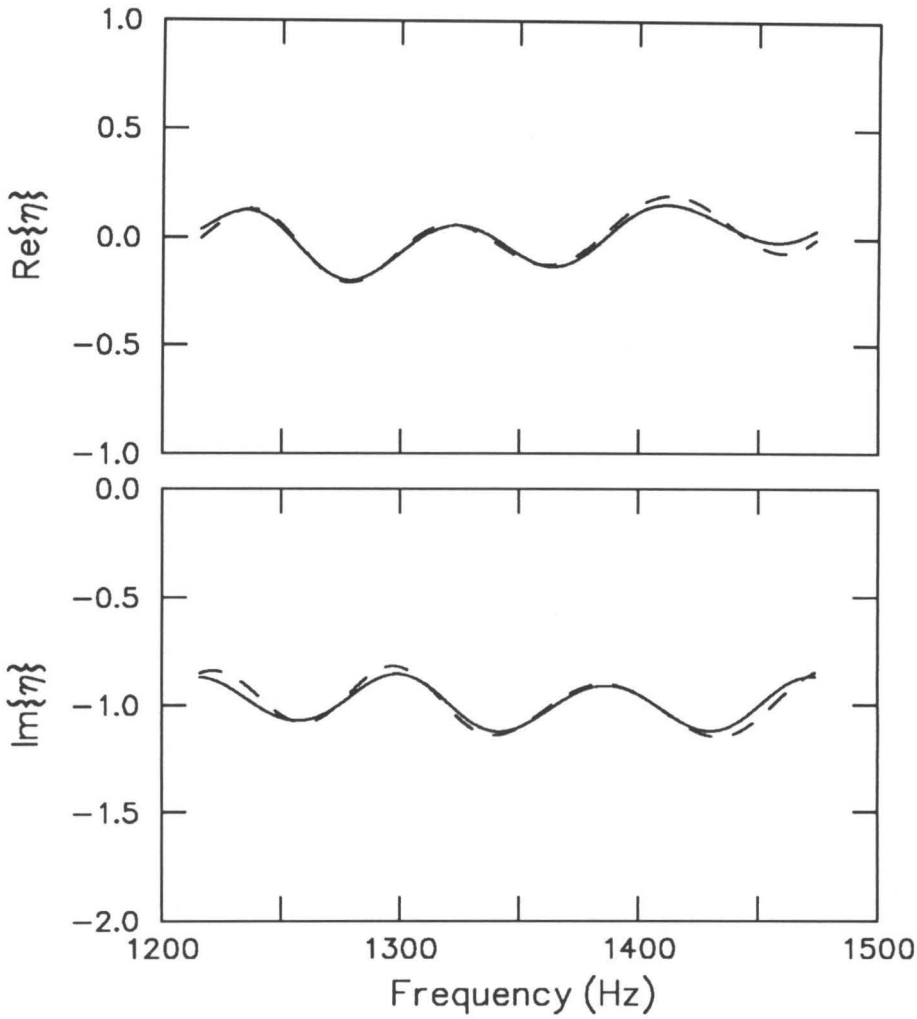

Figure 15. The function $\eta(\omega)$ computed using the data at 0 dB SL from Fig. 6 (— — —). For comparison, the values are shown superimposed on the data from Fig. 14. The differences between the curves, originating principally through changes in the slowly-varying background caused by temporal drift, are small and give an indication of the uncertainty in the analysis.

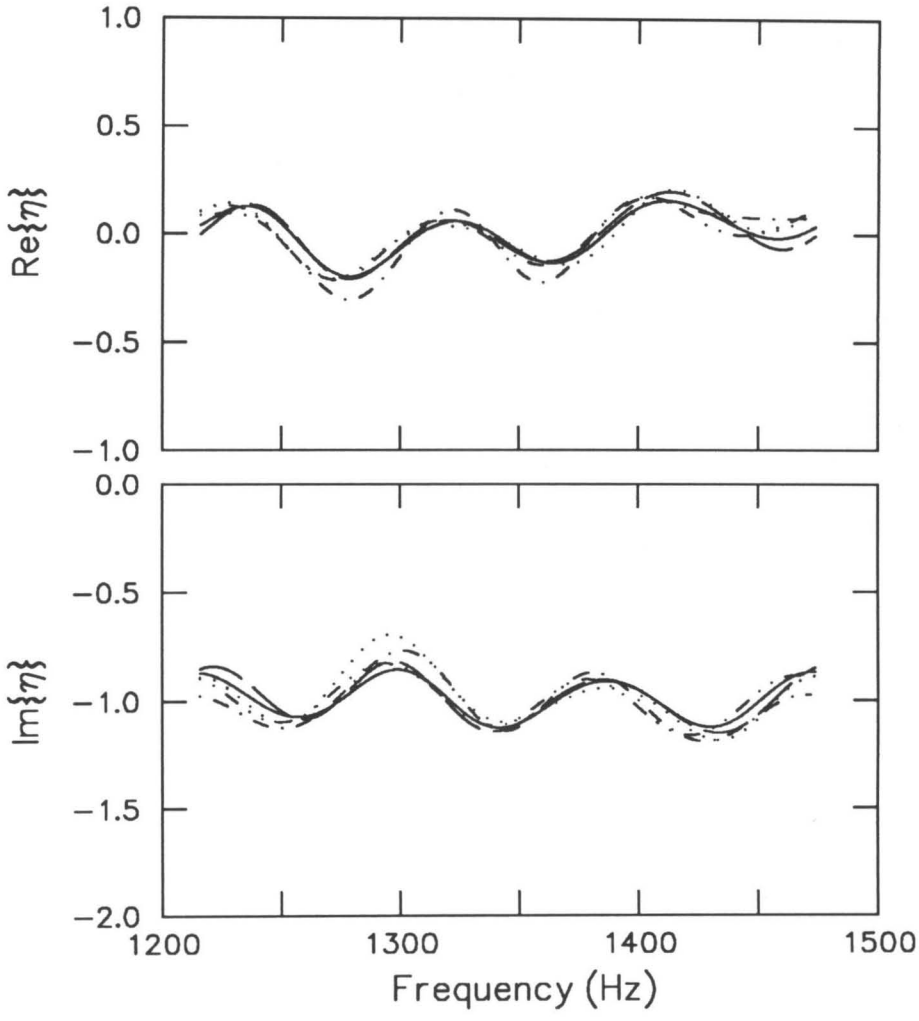

Figure 16. Functions $\eta(\omega)$ computed using three additional measurements of ρ made in the low-level linear regime on the same subject several months later (shown with dotted, dot-dashed, and dot-dot-dashed lines). For comparison, the functions are shown superimposed on those from Fig. 15.

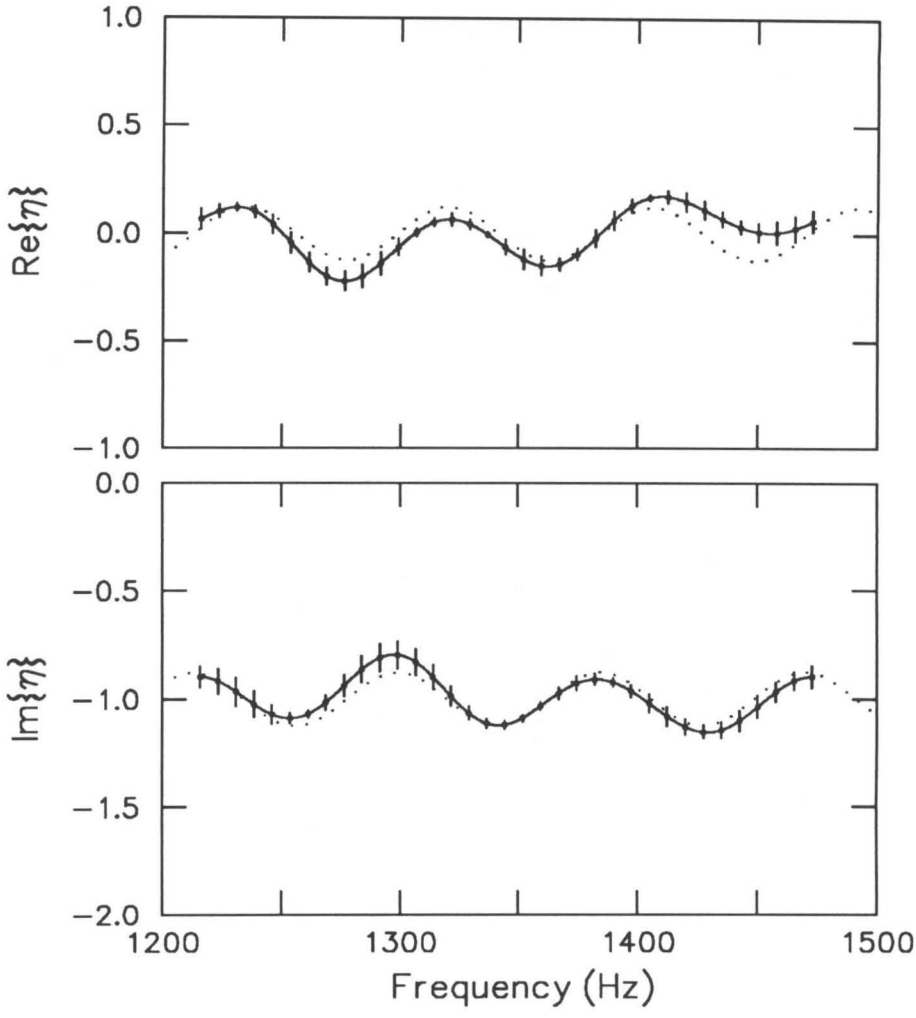

Figure 17. An estimate (———) of the function $\eta(\omega)$ computed by averaging the functions shown in Fig. 16 and plotted with error bars representing standard deviations. Fitting the model of Eq. (34) separately to each of the five data sets and averaging the results yields the parameter estimates given in the text. Shown for comparison (·····) are the predictions of the model using those average parameter values.

F. A consistency check

In verifying the predictions of the empirical form (26) of the traveling-wave ratio, we have determined an estimate of the product qR, which can be expressed in terms of η through Eq. (34):

$$qR \approx \mathrm{Re}\{\eta\} \; - \; i[1 + \mathrm{Im}\{\eta\}] \; . \tag{35}$$

Power series (23) for $\rho(\omega)$ predicts that knowledge of qR determines all higher-order terms in the expansion.

Verification of that prediction is simplified by noting that the empirical form for R implies the existence of a one-to-one correspondence between terms in the power series and spectral peaks in the Fourier transform of $\rho(\omega)$. That correspondence follows from the fact that the Fourier transform of $e^{-i\omega\tau}$ is proportional to the δ-function $\delta(t - \tau)$. Consequently, the power series predicts that spectral peaks should occur in geometric progression, with the ratio of adjacent peaks assuming the approximate value

$$\frac{(\mathrm{peak})_{n+1}}{(\mathrm{peak})_n} \approx \langle |q| \bar{R} e^{i(\omega_0 \tau - \phi)} \rangle \tag{36}$$

The angled brackets indicate that the Fourier transform has "averaged" the parameters over the transformed frequency interval. Thus, when plotted on the appropriate scales, the spectral peaks should be approximately colinear.

Figure 18 reproduces the amplitude and phase of the spectrum of $\mathrm{Im}\{\rho(\omega)\}$. Shown for comparison are straight lines whose slopes were determined from Eq. (36) using parameter values from the model fit to the function η shown in Fig. 14. The foregoing analysis correctly predicts both the approximate colinearity and the complex ratio of adjacent spectral peaks. By reducing the measurement noise floor even further, one could presumably verify the predictions for spectral peaks of even higher order.

G. Estimating q and $\bar{R}$ individually

The amplitude of the oscillations in η depend on the amplitude of the traveling-wave ratio through the expression $|q|\bar{R}$, where $|q|$ depends on unknown properties of the middle-ear. If $|q|$ is close to one, however, the oscillation amplitude is determined principally by the value of $\bar{R}$. Figure 19 shows values of $|q|$ predicted by published models of the "average"

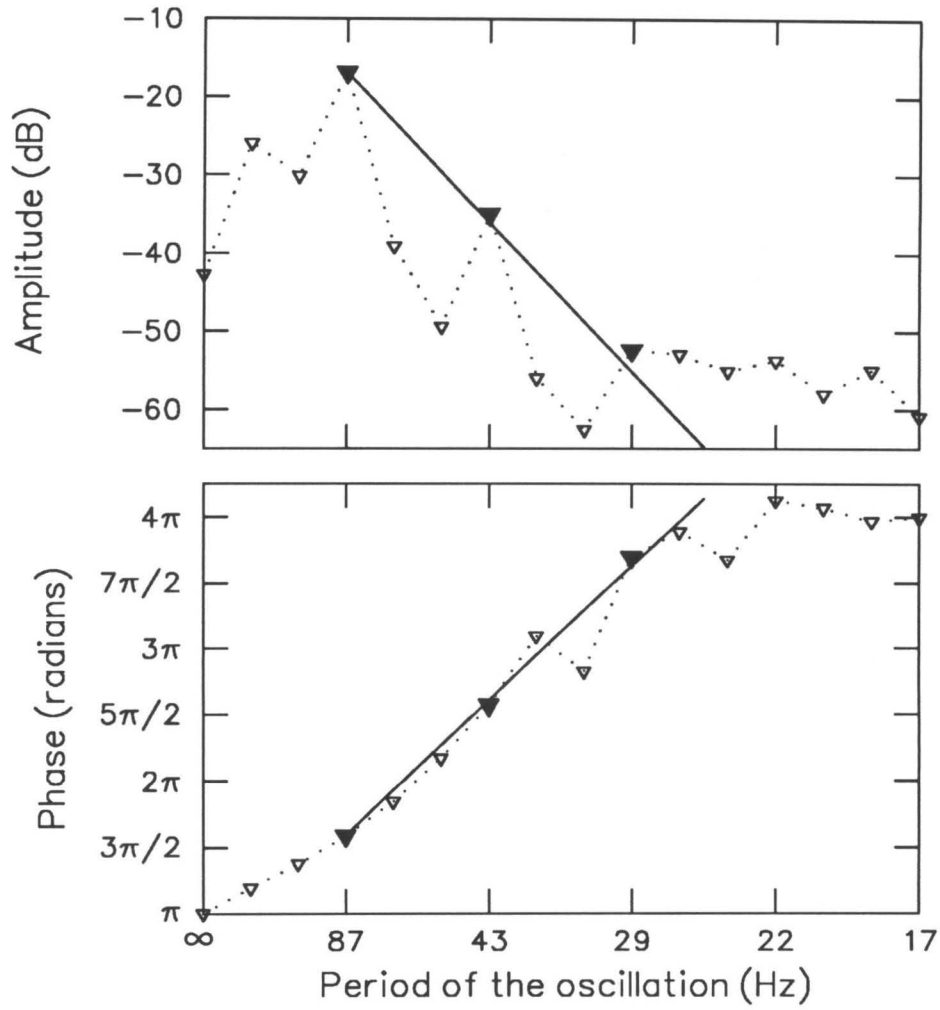

Figure 18. The inverse Fourier transform $\widehat{F}^{-1}\{\mathrm{Im}\{\rho(\omega)\}\}$ ($\triangledown$ connected by $\cdots\cdots$) from Fig. 9 (similar results, omitted for clarity, are obtained using $\widehat{F}^{-1}\{\mathrm{Re}\{\rho(\omega)\}\}$). The spectral peaks corresponding to harmonics of the oscillation period are shown with enlarged solid symbols. The analysis presented above predicts that those peaks occur in geometric progression and should therefore appear colinear on the scales used here. Straight lines, with slopes obtained using the parameter values of Fig. 14, are superimposed for comparison.

human middle ear (Zwislocki 1962; Kringlebotn 1988). Although their predictions differ in detail, the models are in qualitative agreement and predict that q is a slowly-varying function everywhere close to but less than one in magnitude. Reference to Eq. (20) shows that q would be exactly one were the source admittance Y_s zero and the middle-ear perfectly "stiff;" that is, were the eardrum a rigid plate and the ossicular joints rigid (Shera and Zweig 1991c; Shera and Zweig 1992a).

Since $|q| \lesssim 1$, the value $|q|\bar{R} \approx 0.12$ determined from the data thus provides a lower limit on the amplitude of the traveling-wave ratio. Assuming that the middle-ear model predictions are roughly accurate for this subject yields the estimate $|q| \approx 0.7$ in the frequency range of the measurements. Thus, $\bar{R} \approx 0.16$–0.18 in this subject. (The uncertainty reflects only the approximate uncertainty in the determination of the product $|q|\bar{R}$; the uncertainty in $|q|$ is not known.) The corresponding standing-wave ratio, which gives the approximate ratio of the cochlear pressure at a node to that at an antinode, is related to R by

$$\mathrm{SWR} = \frac{1+|R|}{1-|R|}, \tag{37}$$

and is therefore roughly 1.4 near the stapes.

H. Anomalies and other subjects

The analysis above has focused on determining the form of R in a region where ρ has a simple, regular structure. Reference to Fig. 4 indicates, however, that the periodic pattern can fluctuate somewhat erratically and is interrupted by regions where the regular pattern is distorted. Those general features are also found in measurements on other ears. Typical results are given in Figs. 20–25, which illustrate representative measurements of ρ, demonstrate its minimum-phase analyticity properties, and give the corresponding functions η. Although the empirical functions η tend to have more structure than the simple form Eq. (34)—reflecting either an incomplete removal of the background or deviations in R from the approximate form given by Eq. (26)—the data from all subjects support the conclusion that, within the more regular regions, the amplitude of R varies relatively slowly (and nonperiodically) with frequency compared to the phase, in general agreement with the idealized form (26). Figures 24 and 25 provide an example of data collected from an anomalous region flanked by regions of greater regularity. Such regions may reflect underlying anomalies in the mechanical inhomogeneities conjectured to give rise to evoked emission (Manley 1983; Lonsbury-Martin et al. 1988; Shera and Zweig 1992f).

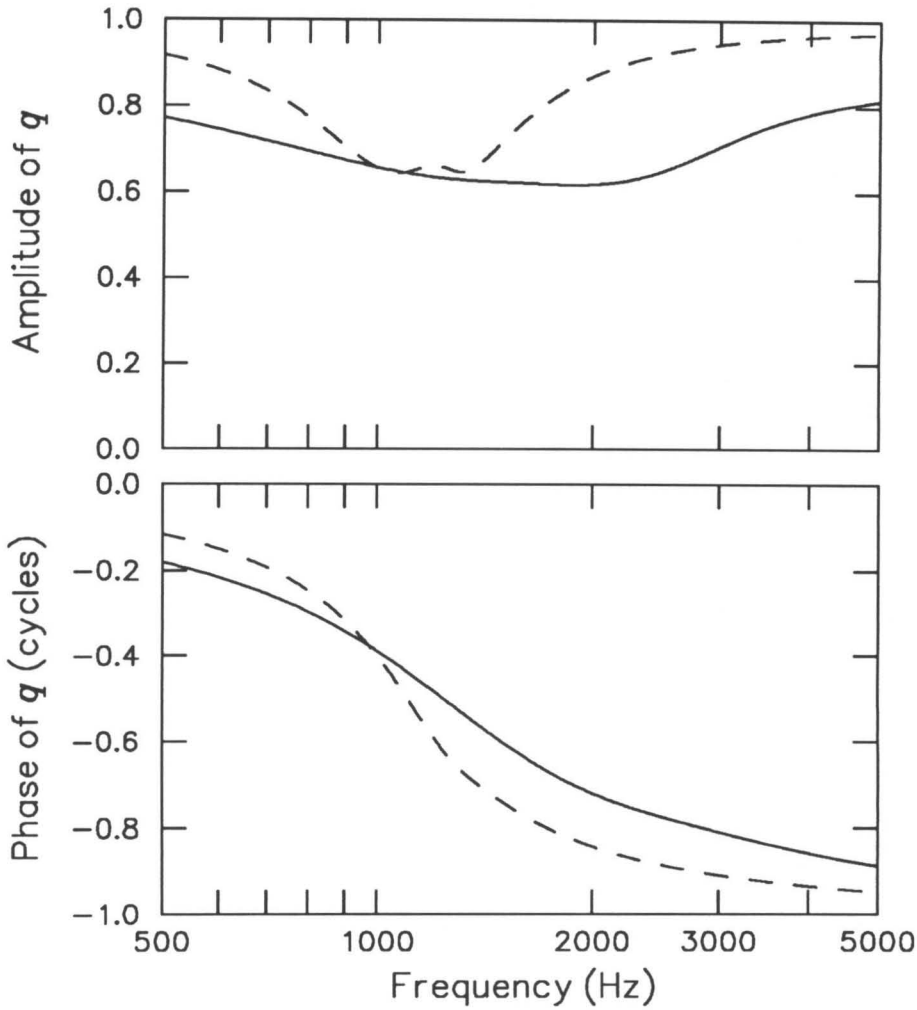

Figure 19. The function $q(\omega)$ predicted by the middle-ear models of Zwislocki (———) and Kringlebotn (— — —). The residual ear-canal space was modeled as a rigid-walled tube of length 1 cm and cross-sectional area 0.4 cm^2. The calculations assume that the source admittance Y_s is zero; more realistic values yield very similar results. Note that q approaches one at low frequencies where the eardrum and ossicular joints become "stiff." The models agree in their prediction that q is everywhere close to but less than one in magnitude.

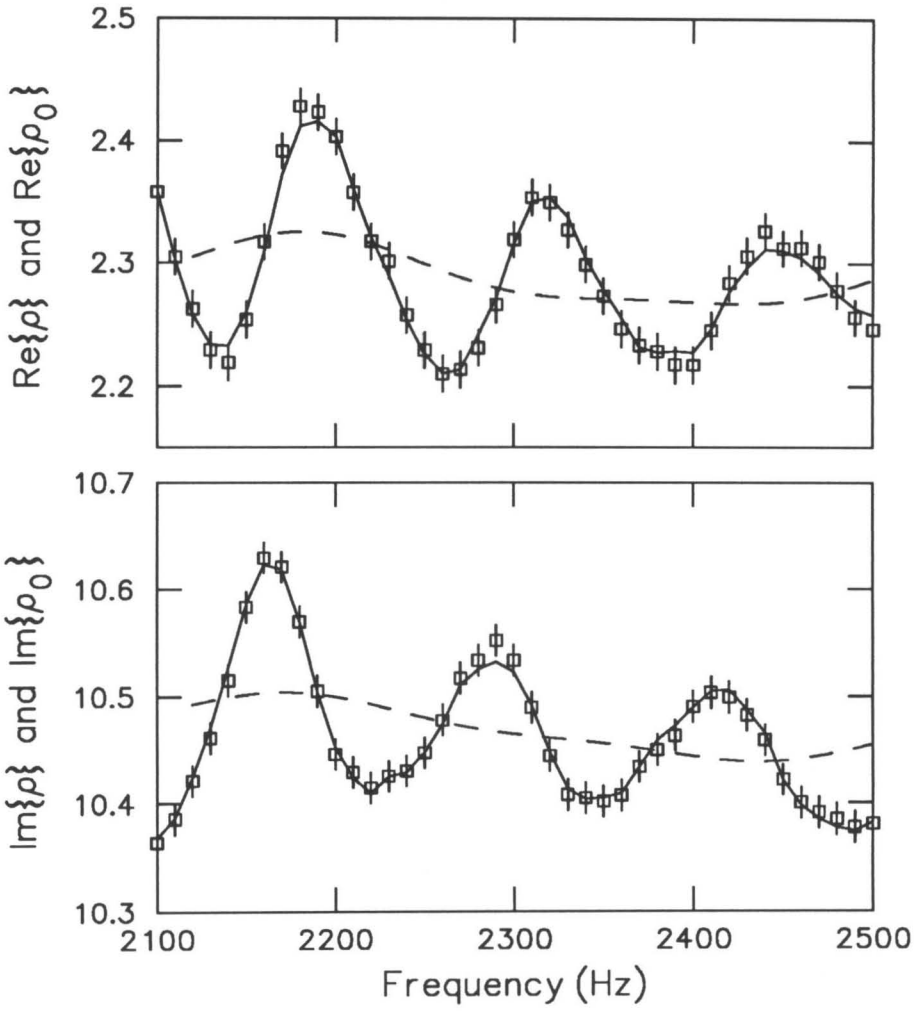

Figure 20. Measurements of $\ln \rho$ in subject CKL-R at approximately 5 dB SL together with smoothed, minimum-phase fits (———) to the measurements. The error bars correspond to 0.125 dB in the amplitude and 0.8° in the phase. The dashed line (— — —) represents the estimate of $\ln \rho_0$ obtained by filtering.

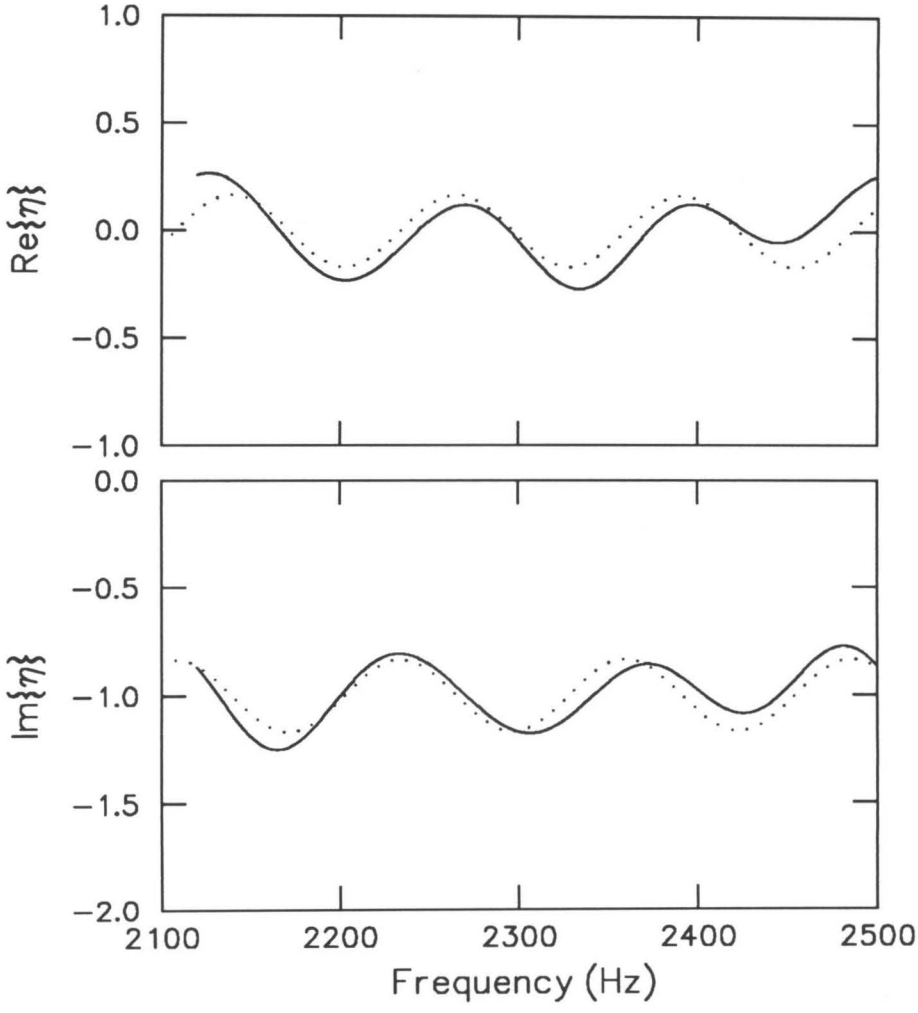

Figure 21. The function $\eta(\omega)$ computed from the data of Fig. 20 (———) and filtered to remove high-frequency noise. Shown for comparison (·····) are the predictions of Eq. (34) with parameter values $|q|\widetilde{R} = 0.17$, $\tau = 7.9$ ms, and $\phi = 1.7$ radians. The reference frequency ω_0 has the value $\omega_0/2\pi = 2300$ Hz.

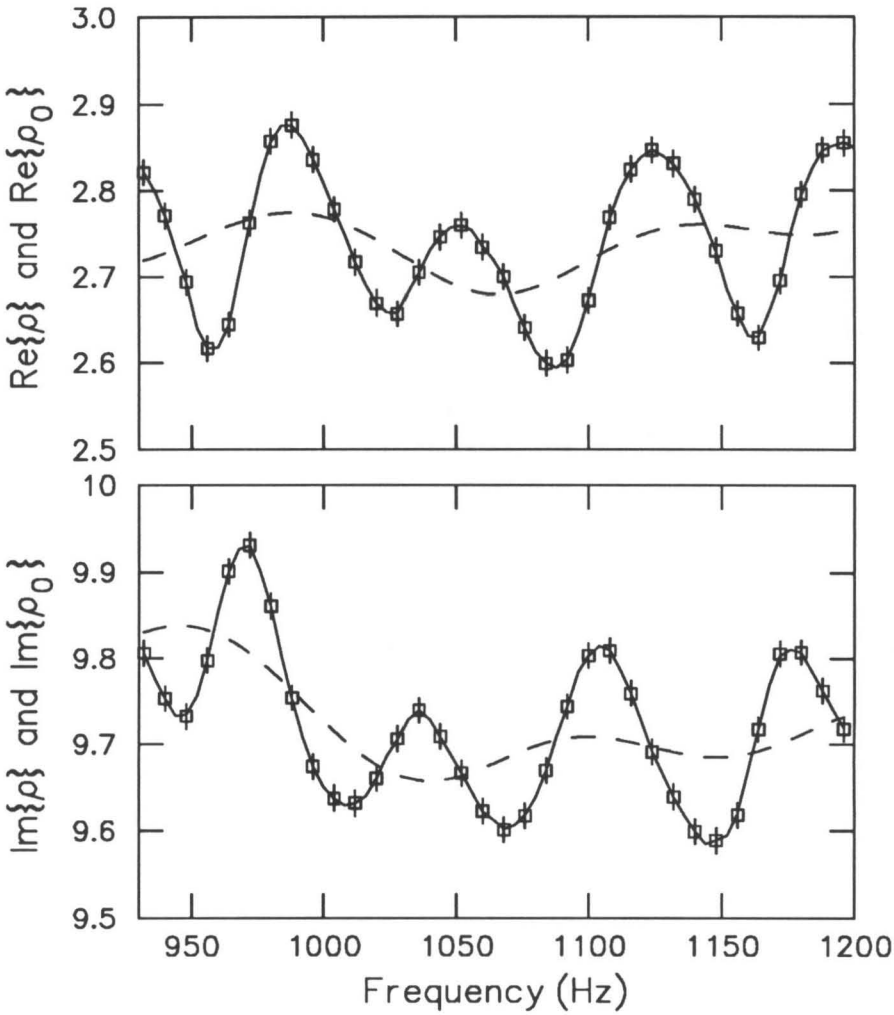

Figure 22. Measurements of $\ln \rho$ in subject CKL-L at approximately 5 dB SL together with smoothed, minimum-phase fits (———) to the measurements. The error bars correspond to 0.125 dB in the amplitude and 0.8° in the phase. The dashed line (— — —) represents the estimate of $\ln \rho_0$ obtained by filtering.

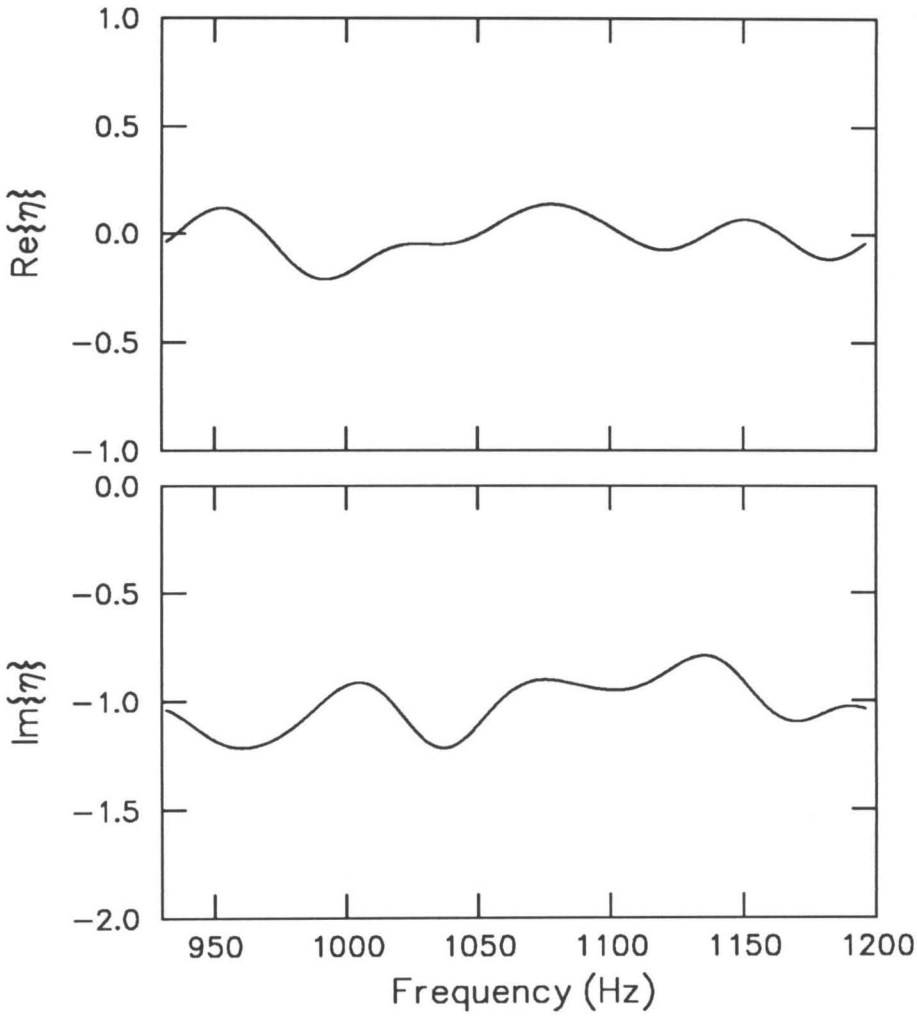

Figure 23. The function $\eta(\omega)$ computed from the data of Fig. 22 (———) and filtered to remove high-frequency noise.

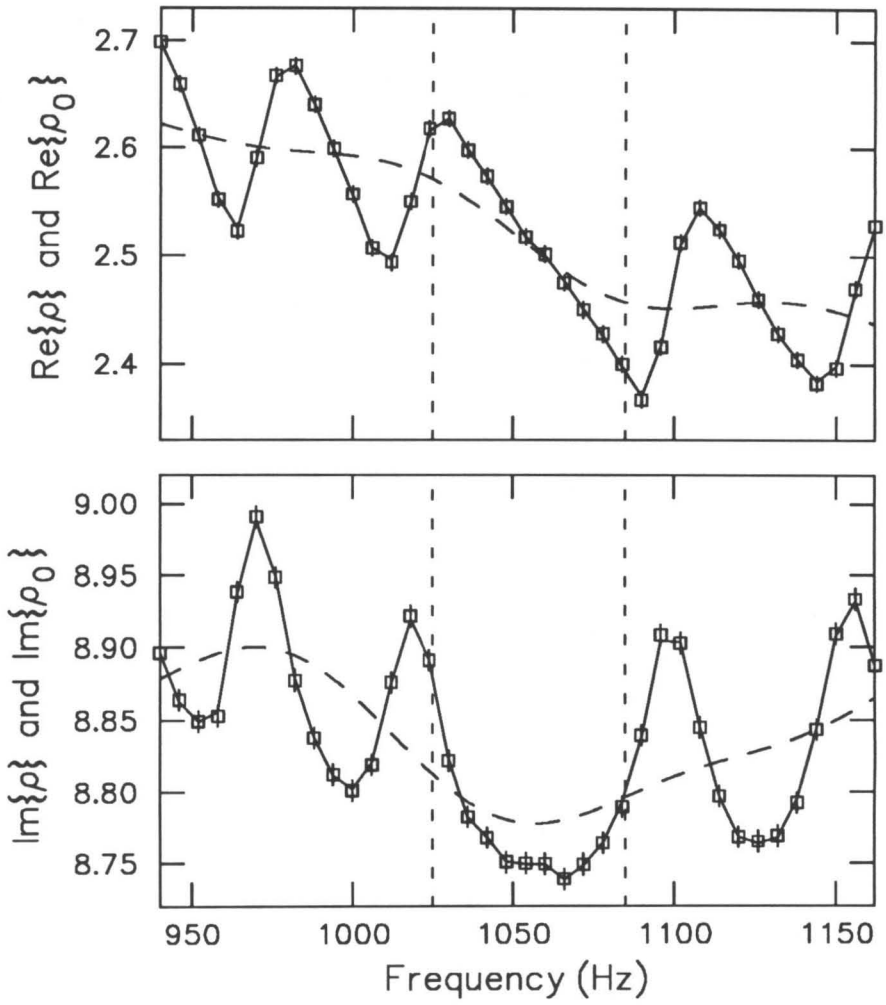

Figure 24. Measurements of $\ln \rho$ in subject MGC-R at approximately 5 dB SL together with smoothed, minimum-phase fits (———) to the measurements. The error bars correspond to 0.06 dB in the amplitude and 0.4° in the phase. The dashed line (— — —) represents the estimate of $\ln \rho_0$ obtained by filtering. Note the presence of an anomalous region, centered about 1050 Hz and delimited by short-dashed lines, flanked by regions of more regular behavior.

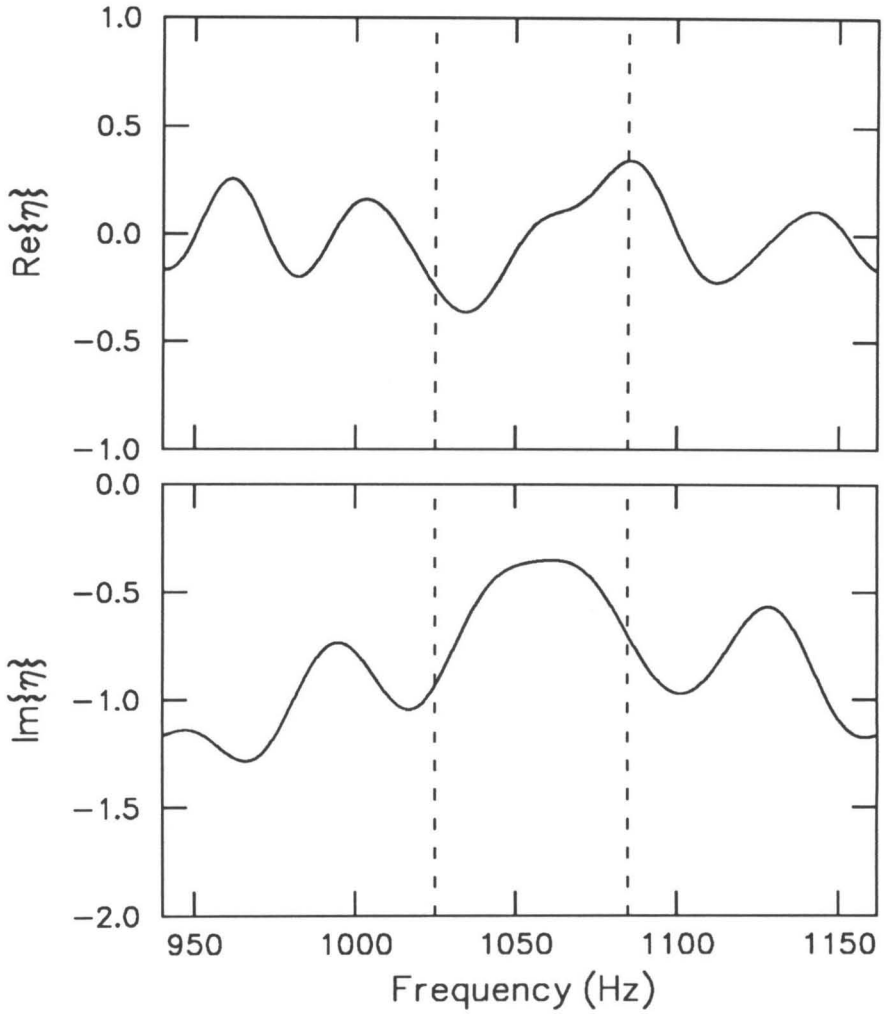

Figure 25. The function $\eta(\omega)$ computed from the data of Fig. 24 (———) and filtered to remove high-frequency noise. The anomalous region centered near 1050 Hz divides the data into two regions flanked by intervals of more regular behavior. The parameter $\tau \approx 22$ ms used in the computation was estimated from the data to the left of the anomaly.

VI. Discussion

A. Interpreting the approximate form for R

The amplitude of the cochlear traveling-wave ratio is a relatively slowly-varying and nonperiodic function of frequency, suggesting that the mechanical inhomogeneities responsible for wave reflection are uncorrelated with the periodicities observed in the microstructure of threshold hearing curves. Although the amplitude of R varies slowly, its phase rotates rapidly. The observed periodicities thus arise predominantly from the sinusoidal variation in relative phase between the forward- and backward-traveling waves at the stapes; as the frequency varies monotonically, the phase $e^{-i\omega\tau}$ passes alternately through plus and minus one, giving rise to the peaks and valleys in the measured ear-canal pressure [cf. Eq. (1)].

In the time domain, the locally linear phase corresponds to a delay, presumably given by the round-trip travel time to and from the site of generation of the backward-traveling wave (Neely et al. 1988). The values τ found here are consistent with emission latencies reported elsewhere (e.g., Norton and Neely 1987).

1. Variation of the delay with frequency

The approximate variation of τ with frequency can be obtained as follows. Measurements of the latency L of tone-burst-evoked emissions indicate that the travel time varies inversely with frequency (Wilson 1980; Norton and Neely 1987; Zweig et al. 1992), suggesting that the emissions originate in a relatively small region of the cochlea appropriate to their frequency, presumably near the peak of the corresponding transfer function (Shera and Zweig 1992f). Consistency with the latency measurements thus requires

$$L \approx \frac{d\theta}{d\omega} \propto 1/\omega \,, \tag{38}$$

where θ denotes the phase of R. Contributions to the latency arising from the middle ear have been assumed small. Solving the differential equation for θ yields,

$$\theta(\omega) = 2\pi\alpha \ln(\omega/\omega_{c_0}) \,, \tag{39}$$

where α is a real integration constant and ω_{c_0} is the maximum frequency represented along the organ of Corti. Although introduced as in integration constant, α may vary slowly with frequency.

One thus obtains an approximate local form for $R(\omega)$ incorporating the more global variation in latency with frequency:

$$R(\omega) \approx R_1 e^{-2\pi i \alpha \ln(\omega/\omega_{c_0})} , \tag{40}$$

where R_1 is a slowly-varying real function of frequency.

One can recover the local empirical form (26) in any neighborhood by expanding the phase,

$$\theta = 2\pi\alpha \ln(\omega/\omega_{c_0}) , \tag{41}$$

in a Taylor series about some arbitrary reference frequency ω_1:

$$\theta(\omega) = \theta(\omega_1) \; + \; \left.\frac{d\theta}{d\omega}\right|_{\omega_1} (\omega - \omega_1) \; + \; \cdots . \tag{42}$$

Evaluating the derivative yields,

$$\theta(\omega) \approx \theta_1 \; + \; 2\pi\alpha(\omega - \omega_1)/\omega_1 , \tag{43}$$

where $\theta_1 \equiv \theta(\omega_1)$ is a constant and the derivative $d\alpha/d\omega$ is, by definition, small and has therefore been neglected. In a neighborhood about ω_1 the traveling-wave ratio therefore has the approximate form

$$R(\omega) \approx R_1 e^{-i\theta_1} e^{-i(\omega-\omega_1)\tau_1} , \equiv R_1' e^{-i(\omega-\omega_1)\tau_1} , \tag{44}$$

where R_1' is slowly-varying, and the local delay τ_1 has the value

$$\tau_1 = 2\pi\alpha/\omega_1 . \tag{45}$$

B. Another way of measuring the background?

This paper has introduced a filtering technique for separating the oscillatory component in the measured ear-canal pressure from the smooth background determined, among other things, by unknown characteristics of the middle ear. The method, outlined in the Appendix, requires only a single measurement at low sound-pressure levels, thereby allowing each measurement to serve as its own control, both against shifts in the background that occur during the course of the measurement and against nonlinearities in the stimulus-delivery and recording system.

The vanishing of the oscillatory component with increasing intensity seen in Fig. 4 suggests defining an alternative background, denoted ρ_∞, by the limit

$$\rho_\infty(\omega) \equiv \lim_{A\to\infty} \rho(\omega; A) \,, \tag{46}$$

where, in practice, the limit is achieved for stimulus amplitudes $A > A^1$.

The alternative background ρ_∞, which provides the basis for the "vector subtraction" method introduced by Kemp (Kemp 1979; Kemp and Chum 1980), was not employed here because a low-frequency temporal shift—perhaps due to static pressure changes in the middle-ear cavities, temperature variations in the recording microphone, or perhaps even an efferent modulation of cochlear mechanics—made it difficult to measure ρ_∞ with sufficient accuracy. If these speculations concerning the origin of the shift are correct, one expects it to originate either in the microphone transfer function K_o or in the middle-ear cavity impedance Z_{cav}, which manifests itself through the transfer coefficients $\left(\begin{smallmatrix} a & b \\ c & d \end{smallmatrix}\right)$ (Shera and Zweig 1992a). Note that if the shift arises predominantly through K_o, the functions p and q remain unaffected. It remains, however, an outstanding experimental question whether one can make the identification

$$\rho_0 \stackrel{?}{=} \rho_\infty \,. \tag{47}$$

VII. Summary

1. Accurate measurements of stimulus-frequency evoked otoacoustic emissions have been made in the low-level linear regime. Unlike the measurements reported by Zwicker and Schloth (1984), the measurements described here are consistent with both causal and minimum-phase behavior.
2. The measured response, expressed in the form of the dimensionless ratio $\rho(\omega)$, consists of an oscillatory component $\Delta(\omega)$ superimposed on a slowly-varying "background" ρ_0. A novel smoothing technique was developed and used to separate those two components. Whereas the background is determined principally by the acoustic properties of the recording system and middle-ear, the oscillatory component originates through the reflection of forward-traveling waves, presumably by mechanical inhomogeneities in the apical turns of the cochlea. The oscillatory component $\Delta(\omega)$ can be expressed

as a power series in the dimensionless traveling-wave ratio, $R(\omega)$, which provides a measure of the net reflected wave, relative to the forward-traveling wave, at the basal end of the cochlea near the stapes.

3. The extracted oscillatory component $\Delta(\omega)$ was analyzed to determine the principal frequency variation of $R(\omega)$, which was shown, locally, to have the approximate form

$$R(\omega) \approx R_0 + \bar{R}e^{-i[(\omega-\omega_0)\tau+\phi_0]}, \tag{48}$$

where $\bar{R}(\epsilon\omega)$ and $\tau(\epsilon\omega)$ are both real, slowly-varying functions of frequency ($\epsilon \ll 1$); the phase shift ϕ_0 is a real constant. Although the magnitude of any additional slowly-varying component $R_0(\epsilon\omega)$ is not determined by the measurements reported here, other published measurements suggest that $|R_0/\bar{R}| \ll 1$. Typically, $\bar{R} = O(1/5)$ and $\tau \approx 12$ ms at frequencies $\omega_0/2\pi$ near 1300 kHz. In individual subjects, the delay τ can be estimated with this technique to within a tenth of a millisecond.

4. The amplitude of the cochlear traveling-wave ratio is a relatively slowly-varying and nonperiodic function of frequency, suggesting that the distribution of inhomogeneities is uncorrelated with the periodicities observed in the microstructure of threshold hearing curves. Although the amplitude of R varies slowly, its phase rotates rapidly. As conjectured by Kemp (1980), the observed periodicities arise predominantly from the sinusoidal variation in relative phase between the forward- and backward-traveling waves at the stapes. The locally linear phase presumably arises as the result of wave propagation delays due to a total round-trip travel time τ from the stapes to the point of reflection and back again. A model in which the orderly, almost periodic pattern of maxima and minima in the spectra of evoked emissions emerges naturally from the scattering of cochlear waves by what may be an essentially random pattern of inhomogeneities in the organ of Corti is presented in a companion paper (Shera and Zweig 1992f).

Acknowledgments

The authors thank Jennifer McDowell for her invaluable assistance with the measurements and gratefully acknowledge her remarkable patience as an experimental subject. This work was supported, in part, by DARPA and AFOSR contract N00014-86-C0399, the Theoretical Division of Los Alamos National Laboratory, and a National Science Foundation Graduate Fellowship to C. A. S.

Appendix A: Smoothing to Extract the Background

This Appendix defines more explicitly the smoothing operation used to extract the background ρ_0.

Unlike the more familiar case of time-domain filtering, the oscillatory component to be removed occurs here in the frequency response. Smoothing involves convolving ρ, wiggles and all, with a smoothing function S of finite bandwidth (e.g., a Gaussian):

$$\rho_0 = S \otimes \rho \, . \tag{A1}$$

Here, the convolution is equivalent to a multiplication in the time domain. For example, let $F\{\cdot\}$ represent the operation of Fourier transformation and L the inverse Fourier transform of the smoothing function:

$$L = F^{-1}\{S\} \, . \tag{A2}$$

(Note that L will have a low-pass characteristic in the time domain.) Then

$$\rho_0 = F\{L \times F^{-1}\{\rho\}\} \, , \tag{A3}$$

when the width of the smoothing function (filter cutoff) is chosen appropriately.

Such filtering preserves the causal analyticity properties of ρ. Since ρ is causal (Fig. 8), the corresponding impulse response $F^{-1}\{\rho\}$ vanishes for negative times. So, therefore, does $L \times F^{-1}\{\rho\}$, implying that the function ρ_0 extracted in this way is also causal.[16]

Ideally, the filter L should have a sharp spectral cutoff (in this case, a sharp cutoff in the time domain) but avoid prolonged ringing in the impulse response (i.e., in the frequency response or smoothing function S). Here we approximate those ideal characteristics by employing one of a class of "recursive-exponential" filters L_n, defined by

$$L_n(t, t_c) \equiv 1/\Gamma_n(\lambda_n t/t_c) \, , \tag{A4}$$

[16] An estimate of ρ_0 guaranteed to have the same minimum-phase behavior as ρ is given by

$$\rho_0 = \exp\left[F\{L \times F^{-1}\{\ln \rho\}\}\right] \, . \tag{16.1}$$

Numerically, this estimate is essentially indistinguishable from the estimate obtained by filtering ρ directly.

where t_c is the filter cutoff and Γ_n is defined recursively:

$$\Gamma_{n+1} = e^{\Gamma_n - 1} , \quad \text{with} \quad \Gamma_1(t) = e^{t^2} . \tag{A5}$$

The scale factor λ_n is set by the requirement that the filter amplitude be $1/e$ at the cutoff point t_c:

$$\lambda_n = \sqrt{\gamma_n}, \text{ where } \gamma_{n+1} = \ln(\gamma_n + 1) \text{ with } \gamma_1 = 1 . \tag{A6}$$

The filters L_n have no poles or other unpleasantness to contribute exponentially-damped sinusoids to the impulse response.

The filters $L_n(t, t_c)$ are defined to have widths Δt such that $\Delta t / t_c = 1$. The width Δf of the corresponding smoothing function $S_n(f, f_c) = F\{L_n(t, t_c)\}$ satisfies

$$\Delta f / f_c \gtrsim 1/\pi , \tag{A7}$$

where $f_c \equiv 1/t_c$. The lower limit of the inequality is attained with the Gaussian smoothing function ($n = 1$).

As an example, the impulse response, or smoothing function $S_n(f, f_c)$ corresponding to the filter $L_n(t, t_c)$ is illustrated in Fig. A1 for two cases: a simple Gaussian (i.e., $n = 1$) and the 10th-order filter L_{10} used to extract ρ_0. Despite the sharp spectral cutoff (see Fig. 9), the smoothing function S_{10} displays little ringing (note the absence of ringing at the "cutoff-period" f_c in the function ρ_0 shown in Fig. 10).

Figures A2 and A3 indicate the nature of the systematic errors introduced into the analysis by the choice of smoothing filter. The figures plot the smooth background ρ_0 and the corresponding function η computed using the Gaussian smoothing function S_1. The results obtained in the text using the function S_{10} are given for comparison (results for orders $n > 2$ are essentially independent of n). The Gaussian filter leaves clearly visible oscillations in the background.

Although one might naively expect the amplitude of the oscillations in η to be reduced correspondingly, Fig. A3 shows that those oscillations have, if anything, increased. To understand this, consider the function $\rho(\omega; R)$ as a function of R. Ideally, smoothing should yield the background function $\rho(\omega; 0)$. If the spectral cut-off is insufficiently sharp, however, filtering will (to first order in R) instead yield the function $\rho(\omega; \epsilon R)$, where ϵ is

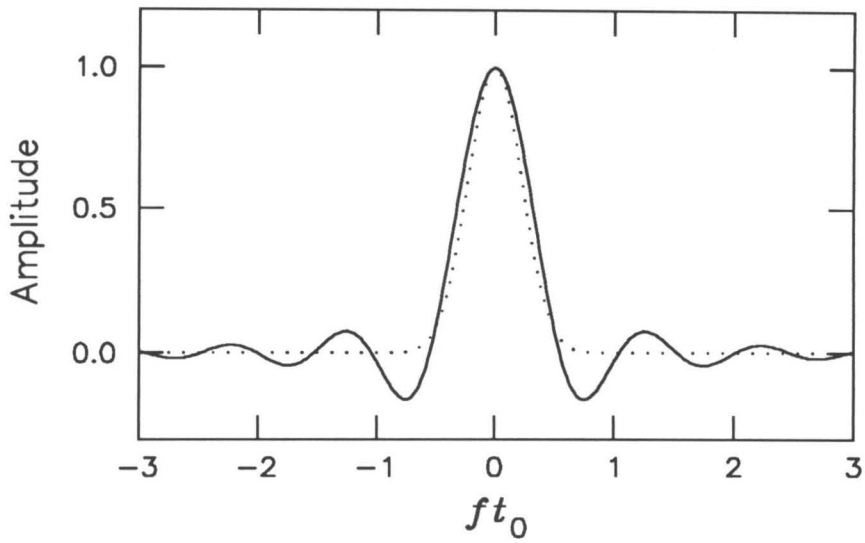

Figure A1. The smoothing function $S_n(f, f_c)$ representing the Fourier transform (impulse response) of the recursive-exponential filter $L_n(t, t_c)$ illustrated for two values of n: (———) smoothing function for the 10th-order filter L_{10} used to extract ρ_0; (·····) a Gaussian smoothing function, corresponding to $n = 1$. The abscissa represents the dimensionless frequency f/f_c, and the smoothing functions are normalized to a maximum value of one. Despite the sharp spectral cutoff (cf. Fig. 9), the smoothing function S_{10} displays only minimal ringing.

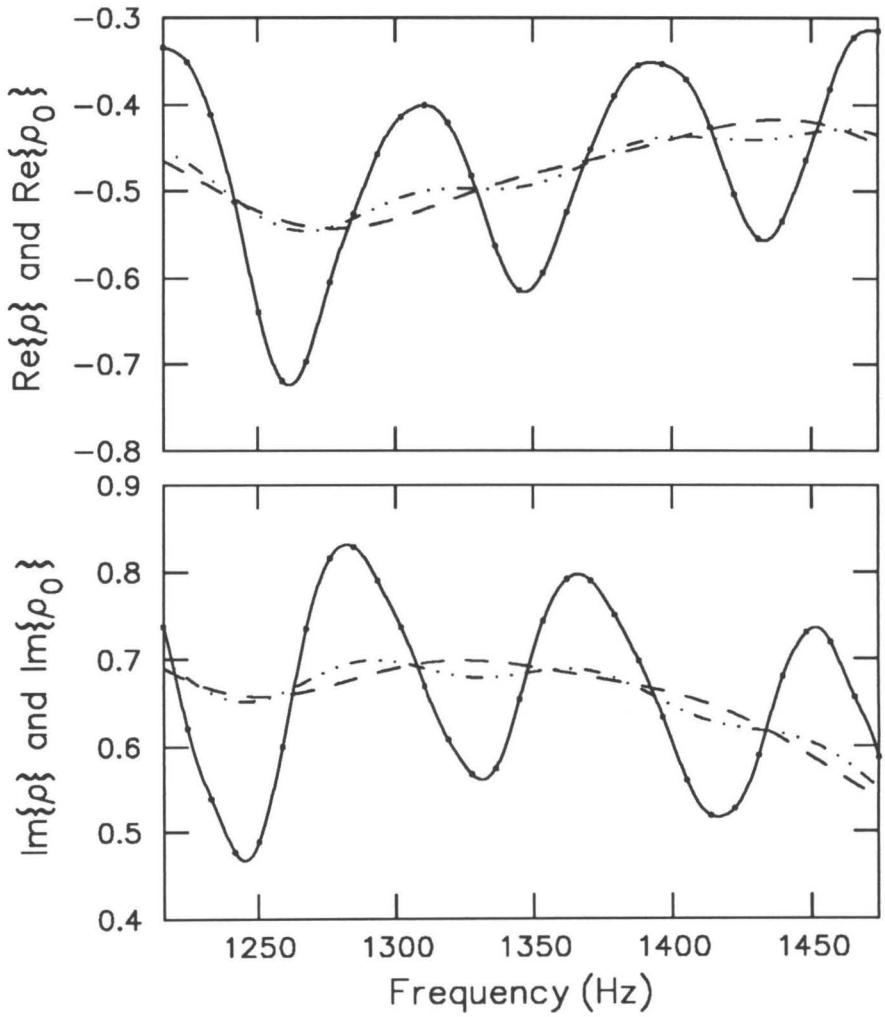

Figure A2. The background $\rho_0(\omega)$ obtained by (under)smoothing the data segment of Fig. 9 with the Gaussian smoothing function S_1 ($\cdots\!-\!\cdots$) using the cut-off period employed earlier (i.e., $f_c = 130$ Hz). Figure 10, superposed for comparison, plots ρ and the smooth background ρ_0 extracted using the function S_{10}.

nonzero but presumably small (with $0 \leq |\epsilon| \leq 1$). Although the oscillations in the corresponding function Δ, defined by $\Delta = \rho(\omega; R)/\rho(\omega; \epsilon R) - 1$, clearly decrease in amplitude, the same is not true of the logarithm. Indeed, taking the logarithm and expanding in power series yields [cf. Eq. (25)]

$$\ln \Delta \approx \ln[(1-\epsilon)p] + \ln R + (1+\epsilon)qR \quad \left(|qR| \ll 1\right) . \tag{A8}$$

The coefficient of the term proportional to R (and hence the amplitude of the oscillations in η) therefore increases with the filtering error ϵ. In the limit $\epsilon \to 1$, the oscillations in η have twice their proper amplitude.

Figures A4 and A5 illustrate the errors introduced by over (rather than under) smoothing. As above, the figures plot the background ρ_0 and the corresponding function η computed using the filter L_{10} and a cutoff period of 220 Hz. Although the resulting estimate of the background is probably too smooth, the function η remains relatively unaffected.

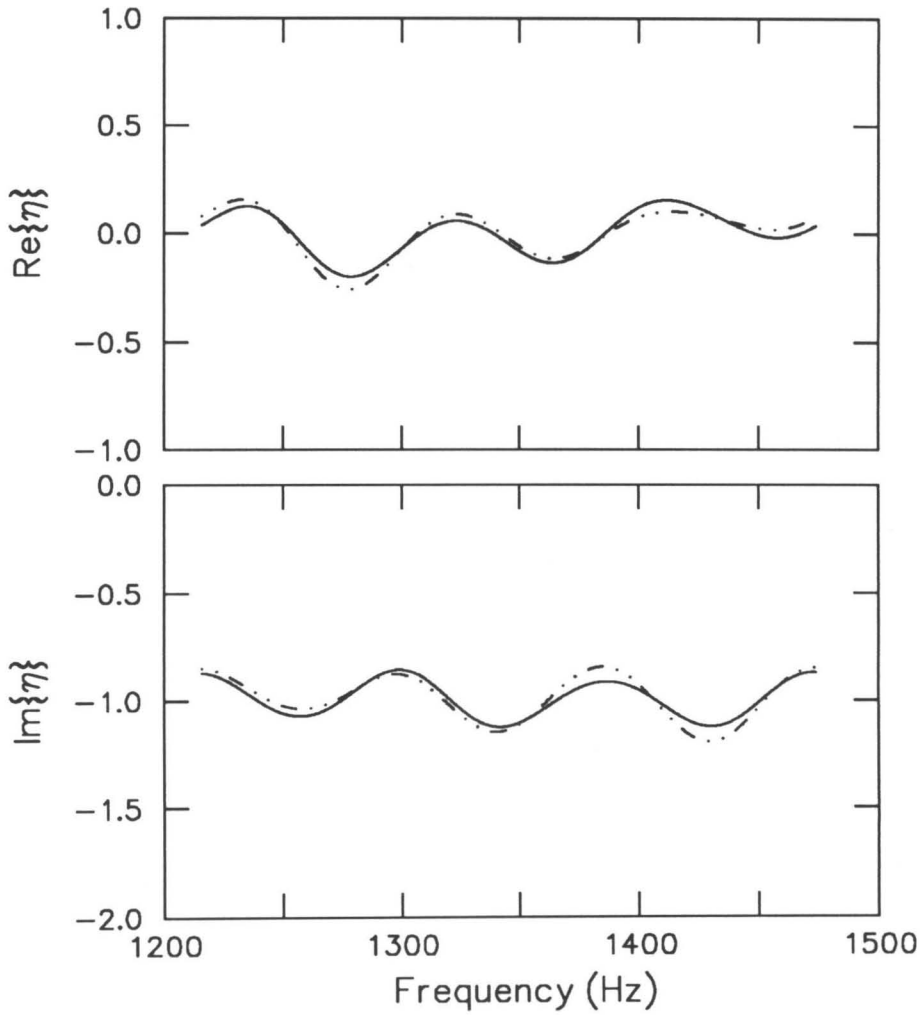

Figure A3. The function $\eta(\omega)$ computed using the background from Fig. A2 extracted using the Gaussian filter L_1 (· · — · · —). For comparison, the figure is shown superimposed on the data from Fig. 14, for which the background was extracted using the filter L_{10}. Although differences are small, the oscillations have generally increased slightly in amplitude.

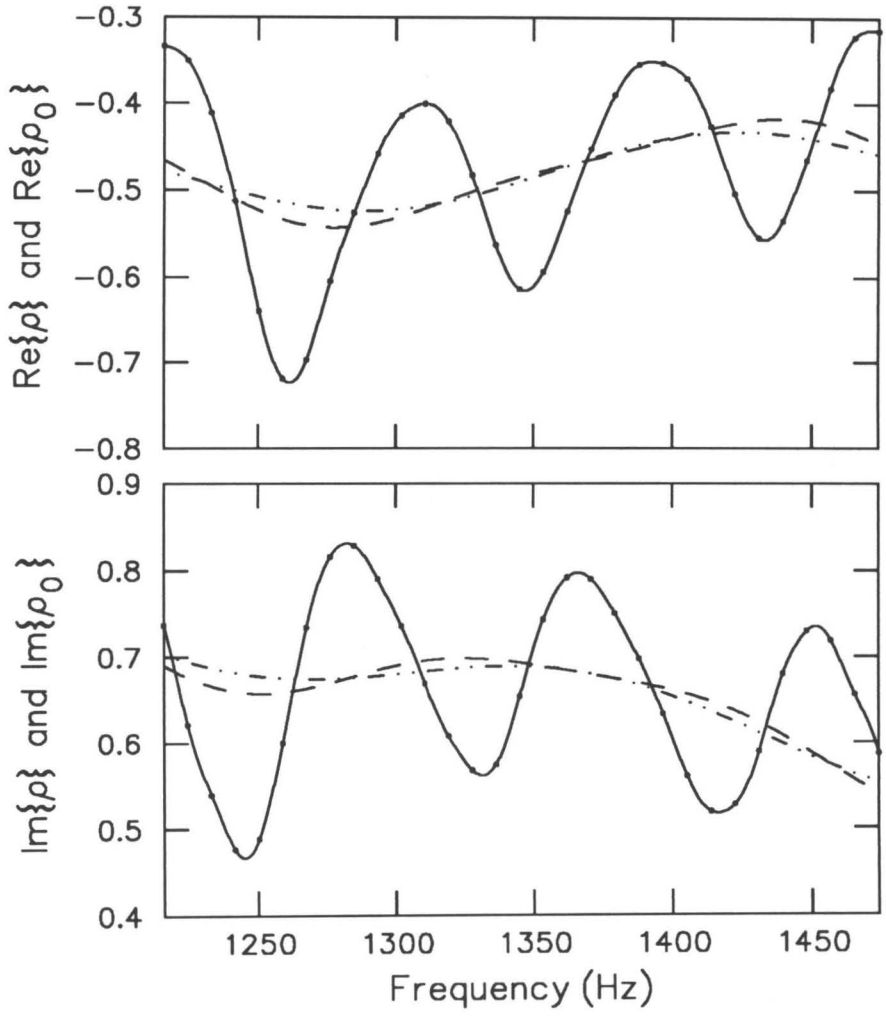

Figure A4. The background $\rho_0(\omega)$ obtained by filtering the data segment of Fig. 9 with the filter L_{10} using a cut-off period $f_c = 220$ Hz (·· — ·· —) so that the resulting background is considerably smoother. Figure 10, superposed for comparison, plots ρ and the background ρ_0 extracted using a cutoff period of 130 Hz.

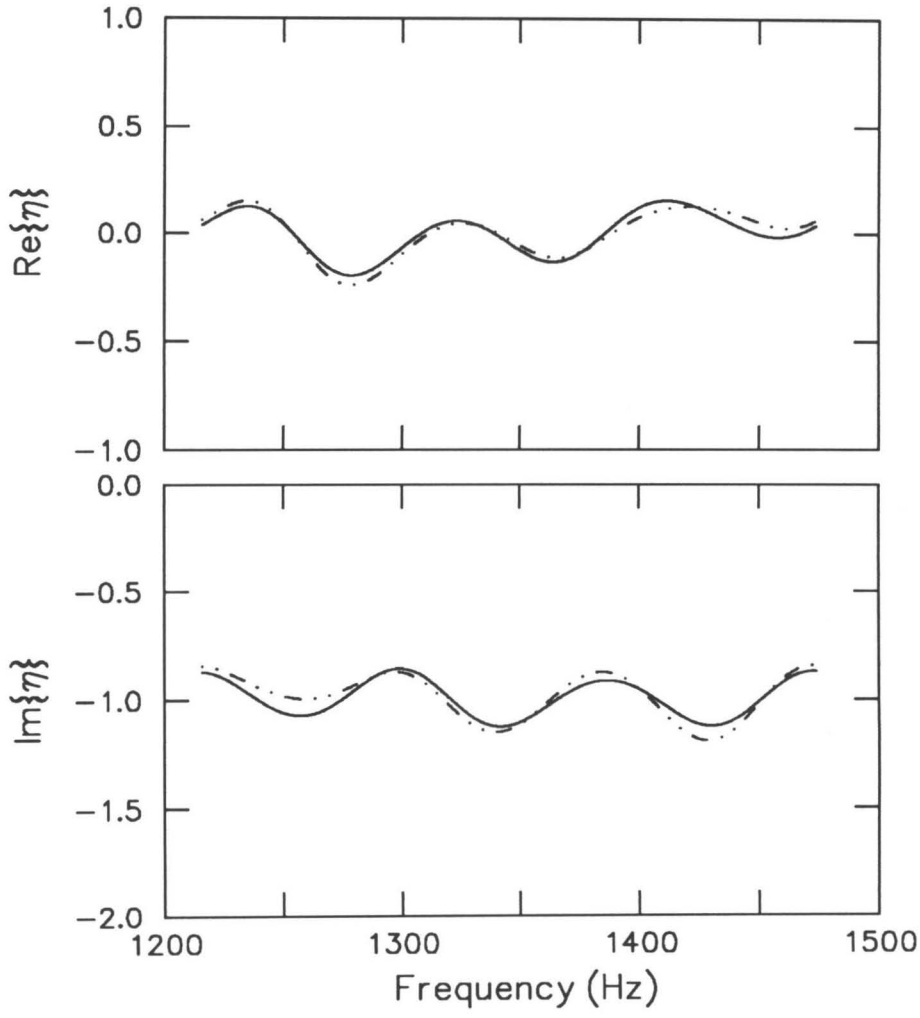

Figure A5. The function $\eta(\omega)$ computed using the (over)smooth background from Fig. A4 extracted using the filter L_{10} and a cutoff period of 220 Hz (·· — ·· —). For comparison, the figure is shown superimposed on the data from Fig. 14, for which the background was extracted using a cutoff period of 130 Hz.

References

von Békésy, G. (1960). *Experiments in Hearing.*New York: McGraw-Hill.

Blackham, R. C., J. A. Vasil, E. S. Atkinson, and R. W. Potter (1987). "Measurement modes and digital demodulation for a low-frequency analyzer," *Hewlett-Packard Journal* **38**(1), 17–25.

Bode, H. (1945). *Network Analysis and Feedback Amplifier Design.*Princeton: Van Nostrand Reinhold.

Elliot, E. (1958). "A ripple effect in the audiogram," *Nature* **181**, 1076.

Helmholtz, H. L. F (1863). *Die Lehre von den Tonempfindungen als physiologische Grundlage für die Theorie der Musik.*Braunschweig: Vieweg. Trans. by A. J. Ellis, *On the Sensations of Tone as a Physiological Basis for the Theory of Music.* New York: Dover, 1954.

Horst, J. W., H. P. Wit, and R. J. Ritsma (1983). "Psychophysical aspects of cochlear acoustic emissions ('Kemp tones').," in *Hearing — Physiological Bases and Psychophysics*, edited by R. Klinke and R. Hartmann, 89–94. Berlin: Springer Verlag.

Kemp, D. T. (1978). "Stimulated acoustic emissions from within the human auditory system," *J. Acoust. Soc. Am.* **64**, 1386–1391.

Kemp, D. T. (1979). "The evoked cochlear mechanical response and the auditory microstructure — Evidence for a new element in cochlear mechanics," *Scand. Audiol. Suppl.* **9**, 35–47.

Kemp, D. T. and R. A. Chum (1980). "Observations on the generator mechanism of stimulus frequency acoustic emissions — Two tone suppression," in *Psychophysical Physiological and Behavioural Studies in Hearing*, edited by G. Van Den Brink and F. A. Bilsen, 34–42. Delft: Delft University Press.

Kemp, D. T. (1980). "Towards a model for the origin of cochlear echoes," *Hearing Res.* **2**, 533–548.

Kemp, D. T. and A. M. Brown (1983). "An integrated view of cochlear mechanical nonlinearities observable from the ear canal," in *Mechanics of Hearing*, edited by E. de Boer and M. A. Viergever, 11–18. Delft: Delft University Press.

Kemp, D. T. and A. M. Brown (1983). "A comparison of mechanical nonlinearities in the cochlae of man and gerbil from ear canal measurements," in *Hearing — Physiological Bases and Psychophysics*, edited by R. Klinke and R. Hartmann, 75–82. Berlin: Springer–Verlag.

Konishi, S. and G. Zweig (1989). "Smoothing causal functions," in preparation.

Kringlebotn, M. (1988). "Network model for the human middle ear," *Scand. Audiol.* **17**, 75–85.

LePage, E. L. (1987). "Frequency-dependent self-induced bias of the basilar membrane and its potential for controlling sensitivity and tuning in the mammalian cochlea," *J. Acoust. Soc. Am.* **82**, 139–154.

LePage, E. L. (1990). "Helmholtz revisited: Direct mechanical data suggest a physical model for dynamic control of mapping frequency to place along the cochlear partition," in *Mechanics and Biophysics of Hearing*, edited by P. Dallos, C. D. Geisler, J. W. Matthews, M. A. Ruggero, and C. R. Steele, 278–285. Berlin: Springer–Verlag.

Lonsbury-Martin, B.L., G.K. Martin, R. Probst, and A.C. Coats (1988). "Spontaneous otoacoustic emissions in the nonhuman primate. II. Cochlear anatomy," *Hearing Res.* **33**, 69–94.

Lynch, T. J., V. Nedzelnitsky, and W. T. Peake (1982). "Input impedance of the cochlea in cat," *J. Acoust. Soc. Am.* **72**, 108–130.

Manley, G. A. (1983). "Frequency spacing of acoustic emissions: A possible explanation," in *Mechanisms of Hearing*, edited by W. R. Webster and L. M. Aitkin, 36–39. Clayton, Australia: Monash University Press.

Mott, J. B., S. J. Norton, S. T. Neely, and W. B. Warr (1989). "Changes in spontaneous otoacoustic emissions produced by acoustic stimulation of the contralateral ear," *Hearing Res.* **38**, 229–242.

Neely, S. T., S. J. Norton, M. P. Gorga, and W. Jesteadt (1988). "Latency of auditory brain-stem responses and otoacoustic emissions using tone-burst stimuli," *J. Acoust. Soc. Am.* **83**, 652–656.

Norton, S. J. and S. T. Neely (1987). "Tone-burst-evoked otoacoustic emissions from normal-hearing subjects," *J. Acoust. Soc. Am.* **81**, 1860–1872.

Papoulis, A. (1977). *Signal Analysis.*New York: McGraw-Hill.

Peisl, W. (1988). "Simulation von zeitverzögerten evozierten oto-akustischen Emissionen mit Hilfe eines digitalen Innenohrmodells," in *Fortschritte der Akustik—DAGA '88.* Bad Honnef: DPG-GmbH..

Peterson, L. C. and B. P. Bogert (1950). "A dynamical theory of the cochlea," *J. Acoust. Soc. Am.* **22**, 369–381.

Shera, C. A. and G. Zweig (1991a). "A symmetry suppresses the cochlear catastrophe," *J. Acoust. Soc. Am.* **89**, 1276–1289.

Shera, C. A. and G. Zweig (1991b). "Reflection of retrograde waves within the cochlea and at the stapes," *J. Acoust. Soc. Am.* **89**, 1290–1305.

Shera, C. A. and G. Zweig (1991c). "Phenomenological characterization of eardrum transduction," *J. Acoust. Soc. Am.* **90**, 253–262.

Shera, C. A. and G. Zweig (1992a). "Middle-ear phenomenology: The view from the three windows," submitted to *J. Acoust. Soc. Am.*

Shera, C. A. and G. Zweig (1992b). "Analyzing reverse middle-ear transmission: Noninvasive *Gedankenexperiments*," submitted to *J. Acoust. Soc. Am.*

Shera, C. A. and G. Zweig (1992c). "An empirical bound on the compressibility of the cochlea," submitted to *J. Acoust. Soc. Am.*

Shera, C. A. and G. Zweig (1992f). "Spectral periodicity without spatial corrugation: On the origin of evoked otoacoustic emission," in preparation.

Slater, J. C. (1942). *Microwave Transmission.*New York: McGraw-Hill.

Strube, H. W. (1985). "A computationally efficient basilar-membrane model," *Acustica* **58**, 207–214.

Strube, H. W. (1989). "Evoked otoacoustic emissions as cochlear Bragg reflections," *Hearing Res.* **38**, 35–45.

Whitehead, M. L. (1991). "Slow variations in the amplitude and frequency of spontaneous otoacoustic emissions," *Hearing Res.* **53**, 269–280.

Wilson, J. P. (1980). "Evidence for a cochlear origin for acoustic re-emissions, threshold fine-structure and tonal tinnitus," *Hearing Res.* **2**, 233–252.

Zweig, G. (1976). "Basilar membrane motion," in *Cold Spring Harbor Symposia on Quantitative Biology, volume XL, 1975*, 619–633. Cold Spring Harbor: Cold Spring Harbor Laboratory.

Zweig, G. and S. Konishi (1987). "Constraints on measurements of causal or minimum-phase systems," accepted for publication in *J. Acoust. Soc. Am.*

Zweig, G. (1991). "Finding the impedance of the organ of Corti," *J. Acoust. Soc. Am.* **89**, 1229–1254.

Zweig, G., J. E. McDowell, and C. A. Shera (1992). "Latency of tone-burst-evoked otoacoustic emissions," in preparation.

Zwicker, E. and E. Schloth (1984). "Interrelation of different oto-acoustic emissions," *J. Acoust. Soc. Am.* **75**, 1148–1154.

Zwislocki, J. (1962). "Analysis of the middle-ear function. Part I: Input impedance," *J. Acoust. Soc. Am.* **34**, 1514–1523.

Zwislocki-Mościcki, J. (1948). "Theorie der Schneckenmechanik: Qualitative und quantitative Analyse," *Acta Otolaryngol. Suppl.* **72**, 1–112.

Spectral Periodicity without Spatial Corrugation: On the Origin of Evoked Otoacoustic Emission

Christopher A. Shera and George Zweig

Hearing Research Laboratory
Signition, Inc.
P.O. Box 1020
Los Alamos, New Mexico 87544

Theoretical Division
Los Alamos National Laboratory
Los Alamos, New Mexico 87545

and

Physics Department
California Institute of Technology
Pasadena, California 91125

ABSTRACT

Current models for the generation of evoked otoacoustic emissions (e.g., Strube 1985; Peisl 1988; Strube 1989) explain the striking periodicity in their frequency spectra by suggesting that the observed periodicity originates through the reflection of forward-traveling waves off a corresponding periodicity, or corrugation, in the mechanics of the cochlea. Although measurements of cochlear anatomy find no such corrugation, they do indicate a considerable disorganization in the arrangement of outer hair cells (Lonsbury-Martin et al. 1988). This paper demonstrates how the periodicity observed in the spectra of evoked emissions can emerge spontaneously through the reflection of cochlear waves, despite an underlying irregularity in the micromechanics of the organ of Corti responsible for that reflection. In the process, measurements of the cochlear traveling-wave ratio (Shera and Zweig 1992e) are used to deduce constraints on the form of the wavelength of the traveling wave near the peak of the wave envelope.

Contents

Introduction

Evoked otoacoustic emissions recorded in the human ear canal often have a remarkably simple structure, their frequency spectra consisting of a series of regularly-spaced, almost periodic peaks and valleys. Since the cochlea maps frequency into position, the observed spectral periodicity has been explained by suggesting that it mirrors an underlying spatial corrugation in the mechanics of the cochlea (e.g., Strube 1985; Peisl 1988; Strube 1989), which is thus conjectured to manifest a discrete translational symmetry much like that of a crystal.

Anatomical studies, however, provide no evidence for such periodicity in the mechanics, noting instead a "generalized irregularity" and "cellular disorganization" characterizing the arrangement of outer hair cells in the apical turns of the primate cochlea (Lonsbury-Martin et al. 1988). In regions where some regularity in the mechanics is found (e.g., in the "scalloping" patterns produced by the occasional appearance and disappearance of a fourth row of outer hair cells), it appears uncorrelated with the emission spectra measured at corresponding frequencies in the same ear (Lonsbury-Martin et al. 1988; Martin et al. 1988). Anatomically, the organ of Corti appears more chaotic than crystalline.

The analysis presented in this paper shows how the simple periotic periodicity observed in the spectra of evoked emissions can emerge spontaneously from such spatial disorder through the scattering of reflected wavelets and their amplification at low levels by the "lasing" action of the cochlea (Zweig 1991), even when the scattering medium is apparently random and disordered.

The regular oscillations apparent in the emission spectra are reflected in the form of the cochlear traveling-wave ratio, which represents the ratio of the forward and backward-traveling waves at the stapes. That ratio has been measured noninvasively (Shera and Zweig 1992e) and found, locally, to have a roughly constant amplitude and a linear phase. The periodicities in the emission spectra result from the cyclic circling of the phase as the frequency changes monotonically. This paper seeks to understand the simple empirical form of the traveling-wave ratio, identifies constraints it places on models of cochlear mechanics, and demonstrates that it can emerge naturally from the scattering of incident waves by disordered inhomogeneities in the organ of Corti.

A. Overview

The paper begins with an examination of the empirical form of the cochlear traveling wave ratio $R(\omega)$. Section II provides a theoretical framework for understanding the origin of evoked emissions and the empirical form of $R(\omega)$ by incorporating mechanical inhomogeneities into a simple, scaling model of cochlear mechanics. An approximate expression for R is obtained in the form of a scattering integral. As a simple consequence, the long latency typical of evoked emission in human ears is shown to require that the scattering inhomogeneities break the approximate scaling symmetry, confirming arguments that "wave-related" reflection mechanisms cannot account for primate evoked emission (Kemp 1986; Strube 1989). Section III applies the framework to demonstrate how an approximate periodicity in the spectra of evoked emissions can emerge from the scattering of incident waves by disordered inhomogeneities in cochlear mechanics. Constraints that the mechanism places on the form of the wavelength of the traveling wave near the peak of the wave envelope are identified. The analysis is contrasted with the model of Strube (1989), in which evoked emissions are conjectured to originate as cochlear 'Bragg reflections' scattering from pre-existing corrugations in the mechanics. Finally, Sec. IV obtains solutions to the inverse scattering problem, inverting measurements of R to determine the nature of the mechanical inhomogeneities responsible for evoked emission.

I. The Empirical Form of the Traveling-Wave Ratio

Figure 1 shows a typical measurement of stimulus-frequency emissions, plotting the amplitude of the pressure measured in the ear canal as the frequency of a quiet stimulus tone is varied along the abscissa (Shera and Zweig 1992e). The measured pressure shows oscillations with a period $\Delta f/f \approx 1/12$ superposed on a slowly-varying background. Whereas the background is determined principally by the acoustic properties of the measuring apparatus and the middle ear, the roughly periodic oscillations arise from the alternating constructive and destructive interference between the stimulus tone and a reflected wave originating in the cochlea (Kemp 1978; Kemp 1980). The cochlear traveling-wave ratio $R(\omega)$ gives the amplitude and phase of that reflected wave—relative to those of the original, forward-traveling wave—evaluated at the basal end of the cochlear spiral.

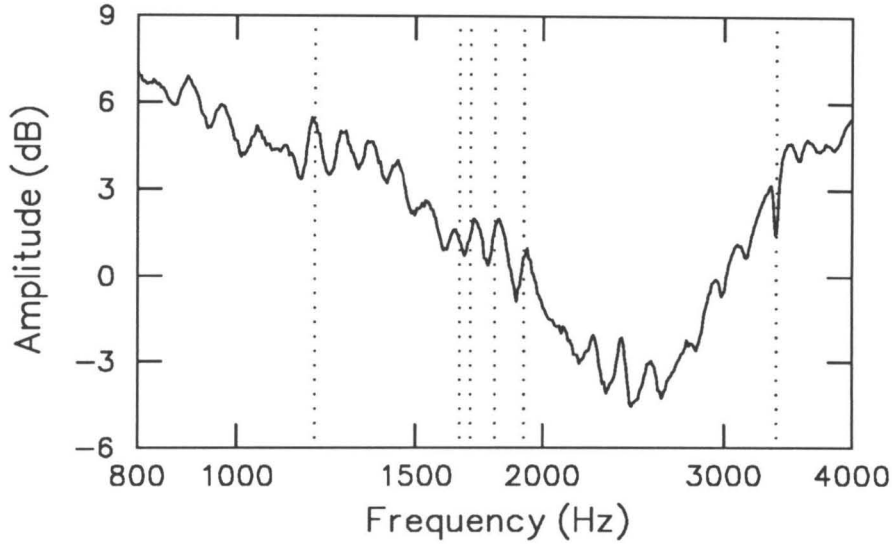

Figure 1. Typical stimulus-frequency emission curve measured in the human ear canal (subject JEM-R) at roughly 20 dB above threshold (Shera and Zweig 1992e). Roughly periodic oscillations arising from interference between the stimulus tone and a reflected wave originating in the cochlea appear superposed on a more slowly-varying background. The vertical dotted lines (·····) indicate the frequencies of the known spontaneous emissions.

Noninvasive measurement of the frequency-dependence of the traveling-wave ratio in human ears (Shera and Zweig 1992e) indicates that $R(\omega)$ has the approximate form

$$R(\omega) \approx R_0(\epsilon\omega)e^{-2\pi i\phi \ln(\omega/\omega_{c_0})} , \tag{1}$$

where the parameter ϵ indicates that $R_0(\epsilon\omega)$ varies slowly with frequency compared to the phase ($\epsilon \ll 1$). The frequency scale ω_{c_0} represents the maximum frequency of hearing and the real constant ϕ determines the rate at which the phase varies with frequency.

Expanding the phase,

$$\theta(\omega) = 2\pi\phi \ln(\omega/\omega_{c_0}) , \tag{2}$$

in a Taylor series about some arbitrary reference frequency demonstrates that the phase is, locally, linear. For example, in a neighborhood about ω_1

$$R(\omega) \approx R_0' e^{-i(\omega-\omega_1)\tau_1} , \tag{3}$$

where

$$\tau_1 \equiv \tau(\omega_1) = \left.\frac{d\theta}{d\omega}\right|_{\omega_1} = 2\pi\phi/\omega_1 . \tag{4}$$

As the frequency varies monotonically, the phase $e^{-i(\omega-\omega_1)\tau}$ passes alternately through plus and minus one, giving rise to the peaks and valleys—with an oscillation period $\Delta f \approx 1/\tau$—measured in the ear-canal pressure. Typical values near 1 kHz are $|R_0| \approx 0.2$ and $\tau \approx 12$ ms (Shera and Zweig 1992e).

In the time domain, the slope of the phase corresponds to the group delay, presumably given by the round-trip travel time to and from the site of generation of the backward traveling wave (Neely et al. 1988). Equation (4) indicates that the delay varies inversely with frequency, consistent with measurements of the latency of tone-burst-evoked emissions (Wilson 1980; Norton and Neely 1987; Zweig et al. 1992), which suggest that evoked emissions originate in a relatively small region of the cochlea appropriate to their frequency, presumably near the peak of the corresponding transfer function.

II. Scattering from Mechanical Inhomogeneities

Evoked emissions have been conjectured to arise from the reflection of forward-traveling waves by inhomogeneities in the structure and mechanics of the cochlea (e.g., Manley 1983; Lonsbury-Martin et al. 1988; Strube 1989). This section introduces a framework for exploring the effects of small inhomogeneities superimposed on the more gradual spatial variation of parameters responsible for the frequency-position map. Subsequent sections apply the framework to understanding the origin of the empirical form of the traveling-wave ratio. When appropriate, illustrative examples are drawn from the simplest model that displays many of the more interesting characteristics of the real cochlea (Zweig 1991). That model, deduced from measurements of basilar-membrane motion, accurately represents the macromechanical motion of the organ of Corti and its basilar membrane in the linear regime.

A. Assumptions and inhomogeneities

In idealized, model cochleae, the impedance of the organ of Corti varies smoothly with position. In the real ear, however, mechanical properties may change discretely from hair cell to hair cell. In addition, the cochlea manifests mechanical imperfections—arising, for example, from natural variability during development or from damage—perturbing the secular variation of parameters responsible for the frequency-position map.[1] For example, the impedance of the organ of Corti may vary somewhat irregularly with position due to variations in the number or spatial orientation of the outer hair cells (Lonsbury-Martin et al. 1988).

Small local variations in the micromechanics of the cochlea perturb the macromechanical traveling wave, giving rise to minute reflected wavelets that scatter back and forth within it as it propagates. Complete characterization of that scattering requires a fully-detailed, three-dimensional description of cochlear geometry, including the intricate microstructure of the organ of Corti. Micromechanical details determine, for example, how the scattered wavelets couple back into the traveling wave, where they combine to form a net backward-traveling wave detectable in the ear canal.

[1] When the cochlear response is nonlinear, the traveling wave can itself induce transient spatial variations in the mechanical characteristics of the organ of Corti. Such "wave-related" mechanisms for generating the mechanical inhomogeneities responsible for evoked emission are inconsistent, however, with the long latencies measured in human ears (see below).

Since a complete description requires measurements of cochlear micromechanics not currently available, we adopt here a more phenomenological approach based on the simple one-dimensional transmission-line model. Any complicated coupling between the scattering of wavelets within the organ of Corti and the macromechanical traveling wave is summarized by an effective, one-dimensional scattering potential. Although such an approach is adequate for exploring the more qualitative mechanisms underlying evoked emission, it cannot, for lack of micromechanical detail, be used to make quantitative predictions for a given distribution of micromechanical inhomogeneities (e.g., for the variations in hair-cell orientation mentioned above).

Mechanisms for creating otoacoustic emissions will thus be described by representing the cochlea as a linear, one-dimensional hydromechanical transmission line. Although simplifications, these assumptions are not gross distortions. For example, the scattering addressed in this paper is most significant at stimulus levels near threshold where cochlear mechanics appears linear. And although the long-wavelength approximation presumably breaks down near the peak of the transfer function, a simple one-dimensional treatment permits elucidation of the scattering mechanisms underlying evoked emission.

The differential pressure P satisfies the wave equation (Shera and Zweig 1991a)

$$\frac{d^2P}{d\chi^2} + \frac{1}{\tilde{\lambda}_\chi^2}P = 0 \,, \tag{5}$$

where $\tilde{\lambda}_\chi$ represents the wavelength, or characteristic impedance. The diacritical tilde indicates that the wavelength includes perturbations arising from mechanical inhomogeneities of the type described above.

Those inhomogeneities scatter waves traveling along the organ of Corti. To analyze that scattering, first imagine "ironing out" the inhomogeneities to obtain a smoothly varying wavelength λ_χ. Traveling-wave solutions for the smooth cochlea can be obtained using the WKB approximation. The mechanical inhomogeneities, or perturbations, can then be reintroduced and their effect on the pressure waves explored using a perturbative scattering series (Shera and Zweig 1991b).

Equation (5) can therefore be written in the inhomogeneous form

$$\frac{d^2P}{d\chi^2} + \frac{1}{\lambda_\chi^2}P = \frac{\varrho}{\lambda_\chi^2}P \,, \tag{6}$$

where the dimensionless scattering potential,

$$\varrho(\chi,\omega) \equiv 1 - \lambda_\chi^2/\tilde{\lambda}_\chi^2 \,, \tag{7}$$

vanishes in the absence of any inhomogeneities. Approximate solutions to the inhomogeneous scattering equation, based on WKB solutions to the homogeneous equation, can be obtained by iteration (Shera and Zweig 1991b).

To simplify the discussion by reducing the number of independent variables, we adopt scaling symmetry for the smooth cochlea (Zweig 1976; Zweig 1991; Shera and Zweig 1991a). Rather than depending on position and frequency independently, the wavelength λ_χ is therefore assumed to depend on those variables only in the combination

$$\beta(x,\omega) = \omega/\omega_c(x) \,, \tag{8}$$

where $\omega_c(x)$ is the frequency-position map. Of course, inhomogeneities in the mechanics typically require a slight breaking of that symmetry.

Equation (6) becomes

$$\frac{d^2P}{d\beta^2} + \frac{1}{\lambda^2}P = \frac{\varrho}{\lambda^2}P \,, \tag{9}$$

where

$$\lambda(\beta) \equiv \lambda_\beta(\beta) = \frac{d\beta}{d\chi}\lambda_\chi \,. \tag{10}$$

The inhomogeneity $\varrho(\beta,\beta_0)$ is now viewed as a function of β and β_0, where $\beta_0 \equiv \omega/\omega_{c_0}$. (Later, when evaluating integrals, it proves helpful to regard these composite variables as representing, respectively, space and frequency—at fixed β_0, the variable β varies only with position.)

1. The empirical wavelength

Rhode's measurements of basilar-membrane motion in the squirrel monkey have been used to obtain an empirical estimate of the wavelength λ by solving the cochlear inverse problem (Zweig 1991). The empirical wavelength, denoted $\lambda^\dagger$ to distinguish it from the more generic wavelength λ, was shown to have the approximate form

$$(4N\lambda^\dagger)^2 \approx 1 - \beta^2 + i\delta\beta + \rho e^{-2\pi i\mu\beta} \,, \tag{11}$$

implying that a section of the organ of Corti responds as though it were a negatively-damped harmonic oscillator ($\delta < 0$) stabilized by a delayed feedback force of strength $\rho > 0$. The time delay corresponds to $\mu \approx 1\frac{3}{4}$ cycles of the local oscillation period. The parameter N represents the approximate number of wavelengths of the traveling wave present in the cochlea in response to sinusoidal stimulation (Zweig et al. 1976).

In the absence of any inhomogeneities, the behavior of the solutions to Eq. (9) for P is determined by the location of the zeroes of λ^2. The parameter values found by Zweig (1991) imply that the empirical wavelength has, among an infinite series of zeroes, two closely-spaced zeros just above the real axis near $\beta = 1$. Those two zeroes create the broad, high peak observed in the measured transfer function. By choosing slightly different parameter values, the locations of those two zeroes can be made to coincide without, as illustrated in Fig. 2, significantly changing the corresponding transfer function. Indeed, requiring that the two zeroes coincide at a given distance from the real axis uniquely determines the parameters δ, ρ, and μ (for μ in a neighborhood of $1\frac{3}{4}$). For ease of analysis, this paper adopts this simpler "double-zero" form for the empirical wavelength $\lambda^\dagger$. The locations of its zeroes are plotted in Fig. 3.

The empirical wavelength $\lambda^\dagger$ was deduced from basilar-membrane transfer functions in the squirrel monkey and is limited in its validity to frequencies above approximately 3 kHz. Although the model is useful for illustrating certain qualitative features of the wavelength and their relationship to the mechanisms responsible for evoked emission, its quantitative predictions cannot be compared with measurements of human otoacoustic emissions made at lower frequencies.

B. The traveling-wave ratio in the Born approximation

Applying the WKB approximation, one can develop the solution P to Eq. (6) as a cochlear scattering series. Since measurements of the traveling-wave ratio typically yield ratios of $O(\frac{2}{10})$, secondary scattering can be neglected (the Born approximation), and one obtains the expression (Shera and Zweig 1991b)

$$R(\beta,\beta_0) \approx -\int_\beta^\infty W^+(\beta',\beta_0)\sigma(\beta',\beta_0)W^+(\beta',\beta_0)\,d\beta' \;+\; O(\sigma^2) \qquad (12)$$

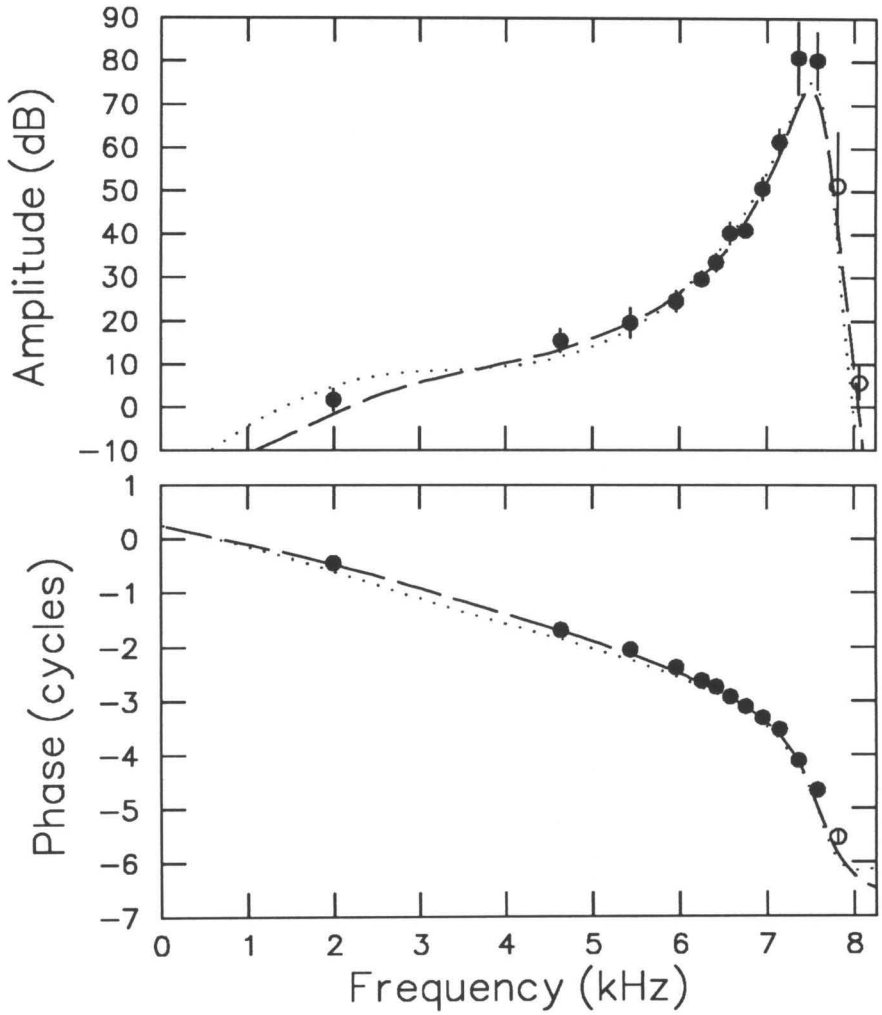

Figure 2. The basilar-membrane transfer function (· · · ·) computed using the wavelength $\lambda^\dagger$ with parameter values determined by requiring that its two zeroes near $\beta = 1$ coincide. The transfer function is compared with extrapolated measurements (•) of basilar-membrane motion and with the transfer function derived from the wavelength obtained by solving the cochlear inverse problem (—— ——); both are taken from Fig. 10 of Zweig (1991). Parameter values are

$$\delta = -0.1223; \quad \rho = 0.1309; \quad \mu = 1.746; \quad N = 5.24; \quad \text{and } \omega_c/2\pi = 7.75 \text{ kHz}.$$

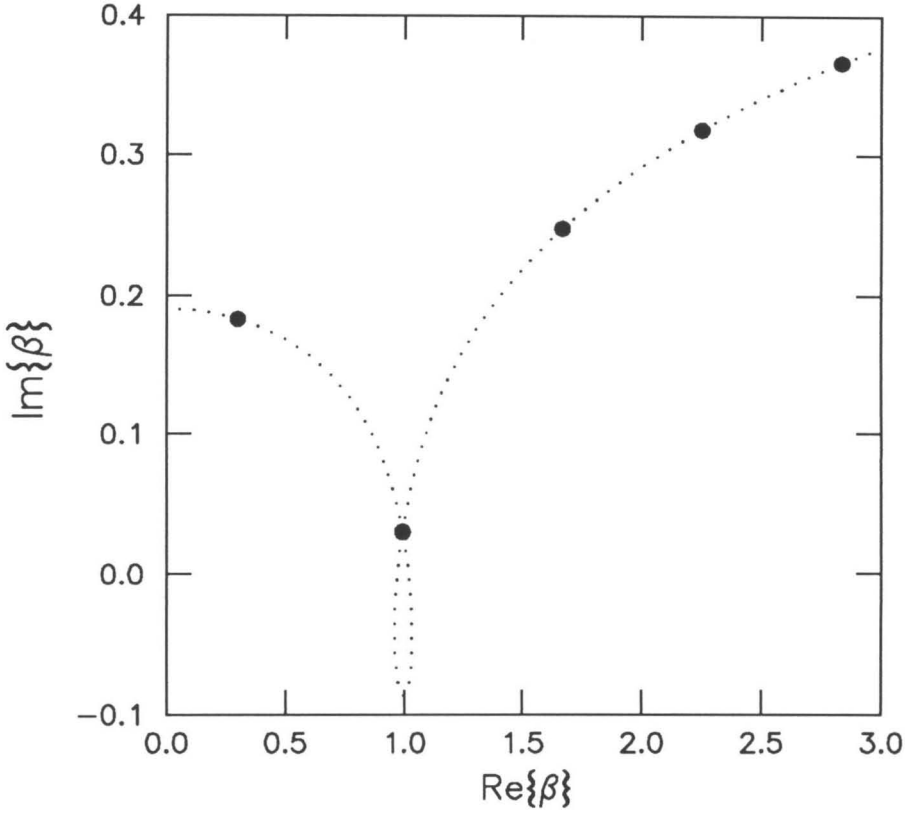

Figure 3. The zeroes (•) of $(\lambda^{\dagger})^2$ in the complex β-plane for the region near $\beta = 1$, computed as in Zweig (1991, Fig. 14). The zero closest to the real axis, denoted $\ddot{\beta}$, is double. The double zero creates the peak of the transfer function. Parameter values are the same as those listed in Fig. 2, and were determined by requiring that $\mathrm{Im}\{\ddot{\beta}\} = 0.03$ with $\mu \approx 1\frac{3}{4}$. An infinite string of zeroes lies on the dotted line outside the range of the figure. Note that all zeroes lie in the upper half of the complex frequency plane, indicating that the model is stable.

for the traveling-wave ratio. Here, the functions

$$W^{\pm}(\beta,\beta_0) \equiv \sqrt{\lambda}\exp\left(\mp i\int_{\beta_0}^{\beta} d\beta'/\lambda\right) \tag{13}$$

represent WKB waves, and

$$\sigma(\beta,\beta_0) \equiv \frac{\varrho(\beta,\beta_0)}{2i\lambda^2} \ . \tag{14}$$

The upper integration limit, shown as '∞' for convenience, indicates that the integration extends to the helicotrema. Because of the rapid fall in $|W^+|$ as β increases above one, the limit '∞' means, in practice, any convenient value of β somewhat greater than one.

We are interested in the traveling-wave ratio evaluated at the basal end of the cochlea where the form and frequency dependence of R has been found from experiment (Shera and Zweig 1992e). At β_0 near the stapes, the traveling-wave ratio becomes

$$R(\beta_0) \equiv R(\beta_0,\beta_0) \approx -e^{+2i\int_0^{\beta_0} d\beta'/\lambda}\int_{\beta_0}^{\infty} \lambda(\beta)\sigma(\beta,\beta_0)e^{-2i\int_0^{\beta} d\beta'/\lambda}\,d\beta \ . \tag{15}$$

Since the wavelength is real at small β, the exponential in front provides a phase shift. Substituting the form for σ yields

$$R(\beta_0) \approx \psi(\beta_0)\int_{\beta_0}^{\infty} \frac{\varrho(\beta,\beta_0)}{\lambda(\beta)} e^{-2i\int_0^{\beta} d\beta'/\lambda}\,d\beta \ , \tag{16}$$

where

$$\psi(\beta_0) \equiv -e^{+2i\int_0^{\beta_0} d\beta'/\lambda}/2i \ \approx \ -e^{+8Ni\beta_0}/2i \qquad (\beta_0 \ll 1) \ , \tag{17}$$

where the real, positive number N, typically of order $O(5)$, is defined by the limit (Zweig et al. 1976)

$$\lim_{\beta\to 0} \lambda = 1/4N \ . \tag{18}$$

C. Evoked emission requires a breaking of scaling symmetry

Equation (1) representing the empirical form of the traveling-wave ratio can be rewritten as

$$R(\beta_0) \approx R_0(\epsilon\beta_0)e^{-2\pi i\phi \ln \beta_0} \ . \tag{19}$$

Comparing this form with Eq. (16) shows that the phase shift $+8N\beta_0$ arising from $\psi(\beta_0)$ has the wrong sign—and, for reasonable values of N, is far too small in magnitude—to

yield the empirical delay. Likewise, the delay cannot originate in the frequency dependence of the lower limit of integration (see Sec. IV). The rapid circling of phase responsible for the measured latency must therefore originate in the function $\varrho(\beta, \beta_0)$. Consequently, the function ϱ must depend on β_0 and cannot be a function of β alone. Were ϱ a function merely of β, the integral would not evaluate to a strong function of β_0, and the phase $\angle R(\beta_0)$ would not depend strongly on frequency.

Equivalently, the scattering potential ϱ describing the inhomogeneities cannot scale. The inhomogeneities responsible for evoked emission cannot, therefore, simply move with the wave envelope, as they would were those inhomogeneities created by the wave itself [e.g., by some nonlinearity in the mechanics acting near threshold as a "source" of backward-traveling waves (de Boer 1983)]. The rapid frequency variation of the phase of R requires a breaking of scaling symmetry. This argument reproduces, in a nutshell, the reasoning underlying the conclusion that "wave-related" reflection mechanisms cannot explain the long latencies of evoked emissions observed in human ears (Kemp 1979; Kemp 1986; Strube 1989).

III. Spectral Periodicity without Cochlear Corrugation

The following heuristic argument shows how an approximate periodicity in the frequency spectra of evoked emissions can emerge from the scattering of cochlear waves by a disordered distribution of inhomogeneities in the organ of Corti. The observed periodicity is shown to be a measure of the real part of the wavelength near the peak of the transfer function.

A. A dominant spatial frequency for scattering

In the following analysis it proves helpful to decompose the inhomogeneity ϱ into its spatial-frequency components. When the inhomogeneities are irregular or random, ϱ will contain contributions from many spatial frequencies. Viewing the inhomogeneities as a function of the dimensionless distance $\gamma \equiv x/l$—where l represents the distance by which the characteristic frequency changes by a factor of e in the basal turns—one obtains

$$\varrho(\gamma, \omega) = \int_{-\infty}^{\infty} \bar{\varrho}(\xi, \omega) e^{2\pi i \xi \gamma} d\xi \ , \tag{20}$$

where ξ is the dimensionless spatial frequency obtained when distances are measured in terms of l. The inverse transform is, of course,

$$\bar{\varrho}(\xi,\omega) = \int_0^\infty \varrho(\gamma,\omega) e^{-2\pi i\gamma\xi} d\gamma \ . \tag{21}$$

Note that since $\varrho(\gamma < 0,\omega) = 0$, the spatial spectral density $\bar{\varrho}(\xi,\omega)$ is a "causal function" (Bode 1945; Zweig and Konishi 1987). Rewriting the Fourier integral in terms of the scaling variables yields

$$\varrho(\beta,\beta_0) = \int_{-\infty}^\infty \bar{\varrho}(\xi,\beta_0) e^{2\pi i\xi \ln(\beta/\beta_0)} d\xi \ . \tag{22}$$

In the Born approximation, the traveling-wave ratio has the value

$$R(\beta_0) \approx \psi(\beta_0) \int_{\beta_0}^\infty \varrho(\beta,\beta_0) k(\beta) e^{-2i\int_{\beta_0}^{\beta} k\, d\beta'} \, d\beta \ , \tag{23}$$

where the wavenumber $k \equiv 1/\lambda$. Thus,

$$R(\beta_0) \approx \psi(\beta_0) \int_{\beta_0}^\infty d\beta\, k e^{-2i\int_{\beta_0}^{\beta} k\, d\beta'} \int_{-\infty}^\infty d\xi\, \bar{\varrho}(\xi,\beta_0) e^{2\pi i\xi \ln(\beta/\beta_0)} \ . \tag{24}$$

Since the logarithm can itself be written as an integral, namely

$$\ln(\beta/\beta_0) = \int_{\beta_0}^{\beta} \frac{d\beta'}{\beta'} \ , \tag{25}$$

the scattering integral becomes

$$R(\beta_0) \approx \psi(\beta_0) \int_{-\infty}^\infty d\xi\, \bar{\varrho}(\xi,\beta_0) \int_{\beta_0}^\infty d\beta\, k e^{i\int_{\beta_0}^{\beta} (2\pi\xi/\beta' - 2k)\, d\beta'} \ , \tag{26}$$

where the order of integration has been interchanged.

The scattering integral (26) can thus be written in the form

$$R(\beta_0) \approx \psi(\beta_0) \int_{-\infty}^\infty d\xi\, \bar{\varrho}(\xi,\beta_0) F(\xi,\beta_0) \ , \tag{27}$$

where

$$F(\xi,\beta_0) \equiv \int_{\beta_0}^\infty d\beta\, k e^{i\int_{\beta_0}^{\beta} (2\pi\xi/\beta' - 2k)\, d\beta'} \ . \tag{28}$$

At fixed β_0, the function F has the form of an integral over position (i.e., over different scattering locations). The following sections use qualitative features of the wavelength to evaluate the scattering integral, focusing first on the integral F. The results are used to show how the observed spectral order can arise dynamically from scattering off a spatially disordered array of inhomogeneities.

1. Integrating over space at fixed frequency

To evaluate the integral F, it is helpful to separate contributions arising from the real and imaginary parts of the wavenumber:

$$F(\xi) = \int_{\beta_0}^{\infty} d\beta \, e^{A(\beta)+i\theta(\beta;\xi)} \tag{29}$$

where

$$A(\beta) \equiv \ln|k| + 2\int_{\beta_0}^{\beta} \mathrm{Im}\{k\}\, d\beta' \,, \tag{30}$$

and

$$\theta(\beta;\xi) \equiv \angle k + \int_{\beta_0}^{\beta} (2\pi\xi/\beta' - 2\mathrm{Re}\{k\})\, d\beta' \,. \tag{31}$$

The dependence on the variable β_0 is weak and has been omitted here for clarity.

To elucidate the qualitative behavior of the integral F, note that its value will be dominated by the region—centered, by definition, about the value $\beta = \hat{\beta}$—near the absolute maximum of A, which occurs near the peak of the transfer function (i.e., near $\beta \approx 1$). As a function of ξ, the function F will then reach a maximum at values ξ such that the phase is stationary when evaluated at $\hat{\beta}$. The next two sections make these arguments more precise.

a) Determining the scattering location

At values of $\beta \approx 1$, the function A reaches a maximum. A maximum occurs both because the wavelength becomes short ($|k|$ becomes large) near "resonance" and, in active models, because of contributions from the second term in Eq. (30) arising from the "lasing" action of the cochlea. Equation (18) implies that the first term is positive (for typical values of N) and of order $\ln(4N)$ or greater. The second term represents any contributions from the gain of the "cochlear amplifier." In passive models, $\mathrm{Im}\{k\}$ is always negative and the two terms in Eq. (30) tend to cancel, thereby reducing and broadening the peak in A. In active models, however, both terms can be positive over some range of β; the resulting peak can be quite high and sharp. For example, the imaginary part of the empirical wavenumber, $k^{\dagger} \equiv 1/\lambda^{\dagger}$, increases many fold just basal to the peak of the transfer function (Zweig 1991). As a consequence, there is an exponential increase in energy transfer to the traveling wave just before the sign of $\mathrm{Im}\{\lambda^{\dagger}\}$ reverses and the accumulated

wave energy is deposited in the organ of Corti. These remarks are illustrated in Fig. 4, which plots the function $A(\beta)$ for the wavelength $\lambda^\dagger$.

The value of β at which A reaches its global maximum thus fixes the scattering location $\hat{\beta}$, defined so that

$$A(\beta) \leq A(\hat{\beta}) \quad \forall \beta \, . \tag{32}$$

Expanding A in a Taylor series about the $\hat{\beta}$ yields

$$A/\hat{A} = 1 - \tfrac{1}{2}\alpha \, \Delta\beta^2 + O(\Delta\beta^3) \, , \tag{33}$$

where $\Delta\beta \equiv \beta - \hat{\beta}$, and

$$\alpha \equiv \frac{1}{A} \left. \frac{d^2 A}{d\beta^2} \right|_{\beta=\hat{\beta}} \, , \tag{34}$$

with $\alpha > 0$.

The approximate width of the peak can be obtained from the Taylor series:

$$\Delta\beta \approx \sqrt{2/\alpha\hat{A}}. \tag{35}$$

If A is sharply peaked (i.e., if $\Delta\beta \ll 1$), the scattering location $\hat{\beta}$ is well defined. The magnitude of the scattering integral is then determined principally by a small region, identified with a neighborhood of size $\pm\Delta\beta$ about $\hat{\beta}$, in the immediate vicinity of the peak of the transfer function. (The diacritical hat, which indicates that the underlying function is evaluated at the scattering location, was chosen to resemble a "peak" in anticipation of this result.) This finding is consistent with measurements of emission spectra and latency (Norton and Neely 1987), which suggest that emissions arise in a relatively small region that moves with the wave envelope.

In addition to its role in determining the scattering location—and thus, as shown below, the phase of R—the function $A(\beta)$ controls, in combination with the scattering potential ϱ, the amplitude of the traveling-wave ratio. When the maximum in A is large, the corresponding inhomogeneities can be relatively small; the combination will still produce traveling-wave ratios of the size, typically of order $O(\frac{2}{10})$ or greater, measured experimentally. By contrast, models in which A remains relatively small (e.g., the generic passive model illustrated in Fig. 4), require gross inhomogeneities to generate measurable emissions.

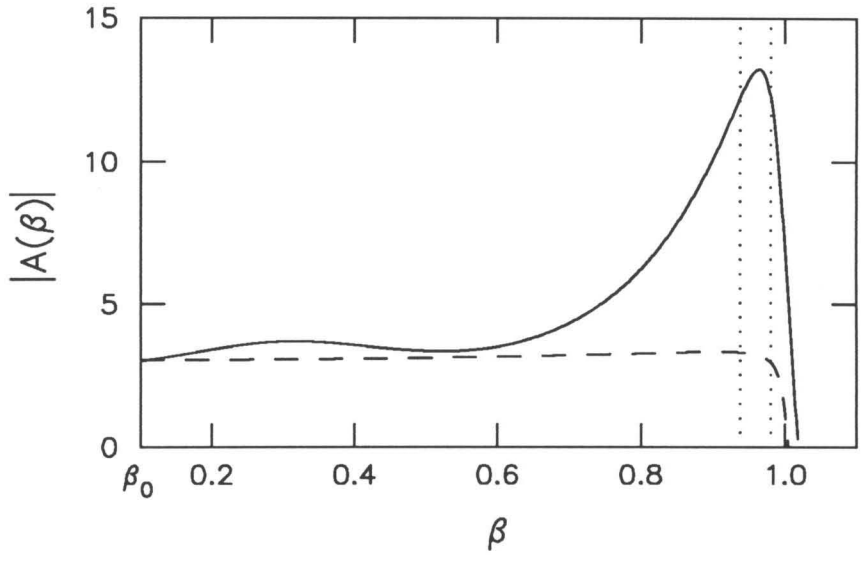

Figure 4. The function $A(\beta)$ computed using two example wavelengths: (———) the empirical wavelength $\lambda^{\dagger}$ and (— — —) a generic passive wavelength obtained from $\lambda^{\dagger}$ by setting $\rho = 0$ and $\delta = +0.02$. The function A was evaluated at fixed frequency ($\beta_0 = 1/10$). The vertical dotted lines (·····), placed at values β such that $A(\beta) = \hat{A} - 1$, delimit the neighborhood about the peak at $\hat{\beta}$ defining the scattering region. In the passive model, that neighborhood is large, spanning essentially all $\beta < 1$. Note that Eq. (18) implies that $A(\beta_0) \approx \ln 4N$.

b) Determining the dominant spatial frequency

The position of the maximum in the amplitude of the integrand selects the principle scattering location $\hat{\beta}$. This section shows how the existence of a stationary point in the phase selects a principle spatial frequency as making the dominant contribution to that scattering.

The phase θ in the exponential in Eq. (29) for F contains the dependence on the mechanical inhomogeneities, specifically on their spatial frequency ξ:

$$\theta(\beta;\xi) = \angle k + \int_{\beta_0}^{\beta} 2\pi\xi/\beta' - 2\,\mathrm{Re}\{k\}\,d\beta' \,. \tag{36}$$

The first term, $\angle k$, is small and changes relatively slowly with position, going smoothly from values close to zero at small β where the wavelength is real to values near $-\pi/2$ above "resonance."[2]

The second term, however, is large and can rotate rapidly with β. For example, since the spatial frequencies characteristic of variation at the level of a hair cell are typically of $O(500)$ or greater, one expects $2\pi\xi \gg 1$. Similarly, the wavenumber $\mathrm{Re}\{k\}$ is large, even at $\beta \ll 1$, where, by Eq. (18), $k \approx 4N$, with the real number N being typically of $O(5)$. Since the wavelength decreases with distance from the stapes, $\mathrm{Re}\{k\}$ becomes even larger as the wave approaches the scattering location, $\hat{\beta}$.

Since the integrand in Eq. (36) is everywhere large, the phase θ rotates rapidly with β and contributions to the integral F from nearby locations largely cancel except near stationary points of θ, which occur at zeroes of the derivative (Papoulis 1968; Friedman 1969):

$$0 = \left.\frac{\partial\theta}{\partial\beta}\right|_{\hat{\beta}} \approx \frac{2\pi\xi}{\hat{\beta}} - 2\,\mathrm{Re}\{1/\hat{\lambda}\}\,, \tag{38}$$

---

[2] The argument for neglecting contributions to the derivative of θ arising from $\angle k$, valid in generic passive models, becomes stronger when considering the empirical wavelength $\lambda^{\dagger}$. First, note that

$$\angle k = -\angle\lambda = -\tfrac{1}{2}\angle\lambda^2 \,. \tag{2.1}$$

The two closely-spaced zeroes near $\hat{\beta}$ responsible for the broad transfer-function peak make the derivative of the square of the wavelength small near the peak of the transfer function (Zweig 1991):

$$\left.\frac{d(\lambda^{\dagger})^2}{d\beta}\right|_{\hat{\beta}} \approx 0 \,. \tag{2.2}$$

Consequently,

$$\frac{d\angle k}{d\beta} = -\frac{1}{2}\frac{d\angle(\lambda^{\dagger})^2}{d\beta} \approx 0 \tag{37}$$

near $\hat{\beta}$, as required.

where contributions from $\angle k$ have been neglected. For consistency, the stationary-phase condition has been evaluated at the scattering location $\hat{\beta}$.

Equation (38) determines the spatial frequency $\bar{\xi}$ at which the phase is stationary and the function F therefore maximal:

$$\bar{\xi} = 2\hat{\beta}\,\mathrm{Re}\{1/\hat{\lambda}\}/2\pi\ . \tag{39}$$

The stationary-phase condition (38) thus determines the existence of a dominant spatial frequency. When the traveling-wave ratio is found from Eq. (27) by integrating over ξ, only those spatial frequencies in the neighborhood of $\bar{\xi}$ contribute to the net reflected wave. Since scaling symmetry is only an approximate local symmetry, the dominant spatial frequency $\bar{\xi}$ depends on position within the cochlea. For example, $\mathrm{Re}\{1/\hat{\lambda}\}$ presumably varies as the shape of the traveling-wave envelope changes with characteristic frequency.

The dominant spatial frequency $\bar{\xi}$ determined by Eq. (39) is well defined only if $\mathrm{Re}\{1/\lambda\}$ is slowly varying in a neighborhood about $\hat{\beta}$. The size of that neighborhood is determined by the width of the maximum in the function $A(\beta;\xi)$, defined by Eq. (30). The sharper that peak in A—or, equivalently, the better determined the scattering location $\hat{\beta}$—the smaller need be the neighborhood about $\hat{\beta}$ within which $\mathrm{Re}\{1/\lambda\}$ remains roughly constant.

As an example, Fig. 5 plots $|F(\xi)|$ computed, at fixed frequency β_0, as a function of spatial frequency ξ using the empirical wavelength $\lambda^{\dagger}$. As predicted by the foregoing analysis, the integral is sharply peaked about the spatial frequency $\bar{\xi}$ given by Eq. (39). As discussed below, the integral $F(\xi)$ thus serves as a bandpass spatial filter through which the inhomogeneities ϱ are passed to generate the net reflected wave.

c) Another perspective

The heuristic arguments outlined above for determining the behavior of $F(\xi)$ can be inverted and the process viewed from a different perspective. Rather than first determining the scattering location and then evaluating the stationary-phase condition at $\hat{\beta}$ to determine $\bar{\xi}$, one can view the stationary-phase condition as determining β as an implicit function of ξ. In this view, Eq. (38) determines the function $\beta(\xi)$. The integral $F(\xi)$ will then be maximal at that value of ξ for which $\beta(\xi) = \hat{\beta}$, where $\hat{\beta}$ locates the maximum of $A(\beta)$. That value of ξ is, of course, simply $\bar{\xi}$, as defined by Eq. (39).

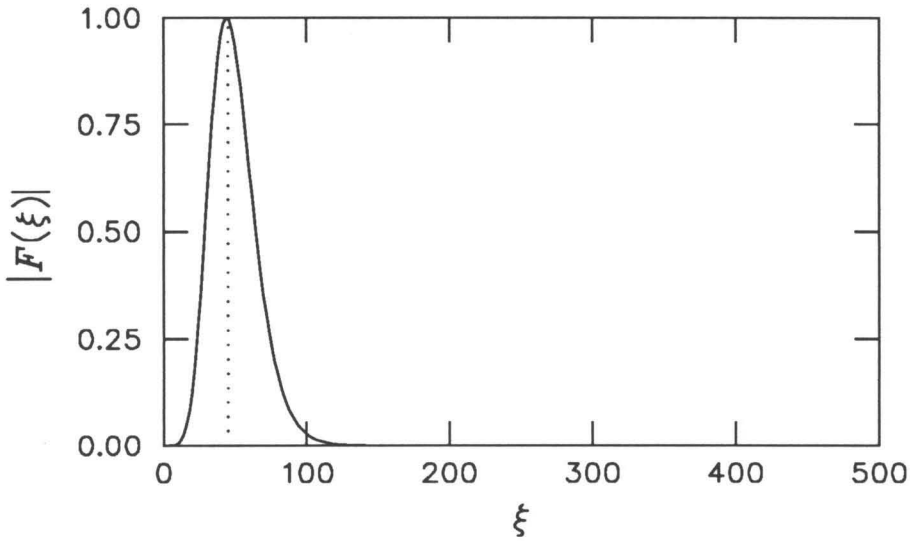

Figure 5. The function $|F(\beta_0, \xi)|$ computed as a function of spatial frequency ξ from Eq. (23) using the empirical wavelength $\lambda^{\dagger}$. The integral F was evaluated at fixed frequency ($\beta_0 = 1/10$) and has been normalized to a maximum value of one. The maximum value along the abscissa corresponds to the approximate spatial frequency ($\Delta x = l/\xi \approx 10$ μm with $l = 1/2$ cm) characteristic of variations at the level of a hair cell (Beecher 1974). The vertical dotted line (·····) indicates the dominant spatial frequency $\bar{\xi}$—here, $\bar{\xi} \approx 45$, corresponding to roughly 10 hair cells—computed from Eq. (39).

2. Integrating over spatial frequency

An irregular distribution of mechanical inhomogeneities represents a superposition of inhomogeneities at many spatial frequencies. The net backward-traveling wave then emerges, when the system is linear, as a simple integral over contributions from each spatial frequency. As shown here, however, not all spatial frequencies reflect equally. The sharp peak in $A(\beta)$—which results, in the squirrel monkey, from the behavior of the imaginary part of the wavelength basal to the characteristic frequency point—selects one distance scale, determined by the real part of the wavelength, as special. The scattering of wavelets and their amplification by the "lasing" action of the cochlea thus serves as a sort of dynamic "spatial filter," enhancing contributions from inhomogeneities arrayed with spatial period $\bar{d}$ given by

$$\bar{d} = l/\bar{\xi} \approx 2\pi l/2\hat{\beta}\,\mathrm{Re}\{1/\hat{\lambda}\}\,. \tag{40}$$

Eq. (40) can be simplified whenever the wavelength satisfies

$$|\angle\hat{\lambda}| = \left|\frac{\mathrm{Im}\{\hat{\lambda}\}}{\mathrm{Re}\{\hat{\lambda}\}}\right| \ll 1\,. \tag{41}$$

When that inequality is valid

$$\mathrm{Re}\{1/\hat{\lambda}\} \approx 1/\mathrm{Re}\{\hat{\lambda}\} \approx 1/\hat{\lambda}\,; \tag{42}$$

and consequently

$$\bar{\xi} \approx 2\hat{\beta}/\mathrm{Re}\{\hat{\lambda}\}\,, \tag{43}$$

where $\lambda = 2\pi\lambda$.

In terms of the conventional wavelength λ_x, related to λ by the expression (Shera and Zweig 1991a; Zweig 1991)

$$\lambda_x = 2\pi\frac{dx}{d\beta}\lambda = \frac{2\pi l}{\beta}\lambda\,, \tag{44}$$

the spatial period $\bar{d}$ can then be written

$$\bar{d} = \tfrac{1}{2}\mathrm{Re}\{\hat{\lambda}_x\}\,. \tag{45}$$

For the empirical wavelength, $\hat{\beta}$ represents the approximate location of the positive-going zero crossing of $\mathrm{Im}\{\lambda^{\dagger}\}$. At that point, the power flow reverses sign and wave energy is dumped into the organ of Corti. Thus, in a neighborhood about $\hat{\beta}$ the empirical wavelength satisfies inequality (41), and Eq. (45) is valid. In other words, the "lasing" action of the cochlea selectively amplifies wavelets scattered from mechanical inhomogeneities arrayed with a spatial frequency determined by the Bragg condition (Ashcroft and Mermin 1976) at resonance.

B. The corresponding spectral periodicity

Because the cochlea maps frequency into position, the dominance of one spatial frequency in generating the reflected wave creates a corresponding periodicity in the spectra of evoked emissions. To see this most easily, consider the limit in which the "filter" $F(\xi)$ is quite narrow, so that contributions from other than the dominant spatial frequency can be neglected.

In other words, approximate the effective inhomogeneity, obtained through filtering, by a δ-function in spatial frequency:

$$\bar{\varrho}_{\rm eff}(\xi,\beta_0) \equiv F(\xi)\bar{\varrho}(\xi,\beta_0) \approx \bar{\varrho}_1(\beta_0)\delta(\xi-\bar{\xi})\,. \tag{46}$$

Inverting the spatial Fourier transform to obtain the the potential yields

$$\varrho_{\rm eff}(\beta,\beta_0) = \bar{\varrho}_1(\beta_0)e^{2\pi i\bar{\xi}\ln(\beta/\beta_0)}\,. \tag{47}$$

Consequently,

$$R(\beta_0) \approx \bar{\varrho}_1(\beta_0)\psi(\beta_0)\int_{\beta_0}^{\infty}\frac{e^{2\pi i\bar{\xi}\ln(\beta/\beta_0)}}{\lambda(\beta)}e^{-2i\int_{\beta_0}^{\beta}d\beta'/\lambda}\,d\beta \tag{48}$$

$$= \bar{\varrho}_1(\beta_0)\psi(\beta_0)e^{-2\pi i\bar{\xi}\ln\beta_0}\int_{\beta_0}^{\infty}\frac{e^{2\pi i\bar{\xi}\ln\beta}}{\lambda(\beta)}e^{-2i\int_{0}^{\beta}d\beta'/\lambda}\,d\beta\,. \tag{49}$$

Note that the integral (with limits β_0 to '∞') is nothing more than a number whose value is determined principally by the region near the peak of the transfer function. For $\beta_0 \ll 1$, the frequency dependence enters almost entirely through the phase factor

$$e^{-2\pi i\bar{\xi}\ln\beta_0} = e^{-2\pi i\bar{\xi}\ln(\omega/\omega_{c_0})}\,. \tag{50}$$

Locally, the traveling-wave ratio therefore has an approximately constant amplitude and a linear phase, in agreement with the form determined empirically (Shera and Zweig 1992e). Comparing Eq. (49) with its empirical counterpart, Eq. (1) for $R(\omega)$, determines the value of the dominant spatial frequency $\bar{\xi}$:

$$\bar{\xi} = \phi\,. \tag{51}$$

Because more than a single spatial frequency contributes to the traveling wave ratio, the simple relationships derived here are only approximate. The traveling-wave ratio measured in any individual subject will show fluctuations about these idealized forms (Shera and Zweig 1992e).

1. Simulated emissions

As an example, Figs. 6 and 7 give the results of a simulation, based on the empirical wavelength $\lambda\!\!\!^{\dagger}$, in which inhomogeneities in the mechanics of the organ of Corti were introduced by randomly varying the strengths of the fast and slow feedback forces. Those two forces are responsible, respectively, for creating a net negative damping and for stabilizing the resulting oscillator. The form of the inhomogeneities is motivated by the conjecture that the feedback strengths are likely to depend on the number and orientation of the outer hair cells, which vary rather irregularly with position in primates (Lonsbury-Martin et al. 1988). The figures give both the traveling-wave ratio $R(\omega)$ and the corresponding oscillations produced in the cochlear input impedance

$$Z(\omega; R)/Z(\omega; 0) = \frac{1 + R(\omega)}{1 - R(\omega)} \, . \tag{52}$$

In actual measurements made in the ear canal, the recorded emissions have, of course, been filtered by the middle ear, thereby altering their apparent amplitude and phase, and appear superposed on a slowly-varying background as in Fig. 1.

The parameter values were varied in such a way that the distance between the double zero in $\lambda\!\!\!^{\dagger}$ and the real axis varied randomly at the level of the hair cell. The resulting wobbles in the location of the double zero are illustrated in Fig. 8. To give an indication of the variability, Figs. 9 and 10 overlay the results from a number of simulations, each computed for a different set of similar, random inhomogeneities.

Although the inhomogeneities responsible for the wave scattering are disordered at the level of the hair cell (the parameters change discontinuously every 10 μm), the resulting simulated emissions show considerable spectral regularity, with peaks and valleys arrayed nearly periodically, in agreement with experiment. The phase of R varies almost linearly,

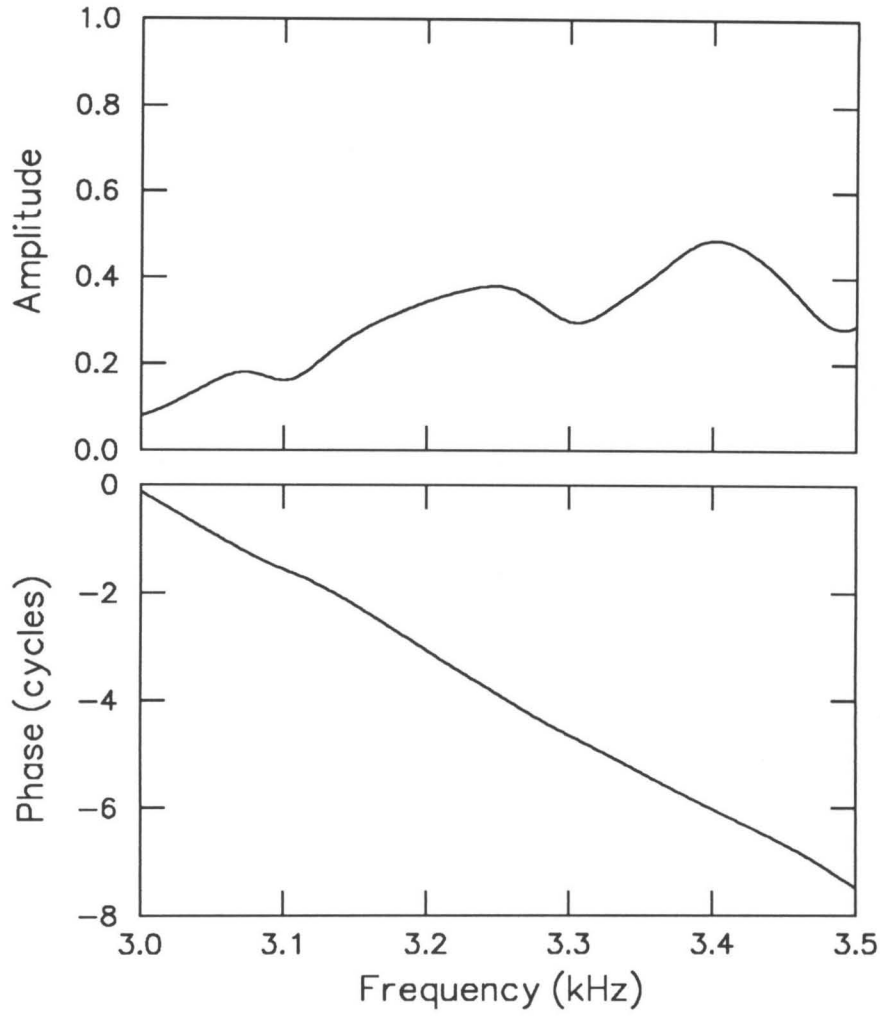

Figure 6. The traveling-wave ratio $R(\omega)$ computed (to all orders in the scattering potential) from a simulation, based on the empirical wavelength $\lambda^{\dagger}$, in which the strengths of the fast and slow feedback forces are varied randomly at the level of the hair cell (i.e., the feedback strengths change discontinuously every 10 μm). The frequency range of the figure was chosen to correspond with the lowest frequencies for which the empirical wavelength is believed valid in the squirrel monkey. As predicted, the phase $\angle R$ is almost linear, varying approximately as $-2\pi\bar{\xi}\ln(\omega/\omega_{c_0})$, in qualitative agreement with the empirical result. By contrast, the amplitude $|R|$ varies more slowly; its fractional change over intervals of size $\Delta f \approx 70$ Hz—corresponding to a full rotation of the phase—is typically small. Note that in this example $|R|$ generally increases at higher frequencies; comparison with Fig. 8 shows that this reflects a general *increase with* characteristic frequency in the rms-value of the underlying inhomogeneities.

changing by about 7 cycles over the range of the figure and yielding an average frequency spacing Δf of approximately

$$\Delta f \approx 500 \text{ Hz}/7 \approx 70 \text{ Hz}, \tag{53}$$

in agreement with the periodicity predicted by the relation

$$\begin{aligned} \Delta f/f \approx 1/\phi &= 1/\bar{\xi} \\ &= 2\pi/2\hat{\beta}\,\mathrm{Re}\{1/\hat{\lambda}\} \\ &\approx \tfrac{1}{2}\,\mathrm{Re}\{\hat{\lambda}^{\dagger}\}/\hat{\beta} = \tfrac{1}{2}\,\mathrm{Re}\{\hat{\lambda}_x^{\dagger}\}/l \quad (|\angle\hat{\lambda}| \ll 1)\,. \end{aligned} \tag{54}$$

Note that $|R|$ varies slowly in comparison with the phase, in agreement with the empirical result (Shera and Zweig 1992e).

A simple, qualitative way to model the level-dependence of the predicted emissions is to suppose that raising the stimulus level has the effect of decreasing the strengths of the feedback forces, thereby increasing δ towards zero and decreasing ρ. Here, we mock up those parameter variations by assuming that raising the stimulus level moves the double zero in $\lambda^{\dagger}$ further from the real axis, thereby reducing and broadening the peak of the corresponding transfer function in a manner qualitatively consistent with the trends observed experimentally.

Figures 11 and 12 show the results of varying the effective stimulus level in this way. The underlying inhomogeneities are those shown in Fig. 8. Despite the simplicity of the assumptions, the simulation captures many of the qualitative features seen experimentally. Note, for example, that whereas the amplitude of the oscillations is a strong function of "level," their period and phase vary only slightly (indeed, they remain here essentially unchanged), characteristics that are observed experimentally (Shera and Zweig 1992e). These results originate in the differential behavior of the real and and imaginary parts of the wavelength: whereas $\mathrm{Im}\{1/\lambda^{\dagger}\}$, which determines the gain of the "cochlear amplifier," depends strongly on level (the location of the zeroes), $\mathrm{Re}\{1/\lambda^{\dagger}\}$, which determines the dominant spatial frequency $\bar{\xi}$, varies considerably less.

Although the linearity of the model renders it unsuitable for exploring spontaneous emissions, it is interesting to note that introducing a localized perturbation in the mechanics somewhat larger than those employed above often results in the generation of a sharp

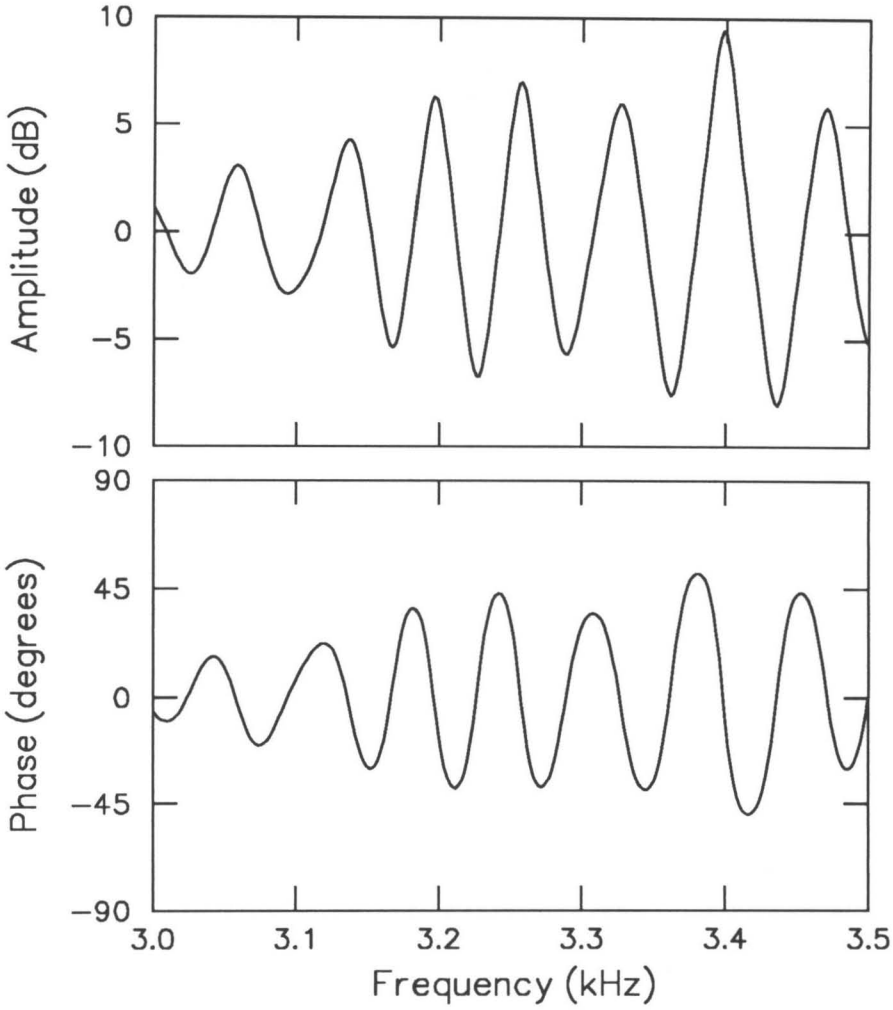

Figure 7. Simulated stimulus-frequency emissions "recorded" at the basal end of the cochlea. The figure plots the cochlear input impedance normalized to its value in the absence of apical reflections (i.e., to its value at high stimulus amplitudes or in the corresponding "smooth" cochlea):

$$Z(\omega; R)/Z(\omega; 0) = \frac{1+R}{1-R} .$$

The functions Z were computed from the simulation described in Fig. 6 in which the cellular feedback forces are varied randomly at the level of the hair cell. Despite the stochastic nature of the inhomogeneities, the amplitude and phase of the cochlear input impedance manifest a pronounced periodicity, with peaks and valleys arrayed at intervals predicted by Eq. (54). Consistent with its identity as a ratio of driving-point impedances (Bode 1945), the simulated emission curve represents a minimum-phase function.

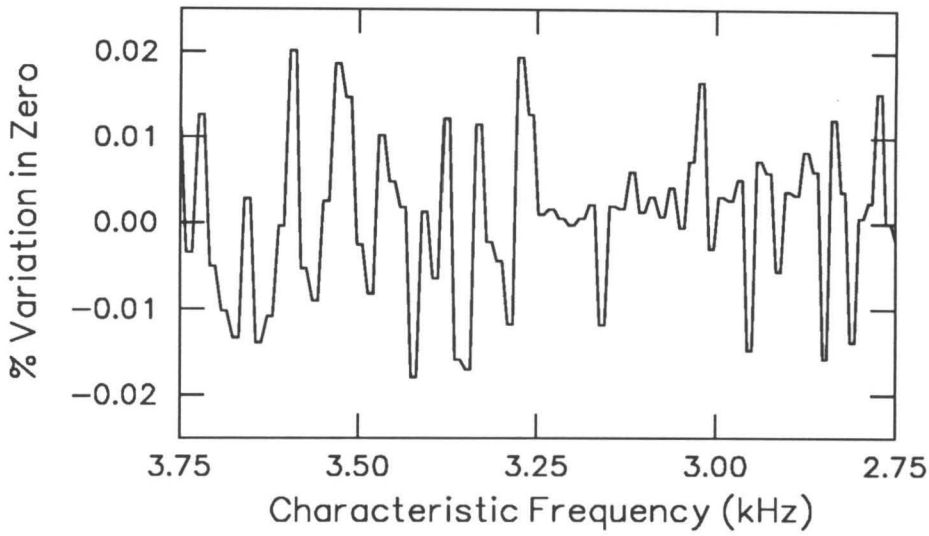

Figure 8. A representation of the inhomogeneities used in the simulations shown in Figs. 6 and 7. The figure plots deviations in $\mathrm{Im}\{\ddot{\beta}\}$, where $\ddot{\beta}$ is the double zero of $\lambda^{\dagger}(\beta)$ found near the real axis close to $\beta \approx 1$. The zero location, expressed as percent deviation from its unperturbed value—which is the same as that shown in Fig. 3—is plotted as a function of the local characteristic frequency $\omega_c(x)/2\pi$. Note that the characteristic-frequency axis is reversed (the distance x from the stapes increases along the abscissa). The zero location was changed every 10 μm by picking random deviations from a Gaussian distribution with a width corresponding to 0.01%. The width of the distribution was chosen to yield a traveling-wave ratio of mean amplitude $|R| \sim 2/10$ similar to that measured experimentally (Shera and Zweig 1992e). However, since the analysis assumes an effective, one-dimensional scattering potential, the inhomogeneities used here—in particular, their absolute magnitude—cannot currently be related to corresponding micromechanical perturbations in the organ of Corti.

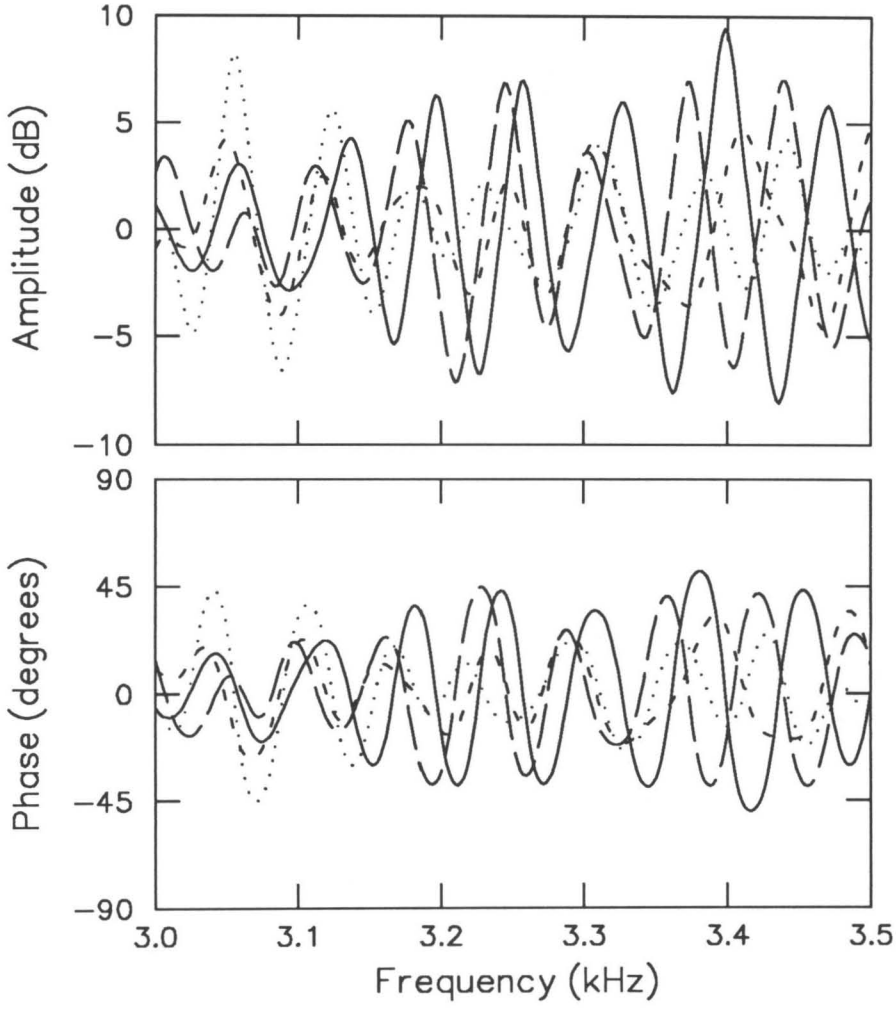

Figure 9. Simulated stimulus-frequency emissions computed as in Fig. 7, which is overlaid for comparison (———), using different sets of random inhomogeneities of the type shown in Fig. 8.

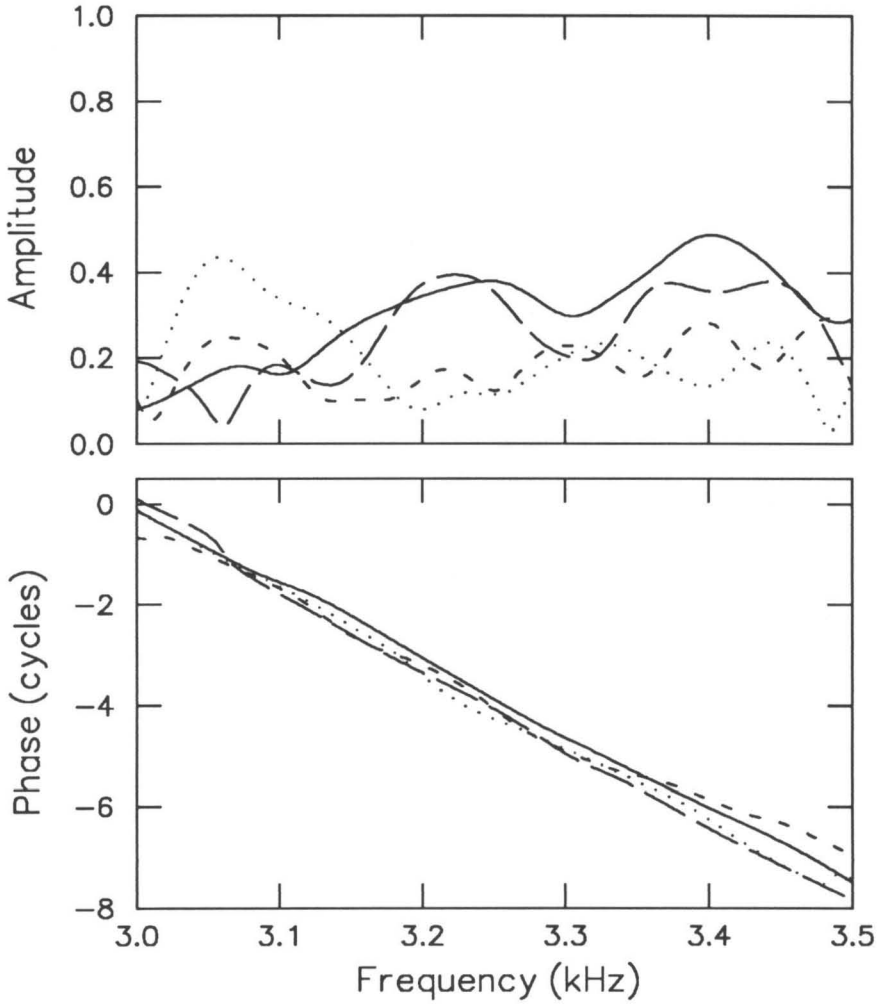

Figure 10. Traveling-wave ratios $R(\omega)$ corresponding to the simulated emissions shown in Fig. 9.

peak in $|Z(\omega)|$ and concomitant values of $\mathrm{Re}\{Z\} < 0$, indicating that the model is "emitting" energy at these frequencies (i.e., the traveling-wave ratio is greater than one). This occurs despite the fact that all spectral zeroes characterizing each of the many oscillators making up the organ of Corti are in the upper half of the complex-frequency plane (individually, the oscillators are stable). The appearance of this instability (a "spontaneous emission") thus arises as a collective response to the presence of a localized perturbation in the mechanics.

C. Comparison with a corrugated cochlea

To explain the roughly periodic structure of the spectra of evoked emissions, Strube (1989) recently proposed that evoked otoacoustic emissions originate as cochlear Bragg reflections scattering from an as yet unidentified periodic corrugation in the mechanics of the cochlea. In that model, the cochlea manifests a discrete translational symmetry characterized by some length scale Δx. That crystalline structure is, of course, superimposed on the more gradual monotonic variation of the mechanics responsible for the variation in characteristic frequency with position. The periodicities observed in the emission spectra are a direct reflection of this underlying washboarding in cochlear mechanics. Indeed, the observed frequency spacing Δf at frequency f in the emission spectra is given, as a function of Δx, by the equation

$$\Delta f / f = \Delta x / l \, . \tag{55}$$

Equations (54) and (55) become equivalent under the substitution $\mathrm{Re}\{\hat{\lambda}_x\} \rightarrow 2\Delta x$. In the analysis presented here, the length scale determining the frequency spacing Δf arises not as the result of some pre-existing cochlear corrugation, but dynamically from the scale provided by the wavelength at resonance. As an illustration, Fig. 13 shows a snapshot of the forward-traveling pressure wave generated by a pure tone, computed using the empirical wavelength $\lambda^{\dagger}$. Superimposed on the figure is a grid of constant spacing $\Delta x = \bar{d} = \frac{1}{2}\mathrm{Re}\{\hat{\lambda}_x\}$. (Note that the corresponding spacing $\Delta\beta \approx \beta\Delta x/l$ varies with position.) In the model of Strube (1989), the cells correspond to a pre-existing washboarding in the mechanics, and perhaps the anatomy, of the cochlea. In the analysis presented here, however, the length scale Δx emerges dynamically and has no objective correlate independent of the traveling wave.

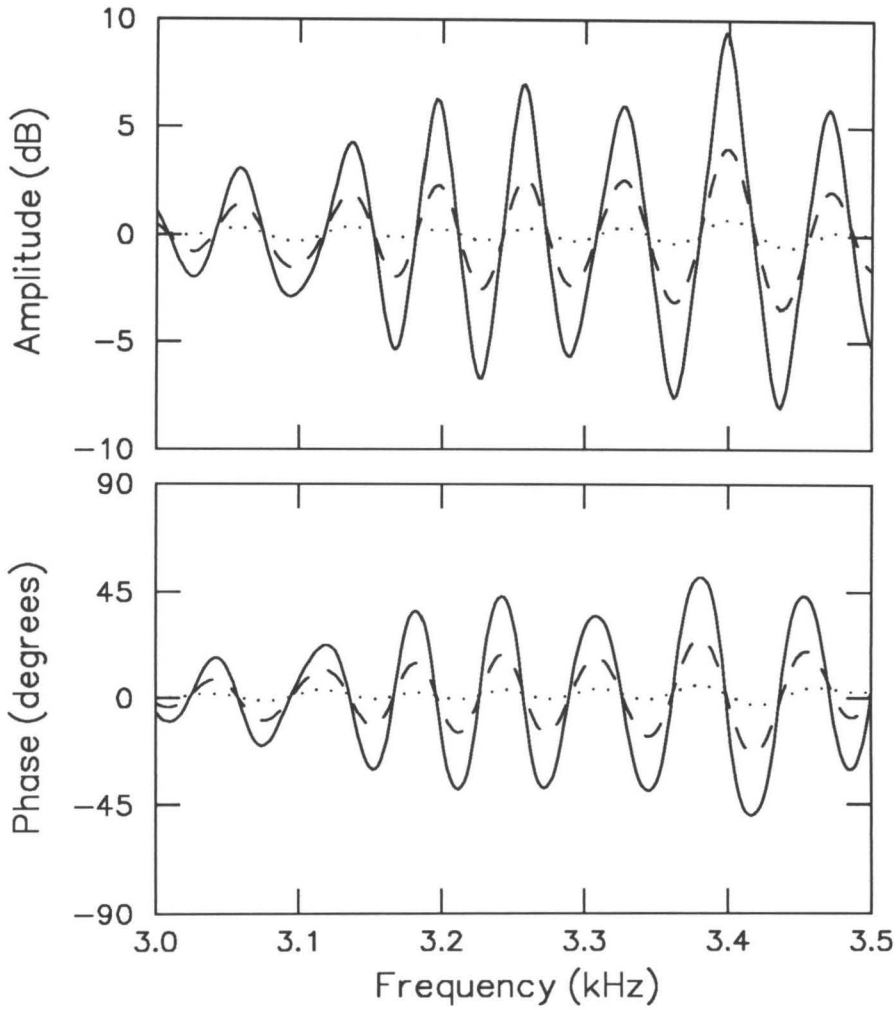

Figure 11. Simulated stimulus-frequency emissions computed for varying "stimulus levels" using the inhomogeneities shown in Fig. 8. The effective stimulus level was increased by moving the double zero in $\lambda^{\dagger}$ further from real axis, thereby lowering and broadening the peak in the corresponding transfer function. The dashed line (— — —), corresponding to a zero location of $\mathrm{Im}\{\ddot{\beta}\} = 0.033$, was computed using the parameter values

$$\delta = -0.1163; \quad \rho = 0.1268; \quad \text{and } \mu = 1.746.$$

The dotted line line (·····), corresponding to a zero location of $\mathrm{Im}\{\ddot{\beta}\} = 0.04$, was computed using the parameter values

$$\delta = -0.1024; \quad \rho = 0.1175; \quad \text{and } \mu = 1.745.$$

Figure 7, computed using parameter values listed in Fig. 2, is overlaid for comparison (———).

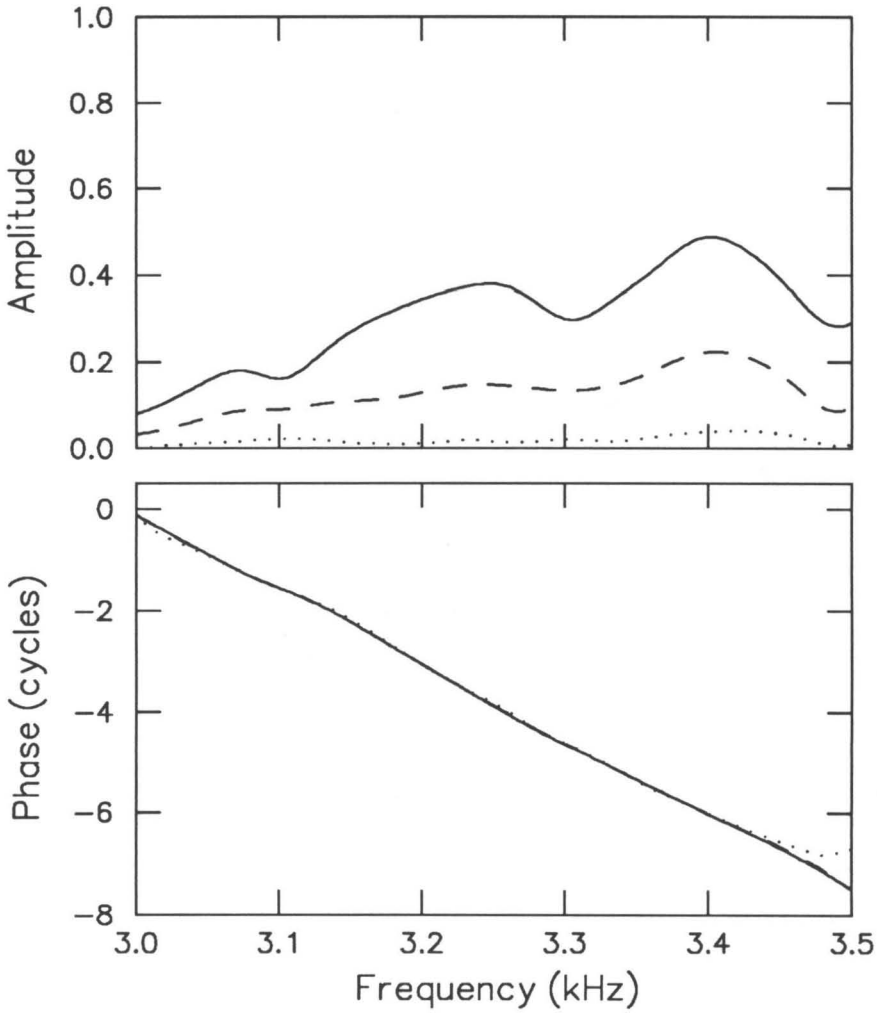

Figure 12. Traveling-wave ratios $R(\omega)$ corresponding to the simulated emissions shown in Fig. 11.

In a corrugated cochlea, the scattering location is determined not by the position of the maximum in A, but rather by the stationary-phase condition (Strube 1989). Given a spatial period Δx, scattering occurs at locations where the wavelength λ_x satisfies

$$2\mathrm{Re}\{1/\lambda_x\} = 1/\Delta x \ , \tag{56}$$

which, when inequality (41) is satisfied, reduces to the Bragg condition obtained by Strube (1989):

$$\tfrac{1}{2}\mathrm{Re}\{\lambda_x\} = \Delta x \ . \tag{57}$$

The analysis presented here does not, of course, rule out the possibility that the cochlea is actually corrugated (at the predicted or any other spatial frequency), but demonstrates that such corrugation, although sufficient, is not necessary for the generation of otoacoustic emissions. Indeed, unless the ostensible corrugations are large and "spectrally pure" (or happen to coincide with the spatial frequency $\bar{\xi}$), the mechanism described here will, in effect, filter them out in favor of spatial-frequency components close to $\bar{\xi}$ and perhaps present in the scattering potential only as "spatial noise."

Note that Strube's identification of the mechanism underlying wave reflection in a corrugated cochlea with the phenomenon of Bragg reflection is somewhat problematic. Bragg reflection occurs in crystalline materials in which incident waves of constant wavelength reflect off a large number of equally-spaced scattering centers (Ashcroft and Mermin 1976). The wavelets reflected from each plane of the crystal add coherently—and the phase of the scattering integrand is therefore stationary—when the wavelength coincides with half the crystal spacing (normal incidence). In the cochlea, however, the wavelength of the incident wave changes continually with position, and consequently no more than perhaps a couple scattering centers can ever contribute coherently to the reflected wave (cf. Fig. 13).

D. Connection with round-trip travel time

Section I showed how the empirical phase constant ϕ determines the value of the group delay through Eq. (4). Since ϕ and $\bar{\xi}$ are related through Eq. (51), the overall consistency of the analysis requires a connection between the round-trip travel time to and from the site of reflection and the dominant spatial frequency. That relationship, established here

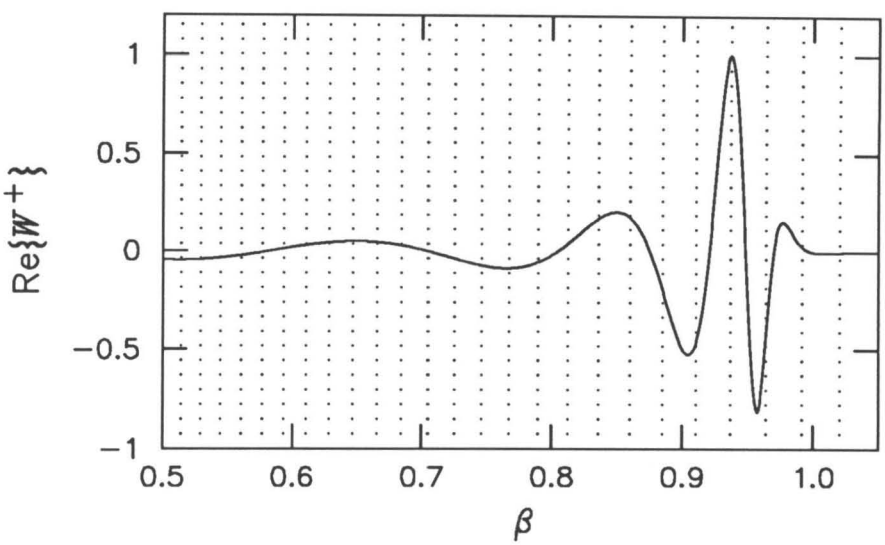

Figure 13. Temporal snapshot of the real part of the WKB approximation W^+ to the forward-traveling pressure wave normalized to unity at the peak, computed using the empirical wavelength $\lambda^\dagger$. The vertical dotted lines demarcate regions of constant width corresponding to the spatial frequency $\bar{\xi} \approx 45$ computed from the model (and representing the approximate distance, roughly 100 μm, spanned by 10 hair cells). Note that the wavelength is continually changing with position, so that even were the cochlea corrugated, no more than a *couple scattering* centers could contribute coherently to the reflected wave.

by direct computation, suggests another viewpoint from which to understand the origin of spectral periodicity in evoked emission.

The round-trip propagation time is given by

$$\tau_{\rightleftharpoons}(\omega) = 2\,\mathrm{Re}\int_0^{\hat{x}} \frac{dx}{c(x,\omega)}\,, \tag{58}$$

where $c(x,\omega)$ is the group velocity of the waves on the organ of Corti, and $\hat{x}$ represents the location of wave reflection. The group velocity is given by

$$c^{-1} = \frac{\partial k_x}{\partial \omega} = \frac{\partial \beta}{\partial \omega}\frac{d}{d\beta}\left(\frac{\partial \beta}{\partial x}k\right)\,, \tag{59}$$

where k_x is the local wavenumber $1/\lambda_x$. Thus,

$$\tau_{\rightleftharpoons}(\omega) = 2\,\mathrm{Re}\int_{\beta_0}^{\hat{\beta}} \frac{\partial \beta}{\partial \omega}\frac{d}{d\beta}\left(\frac{\partial \beta}{\partial x}k\right)\frac{\partial x}{\partial \beta}\,d\beta \tag{60}$$

$$= \frac{2}{\omega}\,\mathrm{Re}\int_{\beta_0}^{\hat{\beta}} \frac{d}{d\beta}\Big(\beta k\Big)\,d\beta \tag{61}$$

$$= \frac{2}{\omega}\,\mathrm{Re}\{\beta k\}\Big|_{\beta_0}^{\hat{\beta}}\,. \tag{62}$$

Since the wave slows down considerably as it approaches the resonance location, contributions to the travel time coming from the lower limit of integration (i.e., the basal region of the cochlea) can be neglected. Thus,

$$\tau_{\rightleftharpoons}(\omega) \approx \frac{2}{\omega}\hat{\beta}\,\mathrm{Re}\{1/\hat{\lambda}\}\,. \tag{63}$$

If the real part of the wavelength at the scattering location changes slowly, the round-trip travel time varies inversely with frequency, in agreement with measurements of the echo latency (Wilson 1980; Norton and Neely 1987; Zweig et al. 1992). Equating Eqs. (4) and (63)—that is, latency τ with round-trip travel time $\tau_{\rightleftharpoons}$—yields the expression

$$\phi = 2\hat{\beta}\,\mathrm{Re}\{1/\hat{\lambda}\}/2\pi = \bar{\xi}\,, \tag{64}$$

which relates, via the real part of the wavelength near resonance, the rate of phase rotation of the traveling-wave ratio (and hence the emission latency) to the dominant spatial frequency for scattering, in agreement with Eq. (51).

The connection with round-trip travel times to and from the site of reflection suggests an equivalent, but perhaps more physically intuitive, way of understanding the origin of the regular, almost periodic pattern characteristic of emission spectra. Interpreted in the time domain, the observed spectral regularity implies that the emission latency is well defined and, locally, a slowly-varying function of frequency. Reference to Eq. (63) indicates that $\tau_{\rightleftharpoons}$ will have a well-defined value at frequency ω if (1) the scattering location $\hat{\beta}$ is well determined, and (2) the function $\mathrm{Re}\{1/\lambda\}$ varies slowly at that location. These conditions are, of course, just those derived above in Sec. III.A.

IV. Solving the Inverse Problem

This section provides another perspective on the analysis presented above, combining theory and experiment to "invert" the measurements of R to obtain the form of the scattering potential ϱ. The inverse scattering problem has, however, no unique solution; two possibilities are discussed, the first corresponding to the corrugated-cochlea model (Strube 1989) and the second to the dynamic spatial-filtering mechanism outlined in Sec. III.

A. The inverse scattering problem

In Sec. I the empirical traveling-wave ratio was shown to have the approximate local form (Shera and Zweig 1992e)

$$R(\beta_0) \approx R_0 e^{-2\pi i \phi \ln \beta_0} , \tag{65}$$

where R_0 varies only slowly with frequency relative to the phase. Consequently,

$$\frac{dR}{d\beta_0} \approx -\frac{2\pi i \phi}{\beta_0} R . \tag{66}$$

In humans, $2\pi\phi \approx 80$ and $\beta_0 \approx 1/20$ at a typical emission frequency of 1 kHz. Thus,

$$\left| \frac{d \ln R}{d\beta_0} \right| = O(1600) . \tag{67}$$

Corresponding to these experimental results are the theoretical expressions derived in Sec. II. In the Born approximation, the traveling-wave ratio was shown to have the form

$$R(\beta_0) \approx \psi(\beta_0) \int_{\beta_0}^{\infty} \varrho(\beta, \beta_0) q(\beta)\, d\beta ; \tag{68}$$

where,

$$q(\beta) \equiv e^{-2i\int_0^\beta d\beta'/\lambda}/\lambda(\beta)\,, \tag{69}$$

and

$$\psi(\beta_0) \equiv -e^{+2i\int_0^{\beta_0} d\beta'/\lambda}/2i\,. \tag{70}$$

Differentiating Eq. (68) for R yields

$$\frac{dR}{d\beta_0} \approx \frac{2i}{\lambda(\beta_0)}R(\beta_0) \;-\; \psi(\beta_0)\varrho(\beta_0,\beta_0)q(\beta_0) + \;\psi(\beta_0)\int_{\beta_0}^{\infty}\frac{\partial\varrho(\beta,\beta_0)}{\partial\beta_0}q(\beta)\,d\beta\,. \tag{71}$$

Since

$$\lambda(\beta_0) \approx 1/4N\,, \tag{72}$$

the derivative can be simplified to the form

$$\frac{dR}{d\beta_0} \approx 2Ni\big[4R(\beta_0) \;-\; \varrho(\beta_0,\beta_0)\big] \;+\; \psi(\beta_0)\int_{\beta_0}^{\infty}\frac{\partial\varrho(\beta,\beta_0)}{\partial\beta_0}q(\beta)\,d\beta\,. \tag{73}$$

Comparison with Eq. (66) shows that the first term in brackets has the wrong sign to provide the dominant contribution to the derivative. In addition, both bracketed terms are far too small, given reasonable values of N and $|\varrho|$, to yield the empirical result. Consequently, we neglect those terms and approximate the derivative by

$$\frac{dR}{d\beta_0} \approx \psi(\beta_0)\int_{\beta_0}^{\infty}\frac{\partial\varrho(\beta,\beta_0)}{\partial\beta_0}q(\beta)\,d\beta\,. \tag{74}$$

Equations (68) and (74) for R and $dR/d\beta_0$ provide the theoretical counterparts to Eqs. (65) and (66) deduced from experiment. The inverse scattering problem is then to find forms for the potential ϱ that yield the experimental result.

B. A corrugated cochlea

The most straightforward way to solve the equations and make the theoretical expressions yield the empirical results is to assume that

$$\frac{\partial\varrho(\beta,\beta_0)}{\partial\beta_0} = -\frac{2\pi i\phi}{\beta_0}\varrho(\beta,\beta_0)\,. \tag{75}$$

When this expression for $\partial\varrho/\partial\beta_0$ is substituted into Eq. (74) for $dR/d\beta_0$, it yields an equation of the empirical form (66). To see this, note that solving Eq. (75) for ϱ yields

$$\varrho(\beta,\beta_0) \approx b(\beta)e^{+2\pi i\phi \ln(\beta/\beta_0)} , \tag{76}$$

where $b(\beta)$ is an undetermined function of β. Substituting this expression for ϱ into Eq. (68) yields

$$R(\beta_0) \approx \psi(\beta_0)e^{-2\pi i\phi \ln \beta_0} \int_{\beta_0}^{\infty} b(\beta)e^{+2\pi i\phi \ln \beta} q(\beta)\, d\beta , \tag{77}$$

which, after making the identification

$$R_0 = \psi(\beta_0) \int_{\beta_0}^{\infty} b(\beta)e^{+2\pi i\phi \ln \beta} q(\beta)\, d\beta , \tag{78}$$

has precisely the form determined empirically.

The exponential mapping between characteristic frequency and position implies that

$$e^{+2\pi i\phi \ln(\beta/\beta_0)} = e^{+2\pi i\phi x/l} . \tag{79}$$

Therefore, the exponential in ϱ is a periodic function of position, oscillating with dimensionless spatial frequency ϕ. The inhomogeneity appears as a product of a scaling function $b(\beta)$ and a symmetry-breaking function depending only on position. In this case, the mechanical inhomogeneities oscillate sinusoidally at a well-defined spatial frequency. When spatial periodicities of period Δx are introduced into the mechanics, corresponding periodicities of period Δf, where

$$\Delta f/f = \Delta x/l , \tag{80}$$

are created in the emission spectra; spatial periodicity in, spectral periodicity out. This solution to the inverse problem reduces to the corrugated-cochlea model of Strube (1989).

C. Dynamic spatial filtering

The solution to Eq. (66) found above is not, however, unique; another solution can be obtained as follows. Recall that by decomposing the inhomogeneity into its spatial frequency components, R can be written

$$R(\beta_0) \approx \psi(\beta_0) \int_{-\infty}^{\infty} d\xi\, \bar{\varrho}(\xi,\beta_0) \int_{\beta_0}^{\infty} d\beta\, q(\beta)e^{2\pi i\xi \ln(\beta/\beta_0)} , \tag{81}$$

so that

$$\frac{dR}{d\beta_0} \approx -\frac{2\pi i}{\beta_0}\psi(\beta_0)\int_{-\infty}^{\infty} d\xi\, \bar{\varrho}(\xi,\beta_0)\xi \int_{\beta_0}^{\infty} d\beta\, q(\beta)e^{2\pi i\xi \ln(\beta/\beta_0)}\ , \tag{82}$$

where $\partial\bar{\varrho}(\xi,\beta_0)/\partial\beta_0$ has been assumed small.

Assume, now, that the integral $\int qe^{2\pi i\xi \ln\beta}d\beta$ has the form of a δ-function in spatial frequency:

$$\int_{\beta_0}^{\infty} q(\beta)e^{2\pi i\xi \ln\beta}\, d\beta \approx A(\xi)\delta(\xi-\bar{\xi}) \quad \text{with } \bar{\xi}=\phi\ . \tag{83}$$

With that assumption, R and its derivative become

$$R(\beta_0) \approx R_0(\beta_0)e^{-2\pi i\phi \ln\beta_0}\ , \tag{84}$$

where

$$R_0(\beta_0) \equiv \psi(\beta_0)\bar{\varrho}(\phi,\beta_0)A(\phi)\ ; \tag{85}$$

and

$$\frac{dR}{d\beta_0} \approx -\frac{2\pi i\phi}{\beta_0}R(\beta_0)\ , \tag{86}$$

in agreement with the empirical results. Unlike the case of the corrugated cochlea, the inhomogeneities ϱ need have no particular spectral content—indeed, they can be completely random—as long as $\bar{\varrho}(\phi,\beta_0)\neq 0$. The appropriate spatial frequency component is extracted from the spectrum $\bar{\varrho}$ dynamically.

This dynamic spatial-filtering mechanism is, of course, but an idealized version of that outlined in Sec. III. Figure 5 shows that the integral $\int qe^{2\pi i\xi \ln\beta}d\beta$, which is simply the function F, is sharply peaked about the value $\xi=\bar{\xi}$, resembling the δ-function $\delta(\xi-\bar{\xi})$ used here. As shown above, the constant ϕ responsible for the observed frequency spacing Δf is determined by the value of the wavelength at resonance:

$$\phi \approx 2\hat{\beta}\,\mathrm{Re}\{1/\hat{\lambda}\}/2\pi\ . \tag{87}$$

In this solution to the inverse problem, the observed periodicity is not an input to the model, but emerges as a consequence of the dynamics.

V. Discussion

Because the cochlea maps frequency into position, it is natural to associate a length scale Δx with the observed spectral period Δf characterizing the threshold hearing curve and the spectra of evoked emissions. The two intervals are related by

$$\Delta x/l = \Delta f/f \ , \tag{88}$$

an equation obtained by differentiating the exponential form of the frequency-position map. Current models require that the frequency spacing Δf originate with a corresponding corrugation (of spatial period Δx) in the organ of Corti. This paper has shown, however, that the length scale Δx can arise dynamically, and need have no objective correlate in the mechanical structure of the cochlea. In this analysis, the frequency spacing Δf reflects not some pre-existing corrugation in cochlear mechanics, but arises from the length scale provided by the wavelength of the traveling wave near "resonance."

The frequency spacing Δf of the emission spectra thus provides a noninvasive measure of the real part of the wavelength near the peak of the transfer function. For example, experiments indicate that whereas R_0 appears to be a strong function of stimulus amplitude (rapidly going to zero at higher levels), the constant ϕ determining the frequency spacing Δf is essentially independent of level (e.g., Zwicker and Schloth 1984; Shera and Zweig 1992e). The theory outlined here thus predicts that $\mathrm{Re}\{1/\hat{\lambda}\}$, which determines ϕ, is largely independent of stimulus level. By contrast, the imaginary part of the wavelength, responsible for the observed variation in the amplitude of R, presumably depends considerably on stimulus amplitude.

The focus of this paper is complementary to the subject of an earlier paper (Shera and Zweig 1991a). Both combine measurements and analysis to deduce empirical constraints on the form of the wavelength of the traveling pressure wave. But whereas the earlier paper focuses on the properties of the wavelength in the basal, small-β region of the cochlea corresponding to the tails of the transfer functions, this paper explores the region near $\beta = 1$ about the peak of the wave envelope. Whereas the earlier paper concerns itself principally with cochlear mechanics at sound-pressure levels above 60 dB, deducing the existence of a tapering symmetry that guarantees that waves traveling through the basal

turn suffer little reflection, here the analysis focuses on the low-level, linear regime and identifies characteristics of the wavelength necessary for the generation of evoked emissions with the amplitude and spectral periodicity observed experimentally.

This paper assumes scaling symmetry in order to simplify the evaluation of scattering integrals that are dominated by the value of the integrand in a small region about the peak of the transfer function. Although measurements of basilar-membrane motion (Rhode 1971; Gummer et al. 1987) have shown that scaling symmetry is operative in the basal turns of the cochlea, that symmetry appears to be broken at the lower characteristic frequencies for which human evoked emission, measured in the ear canal, is strongest. Even at low frequencies, however, there remains a local continuity in the shape of the transfer functions—and hence, presumably, in the wavelength—that permits the definition of a local scaling variable near the peak of the response.

Statistical measurements of evoked emissions (e.g., the distribution of amplitude fluctuations about the smooth high-amplitude limit for a stimulus-frequency emission curve) provide constraints on the form of the inhomogeneities and their spatial correlations. For example, deviations from perfect spectral regularity can be quantified by computing correlation functions that relate statistical properties of the frequency spectra of evoked emissions to those present in the underlying spatial inhomogeneities responsible for the reflection. Thus, when coupled with a model of cochlear mechanics, such measurements can, in principle, be used to test whether the underlying inhomogeneities are consistent, for example, with an assumption of randomness at the level of the hair cell. Any comparison between theory and experiment, however, awaits both a model of cochlear mechanics believed valid at the relatively low frequencies typical of evoked emission and a systematic measurement of the statistical properties of emissions.

Although correlation functions and other expectation values defined over an ensemble can be computed from simulations by changing the inhomogeneities responsible for the wave scattering, they are not so easily measured, since the pattern of inhomogeneities is fixed in each subject. To the extent that scaling symmetry is applicable in the "smooth" cochlea, however, certain statistical properties of the emission spectra may be computable in a single subject by invoking an analog of the ergodic principle and replacing averages over an ensemble of inhomogeneities explored at fixed frequency (i.e., over an ensemble of subjects) with averages over frequency (and hence position) assembled from measurements on a single individual.

VI. Summary

This paper has explored the origin of the remarkable regularity apparent in the spectra of evoked otoacoustic emissions and has sought to understand the constraints such spectral order places on models of cochlear mechanics. Contrary to recent arguments (e.g., Strube 1985; Peisl 1988; Strube 1989), the paper has demonstrated that a corresponding corrugation in the mechanics of the organ of Corti is not necessary for generating the observed periodicities. When the wavelength satisfies conditions summarized below—conditions satisfied by the empirical wavelength deduced from measurements in the squirrel monkey (Zweig 1991)—such periodicities can emerge spontaneously through the dynamics of wave propagation and reflection, despite the apparent "irregularity" and "disorganization" of the micromechanics of the organ of Corti that presumably gives rise to that scattering (Lonsbury-Martin et al. 1988).

The following list summarizes the major results and conclusions of the paper.

1. Noninvasive measurements of stimulus-frequency emission in human ears indicate that the traveling-wave ratio, $R(\omega)$, has the approximate form (Shera and Zweig 1992e)

$$R(\omega) \approx R_0(\epsilon\omega)e^{-2\pi i\phi \ln(\omega/\omega_{c_0})} , \tag{89}$$

   where $R_0(\epsilon\omega)$ varies slowly with frequency compared to the phase.

2. An approximate expression for $R(\omega)$ has been given in the form of a scattering integral and used to demonstrate that the long latencies typical of human evoked emission require a breaking of scaling symmetry, confirming arguments (Kemp 1986; Strube 1989) that "wave-related" reflection mechanisms cannot account for primate evoked emission;

3. The empirical form of $R(\omega)$ has been inverted to obtain solutions to the inverse scattering problem. Two qualitatively different solutions were obtained:

   A. In one possible solution, the observed spectral periodicities reflect a pronounced underlying corrugation in the mechanics of the cochlea (Strube 1989). The observed spectral period Δf is then related to the length scale Δx characterizing the spatial washboarding through the equation

$$\Delta f/f = \Delta x/l . \tag{90}$$

This solution achieves spectral periodicity by exploiting the cochlear mapping between frequency and position and requiring a corresponding spatial periodicity in the inhomogeneities causing the reflection. No particular constraints are placed on the form of the wavelength λ. Generic passive models, however, require a substantial inhomogeneity to generate emissions of the size determined empirically.

B. Alternatively, the observed spectral order can emerge spontaneously through a dynamic process of spatial filtering in which, as suggested by the anatomy (Lonsbury-Martin et al. 1988), the micromechanics of the organ of Corti need manifest no particular long-range regularity or organization. To generate a pronounced periodicity despite the lack of regularity in the scattering potential, this solution requires (a) that the function $A(\beta)$, defined by

$$A(\beta) \equiv -\ln|\lambda| + 2\int_{\beta_0}^{\beta} \mathrm{Im}\{1/\lambda\}\, d\beta' \,, \tag{91}$$

have a strong, sharp maximum $\hat{A}$ at some value $\hat{\beta} < 1$; and (b) that $\mathrm{Re}\{1/\lambda\}$ remain roughly constant in a neighborhood about $\hat{\beta}$ of size $\Delta\beta$ proportional to the width of the maximum in $A(\beta)$. Condition (a) guarantees that the scattering region about $\hat{\beta}$ is well defined; condition (b) that inhomogeneities characterized by spatial frequencies ξ lying outside a small neighborhood of $\bar{\xi} = \phi$ contribute little to the net reflected wave (or, equivalently, that the round-trip travel time varies slowly over the scattering region). In this case, the spectral period Δf is determined by the value of the wavelength near the peak of the wave envelope:

$$\Delta f / f \approx 1/\bar{\xi} \,, \tag{92}$$

where

$$\bar{\xi} = 2\hat{\beta}\,\mathrm{Re}\{1/\hat{\lambda}\}/2\pi \,. \tag{93}$$

The observed spectral regularity arises spontaneously through the dynamics of wave propagation and reflection.

The empirical wavelength found by inverting basilar-membrane transfer functions measured in the squirrel monkey satisfies these two conditions, achieving

the sharp maximum in A through the form of the imaginary part of the wavelength, which results in a substantial transfer of energy to the traveling wave basal to the putative scattering location $\hat{\beta}$ (Zweig 1991).

The two possibilities are not, of course, mutually exclusive. When conditions (a) and (b) are satisfied, however, a pronounced corrugation of the mechanics, while sufficient, remains unnecessary for producing the striking periodicities observed in the spectra of evoked emission.

Acknowledgments

This work was supported, in part, by DARPA and AFOSR contract N00014-86-C0399, the Theoretical Division of Los Alamos National Laboratory, and a National Science Foundation Graduate Fellowship to C. A. S.

References

Ashcroft, N. W. and N. D. Mermin (1976). *Solid State Physics.*New York: Holt, Rinehart, & Winston.

Beecher, M. D. (1974). "Pure-tone thresholds of the squirrel monkey," *J. Acoust. Soc. Am.* **55**, 196–198.

Bode, H. (1945). *Network Analysis and Feedback Amplifier Design.*Princeton: Van Nostrand Reinhold.

de Boer, E. (1983). "Wave reflection in passive and active cochlea models," in *Mechanics of Hearing*, edited by E. de Boer and M. A. Viergever, 135–142. Delft: Delft University Press.

Friedman, B. (1969). *Lectures on Applications-Oriented Mathematics.*San Francisco: Holden-Day.

Gummer, A. W., J. W. T. Smolders, and R. Klinke (1987). "Basilar membrane motion in the pigeon measured with the Mössbauer technique," *Hearing Res.* **29**, 63–92.

Kemp, D. T. (1978). "Stimulated acoustic emissions from within the human auditory system," *J. Acoust. Soc. Am.* **64**, 1386–1391.

Kemp, D. T. (1979). "The evoked cochlear mechanical response and the auditory microstructure — Evidence for a new element in cochlear mechanics," *Scand. Audiol. Suppl.* **9**, 35–47.

Kemp, D. T. (1980). "Towards a model for the origin of cochlear echoes," *Hearing Res.* **2**, 533–548.

Kemp, D. T. (1986). "Otoacoustic emissions, travelling waves and cochlear mechanisms," *Hearing Res.* **22**, 95–104.

Lonsbury-Martin, B.L., G.K. Martin, R. Probst, and A.C. Coats (1988). "Spontaneous otoacoustic emissions in the nonhuman primate. II. Cochlear anatomy," *Hearing Res.* **33**, 69–94.

Manley, G. A. (1983). "Frequency spacing of acoustic emissions: A possible explanation," in *Mechanisms of Hearing*, edited by W. R. Webster and L. M. Aitkin, 36–39. Clayton, Australia: Monash University Press.

Martin, G. K., B. L. Lonsbury-Martin, R. Probst, and A. C. Coats (1988). "Spontaneous otoacoustic emissions in the nonhuman primate. I. Basic features and relations to other emissions," *Hearing Res.* **33**, 49–68.

Neely, S. T., S. J. Norton, M. P. Gorga, and W. Jesteadt (1988). "Latency of auditory brain-stem responses and otoacoustic emissions using tone-burst stimuli," *J. Acoust. Soc. Am.* **83**, 652–656.

Norton, S. J. and S. T. Neely (1987). "Tone-burst-evoked otoacoustic emissions from normal-hearing subjects," *J. Acoust. Soc. Am.* **81**, 1860–1872.

Papoulis, A. (1968). *Systems and Transforms with Applications in Optics.*New York: McGraw-Hill.

Peisl, W. (1988). "Simulation von zeitverzögerten evozierten oto-akustischen Emissionen mit Hilfe eines digitalen Innenohrmodells," in *Fortschritte der Akustik—DAGA'88.* Bad Honnef: DPG-GmbH..

Rhode, W. S. (1971). "Observations of the vibration of the basilar membrane in squirrel monkeys using the Mössbauer technique," *J. Acoust. Soc. Am.* **49**, 1218–1231.

Shera, C. A. and G. Zweig (1991a). "A symmetry suppresses the cochlear catastrophe," *J. Acoust. Soc. Am.* **89**, 1276–1289.

Shera, C. A. and G. Zweig (1991b). "Reflection of retrograde waves within the cochlea and at the stapes," *J. Acoust. Soc. Am.* **89**, 1290–1305.

Shera, C. A. and G. Zweig (1992e). "Noninvasive measurement of the cochlear traveling-wave ratio," submitted to *J. Acoust. Soc. Am.*

Strube, H. W. (1985). "A computationally efficient basilar-membrane model," *Acustica* **58**, 207–214.

Strube, H. W. (1989). "Evoked otoacoustic emissions as cochlear Bragg reflections," *Hearing Res.* **38**, 35–45.

Wilson, J. P. (1980). "Evidence for a cochlear origin for acoustic re-emissions, threshold fine-structure and tonal tinnitus," *Hearing Res.* **2**, 233–252.

Zweig, G. (1976). "Basilar membrane motion," in *Cold Spring Harbor Symposia on Quantitative Biology, volume XL, 1975*, 619–633. Cold Spring Harbor: Cold Spring Harbor Laboratory.

Zweig, G., R. Lipes, and J. R. Pierce (1976). "The cochlear compromise," *J. Acoust. Soc. Am.* **59**, 975–982.

Zweig, G. and S. Konishi (1987). "Constraints on measurements of causal or minimum-phase systems," accepted for publication in *J. Acoust. Soc. Am.*

Zweig, G. (1991). "Finding the impedance of the organ of Corti," *J. Acoust. Soc. Am.* **89**, 1229–1254.

Zweig, G., J. E. McDowell, and C. A. Shera (1992). "Latency of tone-burst-evoked oto-acoustic emissions," in preparation.

Zwicker, E. and E. Schloth (1984). "Interrelation of different oto-acoustic emissions," *J. Acoust. Soc. Am.* **75**, 1148–1154.

IX. Epilogue

"What's past is prologue."

—Shakespeare, *The Tempest* (act II, scene i)

By way of conclusion, these final pages—written with the hope of provoking further examination of the ideas presented here—gather together proposals for a number of experiments in hearing naturally suggested by the results of the thesis.

- *Tapering symmetry.* Tapering symmetry was deduced (§I) from measurements of the cochlear input impedance in cat (Lynch et al. 1982). Rigorous comparison with experiment requires additional measurements, in both cats and human cadavers. Those measurements should be made at the basal end of the organ of Corti, provide considerable coverage of low and intermediate frequencies, have known errors, and exhibit the minimum-phase analyticity properties required of driving-point impedances (Bode 1945; Zweig and Konishi 1987). Tapering symmetry predicts that the phase of the cochlear input impedance remains small at low frequencies.

- *The opposing tapers of cochlear geometry.* Tapering symmetry relates the spatial variation of certain geometric and mechanical properties in the basal turns of the cochlea (§I). The opposing tapers of cochlear geometry—whereby the scalae areas and the width of the basilar membrane taper in opposite directions—are a natural consequence of that symmetry. To test more rigorously the simple proportionality implied by conventional cochlear models, one can measure the spatial variation of both the scalae cross-sectional area and the volume stiffness of the organ of Corti. Ideally, measurements should be made in the same preparations used above to measure the input impedance. In addition to testing the relationships implied by tapering symmetry, the measurements can be compared with the predictions of scaling symmetry (cf. §I).

- *Effective areas of the eardrum.* Measurement of the transfer coefficients of the eardrum—including its two effective areas and their regions of validity—would permit incorporation of a phenomenological model of eardrum transduction into models of the middle ear and allow a meaningful comparison between the predictions of eardrum models and experiment (§III). The standard methodology should include using the

constraints imposed by causality to check and "improve" the measurements (Zweig and Konishi 1987), which can then be examined for minimum-phase behavior and consistency with the principle of reciprocity.

- *Deconstruction of middle-ear mechanics.* Systematic, invasive measurements of the transfer coefficients of the middle ear and its components in a series of individual preparations (preferably feline and/or cadaver) would permit a more rigorous comparison between middle-ear models and experiment. Current models are based almost exclusively on "average" measurements and remain incompletely tested, even at low frequencies. For example, models predict both "forward" and "reverse" transfer functions, but the latter have never been compared with experiment. Although middle-ear transduction characteristics are conveniently factored into a product of component transformations, the regions of validity for that factorization remain largely unknown. The validity of the program of middle-ear deconstruction must be therefore established experimentally. As always, measurement consistency should be examined using constraints (such as causality and reciprocity) that overdetermine the system.
- *Stapes reflection coefficient.* Measurement of middle-ear transfer coefficients and cochlear input impedance can be combined to calculate the basal reflection coefficient for retrograde waves incident upon the stapes (§II). Those results can be compared with the predictions of middle-ear models. The basal reflection coefficient has important consequences for understanding combination-tone and other similar experiments in which the middle ear is driven in reverse (§V). In addition, differences in the amplitude of that reflection coefficient induced by variations in middle-ear size correlated to gender may underly the observation that spontaneous emissions are found more frequently in females than in males.
- *Noninvasive measurement of middle-ear scattering coefficients.* Combining the analysis techniques presented in chapters V and VII allows one to measure certain combinations of middle-ear scattering coefficients noninvasively. Those measurements can be used to test the common theoretical assumption that the action of the middle-ear can be idealized as that of a simple mechanical transformer (Shera and Zweig 1992g). Especially interesting would be a comparison between such measurements and the

predictions of a middle-ear model whose parameter values have been estimated by comparison with the middle-ear input impedance in the same subject (Shera and Zweig 1992d).

- *Psychophysical Gedankenexperiments.* The *Gedankenexperiment* analyzed in chapter V can be performed psychophysically or, in the spirit of Fahey and Allen (1985), neurophysiologically. The analysis suggests one will find pronounced "resonant peaks" due to wave interference effects within the cochlea.

- *"Dividing out" the middle ear.* The formalism outlined in chapter V can be used to identify combination- and cancellation-tone experiments in which the unknown transfer characteristics of the middle ear "divide out," greatly simplifying the comparison between theory and experiment.

- *Direct measurement of cochlear compressibility.* Chapter VI used an analysis of psychophysical thresholds in patients with missing or disarticulated middle-ear ossicles (von Békésy 1936; von Békésy 1960) to obtain a tight upper bound on the magnitude of cochlear compressibility. Direct measurements of oval- and round-window volume displacements—made, for example, by measuring stapes displacement with the Mössbauer technique (e.g., Lynch et al. 1982) while recording round-window displacements with a sensitive microphone sealed over the niche (e.g., Moxon 1971)—should be able to corroborate that result.

- *Hearing thresholds in the middleless ear.* Additional psychophysical measurements on the "middleless" ear should be undertaken to verify von Békésy's finding—consistent with a small, but finite compressibility—that hearing in such ears is most sensitive at low frequencies. The prediction that immobilizing the stapes should actually improve hearing in these subjects, especially at higher frequencies, can be tested in animal preparations where measurements of auditory-nerve fiber thresholds can replace psychophysical determination of the hearing threshold. To minimize pressure differences between the oval and round windows, which can drive the cochlea and complicate the interpretation, the experiments should be performed in animals in which the two windows face onto the same cavity or in preparations in which the cavities have been opened widely. Similarly, residual hearing due to compressibility can be expected to

decrease if the impedances of the oval and round windows are made more comparable. For example, removing the stapes while retaining the oval window membrane, which presumably increases the symmetry between the windows, should result in an elevation of hearing thresholds at low frequencies.

- *Emission statistics.* Measurement of amplitude distributions and other statistical properties of stimulus-frequency emissions can be helpful in understanding the distribution of spatial inhomogeneities responsible for the reflection underlying evoked emission (cf. §VIII).
- *Level-dependence of evoked emission.* Measurements of basilar-membrane transfer functions can be "inverted" to find the wavelength of cochlear traveling waves as a function of frequency and stimulus level (Zweig 1991). The qualitative picture of evoked emission presented in §VIII predicts that the observed spectral periodicity (and, as a result, the latency) of evoked emissions provides a measure of the real part of the wavelength near the peak of the wave envelope. By contrast, the amplitude of evoked emissions reflects the value of the imaginary part of the wavelength (which, depending on its sign, may either amplify or diminish the energy in retrograde waves during propagation). Measurements of the level-dependence of emission latency and amplitude suggest that the real and imaginary parts of the wavelength vary quite differently with sound-pressure level. Comparison of these independent determinations of the wavelength and its variation with level would provide a critical test of the model of evoked emission.
- *Emissions and expectations.* Although evoked emissions may originate as an epiphenomenon of mechanical activity in the cochlea, the correlation between their spectra and the microstructure of the hearing threshold curve and the evidence for their control from the central nervous system suggests that the brain may exploit emissions to modify the sensitivity of hearing. Measurements of emissions can be combined with psychophysical experiments to explore whether the mechanics are modified by expectations.
    - For example, the position of extrema in the emission spectra (and, consequently, in the hearing threshold) can be determined from the envelope of the measured

ear-canal pressure in response to tone burst (Zweig et al. 1992). If those tone bursts are masked by noise played to the contralateral ear and the subject asked to detect them, the ear might attempt to obtain greater sensitivity at the tone-burst frequency by modifying (perhaps only locally) the pattern of peaks and valleys in the threshold microstructure. When reflected in the emission spectra, those modifications can be detected noninvasively in the ear canal.

As another example, it would be interesting to explore emissions evoked by transient stimuli under conditions that "confuse" the brain, such as the tone-burst illusion described by Deutsch (Deutsch 1974; Deutsch 1975; Houtsma et al. 1987). Let the letters A and B denote different tones. When the tone sequences "$ABABAB\cdots$" and "$BABABA\cdots$" are presented simultaneously to the right and left ears, respectively, the percepts in the two ears are typically "A–A–A–$\cdots$" and "–B–B–B–$\cdots$." (The perceived pattern is correlated with the handedness of the subject; right handers have a strong tendency to localize the higher frequency tone to the right ear.) By recording emissions evoked by these stimuli, presented first to each ear separately and then together, one can look for any peripheral correlates of central confusion.

References

von Békésy, G. (1936). "Zur Physik des Mittelohres und über das Hören bei fehlerhaftem Trommelfell," *Akust. Zeits.* **1**, 13–23.

von Békésy, G. (1960). *Experiments in Hearing.*New York: McGraw-Hill.

Bialek, W. and H. P. Wit (1983). "Quantum limits to oscillator stability: Theory and experiments on acoustic emissions from the human ear," in *Hearing — Physiological Bases and Psychophysics*, edited by R. Klinke and R. Hartmann, 51–57. Berlin: Springer Verlag.

Bode, H. (1945). *Network Analysis and Feedback Amplifier Design.*Princeton: Van Nostrand Reinhold.

Brownell, W. E., C. R. Bader, D. Bertrand, and Y. de Riebaupierre (1985). "Evoked mechanical responses of isolated cochlear outer hair cells," *Science* **227**, 194–196.

Burns, E. M., E. A. Strickland, A. Tubis, and K. Jones (1984). "Interactions among spontaneous otoacoustic emissions. I. Distortion products and linked emissions," *Hearing Res.* **16**, 271–278.

Deutsch, D. (1974). "An auditory illusion," *Nature* **251**, 307–309.

Deutsch, D. (1975). "Musical illusions," *Sci. Am.* **233**(4), 92–104.

Elliot, E. (1958). "A ripple effect in the audiogram," *Nature* **181**, 1076.

Fahey, P. F. and J. B. Allen (1985). "Nonlinear phenomena as observed in the ear canal and at the auditory nerve," *J. Acoust. Soc. Am.* **77**, 599–612.

Goldstein, J. L. (1967). "Auditory nonlinearity," *J. Acoust. Soc. Am.* **41**, 676–689.

Gold, T. (1948). "Hearing. II. The physical basis of the action of the cochlea," *Proc. Roy. Soc. B.* **210**, 71–72.

Helmholtz, H. L. F (1863). *Die Lehre von den Tonempfindungen als physiologische Grundlage für die Theorie der Musik.*Braunschweig: Vieweg. Trans. by A. J. Ellis, *On the Sensations of Tone as a Physiological Basis for the Theory of Music.* New York: Dover, 1954.

Horst, J. W., H. P. Wit, and R. J. Ritsma (1983). "Psychophysical aspects of cochlear acoustic emissions ('Kemp tones').," in *Hearing — Physiological Bases and Psychophysics*, edited by R. Klinke and R. Hartmann, 89–94. Berlin: Springer Verlag.

Houtsma, A. J. M., T. D. Rossing, and W. M. Wagenaars (1987). "Auditory Demonstrations," compact disk (Phillips 1126-061) prepared at the Institute for Perception Research, Eindhoven, The Netherlands, with support from the Acoustical Society of America.

Jones, K., A. Tubis, G. L. Long, E. M. Burns, and E. A. Strickland (1986). "Interactions among multiple spontaneous otoacoustic emissions," in *Peripheral Auditory Mechanisms*, edited by J. B. Allen, J. L. Hall, A. Hubbard, S. T. Neely, and A. Tubis, 266–273. Berlin: Springer–Verlag.

Kemp, D. T. (1978). "Stimulated acoustic emissions from within the human auditory system," *J. Acoust. Soc. Am.* **64**, 1386–1391.

Kemp, D. T. (1979). "Evidence of mechanical nonlinearity and frequency selective wave amplification in the cochlea," *Arch. Otorhinolaryngol.* **224**, 37–45.

Kemp, D. T. (1979). "The evoked cochlear mechanical response and the auditory microstructure — Evidence for a new element in cochlear mechanics," *Scand. Audiol. Suppl.* **9**, 35–47.

Kemp, D. T. (1980). "Towards a model for the origin of cochlear echoes," *Hearing Res.* **2**, 533–548.

Kemp, D. T., P. Bray, L. Alexander, and A. M. Brown (1986). "Acoustic emission cochleography—Practical aspects," *Scand. Audiol. Suppl.* **25**, 71–95.

LePage, E. L. (1987). "Frequency-dependent self-induced bias of the basilar membrane and its potential for controlling sensitivity and tuning in the mammalian cochlea," *J. Acoust. Soc. Am.* **82**, 139–154.

LePage, E. L. (1990). "Helmholtz revisited: Direct mechanical data suggest a physical model for dynamic control of mapping frequency to place along the cochlear partition," in *Mechanics and Biophysics of Hearing*, edited by P. Dallos, C. D. Geisler, J. W. Matthews, M. A. Ruggero, and C. R. Steele, 278–285. Berlin: Springer–Verlag.

Lonsbury-Martin, B.L., G.K. Martin, R. Probst, and A.C. Coats (1988). "Spontaneous otoacoustic emissions in the nonhuman primate. II. Cochlear anatomy," *Hearing Res.* **33**, 69–94.

Lynch, T. J., V. Nedzelnitsky, and W. T. Peake (1982). "Input impedance of the cochlea in cat," *J. Acoust. Soc. Am.* **72**, 108–130.

Manley, G. A. (1983). "Frequency spacing of acoustic emissions: A possible explanation," in *Mechanisms of Hearing*, edited by W. R. Webster and L. M. Aitkin, 36–39. Clayton, Australia: Monash University Press.

Mott, J. B., S. J. Norton, S. T. Neely, and W. B. Warr (1989). "Changes in spontaneous otoacoustic emissions produced by acoustic stimulation of the contralateral ear," *Hearing Res.* **38**, 229–242.

Moxon, E. C. (1971). "Neural and mechanical responses to electric stimulation of the cat's inner ear," Ph.D. thesis, Massachusetts Institute of Technology.

Norton, S. J. and S. T. Neely (1987). "Tone-burst-evoked otoacoustic emissions from normal-hearing subjects," *J. Acoust. Soc. Am.* **81**, 1860–1872.

Peisl, W. (1988). "Simulation von zeitverzögerten evozierten oto-akustischen Emissionen mit Hilfe eines digitalen Innenohrmodells," in *Fortschritte der Akustik—DAGA'88.* Bad Honnef: DPG-GmbH..

Probst, R., A. C. Coats, G. K. Martin, and B.L Lonsbury-Martin (1986). "Spontaneous, click-, and toneburst-evoked otoacoustic emissions from normal ears," *Hearing Res.* **21**, 261–275.

Probst, R., B. L. Lonsbury-Martin, and G. K. Martin (1991). "A review of otoacoustic emissions," *J. Acoust. Soc. Am.* **89**, 2027–2067.

Rabinowitz, W. M. and G. P. Widin (1984). "Interaction of spontaneous oto-acoustic emissions and external sounds," *J. Acoust. Soc. Am* **76**, 1713–1250.

Ruggero, M. A., N. C. Rich, and R. Freyman (1983). "Spontaneous and impulsively evoked otoacoustic emissions: Indicators of cochlear pathology?" *Hearing Res.* **10**, 283–300.

Shera, C. A. and G. Zweig (1991a). "A symmetry suppresses the cochlear catastrophe," *J. Acoust. Soc. Am.* **89**, 1276–1289.

Shera, C. A. and G. Zweig (1991b). "Reflection of retrograde waves within the cochlea and at the stapes," *J. Acoust. Soc. Am.* **89**, 1290–1305.

Shera, C. A. and G. Zweig (1991c). "Phenomenological characterization of eardrum transduction," *J. Acoust. Soc. Am.* **90**, 253–262.

Shera, C. A. and G. Zweig (1992a). "Middle-ear phenomenology: The view from the three windows," submitted to *J. Acoust. Soc. Am.*

Shera, C. A. and G. Zweig (1992b). "Analyzing reverse middle-ear transmission: Noninvasive *Gedankenexperiments*," submitted to *J. Acoust. Soc. Am.*

Shera, C. A. and G. Zweig (1992d). "Noninvasive estimation of middle-ear transfer characteristics in human cadavers," in preparation.

Shera, C. A. and G. Zweig (1992e). "Noninvasive measurement of the cochlear traveling-wave ratio," submitted to *J. Acoust. Soc. Am.*

Shera, C. A. and G. Zweig (1992g). "Using cochlear nonlinearities to measure the mechanics of the middle ear," in preparation.

Spoendlin, H. (1978). "The afferent innervation of the cochlea," in *Evoked Electrical Activity in the Auditory Nervous System*, edited by R. F. Naunton and C. Fernandez, 21–39. New York: Academic Press.

Spoendlin, H. (1979). "Neural connections of the outer hair cell system," *Acta Otolaryngol.* **87**, 381–387.

Strickland, A. E., E. M. Burns, and A. Tubis (1985). "Incidence of spontaneous otoacoustic emissions in children and infants," *J. Acoust. Soc. Am.* **78**, 931–935.

Strube, H. W. (1985). "A computationally efficient basilar-membrane model," *Acustica* **58**, 207–214.

Strube, H. W. (1989). "Evoked otoacoustic emissions as cochlear Bragg reflections," *Hearing Res.* **38**, 35–45.

Thomas, I. B. (1975). "Microstructure of the pure-tone threshold," *J. Acoust. Soc. Am.* **57** Suppl. 1, S26–S27.

Whitehead, M. L. (1991). "Slow variations in the amplitude and frequency of spontaneous otoacoustic emissions," *Hearing Res.* **53**, 269–280.

Wit, H. P. and R. J. Ritsma (1983). "Sound emission from the ear triggered by single molecules?" *Neurosci. Lett.* **40**, 275–280.

Zenner, H. P., U. Zimmermann, and A. H. Gitter (1987). "Fast motility of isolated mammalian auditory sensory cells," *Biochem. Biophys. Res. Comm.* **149**, 304–308.

Zurek, P. M. and W. W. Clark (1981). "Narrow-band acoustic signals emitted by chinchilla ears after noise exposure," *J. Acoust. Soc. Am.* **70**, 446–450.

Zweig, G. and S. Konishi (1987). "Constraints on measurements of causal or minimum-phase systems," accepted for publication in *J. Acoust. Soc. Am.*

Zweig, G. (1991). "Finding the impedance of the organ of Corti," *J. Acoust. Soc. Am.* **89**, 1229–1254.

Zweig, G., J. E. McDowell, and C. A. Shera (1992). "Latency of tone-burst-evoked otoacoustic emissions," in preparation.

Zwicker, E. and E. Schloth (1984). "Interrelation of different oto-acoustic emissions," *J. Acoust. Soc. Am.* **75**, 1148–1154.